Novel Cucurbituril Complexes as Stimuli-Responsive Supramolecular Systems

Dissertation zur Erlangung des akademischen Grades des

Doktors der Naturwissenschaften (Dr. rer. nat.)

Eingereicht von

STEFAN SCHODER

Im Fachbereich Biologie, Chemie, Pharmazie

am Institut für Chemie und Biochemie

der Freien Universität Berlin

Berlin, 2018

Die vorliegende Arbeit wurde am Institut für Chemie und Biochemie des Fachbereichs Biologie, Chemie, Pharmazie der Freien Universität Berlin im Zeitraum von Juni 2014 bis Juni 2018 unter der Anleitung von Herrn Prof. Dr. Christoph A. Schalley durchgeführt.

1. Gutachter: Prof. Dr. Christoph A. Schalley

2. Gutachter: Prof. Dr. Marcelo Calderón

Tag der Disputation: 15.08.2018

Kurzzusammenfassung

Die Errungenschaften für die Entwicklung molekularer Schalter in organischen Lösungsmitteln können nicht einfach auf wässrige Lösungen übertragen werden. Daher muss das Verständnis für stimuli-responsive supramolekulare Systeme in Wasser angepasst oder neu entwickelt werden.

Die vorliegende Arbeit beschreibt das Entwicklung, die Synthese und die Charakterisierung von neuartigen pH- und redox-responsiven Cucurbit[8]uril (CB[8]) Komplexen in wässriger Lösung. Die konformativen und elektronischen Änderungen nach Zugabe einer externen Eingabe wurden untersucht und die Komplexe wurden in ein funktionales System implementiert.

Allumfassend werden drei stimuli-responsive supramolekulare Systeme in Wasser basierend auf neuartigen CB[8]-Komplexen und deren unterschiedliche Funktionalitäten präsentiert, die nach (De)protonierung entstehen. Diese sind (i) die Feineinstellung der Fluoreszenzeigenschaften eines 2:2-Komplexes, (ii) der Austausch der Gäste eines ternären Komplexes und (iii) Konformationsänderungen zwischen einem 2:2- und einem 2:1-Komplex.

Eine Reihe von neuartigen Bipyridinium-Gästen und deren Komplexierung mit CB[*n*]s wurde untersucht. Der Gast ist ein Fluorophor der einem Twisted Intramolecular Charge Transfer (TICT) Mechanismus folgt, welcher die Emission zum Teil löscht. Komplexierung mit CB[7] hindert die Formation des TICT Zustandes und Komplexierung mit CB[8] führt zur Bildung eines Excimer und starker Fluoreszenzverstärkung. (De)protonierung des Gastes ändert die Emissionseigenschaften. Die Komplexbildung wurde mittels NMR-, UV/Vis- und Photolumineszenzspektroskopie untersucht.

Die Komplexierung einer Serie von unterschiedlich substituierten Phenylpyridinium-Derivaten mit CB[8] wurde untersucht. Ausgehend von diesen Ergebnissen wurde eine orthogonal stimuli-responsives Vielkomponentensystem entworfen. Ein pH-sensitiver und ein redox-sensitiver Gast formen einen heteroternären Komplex mit CB[8]. Beide externen Eingaben resultieren in der Bildung eines homoternären CB[8]-Komplexes, wodurch das System orthogonal schaltbar zwischen drei ternären CB[8]-Komplexen wird. Darüber hinaus wurde ein orthogonal stimuli-responsives self-sorting Netzwerk basierend auf vier Komponenten entwickelt. Die Komplexbildung und das schalten mit externen Eingaben wurde detailliert mittels NMR- und UV/Vis-Spektroskopie analysiert.

Eine pH- und redox-sensitive Achse für CB[*n*]s wurde konzipiert. Der 2:2-Komplex mit CB[8] ist orthogonal stimuli-responsiv und (De)protonierung nach Reduktion resultiert in einer reversiblen Konformationsänderung zwischen einem 2:2- und einem 2:1-Komplex. Komplexbildung und das molekulare Schalten wurden im Detail mittels NMR- und UV/Vis-Spektroskopie analysiert. Für ein mögliches elektrostatisch verriegeltes Rotaxan wurde eine Modifikation der Achse untersucht. Die Komplexbildung und das Redoxverhalten wurden mittels NMR- und UV/Vis-Spektroskopie analysiert.

Abstract

Some of the great achievements for the development of molecular switches in organic solvents cannot simply be translated to aqueous solutions. Therefore, the understanding of stimuli-responsive supramolecular systems in water need to be adjusted or newly developed.

The present thesis describes the design, synthesis and characterization of novel pH- and redox-responsive cucurbit[8]uril (CB[8]) complexes in aqueous solutions. The conformational and electronic changes upon external stimuli were investigated and the complexes were implemented in functional systems.

Overall, three stimuli-responsive supramolecular systems in water are presented which are based on novel CB[8] complexes and their different functionalities emerging upon (de)protonation. These are (i) the tuning of the fluorescence properties of a 2:2 complex, (ii) the exchange of the guests in ternary complexes and (iii) conformational changes between a 2:2 and a 2:1 complex.

A series of novel bipyridinium guests and their complexation with CB[*n*]s was investigated. The guest is a fluorophore that follows a twisted intramolecular charge transfer (TICT) mechanism which quenches the emission in part. Complexation with CB[7] hinders the formation of the TICT state and complexation with CB[8] results in excimer formation and a strong fluorescence enhancement. (De)protonation of the guest leads to a change of the emission properties. The complex formation and the photophysical properties have been analyzed in detail by NMR, UV/Vis and photoluminescence spectroscopy.

The complexation of a series of differently substituted phenylpyridinium derivatives and CB[8] was investigated. Based on these results, an orthogonally stimuli-responsive multicomponent system was designed. A pH-sensitive and a redox-sensitive guest form a heteroternary complex with CB[8]. Each external input results in formation of a homoternary CB[8] complex so that the system becomes switchable between three ternary CB[8] complexes by orthogonal stimuli. Furthermore, an orthogonally stimuli-responsive self-sorting network based on four components has been developed. Complex formation and switching with an external input has been analyzed in detail by NMR and UV/Vis spectroscopy.

A pH- and a redox-sensitive axle for CB[*n*]s has been designed. The 2:2 complex with CB[8] is orthogonally stimuli-responsive and (de)protonation after reduction results in reversible conformational changes between a 2:2 and a 2:1 complex. Complex formation and molecular switching were analyzed in detail by NMR and UV/Vis spectroscopy. For a potential electrostatically interlocked rotaxanes, a modification of the axle was investigated. The complex formation and redox behavior was analyzed by NMR and UV/Vis spectroscopy.

Table of Contents

Abbreviations

A	acceptor	λ_{ex}	excitation wavelength
ACQ	aggregation-caused quenching	λ_s	stokes shift
AIE	aggregation-induced emission	°C	degree Celsius
ALOX	aluminum oxide	(m)M	(milli)molar
aq.	aqueous	m	multiplet
@	encapsulated in	(M)Hz	(mega)hertz
Å	Ångström	mg	milligram
CB[n]	cucurbit[*n*]uril	min	minutes
c	concentration	MSS	metastable state
calcd	calculated	M.P.	melting point
CD	cyclodextrin	m/z	mass-to-charge ratio
CT	charge transfer	(m/µ)L	(milli/micro)liter
D	donor	nm	nanometer
d	doublet	NMR	nuclear magnetic resonance
DMF	*N*,*N*-dimethylformamide	(m/n)s	(milli/nano)seconds
DMSO	dimethyl sulfoxide	p	pentet
D_2O	deuterium oxide	PL	photoluminescence
δ	chemical shift	ppm	parts per million
equiv.	equivalents	RIM	restriction of intramolecular motion
ES	excited state	RIR	restriction of intramolecular rotation
ESI	electrospray ionization	RIV	restriction of intramolecular vibration
ε	energy	q	quartet
GS	ground state	sat.	saturated
h	hour	t	triplet
hept	heptet	TICT	twisted intramolecular charge transfer
(HR)MS	(high resolution) mass spectrometry	TOF	time-of-flight
J	coupling constant	τ	fluorescence decay
K	Kelvin	UV/Vis	ultra violet/visible
LE	locally excited state	Φ	quantum yield
λ_{abs}	absorption wavelength	wt.	weight

1 Introduction

In order to turn on the light, a person needs to flip a switch. The mechanical movement of flipping this switch creates a physical connection between two wires, which in turn closes an electrical circuit – and thus the light is turned on, or off. In a more complex system such as a radio or a computer, a transistor, a semiconductor switching device, it is necessary to amplify or switch electronic signals. These complex machines are not based on only one switch, but rather on numerous combined by a smart design. The switch is therefore an integral component of everyday modern life, and it is important to be able to define its use and capacities. An *external input*, i.e. the person turning on the light, should be able to in induce the *reversible change* between *two states* with *different properties* in a controlled fashion.

On the molecular scale, the concept of switches is a hot topic and investigated intensively. Bistable molecules can be switched between two or more states in response to environmental stimuli, such as changes in pH, light, temperature or the presence of ions and other ligands. This results in electronic or conformational changes in the system which will influence its properties, leading for example to a muscle-like motion, a change in conductivity or a change in the emission behavior. Fostered by the great achievements of the research on molecular switches in the 1990s and early 2000s, the new field of artificial molecular machines emerged. It has gained great attention and its significance was recognized by awarding the Nobel Prize 2016 in chemistry to Fraser STODDART, Jean-Pierre SAUVAGE and Ben FERINGA.[1] They work in the field of supramolecular chemistry, which is in general concerned with the generation and investigation of synthetic molecular systems of greater complexity, organized by non-covalent interactions. They have developed complex molecular systems that can perform various functions, such as a directional rotation,[2] the pumping of a system in an out-of-equilibrium state[3] or the realization of a directional linear movement[4] upon an external input. These artificial molecular machines are often based on supramolecular host-guest complexes, which consist of more than one switch which are combined to perform a specific task.

Each switch within these complex machines follows a simple concept, similar to the earlier example of the light that is been turned on and off. Furthermore, they are based on host–guest interactions and the electronic as well as conformational changes upon an external input. This process can be reversed by a second input and, thereby, the original state of the complex can be restored. In order to obtain a complex which exists in even more than two states, it needs to be addressable by different stimuli. The number of potential outcomes can be increased to four, if the system has two inputs. To access these four different outcomes, the inputs should not be triggered simultaneously, but rather each stimulus should be addressed individually and, therefore, they must be orthogonal.

For the generation of advanced artificial molecular machines, the formation of their host–guest complexes needs to be studied in detail, as well as the conformational and electronic changes of these complexes upon external input. To create new stimuli-responsive complexes with emergent new properties, hosts and guests should be designed and synthesized.

All biochemical processes in nature including natural molecular machines take place in water and, therefore, the investigation and eventual imitation of these processes in the same solvent is of high interest. In addition, principles like sustainability, conservation of resources and recycling must be implemented in every field of society. A great responsibility lies hereby at the chemical research and industry. The concepts of environmentally friendly and sustainable chemistry are collected in the term 'green chemistry'.[5] Consequentially, supramolecular chemists should be able to generate molecular switches in aqueous solutions. This could lead to artificial molecular machines that are fully operational in water. This might lead to functional systems that can be transferred to a physiological environment.

However, the great developments achieved for supramolecular systems in organic solvents cannot simply be translated to aqueous solutions, because these are usually based on non-covalent interactions like hydrogen bonding, which are typically significantly weaker in water. The mechanisms of molecular switches in aqueous solution consequently need to be adjusted or even newly developed. This starts with the basic design of new water-soluble hosts and guests. Commonly used and well-investigated hosts in water are cyclodextrins and cucurbiturils. A large number of well-established host–guest complexes with cucurbiturils are known.[6] Yet, as soon as these are required to be sensitive to an external, the number of known examples significantly decreases. Therefore, new stimuli-responsive guests for cucurbiturils must be designed to create new switchable complexes with emergent properties.

If a toolbox of different stimuli-responsive complexes is finally available, these can be introduced into a larger functional system and transfer their individual properties. This leads the way to the realization of artificial molecular machines in aqueous solutions.

2 Research Objectives

The present thesis aims at the development of new molecular switches in water based on supramolecular host–guest complexes. For this purpose, cucurbiturils are excellent candidates as they are water-soluble, exhibit high binding constants and the driving forces of the complex formation is well understood. Beneficial for the development of new stimuli-responsive systems is the large number of already existing host–guest complexes of cucurbiturils. The main research objectives in this regard will be the design and synthesis of new guests, the formation and analysis of novel host–guest complexes and the investigation of their switching behavior.

The focus is set on the host cucurbit[8]uril (CB[8]) which has the extraordinary feature of the incorporation of a guest dimer inside its cavity. These can either be homodimeric or heterodimeric guest pairs. This allows for the encapsulation of two different guests which are orthogonally stimuli-responsive. Due to the confined space inside the cavity of the host, small changes in guest systems can have a big influence on the binding properties, while the guests must be designed in a smart way. They should be water-soluble, form dimeric guest complexes in CB[8], ideally sensitive to an external input and should bear a free substitution site for the introduction of functional groups to incorporate the resulting complex into larger architectures.

In principle, the library of synthesized guests included the following components: Two electron-poor units, that is, a dicationic bipyridinium and a monocationic phenylpyridinium, as well as an electron-rich counterpart, either a biphenyl or a naphthalene moiety. A part of the building blocks selected are redox-sensitive, another group responds to acids and bases. Extension of this concept by combining these two stimuli led to multicomponent systems that can be addressed orthogonally. This provides the opportunity to study the influence of redox- and pH-stimuli onto host–guest complexes with CB[8] and to explore their emergent properties in a series of five different projects:

(i) The design, synthesis and experimental characterization of novel pH-responsive and fluorescent cucurbit[8]uril complexes based on covalently linked bipyridinium and biphenyl moieties (Figure 1(i), Chapter 3.1)

(ii) The generation of a library of *N*-phenylpyridinium derivatives with different substitutions and their complex formation with cucurbit[8]uril (Figure 1(ii), Chapter 3.2)

(iii) The development and analysis of an orthogonally stimuli-responsive multi component system consisting of a redox-sensitive bipyridinium, a pH-responsive phenylpyridinium and cucurbit[8]uril (Figure 1(iii), Chapter 3.3)

(iv) The synthesis and characterization of the complex formation of an electrostatically interlocked cucurbit[8]uril rotaxane in water based on a covalently linked bipyridinium and naphthalene moieties (Figure 1(iv), Chapter 3.4)

(v) The development of an orthogonally stimuli-responsive molecular switch based on covalently bound redox-sensitive bipyridinium and pH-responsive naphthalene and cucurbit[8]uril (Figure 1(v), Chapter 3.5)

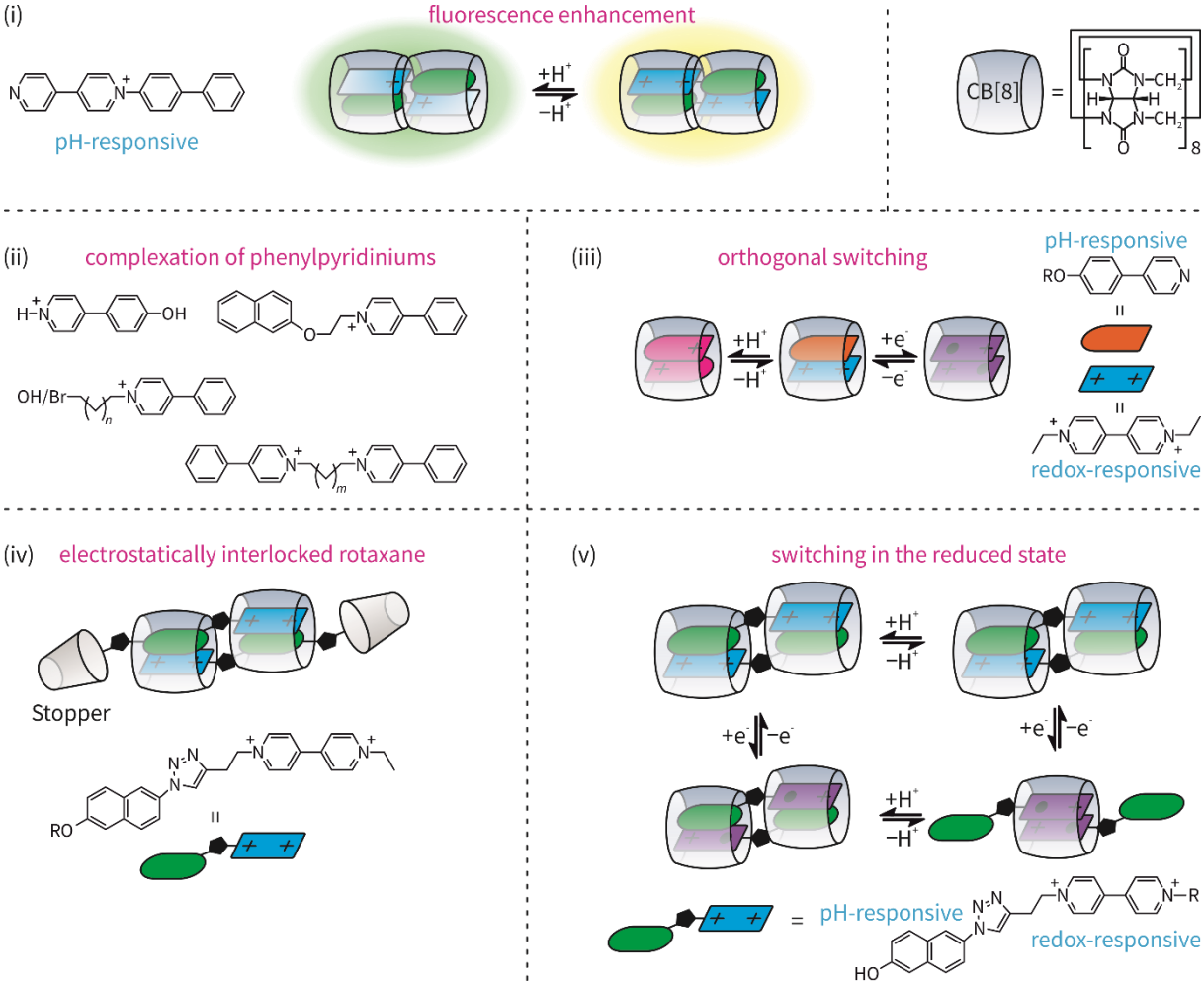

Figure 1. Graphical summary of the research objectives: (i) A pH-responsive 2:2 CB[8] complex that exhibits fluorescence enhancement upon (de)protonation, (ii) phenylpyridinium derivatives with different substitutions for the investigation of complex formation, (iii) an orthogonally responsive multicomponent mixture, (iv) an electrostatically interlocked rotaxane and (v) an orthogonally stimuli-responsive 2:2 CB[8] complex.

3 Background

3.1 Host–Guest Chemistry

Supramolecular chemistry is based on non-covalent interactions between two molecules with a shape difference between the binding partners. If one is a macrocyclic molecule, shaped like a bowl, a ring or a cage, it can act as a host and incorporate a guest molecule. This *host–guest* complex formation is *reversible* and, therefore, the complex is in equilibrium with its individual parts. Figure 2 shows some commonly used macrocycles that are capable of encapsulating inorganic or organic guest molecules.

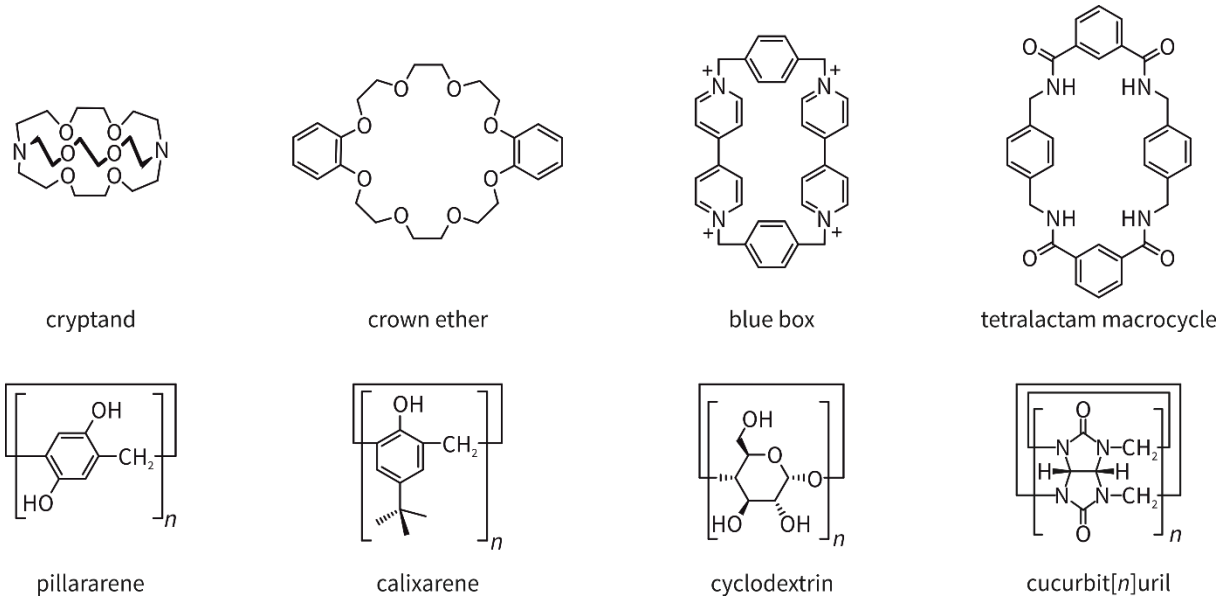

Figure 2. Commonly used macrocyclic molecules for host–guest chemistry in organic solvents or aqueous solutions.

The equilibrium and logically the binding affinity of a supramolecular host–guest complex is strongly dependent on some principle requirements. The guest should have a good fit inside the cavity of the host, meaning the two molecules are *complementary* to each other regarding their size, their shape and their intermolecular interactions. If this requirement is fulfilled, the complex can spontaneously organize without addition of external energy which is termed *self-assembly*. The dissociation of thermodynamically less favored complexes allows for *error correction* since the complex formation is reversible. The processes reach the equilibrium when the system aggregates in the *thermodynamic minimum* state.

When designing a supramolecular system, suitable non-covalent interactions must be chosen. A strong coordinative bond (100–200 kJ · mol^{-1}) might not be reversible and consequently not allow for error correction, and π-π interactions (2–50 kJ · mol^{-1}) might be too weak to form a host–guest

complex.[7] A large number of host–guest systems, especially regarding molecular machines, are based on hydrogen bonding (4–160 kJ · mol^{-1}). Since water competes strongly with hydrogen bonds and solvates charged species efficiently, the binding affinities of host-guest systems typically drop significantly in aqueous environments compared to organic solvents. Host–guest systems therefore must be based on the remaining supramolecular interactions. The most common water-soluble host molecules are cyclodextrins, cucurbiturils, calixarenes and pillararenes (Figure 2). The macrocyclic hosts cyclodextrins and cucurbiturils will be discussed in this thesis.

All these requirements are influenced by factors like solvent interaction, temperature and the molecular composition. Hence, the construction and study of host–guest systems demand careful handling and well-thought design.

3.1.1 Cyclodextrins

VILLIERS discovered and isolated a white powder in 1891,[8] which was later identified as the macrocyclic carbohydrate cyclodextrin (CD). The molecule has a flexible structure with an apolar cavity (Figure 3). Due to the nature of the macrocycle, the height stays the same, but the cavity diameter increases with increasing number monomer units. The most common members of the family of CDs are α-, β- and γ-CD. The Greek letter in front of the name indicates the number of monomeric units (α = 6, β = 7 and γ = 8).

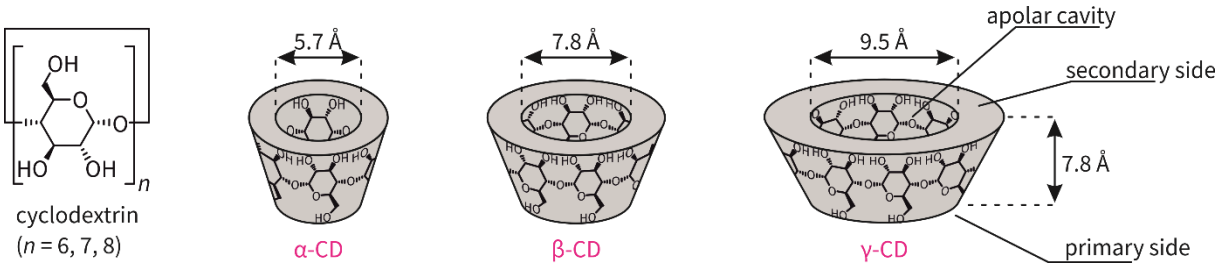

Figure 3. Structure and architecture of cyclodextrins.

CDs have been used far beyond the boundaries of the typical science of carbohydrates. The synthesis of common CDs is relatively simple and uses ordinary starch as the starting material which is treated with easily available enzymes.[9] CDs are used in many fields of science e.g. aroma and food chemistry, cosmetics, pharmaceutics and medicine.[10] The fact that they are reasonably cheap, easy to functionalize, non-toxic and – most important of all – soluble in water, makes them one of the most important groups of host molecules in the wide field of supramolecular chemistry in aqueous media.[11] In the early 1950s, it was discovered that CDs can trap or encapsulate other molecules inside their hydrophobic cavity and since then it is the most commonly used host in aqueous solutions.[12]

Despite their advantages of easy synthesis and good solubility, a major drawback of CDs is their comparatively weak binding constants, with typical values ranging from $k = 10^2$ M^{-1} to $k = 10^4$ M^{-1}.[13] This disadvantage can be overcome by utilization of another common macrocycle in aqueous solution, namely cucurbiturils.

3.1.2 Cucurbiturils

The condensation product of glycoluril and formaldehyde is a highly symmetrical macrocycle with the point group D_{nh},[14] consisting of glycoluril units that are connected by two methylene bridges each (Figure 4).[15] The name cucurbituril was given due to the allegedly similar form to a pumpkin, which belongs to the family of *cucurbitaceae*. The general abbreviation is CB[*n*], with *n* denoting the number of repeating glycoluril units. Most commonly *n* is 5, 6, 7, 8 or 10. A fundamental factor is the fact that the cavity size increases at higher cucurbituril homologues, but the height remains the same at around 9 Å (Table 1).

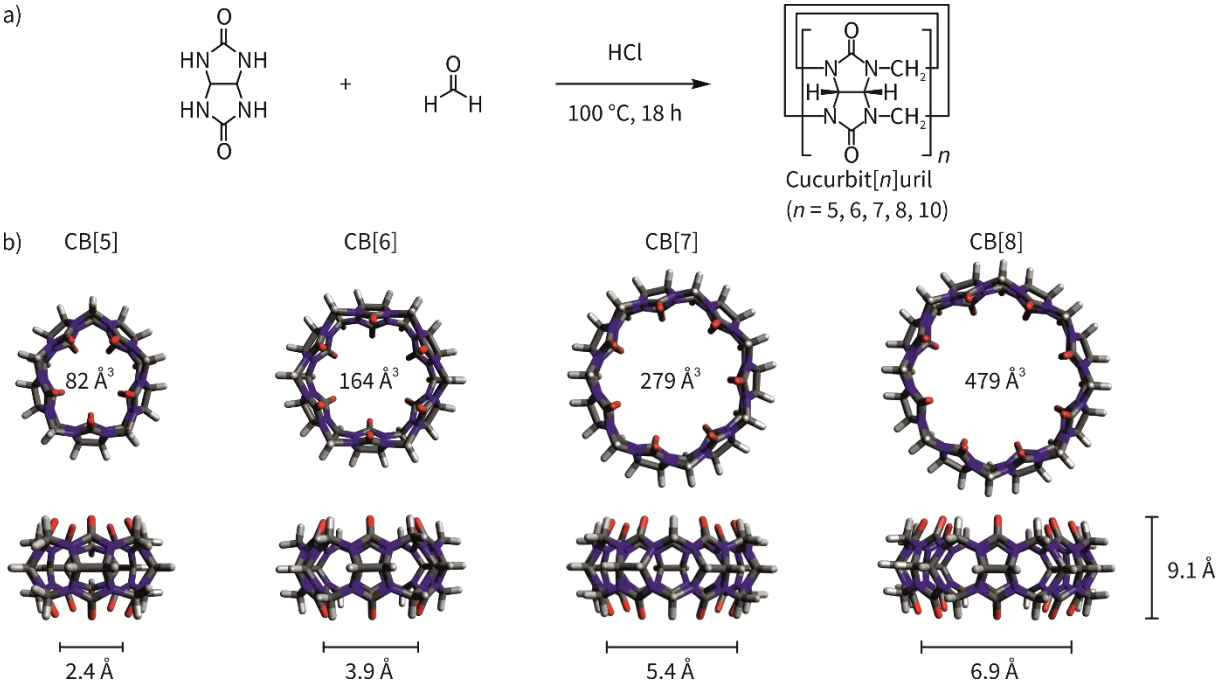

Figure 4. (a) Condensation reaction of glycoluril and formaldehyde yielding a mixture of different cucurbit[*n*]urils and (b) molecules rendered as sticks demonstrating the increasing size with constant height of the macrocycles.

The synthesis of CB[6] was first reported 1905 by BEHREND *et al.*,[16] and a full characterization was performed in 1981 by MOCK.[17] The latter studied the host-guest chemistry of this first cucurbituril derivative in combination with alkyl- and aryl-amines intensively in the 1980s.[18] KIM conducted intensive research in supramolecular architectures with CB[6] in the 1990s,[19] but identified its relatively small cavity size as the big limitation of CB[*n*] chemistry at this time. After the successful synthesis of bigger homologues in the year 2000,[15] the host cucurbituril gained great attention.

However, due to its challenging synthesis and consequently the high price, applications outside of academic research are still rare.

Table 1. Structural parameters for cucubit[*n*]uril (*n* = 5, 6, 7, 8 and 10).

	CB[5][a]	CB[6][b]	CB[7][a]	CB[8][a]	CB[10][c]
portal diameter (Å)	2.4	3.9	5.4	6.9	9.5-10.6
cavity diameter (Å)	4.4	5.8	7.3	8.8	11.3-12.4
cavity volume (Å^3)	82	164	279	479	870
outer diameter (Å)	13.1	14.4	16.0	17.5	20.0
height (Å)	9.1	9.1	9.1	9.1	9.1

[a] based on x-ray crystal structures[15]; [b] based on x-ray crystal structures[20]; [c] based on x-ray crystal structures[21]

The unique architecture of CB[*n*]s features a rigid cavity that is extremely hydrophobic, since no hydrogen-bond-donor or -acceptor moiety is pointing inwards, allowing for encapsulation of hydrophobic compounds.[22] The two symmetrical portals on the other hand consist of electronegative carbonyl rims and bind cationic species,[23] as well as protons, which explains the better solubility of CB[*n*]s in acidic aqueous medium.[24] But the exceedingly high binding constants cannot only be explained by the interaction of the host and the guest, but rather by a *high-energy water* model (Figure 5).[25] The water molecules in the cavity of the CB[*n*]s are structurally and energetically extremely frustrated because of the confined space that they are restricted to. Calculations suggests that they show a lower hydrogen-bond count than bulk water.[26] In the event of the encapsulation of a guest, the cavity water is released out of the hydrophobic environment into the bulk, allowing hydrogen bonding. This causes a high exothermic driving force for complex formation, already explaining high binding constants. Upon binding of the cationic moiety of a charged guest to the carbonyl portals, a number of solvating water molecules is liberated, which is entropically favored.[27] This effect explains the large differences in binding strength between charged and non-charged analogues (Table 2).[28] Another effect is caused by the proportional difference between the cavity and the guest. If the guest is too small to displace all high-energy water molecules, residual water is still present and not the entire energetic potential is released. This plays a crucial role with the large homologue CB[8]. After complexation of dicationic viologen to CB[8], residual water remains in the cavity and therefore, subsequent binding of a second guest is strongly exothermic.[29]

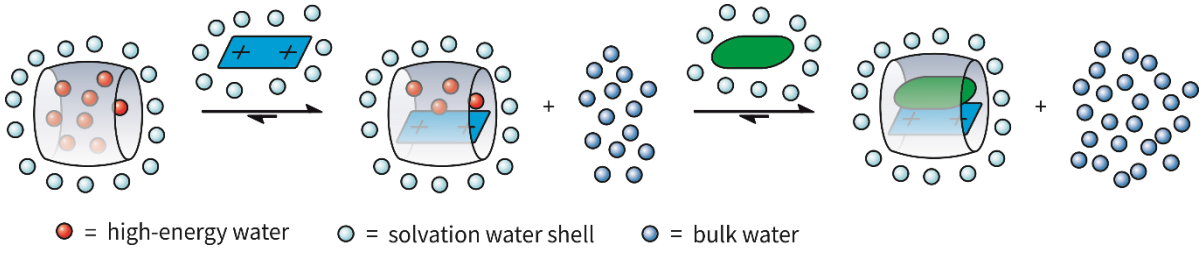

Figure 5. Release of high-energy water upon complexation of guest molecules in cucubituril.

Cucurbit[5]uril is the smallest representative of the CB[*n*]s with half the cavity volume of CB[6].[15] Like the other homologues, the carbonyl groups at the rim can bind cationic species.[30] The cavity, however, can only encapsulate gas molecules like nitrogen and oxygen with ammonium ions acting as a "lid" in the gas phase.[31] In solution, lid-free complexes exist as well.[32]

Cucurbit[6]uril is able to encapsulate small gas molecules, as well as longer alkyl chains.[33] It can host aliphatic ammonium ions because of its larger cavity,[34] but in general it is too small to encapsulate aromatic systems with the exception of a few examples.[35]

The cavity size of cucurbit[7]uril is large enough for inclusion of simple three-dimensional molecules like ferrocene[36] and adamantylammonium[27] derivatives. One of the tightest monovalent non-covalent complexes ever reported in water is the diamantine diammonium guest with an association constant of $k_a = 7.2 \cdot 10^{17}$ M^{-1}.[37] Furthermore, viologen derivatives[38] and their radicals[39] are encapsulated with high binding affinities.

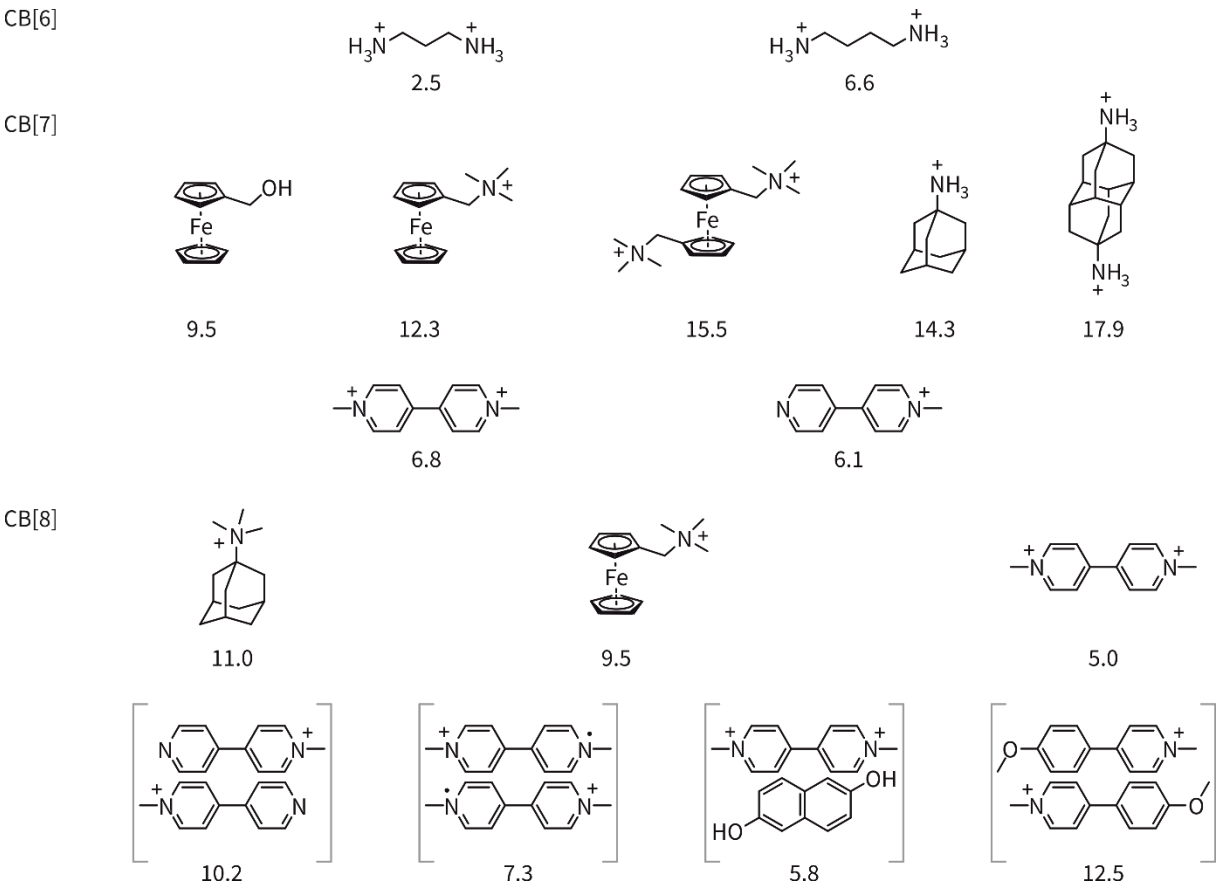

Table 2. Representative examples of common guests of cucurbit[*n*]urils and the corresponding association constants log(*k*); the square brackets symbolize the formation of a ternary complex.[6]

With a cavity volume 1.7 times larger than CB[7], cucurbit[8]uril has similar binding properties to the smaller homologues.[40] It can encapsulate adamantanes,[41] transition metal complexes[42] or bind two fullerenes, one at each rim.[43] The complexation of dications is possible, with smaller association constants than with CB[7], as explained with the high-energy water model. Because of

the bigger cavity size, it is possible to incorporate a second guest molecule to form a ternary complex. In this manner, hetero-[44] and homodimeric[45] guest pairs can be stabilized inside the macrocycle (Figure 6).[1]

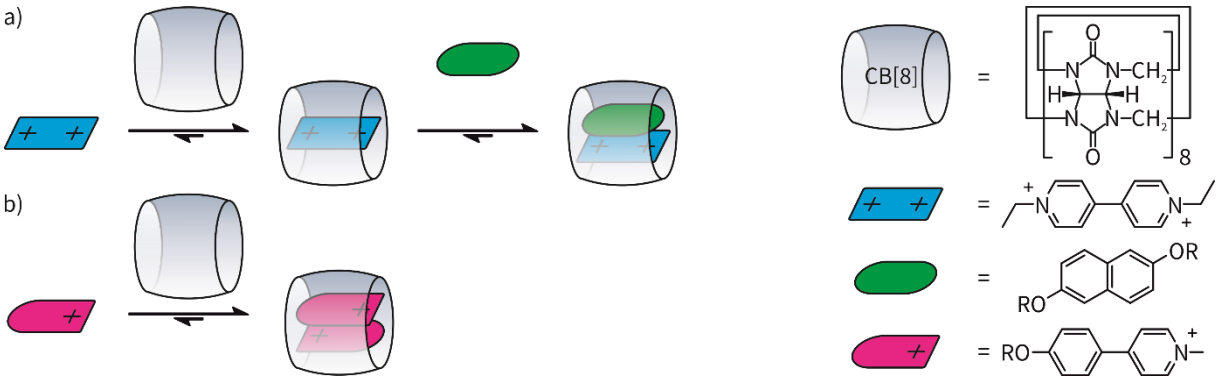

Figure 6. (a) Schematic representation of the encapsulation of a dication (blue) and subsequent incorporation of an electron rich second guest (green) forming a 1:1:1 heteroternary complex with cucurbit[8]uril, (b) encapsulation of phenylpyridinium derivative (pink) forming a 2:1 homoternary complex with cucurbit[8]uril.

The remarkable feature of accommodating two guests simultaneously predestines CB[8] as a linking agent for reversible complex formation. This allows for the design and simple preparation of big supramolecular architectures like linear polymer chains,[46] gels,[47] supramolecular organic frameworks[48] and the functionalization of surfaces.[49]

SCHERMAN and coworkers reported on a supramolecular gel in water based on CB[8] and the viologen-naphthalene binding motif (Figure 7).[50] A commercially available poly(vinyl alcohol) polymer is functionalized with a dicationic viologen (blue) and renewable cellulose with a naphthalene derivative (green). Mixing of the two in water does not change the physical properties of the individual components, but upon addition of CB[8] rapid hydrogel formation takes place. Since the formation of the interconnecting complexes is reversible, the gel exhibits self-healing properties after physical stress.

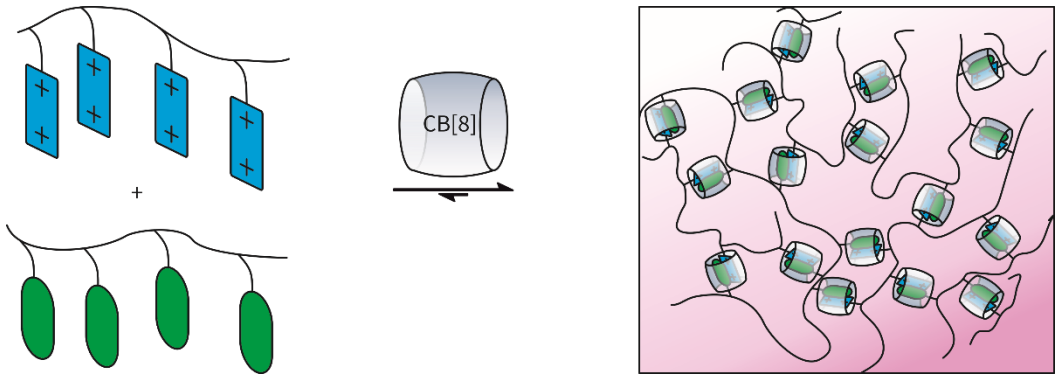

Figure 7. Supramolecular gel based of the viologen-naphthalene heterodimeric guest pair in cucurbit[8]uril.

[1] Even though the term is host–guest chemistry, in this thesis, a 2:1 complex refers to a complex of two guests and one host.

Another highly ordered self-assembly architecture is a supramolecular organic framework (SOF). Li and coworkers presented a three dimensional periodic porous SOF in water based on the phenylpyridinium binding motif and CB[8] (Figure 8).[48a] The tetrahedral monomer unit $\mathbf{X^{4+}}$ of the system consist of a four-times substituted tetraphenyl methane center which allows expansion in all dimensions. The substituents are phenylpyridinium moieties, which form homodimers after encapsulation in the cucurbituril. Mixing of $\mathbf{X^{4+}}$ with CB[8] results in a highly ordered periodic framework that possesses high porosity.

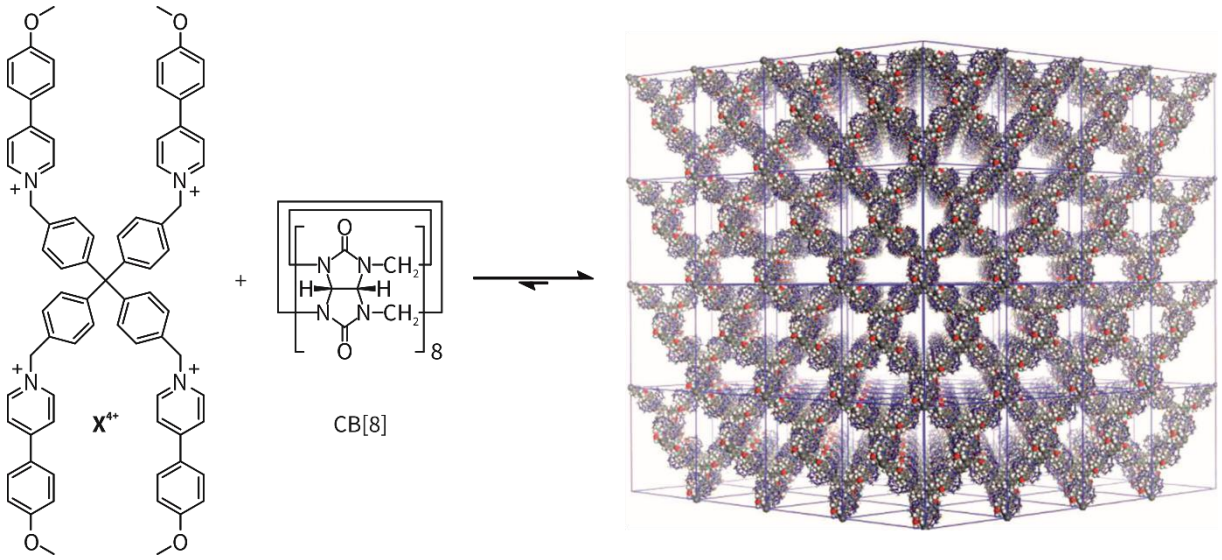

Figure 8. Formation of a three-dimensional supramolecular framework based on the phenylpyridinium homodimer within cucurbit[8]uril. Adapted with the permission from Tian *et al*.[48a] (© 2014 Springer Nature).

Cucurbit[10]uril can bind two organic guests simultaneously inside the cavity, similarly to CB[8], but potential applications in the area of supramolecular polymerization in aqueous media have been explored with limited success.[51] New studies suggest that CB[10] might be able to encapsulate a π-donor-π-acceptor trimer complex in its cavity, which could attract more attention in the next years.[52]

The largest and rather exotic member of the family of the cucurbiturils, CB[14], consists of 14 units of the glycoluril moiety with a 360° twist. Because of this extraordinary feature it does not have a normal cavity like the smaller homologues, but a figure of eight conformation which is furthermore folded stacking the two cavities.[53]

One remote relative to CB[*n*]s is the structurally similar bambus[6]uril.[54] The cyclic hexamer consists of six 2,4-dimethylglycoluril units which are only connected through one methylene bridge each. Therefore, it loses the rigidity that characterizes the CB[*n*]s, but on the other hand gains high affinity and selectivity to certain anions in water.[55]

Even though there are some reports about substituted cucurbiturils, substitution with functional groups and reactions after complex formations are barely available due to the poor solubility, the challenging synthesis and the complicated isolation.[56]

The different association constants of different molecules to cucurbituril (Table 2) enable a controlled release of the guests by addition of a competitive binder (Figure 9). As shown, viologen derivative $\mathbf{V}^{2+}$ is encapsulated by CB[7] with log(*k*) = 6.8 M^{-1} and adamantane derivative **A** binds with log(*k*) = 14.3 M^{-1}.[6] Consequently addition of **A** to a solution of the complex $\mathbf{V}^{2+}$@CB[7] leads to a competitive displacement of the guest resulting in free $\mathbf{V}^{2+}$ and exclusive formation of the complex **A**@CB[7].

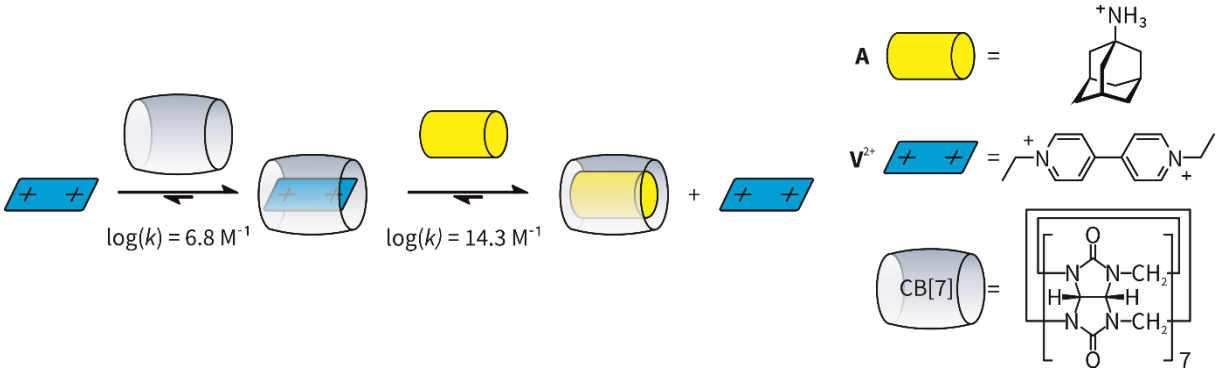

Figure 9. Displacement of the guest $\mathbf{V}^{2+}$ by the competitive binder **A** in a cucurbit[7]uril complex and the corresponding association constants.

3.1.3 Mechanically Interlocked Molecules

A special class of host–guest complexes are mechanically interlocked molecules (MIMs), where two or more molecules are mechanically connected with each other, but do not share any covalent bonds. As a consequence, MIMs cannot be separated into their individual parts without breaking one of the molecules.[57] The two most common architectures are *catenanes* and *rotaxanes* (Figure 10). The name “catenane” derives from the Latin word catena, meaning “chain” and hints to their structure, consisting of two or more topologically linked rings. The word “Rotaxane” is a composite of rota, meaning wheel and axis, meaning axle. Rotaxanes are build from at least one macrocyclic component, which is threaded by a rod-like axle molecule terminated with bulky stopper groups large enough to prevent dethreading. If there are no stoppers attached, or their size not sufficient to stop equilibration of the threading, the complex is referred to as a *pseudorotaxane*. The pseudorotaxane is not a MIM but can play an important role during the synthesis of catenanes and rotaxanes. Other examples for MIMs are knots[58] and Borromean rings,[59] which, similar to catenanes, are also topologically interwoven.

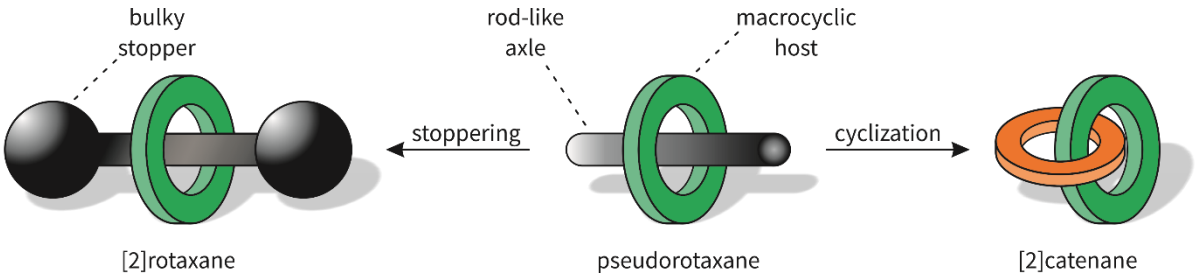

Figure 10. Representation of a [2]rotaxane, a pseudorotaxane and a [2]catenane.

The driving force for the macrocycle to be located on the axle is often a binding station that exhibits host–guest interactions and holds the host on his place. If more than one binding station is on the axle different structures of the rotaxane are possible. STODDARD and coworkers reported a molecular shuttle with two identical binding stations (Figure 11).[60] The electron-deficient macrocycle cyclobis(paraquat-*p*-phenylene) **CBPQT^{4+}** acts as the host. The axle consists of two hydroquinol units connected with polyether chain and stoppered by triisopropylsilyl groups. Since the binding stations are identical, the macrocycle moves back and forth like a molecular shuttle around 1000 times a second. This rotaxane inspired the synthesis of axles with two different binding stations which will be discussed in Chapter 3.2.3.

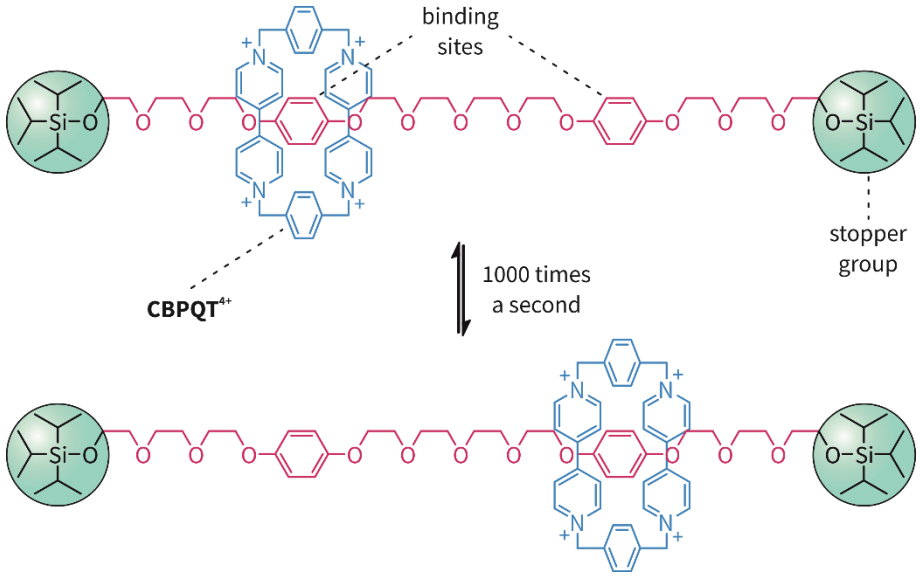

Figure 11. A molecular shuttle in which the macrocycle darts back and forth between two identical binding stations 1000 times per second.

The formation of rotaxanes, catenanes and supramolecular polymers based on cyclodextrins was investigated intensively since the mid-1980s.[61] HARADA and coworkers reported on a rotaxane with a large number of macrocycles with resemblance to a molecular necklace in 1991 (Figure 12a).[61e] A number of α-CDs are penetrated by a polyethylene glycol (PEG) chain which is stoppered after complex formation. The formed polyrotaxane is not soluble in water, but in DMSO, and stable against acids and bases. Based on this supramolecular system, ITO and coworkers presented a so-called slide-ring gel (b).[62] In this approach, the polyrotaxane consists of PEG chains with large

molecular weights that are sparsely populated with α-CDs. After stoppering, the polyrotaxane is soluble in water because around 72% of the PEG units are not shielded by CDs. The CDs are chemically cross-linked and consequently, the polymers are interconnected resulting in a gel. The gel is acid stable, but strong bases can remove the bulky stoppers, which results in the breakdown of the network. The extraordinary property of the gel however is the fact that it is a *topological gel*, in which the polymer network is interlocked by topological restrictions. This means it is flexible and tensile by of a factor of two regarding its length. Physical stress is not harming the polymer network since the polymer strands can rearrange one to each other like pulleys to equalize tension without the breaking of covalent bonds.

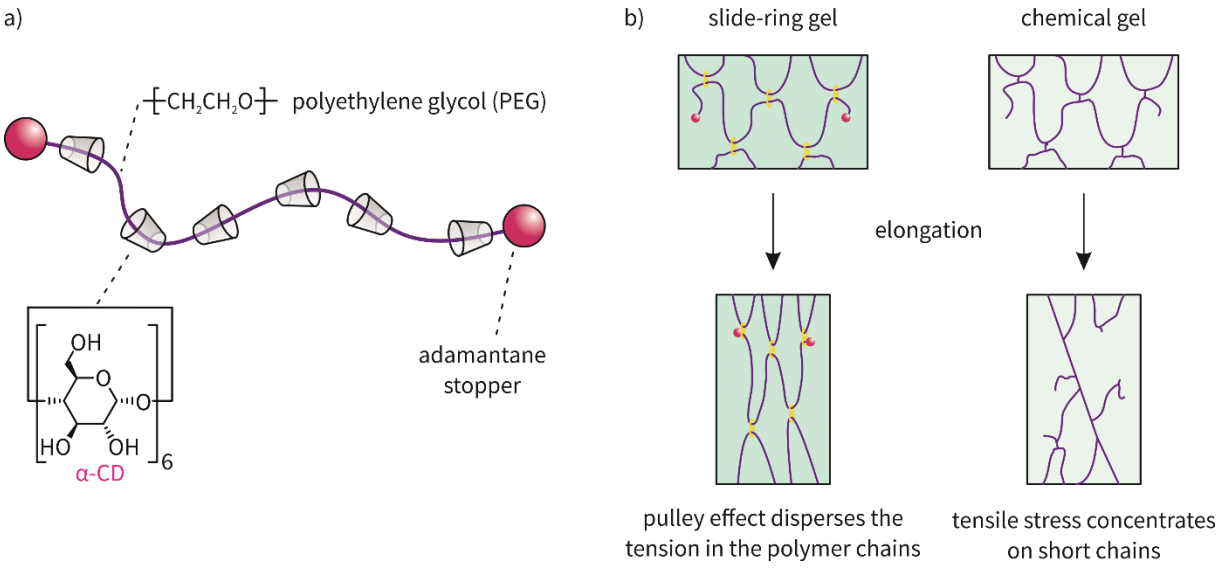

Figure 12. (a) A polyrotaxane based on a PEG axle and α-CDs, (b) the sliding-ring gel with interconnected polyrotaxanes.

A special case of a rotaxane occurs, when the stoppering group is not defined by the fact that it is sterically demanding, but by its electrostatic interactions with the macrocycle. STODDART and coworkers reported on a pseudorotaxane with electrostatic pseudo stopper groups in an organic solvent (Figure 13).[63] The electron-deficient macrocycle cyclobis(paraquat-*p*-phenylene) **CBPQT^{4+}** acts as the host. The axle has an electron-rich 1,5-dioxynaphthalene (DNP) recognition site. Model pseudorotaxane **3@CBPQT^{4+}** is in equilibrium with its individual components because no stopper or speed bump is present (a). Axle **4^{4+}** on the other hand has bipyridinium (BIPY^{2+}) units at both ends of the axle, which are sterically undemanding and therefore do not act as stoppers in the conventional steric sense. If **CBPQT^{4+}** and **4^{4+}** are mixed, pseudorotaxane formation takes place (b). The process is extremely slow because of the strong electrostatic repulsion between the quadruply positively charged **CBPQT^{4+}** and the doubly charged BIPY^{2+} termini; equilibrium is attained after more than one week forming **4^{4+}@CBPQT^{4+}**. Compared to the uncharged model of compound **3** and its pseudorotaxane **3@CBPQT^{4+}**, the bimolecular threading rate constant decreases by approximately ten orders of magnitude. Investigation of the dethreading sheds light onto a peculiar phenomenon: The monomolecular dethreading rate constant of **4^{4+}@CBPQT^{4+}** is decreased strongly, resulting in a

comparatively inert supramolecular species. In other words, the ring is fixed onto the axle once bound to the DNP unit. In conclusion, the pseudorotaxane **4^{4+}@CBPQT^{4+}** exhibits the properties of a rotaxane, but instead of sterically demanding stopper groups it has electrostatic barriers that act as stoppers.

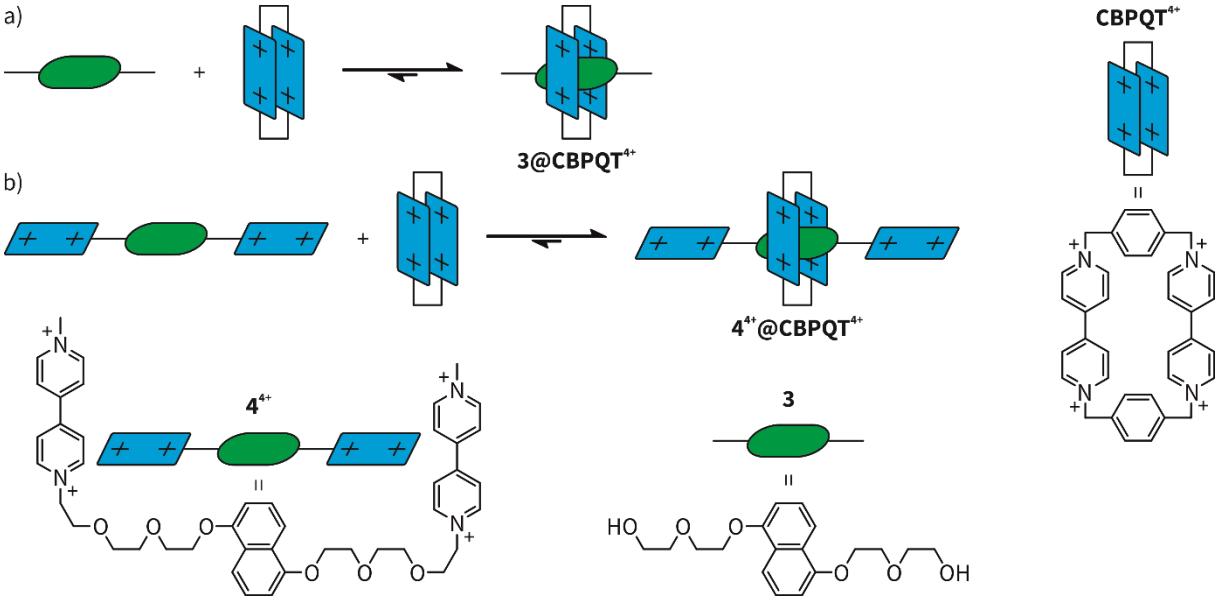

Figure 13. (a) Formation of the host–guest complex **3@CBPQT^{4+}** without stopper groups, (b) formation of the pseudorotaxane **4^{4+}@CBPQT^{4+}** that exhibits properties of a rotaxane because of the strong electrostatic repulsion of the macrocycle and the terminal groups.[63]

3.2 Systems Chemistry

The ability to predict and to influence an outcome of host–guest systems introduces synthetic molecules to the otherwise from biology deriving field of *systems chemistry*.[64] This field is concerned with the investigation of the complexity[65] of multicomponent mixtures, which are governed by molecular interactions. The difference between a complex and a very complicated system can be distinguished in two key properties: *emergence* and *self-organization*.[66] In this context, emergence is defined as the appearance of a property in a system, that is not a characteristic of the individual constituents of the system. By self-organization, a system's internal order increases by consuming energy of its environment. As a relatively young field, most design rules, the mastering of the underlying basic chemistry and the development of the analytical tools of systems chemistry are still to learn.[67]

Nevertheless, unravelling the behavior of individual molecules in multicomponent mixtures and understanding the driving forces which lead to binding or ignoring specific partners in a complex environment could provide insights into the evolution of the biological systems from inanimate matter.[68] For this reason, *self-sorting* of a system must be investigated which can lead to different theoretical outcomes which are combined in a virtual product library, a so-called *dynamic combinatorial library*. If a system can be switched between two of these outcomes in a controlled and reversible way, the realization of a *molecular machine* is possible.[69]

3.2.1 Self-Sorting

Self-assembly can in principle lead to a library of all possible non-covalent complexes derived from the single compounds in the original complex mixture. In case of molecular recognition between individual components, only specific pairs are formed, resulting in so-called self-sorting.[70] The high-fidelity recognition of molecules is a commonplace in biological systems.[71] This idea was transferred to supramolecular systems in 1993 by LEHN and coworkers. When copper(I) ions are added to a mixture of four different bipyridine ligands, only double helices containing the same ligands are formed. However, no crossover of ligands in the same helix was found. This process of self- and non-self-discrimination was described as *self-recognition*.[72]

Self-sorting can be divided into different types depending on their basic operation mechanism.[71] In the case of a homomeric aggregation, meaning that molecules show a high affinity for themselves, the process is called *narcissistic self-sorting*.[73] If molecules have a high affinity for others and heteromeric aggregates are formed, the process is referred to as *social self-sorting*.[74] Another subdivision is made according to the stability of the formed product: *Thermodynamic self-sorting* refers to the product in thermodynamic equilibrium and *kinetic self-sorting* to product species trapped under kinetic control.[75]

An advantage of a thermodynamic self-sorting system is the possibility for error correction since the self-assembly process is reversible. Over time, the mixture converges into the energetically most favorable assembly.[76] ISAACS and coworkers demonstrated a thermodynamic social self-sorting experiment in aqueous solution with twelve components that resulted in the exclusive formation of only six complexes (Figure 14).[77] The complex mixture consisted of macrocyclic hosts CB[6], CB[8] and β-CD and their suitable guests, namely hexane diammonium (**L1**), viologen (**L2**) and naphthalene (**L3**), as well as an adamantane derivative (**L4**), respectively. Furthermore, it contained a potassium-binding cryptand (**L5**), a glycoluril derivative (**L6**) which undergoes dimerization upon self-association and, therefore, narcissistic self-sorting. In addition, a racemic mixture of a glycoluril derivative (**L7** and **L7***) that undergoes an enantiomeric self-recognition triggered by the addition of a palladium species (**L8**). The resulting product mixture could be analyzed by ^{1}H NMR spectroscopy due to the characteristic complexation-induced shifts of the self-sorted components.

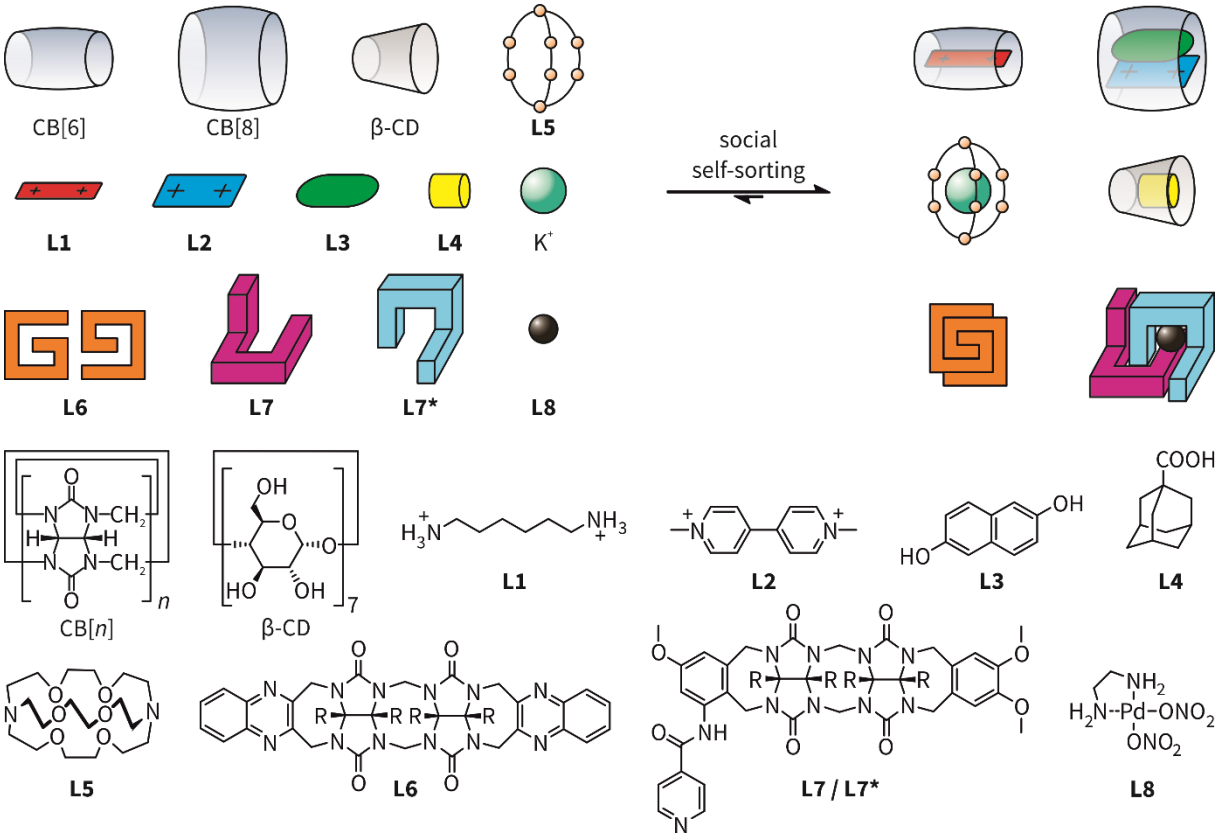

Figure 14. A social self-sorting approach in a complex aqueous solution consisting of twelve components.

To construct larger assemblies by self-sorting, which consist of a number of different building blocks that should be correctly positioned in the resulting complex, it is useful to integrate more binding sites with different motifs into one compound.[76] Thereby, so-called integrative self-sorting can be achieved. SCHALLEY and coworkers reported a simple self-sorting system consisting of macrocyclic hosts CB[7] and CB[8] and suitable guests in an aqueous solution (Figure 15).[78] The non-integrative system (a) with two guests $\mathbf{MV}^{2+}$ and $\mathbf{S1}^{2+}$ results exclusively in the two complexes $\mathbf{MV}^{2+}$@CB[7] and

S1^{2+}@CB[8]. However, the integrative component **S2**$^{4+}$ which consists of covalently connected **MV**$^{2+}$ and **S1**$^{2+}$, forms only the hetero[3]pseudorotaxane **S2**$^{4+}$@CB[7]&CB[8] when mixed with the two hosts in an equimolar fashion (b).

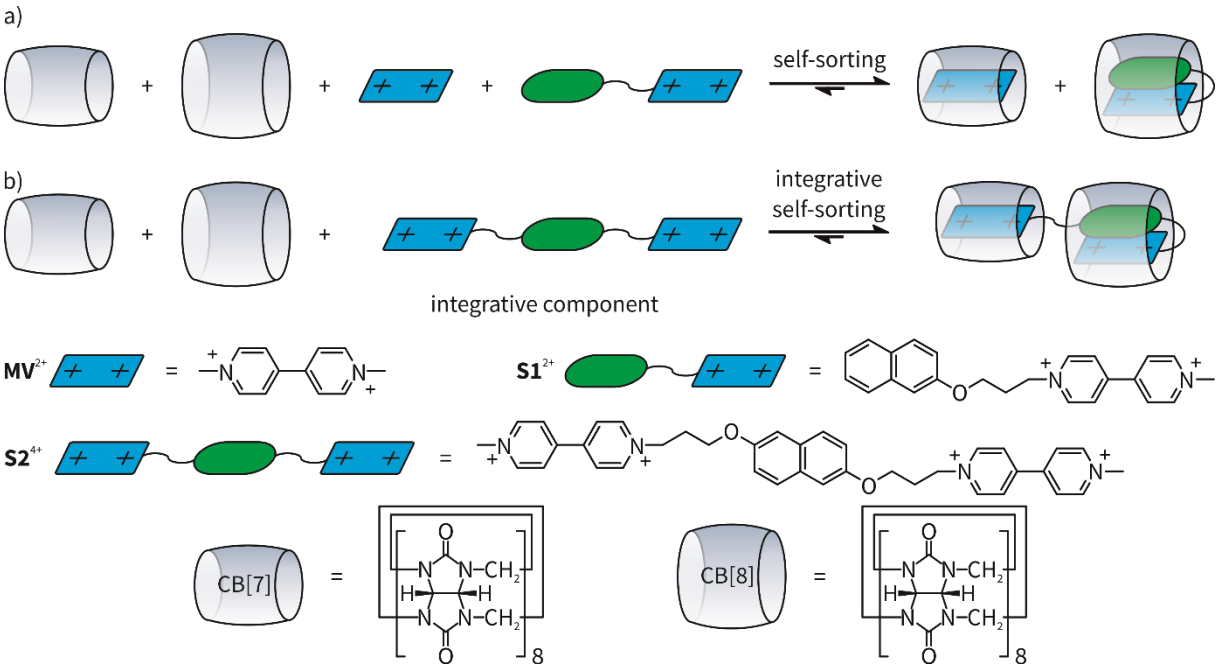

Figure 15. (a) Self-sorting approach with two hosts and two guests and (b) integrative self-sorting with two hosts and a guest with multiple binding sites.

3.2.2 Molecular Machines

The switching of molecules and supramolecular systems between clearly identifiable states is a topic of high interest. The realization of molecular machines can only be achieved if full control over the state of a system is given. The term molecular machines can be categorized into various subgroups such as “motors” and “switches”, which can be clearly differentiated.[79] In a molecular *switch*, for example, the affinity of a host to a binding station is changed and thus, the position of a macrocycle in a rotaxane changes. However, switching back leads to the return of the macrocycle to its original position and undoes any work potentially done. This means that a switch cannot be used to do work progressively. The opposite happens in a molecular motor. After the motor returns to its original position through a different pathway compared to the one they left by, for example after a full 360° directional rotation of a macrocycle, the physical work performed by the machine is not undone. An illustrative example would be a rotating component that winds up a polymer chain.[80] Overall, a switch affects a system as a function of state on the one hand, while a motor, on the other hand, influences a system as a function of the trajectory of its constituents.[81]

To gain control over the molecular machine, an external input is crucial to either trigger an ON/OFF event of a *switch*, or to provide a fuel for a continuously running *motor*.[82] In 2007, STODDART defined three types of external stimuli: a chemical, an electrochemical and a photochemical input.[83]

As an early example of a simple molecular switch, STODDART and coworkers reported an acid-base-responsive [2]rotaxane which consists of a crownether macrocycle and an axle possessing two possible binding stations (Figure 16).[84] Since crownethers show only a small binding affinity toward bipyridinium ($Bipy^{2+}$) cations, but a relatively high affinity to ammonium stations , the host exhibits complete selectivity for this latter recognition site in acidic medium. Deprotonation, however, leads to formation of the amine, which does not have a considerable binding affinity to the host, and consequentially to the relocation of the macrocycle towards the bipyridinium station. Treatment of the rotaxane with acid restores the ammonium binding site and reverses the process.

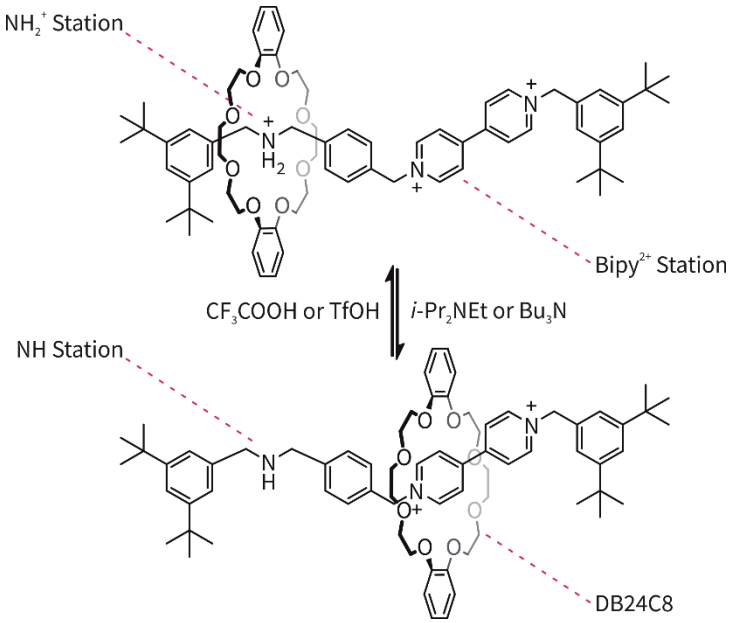

Figure 16. An acid-base controllable [2]rotaxane.

In general, the rapid guest exchange in most weakly binding non-covalent host-guest complexes makes it difficult to extract work from a molecular machine which is solely depending on supramolecular interactions.[81] If the binding affinities in a system are high enough, however, they might be suitable for the use in the assembly of molecular machines. The extraordinarily high binding constants of π-acceptor-π-donor complexes in CB[8] are predestine for that purpose. The one-electron reduction of viologen results in the formation of a monocation radical dimer that is well-stabilized in the cavity of the CB[8]. KIM and coworkers reported on a three-way supramolecular switch based on two redox-sensitive guests (Figure 17).[85] The electron-deficient viologen derivative **MV**$^{2+}$ forms a donor-acceptor complex with the tetrathiafulvalene derivative **TTF** in the host, giving the heteroternary 1:1:1 complex (**MV**$^{2+}$&**TTF**)@CB[8]. Reduction results in the rapid generation of the homoternary 2:1 complex (**MV**$^{+\bullet}$)$_2$@CB[8] and exclusion of the neutral compound **TTF**. A key feature of **TTF** is its oxidation to the monocation radical **TTF**$^{+\bullet}$ that can dimerize and is then stabilized in CB[8] by the formation of the homoternary 2:1 complex (**TTF**$^{+\bullet}$)$_2$@CB[8]. Both, the oxidation and the reduction are fully reversible. Overall, this system can be selectively controlled by redox-stimuli switching between three distinct ternary complexes.

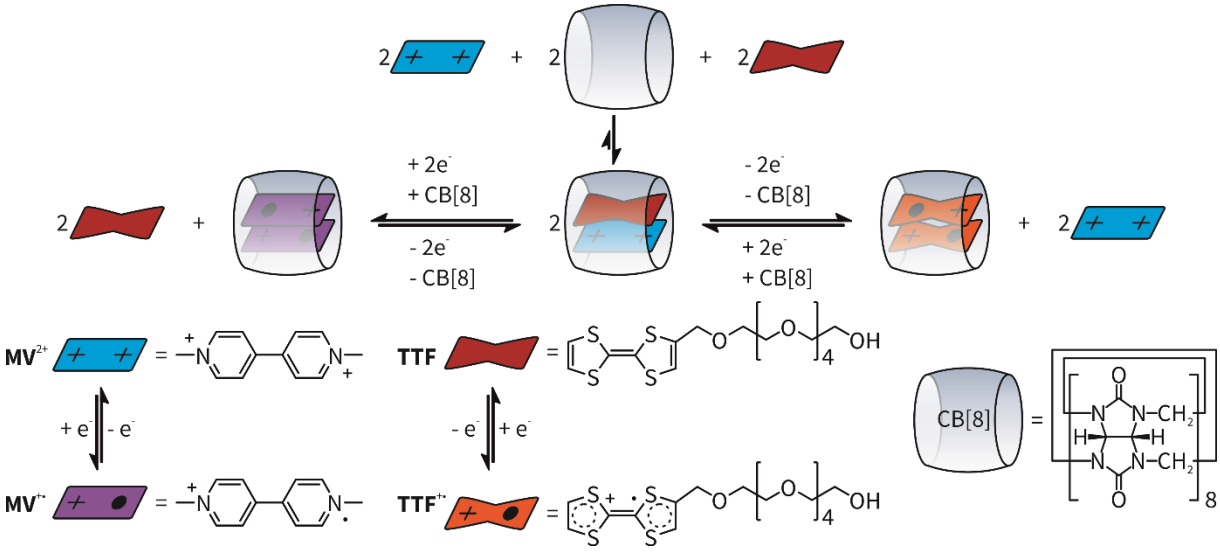

Figure 17. Switching between three distinct ternary cucurbit[8]uril complexes with redox stimuli.

The concept of a molecular machine based on cucurbiturils was extended by SCHERMAN and coworkers who introduced orthogonal switching of a CB[8] complex by redox reactions and light (Figure 18).[86] The host and the two guests, a viologen and a *trans*-azobenzene derivative, form the heteroternary 1:1:1 complex (**MV**$^{2+}$&*t***AB**)@CB[8]. The viologen acts again as the redox-active counterpart forming the 2:1 complex (**MV**$^{+\bullet}$)$_2$@CB[8] upon one-electron reduction which also results in the release of *t***AB** from the complex. Furthermore, photoisomerization of *t***AB** to its *cis*-isomer results in its ejection from the heteroternary 1:1:1 complex due to steric repulsion, yielding free *c***AB**, while the viologen stays encapsulated in the 1:1 complex **MV**$^{2+}$@CB[8]. Both processes, the reduction and the photoisomerization are fully reversible and independent of each other, enabling orthogonal control over the system.

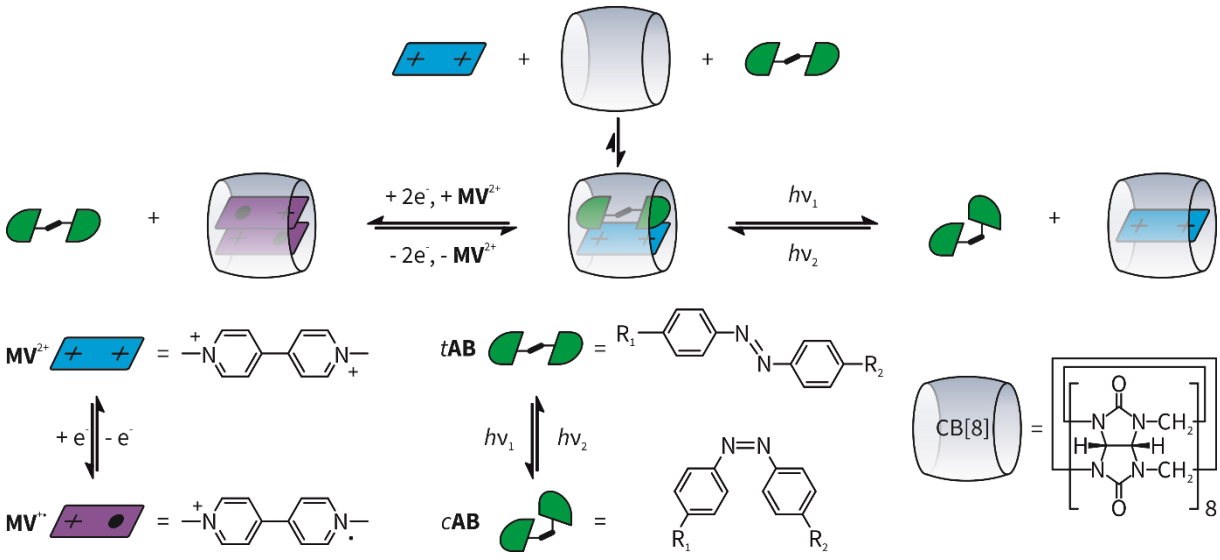

Figure 18. Orthogonal switching of a cucurbit[8]uril complex with redox and light stimuli.

Examples for molecular motors are still rare since the concept is significantly more difficult to realize than a simple molecular switch, as achieving directional movement on the molecular level is a major challenge. Therefore, one example will be presented to show the complexity and the fragility of such a molecular machine. LEIGH and coworkers reported on a rotary molecular motor based on a [2]catenane which is pH-responsive and driven by the addition of just one chemical fuel (Figure 19).[87] The catenane **R**H$^+$ consists of a crown ether (red) that is interlocked with a large macrocycle incorporating an ammonium (blue) and a triazolium (orange) binding station. Furthermore, a gating system of sterically demanding stopper groups ensures directional movement. The disulfide stopper (pink) is base-labile, whereas the hydrazone stopper (green) is acid-labile. If **R**H$^+$ is exposed to basic conditions, the ammonium group is deprotonated making the triazolium group the thermodynamically preferred binding site. Since the hydrazone group is inert under basic conditions, it blocks the movement of the crown ether. The base-labile disulfide group, however, reversibly exchanges with disulfide in bulk solution allowing the macrocycle to pass to the second binding station. Consequently, the transition from compound **R**H$^+$ to **R** was reached by the directional movement in a clock-wise fashion regarding the presentation of the larger ring in Figure 19. When the system is acidified in a second step, the diammonium station is recovered. As the disulfide stopper is locked under these condition, the macrocycle cannot pass. In contrast, the hydrazone stopper undergoes exchange with excess hydrazone in solution *via* a transient aldehyde, thereby allowing the passage of the crownether. Clock-wise directional movement regarding the presentation of the larger ring in Figure 19 leads to compound **R**H$^+$. Overall, a whole 360° directional rotation was achieved by addition of base and subsequently acid. But the system can perform a full rotation by just one additive. If the starting medium is Et_3N in $CHCl_3$ and trichloroacetic acid is added, so the first 180° movement takes place. The triethylamine catalyzes the decarboxylation of the trichloroacetic acid to CO_2 and $CHCl_3$ and the reaction mixture becomes basic promoting the second 180° rotation (see inlet). This means one addition of acid drives a full 360° rotation. Therefore, the whole system is driven by only one chemical fuel, trichloroacetic acid.

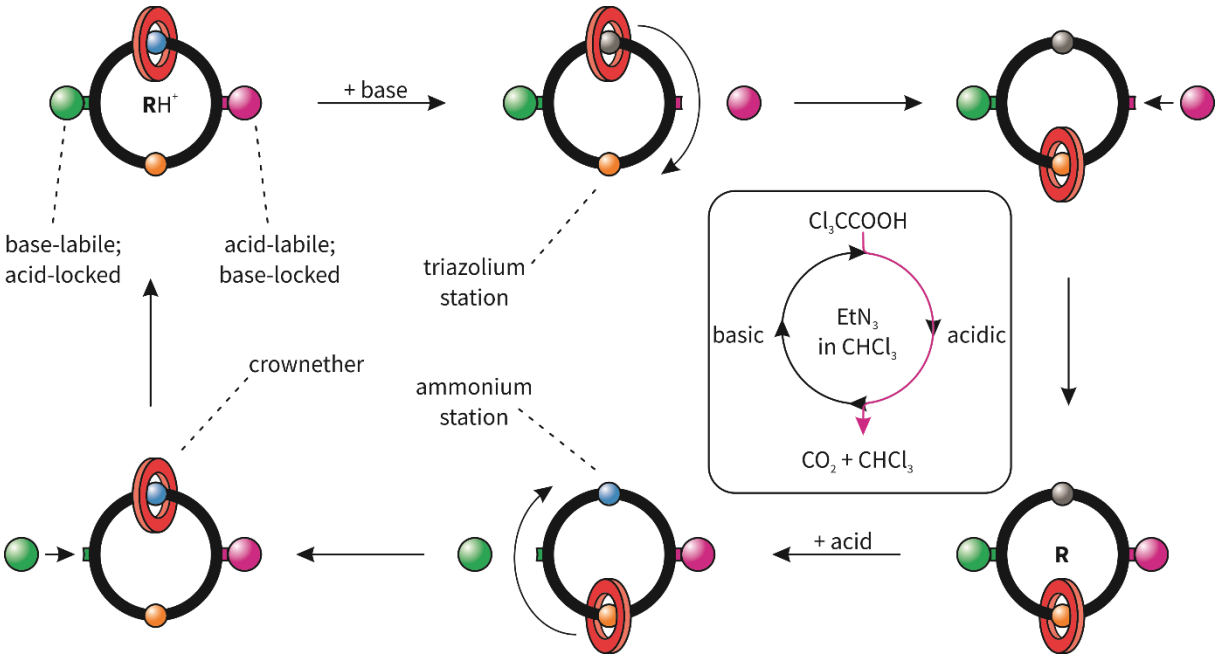

Figure 19. A rotary molecular motor fueled by trichloroacetic acid based on a circular track with two binding stations and a gating system consisting of two locks and the change between acidic and basic conditions by addition of just one chemical fuel (inlet).

3.3 Fluorescence in Supramolecular Complexes

The standard model of fluorescence is described as a three-step mechanism. First, the excitation of an electron from the ground state (GS) to the exited state (ES), second, a non-radiative relaxation to the lowest vibrational level of the ES and a subsequent emission of a photon (Figure 20a). If an energy transfer from a donor group (D) to an acceptor group (A) is involved in a fluorescence mechanism, the structural architecture of a fluorophore plays an important role and will be discussed in detail in Chapter 3.3.2. The whole process can be simplified to the following pathway after excitation: $GS_D \rightarrow ES_D \rightarrow ES_A \rightarrow GS_A$ (b). This energy transfer can result in emission of the acceptor fluorescence or in quenching of the emission.

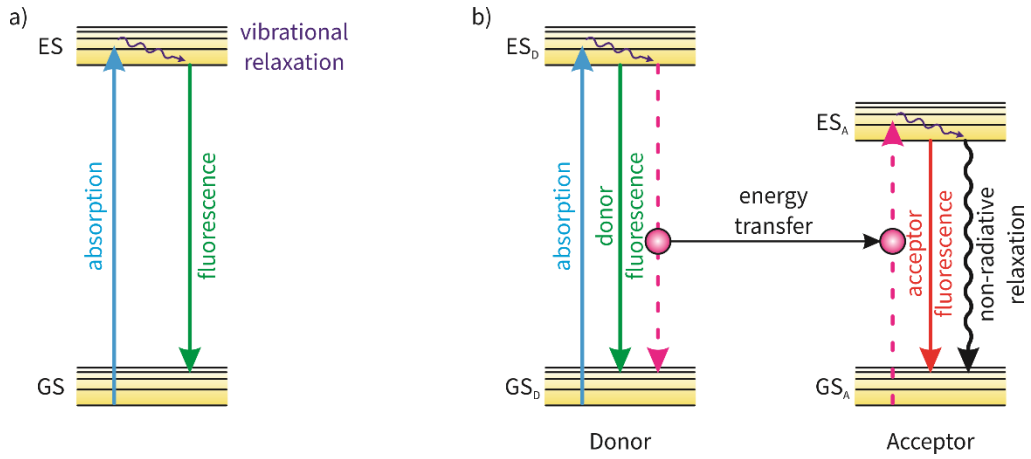

Figure 20. Jabłoński diagrams of (a) the standard model of fluorescence emission after absorption and of (b) a general energy transfer donor–acceptor system; GS = ground state, ES = excited state, GS_D = ground state donor, GS_A = ground state acceptor, ES_D = exited state donor, ES_A = excited state acceptor.

These photophysical processes have usually been studied in highly dilute solutions, to avoid intermolecular interactions between fluorophores. These studies in dilute solutions made a great contribution to the fundamental understanding of luminescence processes at the molecular level, but do not necessarily reflect the interactions and events in concentrated solutions. At higher concentrations, quenching of the luminescence can occur, for example, due to *aggregation-caused quenching* (ACQ).[88] Exemplarily, the perylene derivative **DDPD** is highly luminescent in a dilute THF solution. However, upon addition of water the emission is drastically weakened (Figure 21). The extremely low solubility of **DDPD** in water leads to an increase of the local luminophore concentration and causes aggregation. The aggregates exhibit π-π stacking interactions of the perylene cores, which results in excimer formation. Hence, quenching of the emission occurs.[89] The ACQ effect created various problems in the development of luminescent materials and has furthermore limited the scope for applications of dyes.

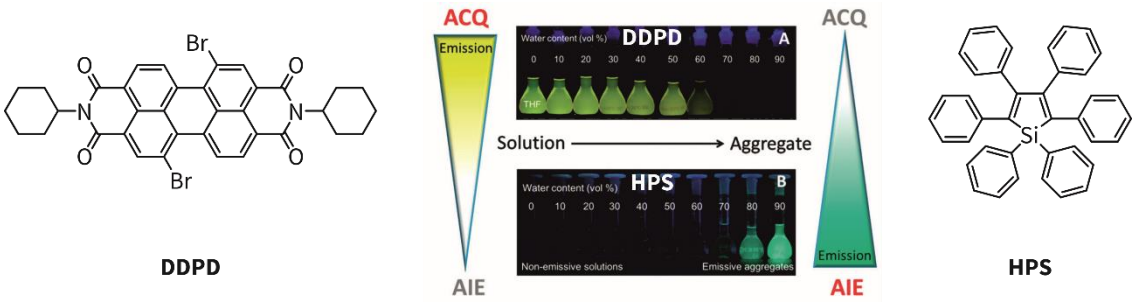

Figure 21. Chemical structures of the chromophores **DDPD** and **HPS** and photographs of solutions/suspensions of the dyes in THF–water mixtures with different water contents. Adapted with permission from reference[90]. Copyright (2014) The Royal Society of Chemistry.

3.3.1 Aggregation-Induced Emission

In 2001, TANG and coworkers observed an interesting phenomenon while working with the silole compound 1-methyl-1,2,3,4,5-pentaphenylsilole.[91] A drop of the compound dissolved in a solvent on a TLC plate was hardly visible under UV light when it was still wet. But after evaporation of the solvent, the dried spot was clearly visible upon irradiation. It was shown that the luminescence enhancement upon aggregation in concentrated solutions or cast into solid films is not limited to this one example.[92] The underlying process was termed *aggregation-induced emission* (AIE).[91] In the proposed mechanism, the *restriction of intramolecular motion* (RIM) is the crucial factor for the fluorescence in the aggregated state. RIM includes *restriction of intramolecular rotation* (RIR) and the *restriction of intramolecular vibrations* (RIV). In the RIV case, the term vibrations unites bending, twisting, flapping, scissoring, etc. This definition of RIM might be broad, but the distinction between RIR and RIV is crucial for the understanding of AIE.[93]

The archetypal AIE luminogen (AIEgen) hexaphenylsilole **HPS** is a propeller shaped non-planar molecule and in dilute solutions the phenyl rotors undergo dynamic rotations (Figure 21). This annihilates the excited states in a non-radiative way and renders the molecule non-luminescent. Upon aggregation, the molecule cannot pack through a π-π stacking process due to the propeller shape and minor intermolecular electronic communication is possible. However, the intramolecular rotation of the aryl moieties is restricted because of the sterically demanding size of the rotors. This RIM effect blocks the non-radiative pathway and opens the radiative channel making compound **HPS** emissive in the aggregate state.[89]

Besides **HPS** derivatives, a great number of other AIEgens with interesting structural features like hydrocarbons,[94] heterocycles,[95] polymers[96] and organometallic compounds[97] were investigated. Linear polyene derivates have a rich structural variety and are synthetically more accessible than **HPS** derivatives.[90] As a simple model system 1,4-distyrylbenzene (**DSB**) was studied in depth (Figure 22). Compound **DSB** is an ACQ luminophore in the *trans* form with strong fluorescence emission in solution and weak emission in the aggregated state. But if the α-olefinic hydrogen atoms

are replaced with methyl groups forming **PPB**, the compound exhibits AIE behavior.[94a] The crystal structures show two very different packing modes. Compound **DSB** packs in a flat conformation of the molecules and allows π-π stacking interactions. This leads to an intermolecular charge transfer and weakens the emission of the aggregate. The methyl groups of **PPB** hinder a packing in this way and a non-planar conformation is adopted. The resulting twisted geometry weakens the intermolecular interaction and prevents a charge transfer.

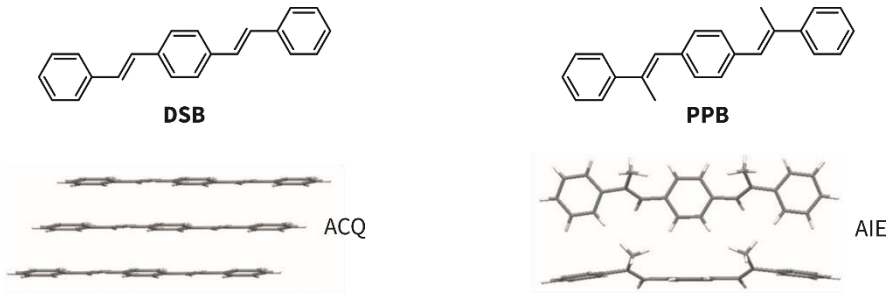

Figure 22. Structure and packing in the solid state of **DSB** and **PPB**. Adapted with permission from reference[89]. Copyright (2011) The Royal Society of Chemistry.

The RIM effect is not only achieved in aggregates or crystals but can be imitated by integrating an AIEgen in a highly ordered macromolecular structure. ZHOU and coworkers reported on a tetraphenylethylene-based zirconium metal-organic framework (MOF) that exhibits a deep-blue fluorescent emission with a strong increase in quantum yield (Figure 23).[98] The metal knots of the MOF are zirconium (IV) clusters. The organic linker monomer (**M**) consists of a fourfold tetraphenylethylene (TPE) core substituted with benzoic acid moieties as coordination sites. TPE is known to be a good AIEgen (purple marked in the structure).[99] Compound **M** displays a bright yellow fluorescence (ϕ = 30%) in the solid state. After MOF formation, however, the strong coordination with the zirconium cluster prevents the free rotation of the aromatic moieties in **M** and enhances the emission drastically. The emission maximum wavelength is blue shifted compared to **M**. The less planar conformation of the monomer units in the MOF compared to free **M** widens the HOMO and LUMO gap, which results in the observed blue shift.

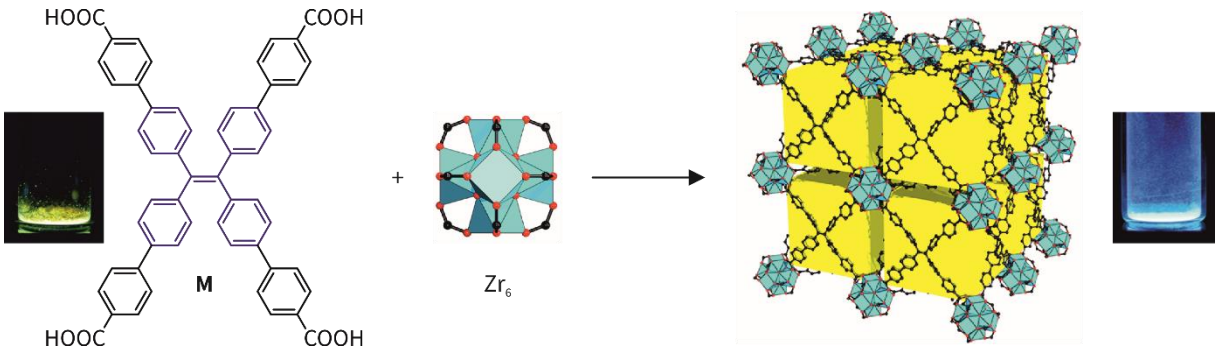

Figure 23. Rigidifying of the TPE based linker **M** by MOF formation with a Zr_6 cluster. Adapted with permission Zhangwen Wei, Zhi-Yuan Gu, Ravi K. Arvapally, Ying-Pin Chen, Roy N. McDougald, Jr., Joshua F. Ivy, Andrey A. Yakovenko, Dawei Feng, Mohammad A. Omary, and Hong-Cai Zhou, *J. Am. Chem. Soc.* **2014**, *136*, 8269–8276. Copyright (2014) American Chemical Society.

3.3.2 Twisted Intramolecular Charge Transfer

A commonly occurring energy transfer process is the *Förster Resonance Energy Transfer* (FRET). In this case, a non-radiative energy transfer from an excited state donor to an acceptor takes place *via* Coulomb interaction. As a consequence, the D–A distance can reach up to 10 nm and is only depending on the relative orientation of the donor emission and acceptor absorption dipole moment (Figure 24a). The *Dexter Energy Transfer* (DET), or Dexter Electron Transfer, features the bilaterally exchange process of electrons of two molecules (intermolecular) or two parts of the same molecule (intramolecular).[100] The D–A distance is limited to < 1 nm and an orbital overlap between the donor and the acceptor is required (b). Since an electron movement takes place, this process is a charge transfer, which includes the formation of short-lived homodimers (excimer) or heterodimers (exciplex) upon excitation. This intermolecular interaction takes places *via* electrostatic attraction. Excimer formation is usually accompanied by a red-shift of the emission wavelength because ES_A is energetically lower than the ES_D. Exciplex formation generally causes quenching of the fluorescence.[101]

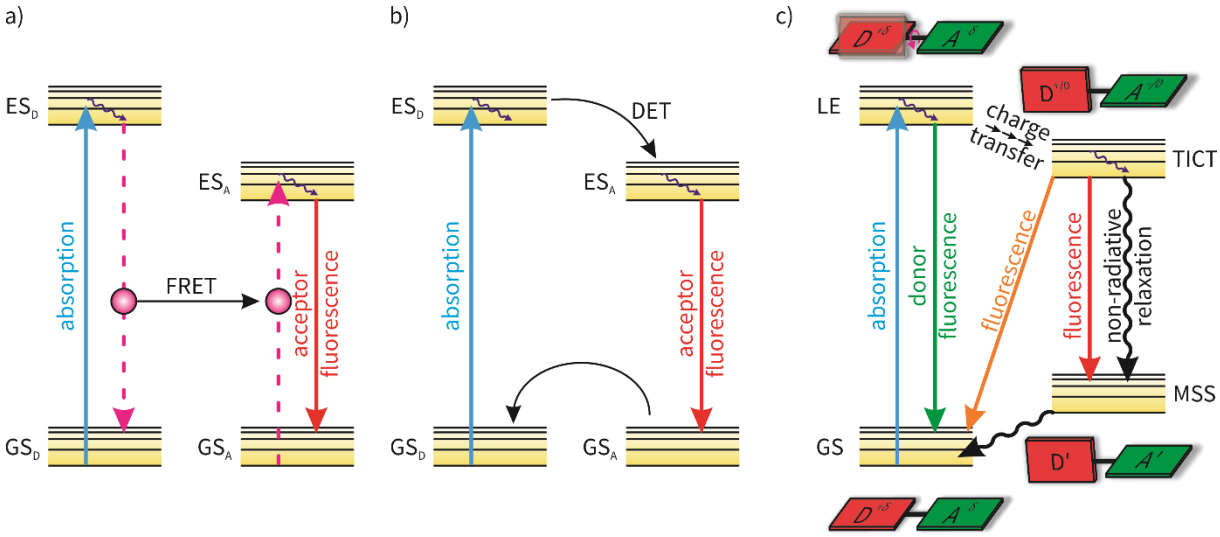

Figure 24. Jabłoński diagrams of (a) the Förster Resonance Energy Transfer (FRET), (b) the Dexter Energy Transfer (DET) and (c) the Twisted Intramolecular Charge Transfer (TICT) dynamics; GS_D = ground state donor, GS_A = ground state acceptor, ES_D = exited state donor, ES_A = excited state acceptor, GS = ground state, LE = locally excited state, MSS = metastable state.

If a donor and a acceptor group are linked by a rotatable bond within one individual molecule, the fluorescence can be influenced by a *Twisted Intramolecular Charge Transfer* (TICT).[102] In the ground state, the planar conformation of the molecule is energetically favored. After excitation to the locally excited state (LE), the donor transfers its excited electron to the acceptor and subsequent intramolecular D-A twisting around the single bond takes place to enable intramolecular charge separation resulting in the TICT state (Figure 24c).[103] Relaxation of the TICT state produces a relaxed perpendicular conformer in the metastable state (MSS), which undergoes a non-radiative relaxation to the GS. It is important to understand, that the TICT mechanism – just like the other charge transfer

phenomena – can quench or enhance the fluorescence emission of a chromophore. In some cases, the LE and the TICT state can coexist and relaxation can exhibit two fluorescence emissions.

The equilibrium in the excited state between the LE and TICT conformations can be compared to other conformational insomerisms. Hence, internal and external factors which alter the stability of the isomers can influence the thermodynamic equilibrium. The nature of the substituents has an extensive effect on the rotation dynamics of the D-A connecting single bond.[104] The rate of TICT formation is depending on the ground state twist angle.[105] Polar solvents provide stabilization of the TICT state and since the polarity of a solvent increases when the temperature is lowered, the activation barrier of the TICT state decreases with lowering the temperature.[106] Viscous solvents on the other hand increase the energy barrier between the LE and the TICT state and the LE emission is favored.[107]

The biphenyl derivatives **B1** and **B2** theoretically fulfil the requirements for a TICT mechanism (Figure 25).[108] Both consist of a push-pull system with a donor group (amine) and an acceptor group (aldehyde). The phenyl rings are connected by a single C-C bond. Furthermore, torsional restrictions were introduced to hinder the rotation around this bond, methyl groups for **B1** and a bridged structure for **B2**. Both compounds exhibit fluorescence emission in apolar solvents. Polar solvents stabilize the charge separation ($D^+ - A^-$) after the energy transfer and quench the emission of **B1** since the TICT mechanism occurs (a). In contrast, **B2** retains its fluorescence due to the prevention of the rotation around the single bond (b).

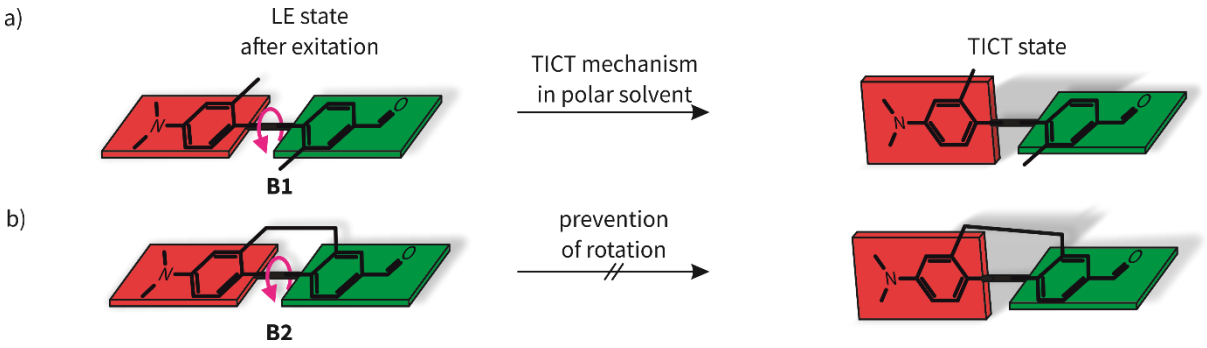

Figure 25. (a) Formation of the TICT state of **B1** after excitation to the LE state and (b) prevention of the formation of the TICT state of **B2** after excitation to the LE state due to covalent modifications.

The prevention of a TICT mechanism by conformational changes of a fluorophore upon complexation was reported on by NAKAMURA and coworkers (Figure 26).[109] Compound **C** consists of two anthracenecarboxamide moieties that are connected *via* a short glycol chain. In solution, the fluorescence is quenched because of the formation of a TICT state upon rotation (indicated by pink arrows). The rotations around the anthracene-CO, the OC-NH and the N-C (benzene) bonds of the chromophore at the locally excited state are possible. Upon complexation of a metal ion, however,

the rotation of the large anthracene moiety is sterically hindered and the TICT state is unfavored opening the radiative decay channel, resulting in an increase of the fluorescence intensity.

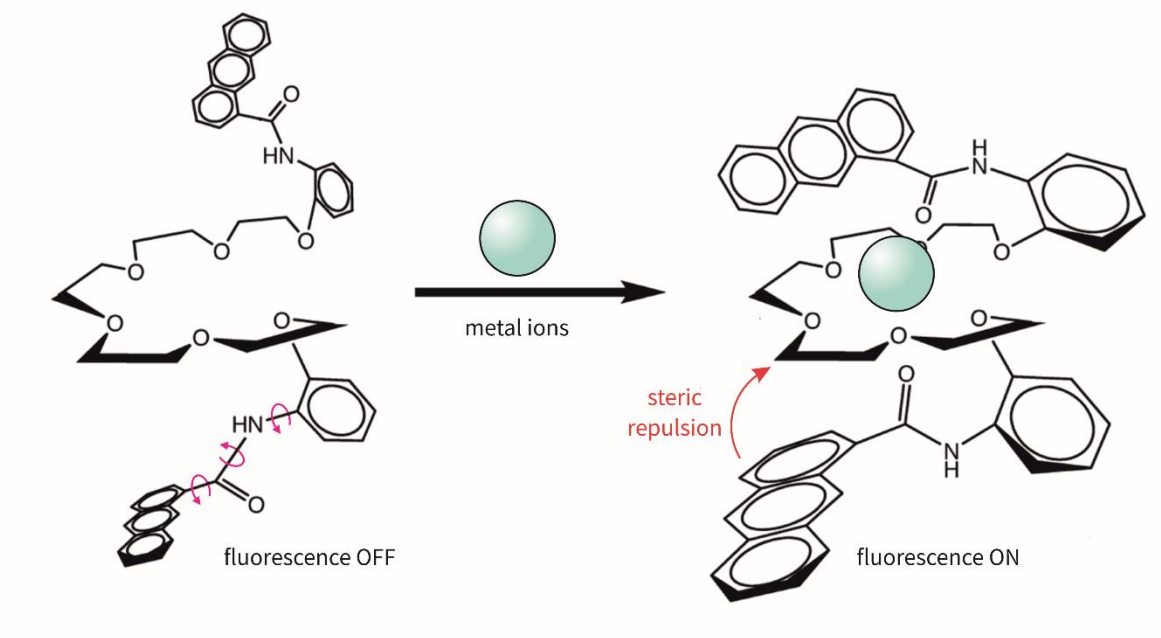

Figure 26. Prevention of the TICT mechanism by hindering of the rotation due to steric repulsion after complex formation. Adapted with permission from reference[109]. Copyright (2009) Japan Society for Analytical Chemistry.

3.3.3 AIE vs TICT

The concepts and mechanisms of the AIE and the TICT mechanisms seem to be the opposite of each other, because the AIE effect and the TICT mechanism are both depending on intramolecular rotations. Therefore, one could think that fluorophores which exhibit quenching in solution due to the formation of a TICT state are fluorescent in the aggregated form due to AIE effect. This led to controversial discussions, but TANG and others try to defend the uniqueness of the AIE phenomenon, by arguing that simply restriction of intramolecular motion (RIR) as explanation for AIE would be to general and insufficient.[99c]

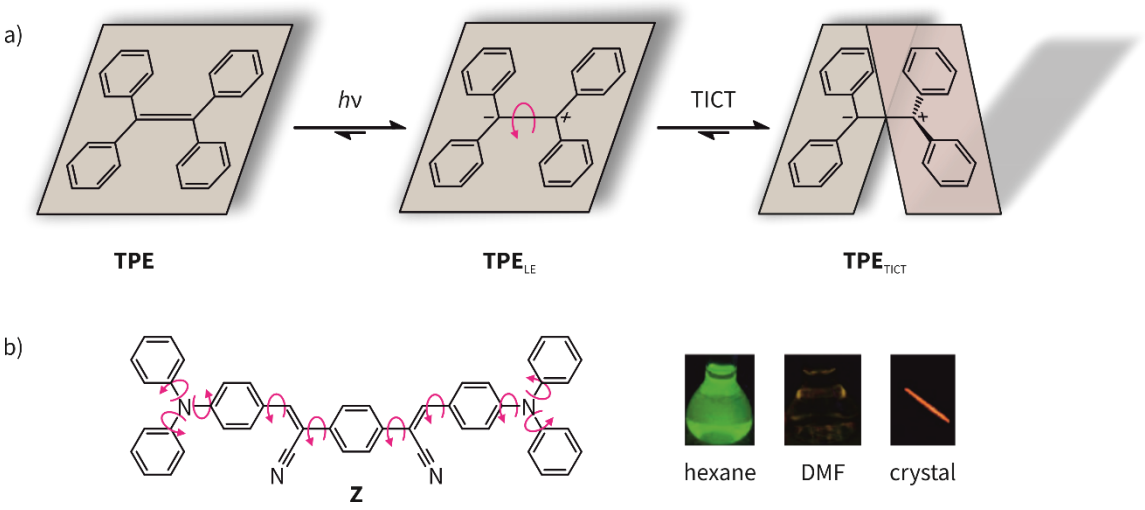

Figure 27. (a) Representation of the TICT mechanism of the AIEgen **TPE** upon excitation and charge transfer in solution and (b) structure of fluorophore **Z** and photographs of its solutions in apolar hexane, polar DMF and a photograph of the crystal under irradiation. Reprinted and adapted with permission from Yan *et al*.[110] (© 2018 Elsevier Inc.).

The simple AIEgen **TPE**, which was shortly discussed before as linker of a MOF, can be described with both concepts (Figure 27a).[99a, 111] In solution, the molecule is non-planar with propeller like phenyl rings as it is often found for AIEgens. After excitation and charge transfer, the LE state corresponds to the zwitterion **TPE**$_{LE}$ which immediately relaxes to the TICT state **TPE**$_{TICT}$. Afterwards, it undergoes a non-radiative decay and, thus, the fluorescence is quenched in solution. If aggregated, the transition to the TICT state and intramolecular rotation of the phenyl rings is restricted because of the confined space. The non-radiative relaxation channel is blocked opening the radiative decay pathway. As a consequence, it is emissive when aggregated.

The more complex fluorophore **Z** consists of two pairs of D–A units (Figure 27b). In solution, the TICT mechanism is easy to explain by the rotation around the single bonds and can be seen with naked eye by studying the solutions. In the apolar solvent hexane, the planar conformation is stabilized, and fluorescence is derived from the LE state. The polar solvent DMF exhibits a redshift and broadening of the emission maximum, which is ascribed to the formation of the TICT state. The crystals of **Z** emit an intense orange-red light with high quantum yield, which clearly reveals its AIE activity.[112] If the AIE effect in the solid state is just attributed to the prevention of the formation of the TICT state, the large shift of the emission wavelength and the great enhancement in quantum yield cannot be fully explained.[110] This means that there has to be more than just the restriction of the TICT mechanism. Other examples show that not every TICT dye is an AIEgen.[113] Besides restriction of rotation (RIR), other RIM processes play an important role in AIE systems.

According to TANG, this makes the AIE phenomenon unique. In consequence it can be stated that different enhancement systems – like TICT, DET and AIE – can partially overlap in their effects, but it is the RIM process alone that is relevant for the AIE activity of molecules.[114]

3.3.4 Changes of Fluorescence Properties by Encapsulation

Host–guest chemistry can be used to change the emission properties of fluorophores by different kinds of interactions. SCHERMAN and coworkers reported on a supramolecular approach for the use of dyes in water by preventing self-aggregation upon encapsulation (Figure 28).[115] The perylene bis(diimide) dye **PDI** is a strong fluorophore in organic solvents, but tends to form aggregates in water and thus, ACQ occurs. CB[8] can complex the fluorophore, and indeed, the addition of the host to a solution of **PDI** results in an increase of the emission intensity since the chromophore is deaggregated and monomerized during the encapsulation process. The host–guest approach to protect the dye from self-aggregation is much more convenient than cumbersome synthetic modifications of the chromophore. In addition, the fluorescence can be switched off by addition of a competitive binder or by addition of a second guest forming a π–donor–acceptor complex inside the cavity of the CB[8].

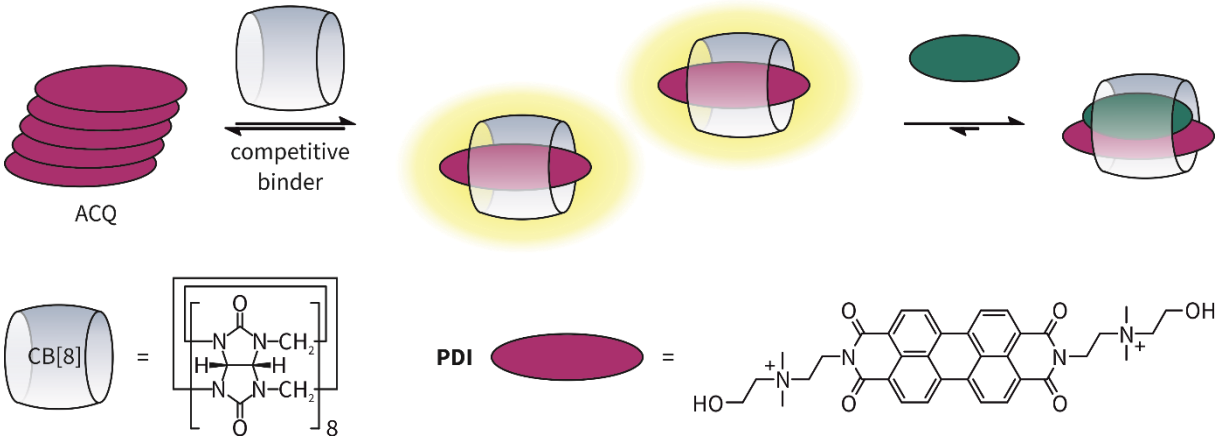

Figure 28. Deaggregation and monomerization of a **PDI** chromophore upon complexation with cucurbit[8]uril.

The idea of preventing ACQ by encapsulating a chromophore was extended by TANG and coworkers by combining a fluorescent guest with a fluorescent host in water (Figure 29).[116] The amphiphilic **TPP-cage** consists of two tetraphenylpyrazine (TPP) molecules which are connected *via* four covalent links. The starting material **TPP-4OH** exhibits AIE behavior. It is non-emissive in solution due to free rotation of the four phenyl rings. After immobilization of the propeller-like structure by covalent modification, the cage features a distinct blue emission after irradiation due to RIM. The cavity of the **TPP-cage** is hydrophobic and can encapsulate the **DPP**. This prevents aggregation of the fluorophore enabling its yellow emission. Since yellow and blue are complementary, the complex **DPP**@**TPP-cage** exhibits white light.

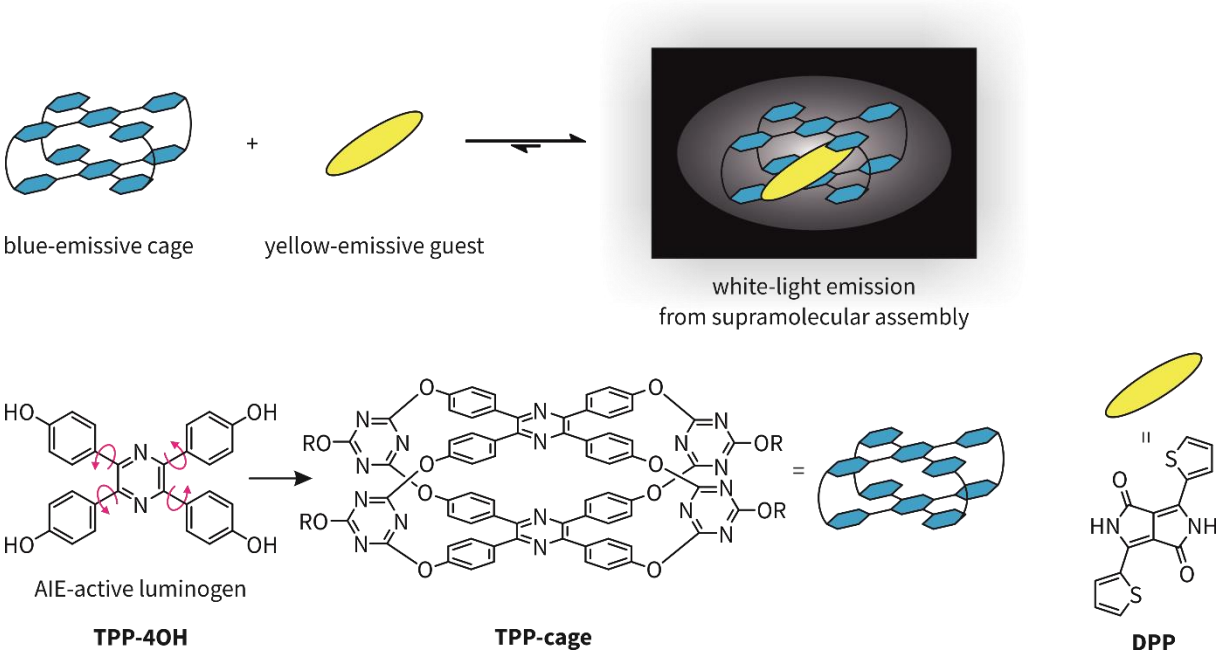

Figure 29. White-light emission from a supramolecular assembly by encapsulation of a yellow-emissive guest in a blue-emissive host

The encapsulation of a guest inside a host cannot only enhance fluorescence properties by prevention of ACQ but also by restriction of intramolecular dynamics of the guest molecule. GALOPPINI and coworkers reported on a fluorescence enhancement upon the encapsulation of a weakly emissive viologen derivative in CB[7] (Figure 30).[117] Compound **DTV**$^{2+}$ is well soluble in aqueous solutions and exhibits a low fluorescence quantum yield (ϕ = 0.01). DFT calculations show that the molecule is twisted in the excited state which hints to the formation of a TICT state. Addition of two equivalents of CB[7] furnishes the complex **DTV**$^{2+}$@CB[7]$_2$, which features a blue shift of the emission wavelength and an increase in quantum yield by a one order of magnitude (ϕ = 0.12). This effect can be contributed to the hindrance of the rotational relaxation of the guest, blocking the TICT mechanism, caused by the encapsulation within the cavity of the host. Since viscose media, like the polymethylmethacrylate polymer (PMMA), prevent the rotation and consequentially the formation of a TICT state, **DTV**$^{2+}$ was mixed with PMMA and spin-coated. The polymer blend exhibits a blue-shifted emission maximum like the complex **DTV**$^{2+}$@CB[7]$_2$.

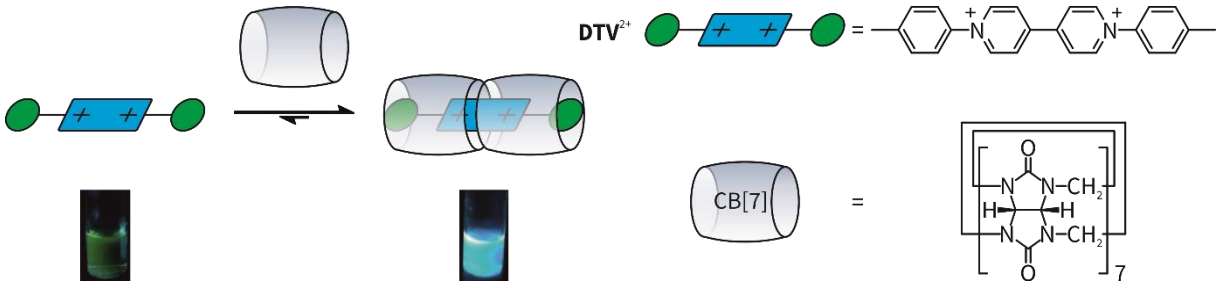

Figure 30. Schematic representation of the encapsulation of **DTV**$^{2+}$ in cucurbit[7]uril and photographs of the aqueous solutions upon irradiation. Adapted with permission from Marina Freitag, Lars Gundlach, Piotr Piotrowiak, and Elena Galoppini, *J. Am. Chem. Soc.* **2012**, *134*, 3358–3366. Copyright (2012) American Chemical Society.

TAO and coworkers reported on a supramolecular approach to a fabricate tunable aqueous solution based on a CB[8] supramolecular polymer (Figure 31). Compound **G1** is well soluble in water and exhibits a blue fluorescence emission. The special feature of **G1** is the presence of two binding sites for CB[8]. Addition of 0.5 equiv. of the host to a solution of the guest furnishes the 2:1 host–guest complex **G1**$_2$@CB[8] with excimer formation inside the cavity of the CB[8]. The formed complex has a bright yellow emission. The carboxylic acid end group of **G1** can act as a second binding site and, thus, addition of an excess of host results in formation of supramolecular polymer SP-**G1**@CB[8] with a green fluorescence. In consequence, the emission color can be tuned by the amount of added CB[8] to a solution of **G1**; e.g. addition of 0.2 equiv. leads to the yellow emission of the complex and the blue emission of free **G1**. Since these colors are complementary, white light emission is achieved. This is in particular special, because the white light emission is realized with just one fluorophore and complements other works that require a mixture of two or more independent color components (see the example above).

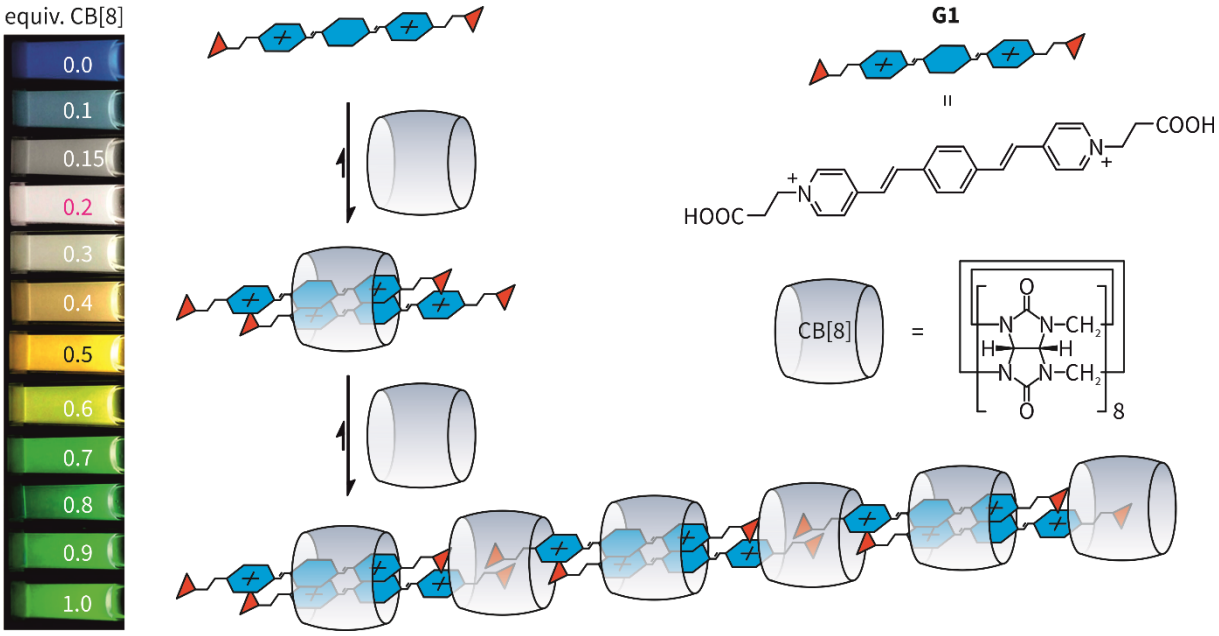

Figure 31. Complex formation of **G1** upon addition of cucurbit[8]uril and photographs of aqueous solutions of **G1** with different amounts of host. Adapted with permission from Xin-Long Ni, Shiyan Chen, Yaping Yang, and Zhu Tao, *J. Am. Chem. Soc.* **2016**, *138*, 6177–6183. Copyright (2016) American Chemical Society.

The emission characteristics of host–guest systems can surpass the ones of single dyes. Not only is the deaggregation by complexation possible, but one supramolecular complex can incorporate the emission properties of two fluorophores. Furthermore, a tuning of the emission of one single dye is possible by addition of different stoichiometries of host. Therefore, host–guest chemistry enhances the field of fluorescence and potentially allows for new applications.

4 Results

4.1 Strong Emission Enhancement in pH-Responsive 2:2 Cucurbit[8]uril Complexes

As a novel guest design, an electron-poor bipyridinium unit and an electron-rich bipyridine unit were linked with each other by just one single bond. This leads to a rigid molecule with a conjugated π-system, creating an intramolecular donor-acceptor system. The resulting series of structurally simple, yet versatile bipyridinium luminophores **2**$^{+}$-**7**$^{+}$ and their supramolecular complexation with cyclodextrins (CDs) and cucurbit[*n*]urils (CB[*n*]s) in aqueous solution is studied (Figure 32).

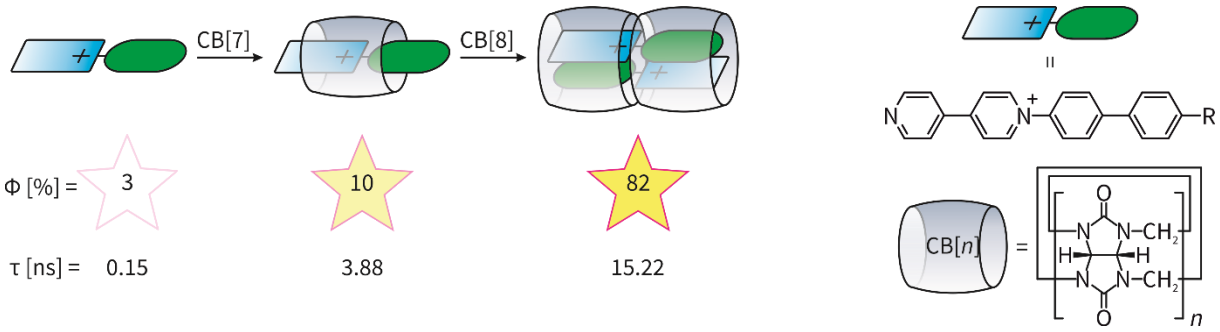

Figure 32. Complexation and emission enhancement of a TICT fluorophore upon addition of macrocyclic hosts CB[7] and CB[8] with exemplary quantum yields and fluorescence decays of compound **2**$^{+}$.

Three approaches for tuning the fluorescence properties of these luminophores were investigated: (i) the covalent modification of the guest, (ii) the complexation with host molecules, and (iii) the (de)protonation of the luminophores and their complexes. It was found that the reversible (de)protonation of the luminophore changes the photophysical properties. In addition, complexation with β-CD, CB[7] and CB[8] has an drastic influence on the emission characteristics. The two tuning parameters (change of pH and host–guest complexation) of the stimuli-responsive system can be combined and are orthogonal to each other.

4.1.1 Synthesis of Bipyridinium Dyes

The water-soluble bipyridinium compounds **2**$^{+}$–**7**$^{+}$ were synthesized in three steps from 4,4'-bipyridine (Scheme 1). First, the Zincke salt **SI1**$^{+}$ is prepared from commercially available 4,4'-bipyridine and 1-chloro-2,4-dinitrobenzene. Zincke reaction of **SI1**$^{+}$ and 4-iodoaniline furnished compound **1**$^{+}$. In the third step, different substituents were introduced by Suzuki reaction of **1**$^{+}$ and the corresponding phenylboronic acids. The products were purified by simple filtration. In addition, **2**$^{+}$ was reacted to the viologen derivative by refluxing with ethyl iodide in DMF, yielding 96% of **8**$^{2+}$.

The chloride salts of $\mathbf{2}^{+}$–$\mathbf{7}^{+}$ and $\mathbf{8}^{2+}$ are yellow powders, soluble in protic, polar solvents and thermally stable (M.P. > 240 °C). Anion exchange was used to obtain the compounds with different counterions which makes the salts soluble in organic solvents.

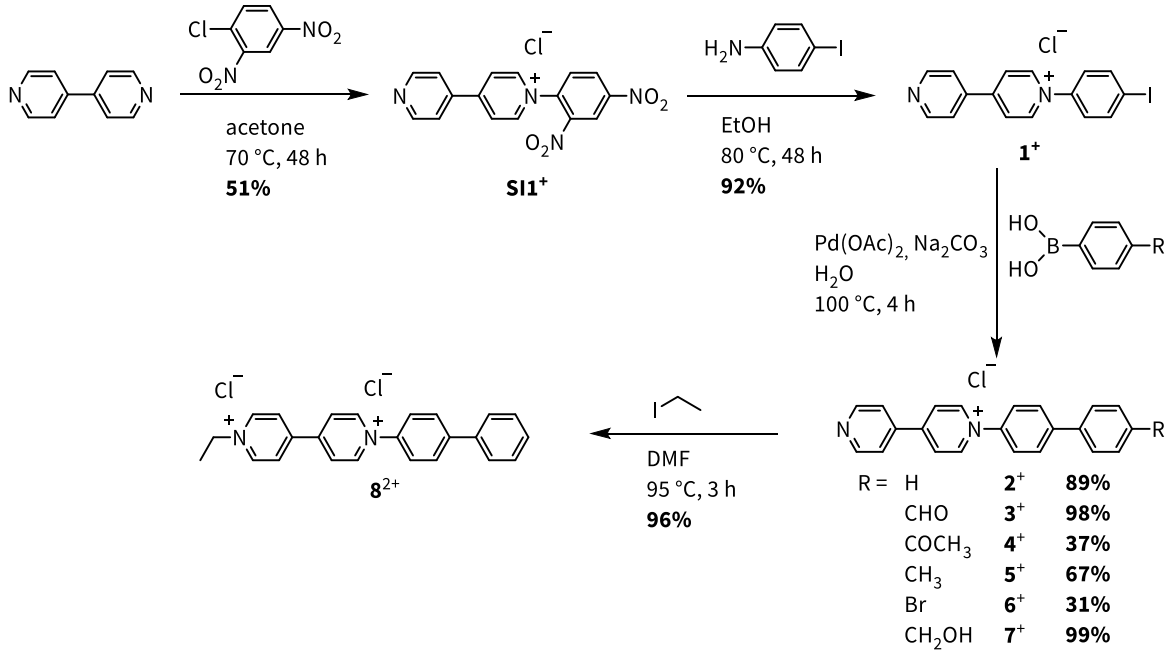

Scheme 1. Synthesis of bipyridinium derivatives $\mathbf{2}^{+}$–$\mathbf{7}^{+}$ and $\mathbf{8}^{2+}$.

4.1.2 Photophysical Properties of the Bipyridinium Dyes

Bipyridinium dyes $\mathbf{2}^{+}$–$\mathbf{7}^{+}$ are fluorophores and the UV/Vis spectra, photographs of the solution upon excitation and photoluminescence (PL) spectra are shown in Figure 33. The photophysical and electrochemical parameters of $\mathbf{2}^{+}$–$\mathbf{7}^{+}$ in solution are summarized in Table 3. The emission wavelengths of the dyes range from 497 nm for $\mathbf{7}^{+}$ to 638 nm for the bromo-substituted $\mathbf{6}^{+}$. The protonated compounds $\mathbf{2}H^{2+}$–$\mathbf{7}H^{2+}$ and compound $\mathbf{8}^{2+}$ display virtually no emission in solution.

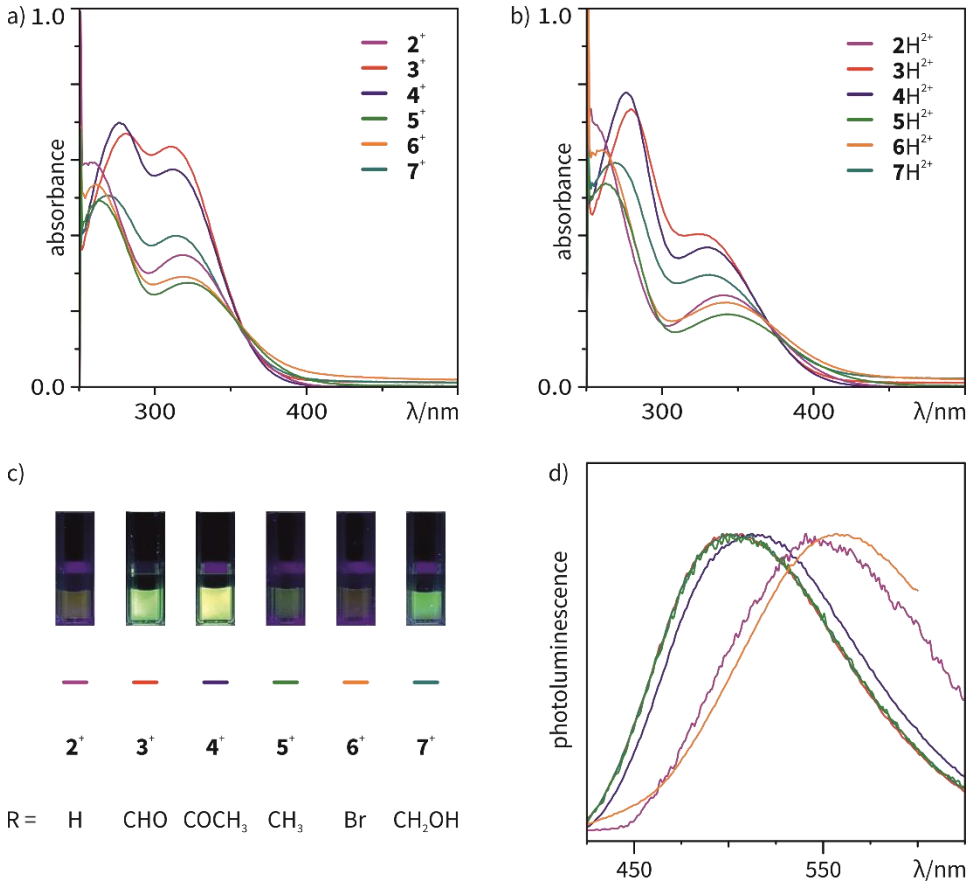

Figure 33. UV/Vis absorption spectra of (a) **2**$^{+}$–**7**$^{+}$ (pH = 10) and (b) **2**H^{2+}–**7**H^{2+} (pH = 4), (c) photographs of aqueous solutions of **2**$^{+}$–**7**$^{+}$ under irradiation of light (λ_{ex} = 366 nm) and (d) normalized PL spectra ($\lambda_{ex} = \lambda_{abs}$) (c = 0.06 mM).

Table 3. Photophysical and electrochemical parameters of **2**$^{+}$–**7**$^{+}$ in aqueous solution.

	R =	λ_{abs} [nm]	λ_{em} [nm][a]	λ_s [10^3 cm^{-1}]	$\varepsilon^{1/2}$ [eV][b]	ε_{HOMO} [eV][c]	ε_{LUMO} [eV][b]	Φ [%][a]
2^{+}	H	318	541	13.0	-1.1	-6.9	-3.7	3
3^{+}	CHO	310	499	12.2	-1.1	-7.1	-3.7	26
4^{+}	$COCH_3$	313	513	12.4	-1.2	-7.0	-3.6	17
5^{+}	CH_3	321	501	11.1	-1.1	-6.9	-3.7	4
6^{+}	Br	318	638	15.8	-1.1	-6.9	-3.8	2
7^{+}	CH_2OH	314	497	11.7	-1.1	-7.0	-3.7	13

[a] $\lambda_{ex} = \lambda_{abs}$; [b] determined by cyclic voltammetry (see Figure 59 in the appendix of Chapter 4.1); [c] determined by On-set approximation.

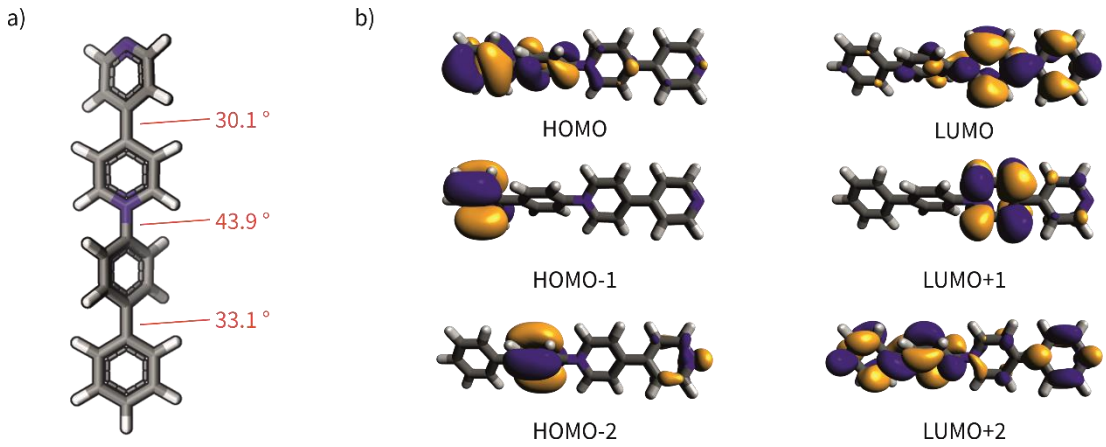

Figure 34. (a) Optimized structure of **2**$^+$ with dihedral angles and (b) selected orbitals of **2**$^+$.

All luminophores show low-energy absorption bands at wavelength between 310–321 nm. In accordance with TD DFT (time-dependent density functional theory) calculations, we attribute these bands to HOMO-LUMO transitions, where the HOMO orbital is centered on the biphenyl moiety and the LUMO on the bipyridyl unit as shown in Figure 34. The substitution has only a minor influence on the relative energies of the frontier orbitals and excitation energies ($\varepsilon^{1/2}$, ε_{HOMO} and ε_{LUMO}), but different substituents drastically affect the quantum yields (Table 3). Unsubstituted **2**$^+$ has a quantum yield of only 3% and the aldehyde substituted **3**$^+$ has a quantum yield of 26%. This is in line with a twisted intramolecular charge transfer (TICT) mechanism in which the locally excited (LE) state relaxes into the twisted intramolecular charge transfer state (TICT state).[102] The barriers for rotation of the aromatic rings around their aryl-aryl C-C and C-N bonds was determined to be smaller than 0.14 eV, which corresponds to 15 kJ·mol^{-1}, which makes a TICT equilibrium possible (Figure 35). This equilibrium partially closes the radiative decay channel of the luminophores and, thus, reduces the emission strength. Different substituents are known to stabilize either the LE or the TICT state,[103-104] and the strong quenching compared to **3**$^+$ demonstrates that the TICT mechanism is favored for **2**$^+$. The presence of a TICT state was further underpinned by TD DFT calculations as illustrated in Figure 36. The computational results are in good accordance with the experimental photophysical data.

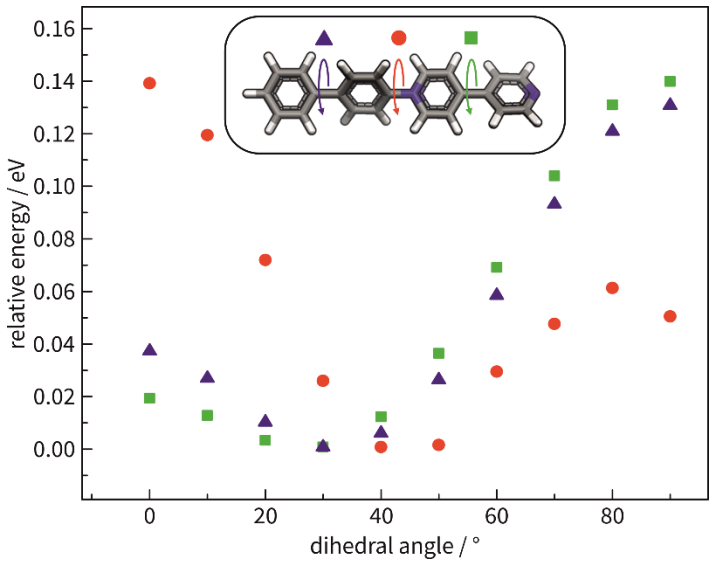

Figure 35. Result of relaxed potential energy surface scans of rotation around the aryl-aryl C-C and C-N bonds between the four aromatic rings of **2**$^+$.

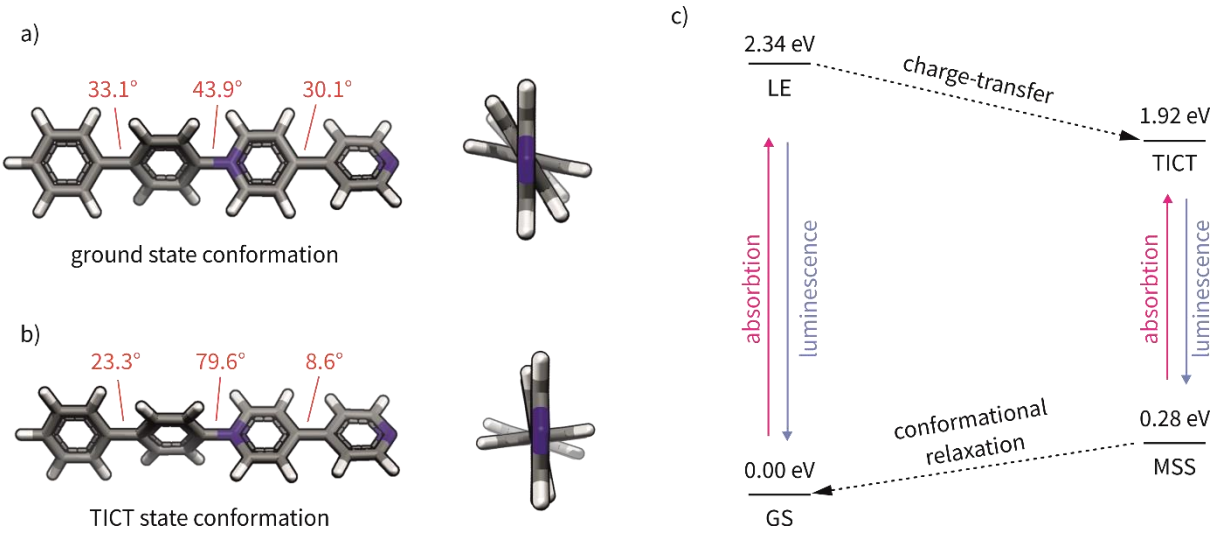

Figure 36. Results of TD DFT calculations and excited state geometry optimization of **2**$^+$: (a) Comparison between ground state and TICT state conformation and (b) schematic energy diagram for the TICT mechanism (GS = ground state, LE = locally enhanced state, TICT = twisted intramolecular charge transfer state, MSS = metastable state).

In order to investigate the TICT mechanism, fluorescence measurements were also conducted in viscose media, where the formation of the TICT state is hindered and, therefore, the opening of a radiative decay channel (LE→GS) takes place.[107] Compound **2**$^+$ in a polymethylmethacrylate (PMMA) polymer matrix (0.02 wt. %) exhibits an emission maximum at 470 nm, independent of the counterion (X^- = PF_6^- or ClO_4^-) (Figure 37a). This finding speaks in favor of the proposed prevention of the TICT state and supports the statement made above.

Compound **3**$^+$ was dissolved in a 1:99 mixture of H_2O and dioxane. The apolar dioxane induces aggregation of the dye. The solution is still fluorescent and, therefore, no aggregation-caused

quenching (ACQ) takes place (b). Hence, the dyes exhibit aggregation-induced emission (AIE) properties.

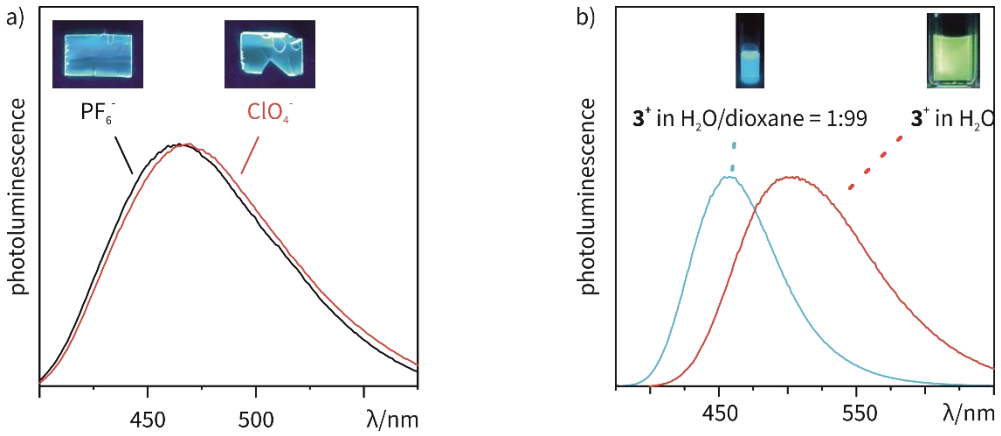

Figure 37. Normalized PL spectra and photographs (inlets) of (a) **2**$^+$ with PF_6^- and ClO_4^- as anions in a polymethylmethacrylate (PMMA) matrix (0.02 wt. %) (λ_{ex} = 366 nm) and (b) **3**$^+$ in a 99:1 mixture of dioxane and H_2O (blue) compared to **3**$^+$ in H_2O (red) (c = 0.06 mM, $\lambda_{ex} = \lambda_{abs}$).

4.1.3 AIE Behavior of Bipyridinium Dyes

Compounds **2**$^+$–**7**$^+$, as well as salts of **2**$^+$ with counterions other than chloride exhibit solid-state luminescence (Figure 38). There are at least three main factors influencing the AIE phenomenon in this system. (i) The restriction of intramolecular motion (RIM), (ii) intermolecular π-π-interactions and (iii) interactions of the fluorophore with the counterion.

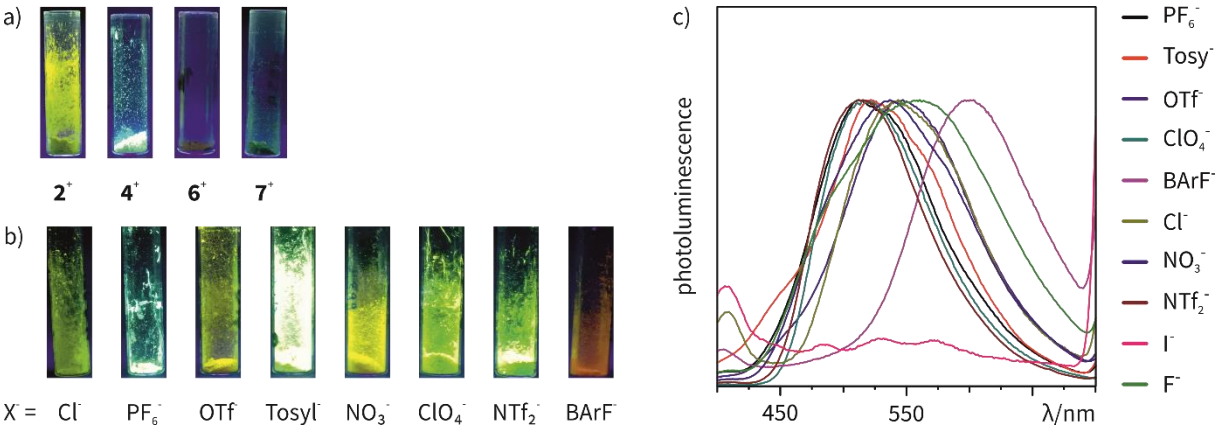

Figure 38. (a) Photographs of **2**$^+$, **4**$^+$, **6**$^+$ and **7**$^+$ with Cl^- counterion and (b) of **2**$^+$ with the denotated anions (λ_{ex} = 366 nm) and (c) normalized PL spectra of suspensions of **2**$^+$ salts with different counterions in hexane (λ_{ex} = 366 nm).

Since the presented system follows a TICT mechanism, the RIM effect must play a prominent role in the solid state as well. It is interesting that no quenching by π-stacking takes place as in the example in Chapter 3.3.1 (Figure 22). To investigate the intermolecular interactions, compound **2**$^+$ was prepared with different counterions and it was possible to obtain several crystal structures of **2**$^+$ with different counterions: [**2**][PF_6], [**2**H][ClO_4]$_2$, [**2**][OTf], [**2**][BF_4] and [**2**H][NO_3]$_2$. It can be observed that intermolecular π-π interactions as well as counterion lone pair-π interactions are present and both

seem to play a role in the solid-state fluorescence (Figure 39-44). Furthermore, the salts of $\mathbf{2}^{+}$ with the denotated anions feature different excitation wavelength ranging from ~475 nm for $\mathbf{2}^{+}$ with PF_6^- counterion to ~575 nm for $\mathbf{2}^{+}$ with $BArF^-$ counterion. An in-depth explanation for the AIE phenomenon cannot be given, since no further fluorescence measurements were conducted of the solid-state compounds and is not focus of this thesis.

The 4,4′-bipyridinium based guest compounds display photochemical properties due to their *para*- or π-quinonoid resonance. Therefore, $\mathbf{2}^{+}$ by itself crystallized with counter ions, BF_4^-, PF_6^- and OTf^-, and the protonated form, $\mathbf{2}H^{+2}$, with counter ions, ClO_4^- and NO_3^-, are analysed for C–C bond rotation flexibility. Three torsion angles α, β and γ as a measure of C–C and N–C bond rotations are shown in Table 4. The a, b and c represent C–C and N–C bond lengths. In the 3-D crystal packing, π-π, C–H···π and, the lone pair-π short contacts between the negative electrostatic potential surface associated with anions and π-aromatic systems are shown in Figure 39-44. The short contacts were also analysed using Hirshfeld Surfaces Analysis as red-hot spots.[118]

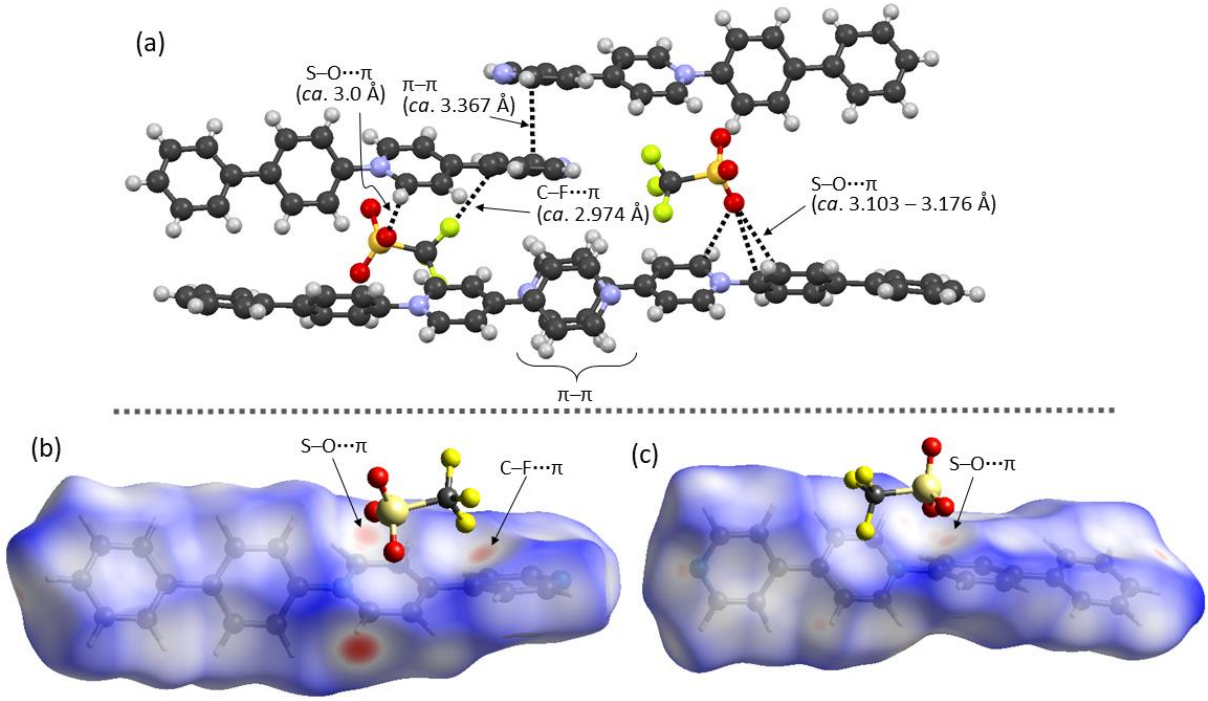

Figure 39. Section of 3-D crystal packing of $\mathbf{2}^{+}\cdot OTf^-$ (a) viewing selected short contacts. Hirshfeld surfaces[118c] displaying short contacts in $\mathbf{2}^{+}\cdot OTf^-$ (b and c). Color scale is between -0.120 (red) and 1.610 (blue) au.

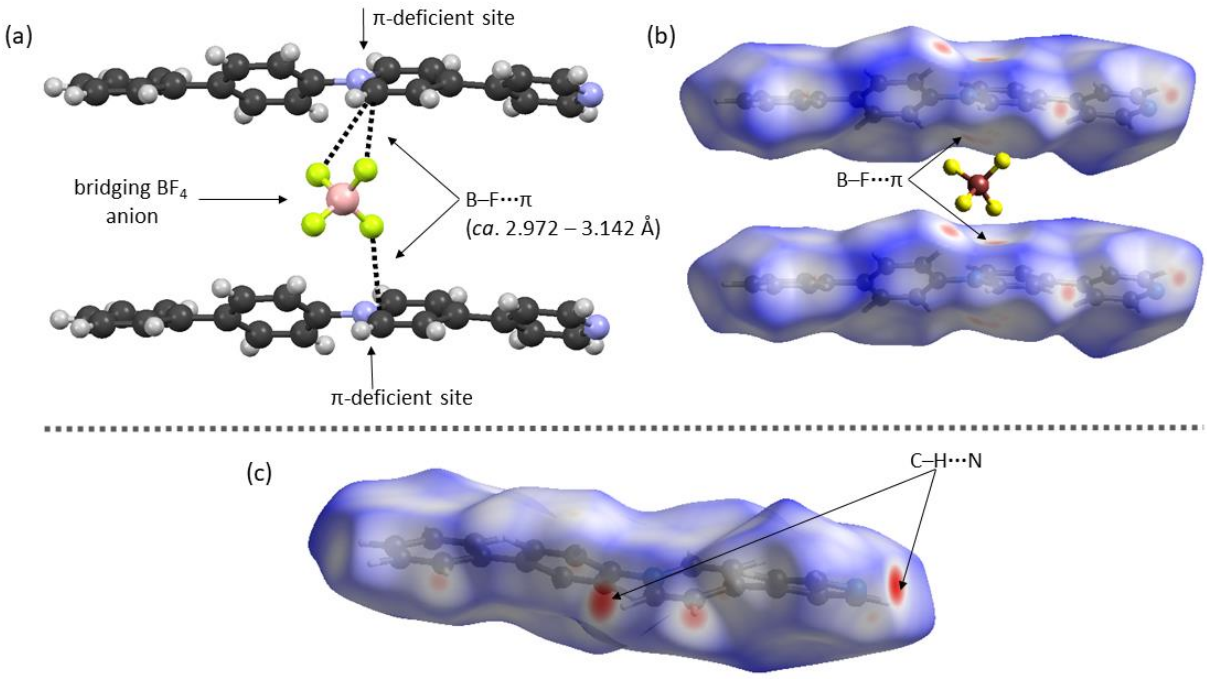

Figure 40. Section of 3-D crystal packing of $\mathbf{2}^{+}\cdot BF_4^-$ (a) viewing selected short contacts. Hirshfeld surfaces displaying short contacts in $\mathbf{2}^{+}\cdot BF_4^-$ (b and c). Color scale is between -0.120 (red) and 1.610 (blue) au.

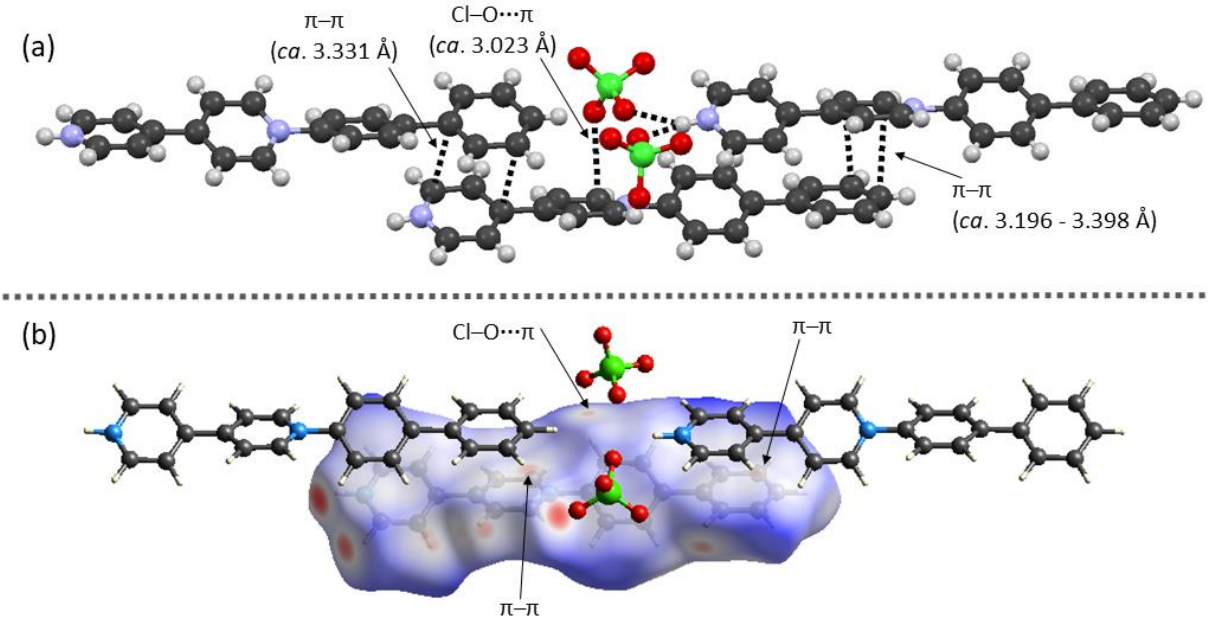

Figure 41. Section of 3-D crystal packing of $\mathbf{2}H^{+2}\cdot[2ClO_4^-]$ (a) viewing selected short contacts. Hirshfeld surfaces displaying short contacts in $\mathbf{2}H^{+2}\cdot[2ClO_4^-]$ (b). Color scale is between -0.369 (red) and 1.750 (blue) au.

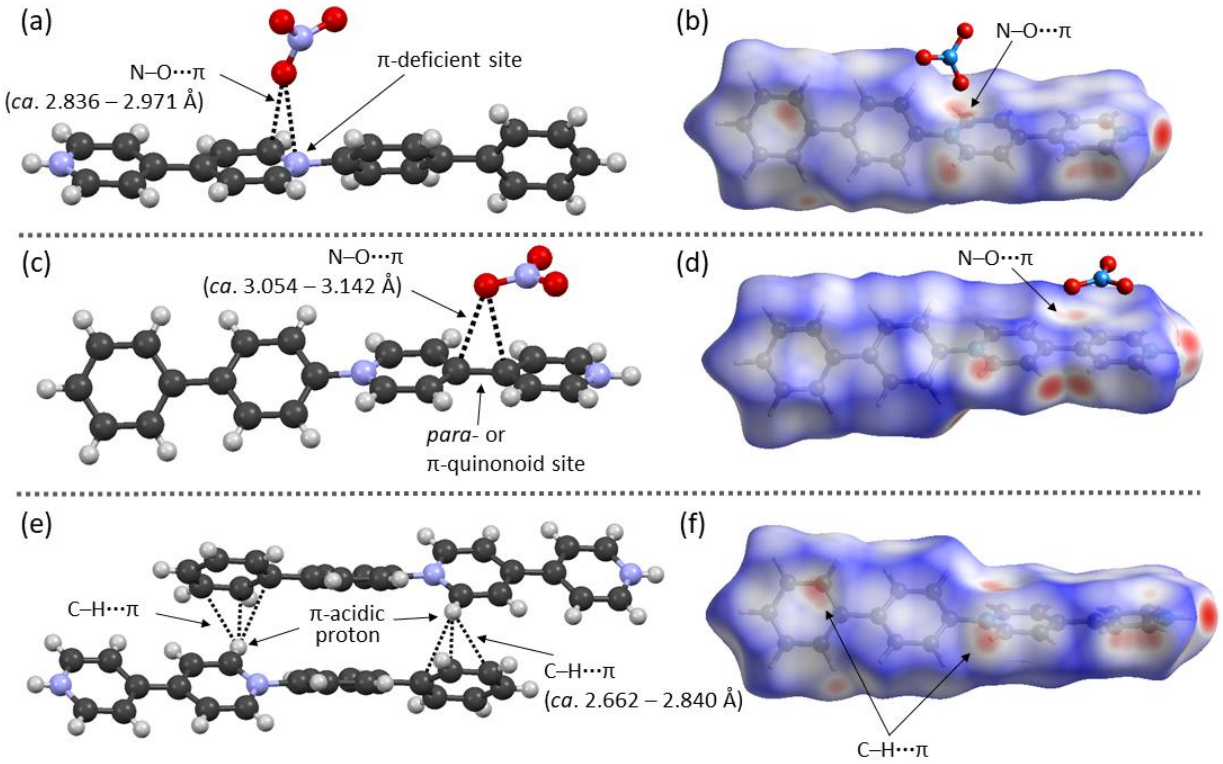

Figure 42. Section of 3-D crystal packing of **2**H^{+2}·[2NO_3^-] (a, c and e) viewing selected short contacts and their respective Hirshfeld surfaces displaying short contacts in **2**H^{+2}·[2NO_3^-] (b, d and f). Color scale is between -0.120 (red) and 1.610 (blue) au.

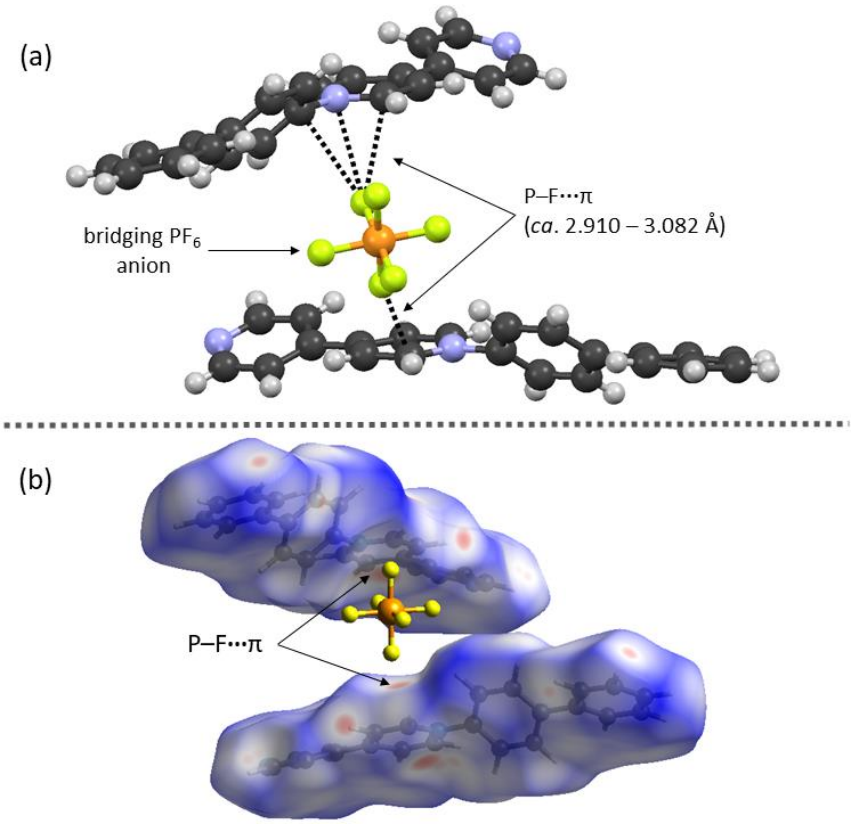

Figure 43. Section of 3-D crystal packing of **2**$^+$·PF_6^- (a) to show selected short contacts and their respective Hirshfeld surface displaying short contacts in **2**$^+$·PF_6^- (b). Color scale is between -0.348 (red) and 1.365 (blue) au.

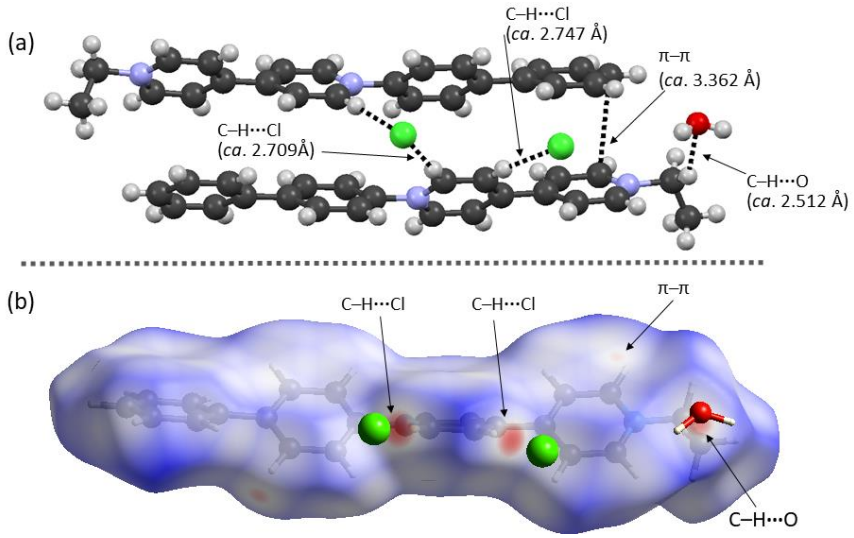

Figure 44. Section of 3-D crystal packing of $\mathbf{8}^{2+}\cdot[2Cl^{-}]$ (a) to show selected short contacts and their respective Hirshfeld surface displaying short contacts in $\mathbf{8}^{2+}\cdot[2Cl^{-}]$ (b). Color scale is between -0.270 (red) and 1.526 (blue) au

Table 4. Solid-state X-ray crystal structure parameters.

Complex	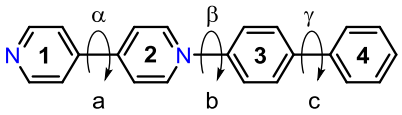 ($\mathbf{2}^{+}$)		
	α [a, Å]	β [b, Å]	γ [c, Å]
$\mathbf{2}^{+}\cdot OTf^{-}$ [a]	150.4(4) [1.473(6)]	131.6(4) [1.446(5)]	17.7(6) [1.490(6)]
	142.6(4) [1.474(6)]	129.5(4) [1.449(5)]	24.1(6) [1.491(6)]
$\mathbf{2}^{+}\cdot BF_4^{-}$	150.0(3) [1.483(4)]	44.0(4) [1.454(3)]	146.4(3) [1.486(4)]
$\mathbf{2}H^{2+}\cdot[2ClO_4^{-}]$ [b]	148.0(8) [1.494(11)]	38.1(11) [1.448(10)]	151.6(8) [1.538(12)]
	153.3(8) [1.465(12)]	36.0(11) [1.466(11)]	149.3(9) [1.550(10)]
	149.2(8) [1.499(11)]	38.3(11) [1.460(10)]	150.0(8) [1.559(12)]
$\mathbf{2}H^{2+}\cdot[2NO_3^{-}]$	170.9(2) [1.488(3)]	141.5(2) [1.454(3)]	156.4(2) [1.488(3)]
$\mathbf{2}^{+}\cdot PF_6^{-}$	22.54(19) [1.482(2)]	42.77(17) [1.452(2)]	144.94(13) [1.491(2)]
$\mathbf{8}^{2+}\cdot[2Cl^{-}]$ [c]	45.6(6) [1.486(5)]	136.9(4) [1.457(4)]	36.3(6) [1.487(5)]
The asymmetric unit contains [a]two crystallographically independent $\mathbf{2}^{+}$ molecules, [b]three crystallographically independent $\mathbf{2}H^{+2}$ molecules and [c] $(\mathbf{2}Et)^{2+}$ as $\mathbf{8}^{2+}$			

4.1.4 Complexation of the Dye with β-CD

The host–guest interactions with water-soluble macrocycles and the emerging photophysical properties should be analyzed and, therefore, the complexation with cyclodextrins was investigated. Aqueous solutions of compound $\mathbf{8}^{2+}$ with α-CD, β-CD and γ-CD were prepared. Figure 45 shows the ^{1}H NMR spectra of the solutions and only in the case of β-CD a complexation induced shift of the signals of the protons can be observed indicating an interaction with the host. This is in line with the expectation, since α-CD is too small to complex aromatic guests and γ-CD is known to encapsulate apolar dimers, which is unfavored in this case because of the charge repulsion of the dicationic moieties.[13, 61a]

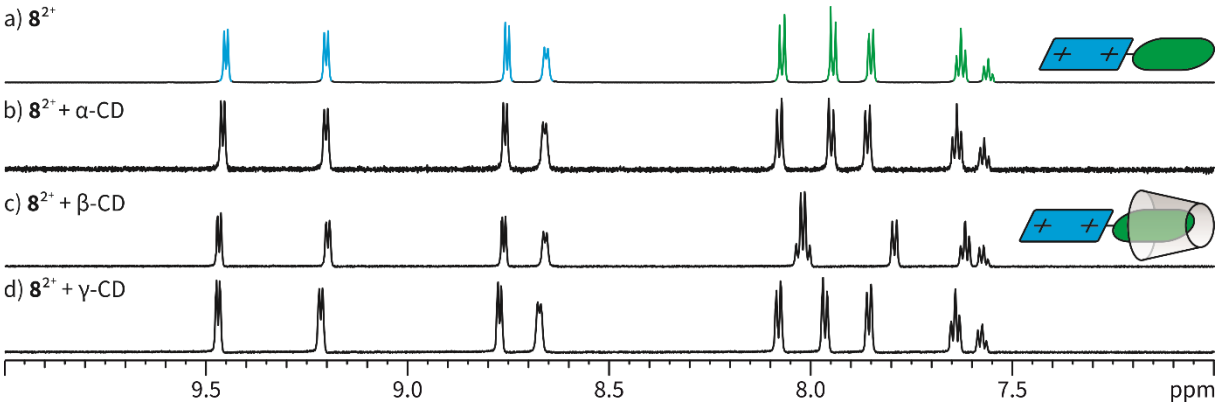

Figure 45. Partial ^{1}H NMR spectra (700 MHz, 298 K, D_2O, 1.0 mM) of (a) $\mathbf{8}^{2+}$, (b) a 1:1 mixture of $\mathbf{8}^{2+}$ and α-CD, (c) a 1:1 mixture of $\mathbf{8}^{2+}$ and β-CD and (d) a 1:1 mixture of $\mathbf{8}^{2+}$ and γ-CD.

The structures of the host–guest complexes with β-CD can be derived from ^{1}H NMR shifts (Figure 46). The change of the shifts of the signals of the biphenyl protons from (a) to (b) indicate complexation of the unpolar moiety by the cyclodextrin furnishing the 1:1 complex $\mathbf{2}H^{2+}$@CD. Since pyridine can be complexed by β-CD,[13] deprotonated $\mathbf{2}^{+}$ has two complexation sites. $\mathbf{2}^{+}$ with two equivalents of β-CD (c) exhibits complexation induces shifts of both, the bipyridyl and the biphenyl moiety indicating the formation of the 1:2 complex $\mathbf{2}^{+}$@CD_2. Addition of only one equivalent of β-CD forms the 1:1 complex $\mathbf{2}^{+}$@CD which is in equilibrium with the 2:1 complex $\mathbf{2}^{+}$@CD_2. Furthermore, the host shuttles between the two binding as represented by the cartoon.

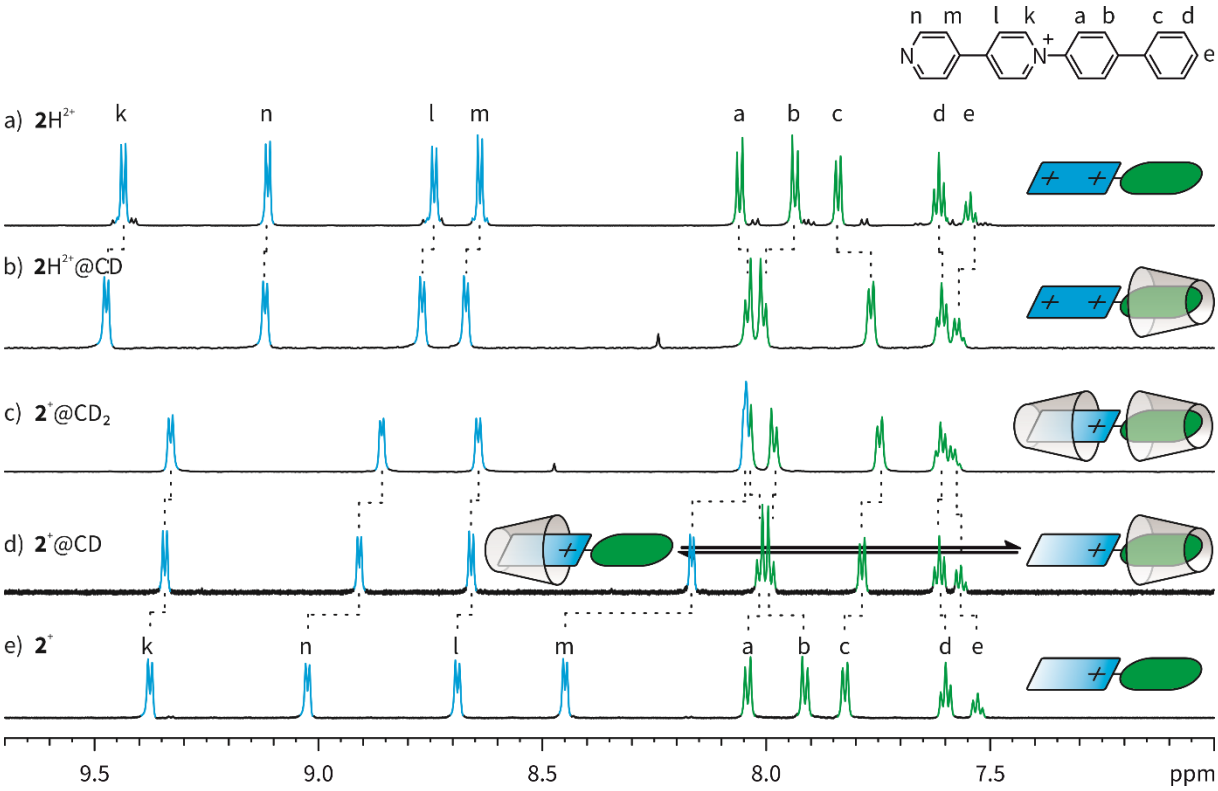

Figure 46. Partial ^{1}H NMR spectra (700 MHz, 298 K, D_2O, 1.0 mM) of (a) **2**H^{2+}, (b) a 1:1 mixture of **2**H^{2+} and β-CD, (c) a 1:2 mixture of **2**$^+$ and β-CD, (d) a 1:1 mixture of **2**$^+$ and β-CD and (e) **2**$^+$; DCl (35% in D_2O) and K_2CO_3 were used to (de)protonate.

The ^{1}H NMR spectra of the β-CD complexes of **3**H^{2+}–**7**H^{2+} and **3**$^+$–**7**$^+$ are shown at the end of the Chapter 4.1 in Figure 60. The complexations follow the same trend and, therefore, the formation of the similar complexes can be assumed.

The stoichiometry of the β-CD complex was investigated by Job plot analysis. The intersection of the fitted lines in the case of **2**H^{2+}@CB[7] confirm the 1:1 stoichiometry (Figure 47 a and b). However, a job plot analysis of **2**$^+$@CB[7] is not conclusive (c), because of the possible existence of the two species, the above described 1:1 and 2:1 complexes **2**$^+$@CD and **2**$^+$@CD_2.[119]

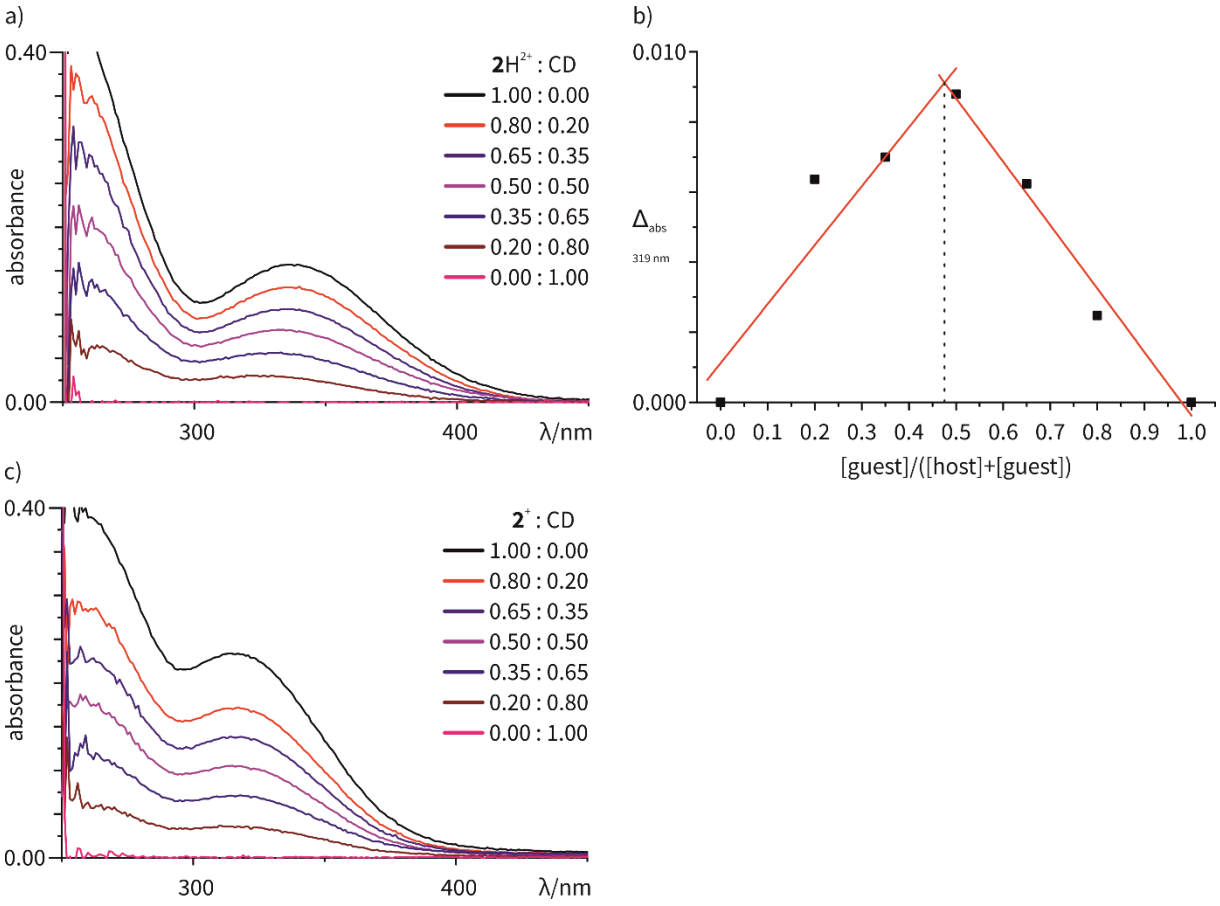

Figure 47. (a) UV/Vis absorption spectra of **2**H^{2+}:β-CD mixtures (pH = 4); overall concentration of a single solution is 0.12 mM. (b) Job plot analysis at 319 nm of the **2**H^{2+} - β-CD complex indicating a 1:1 stoichiometry in the form of **2**H^{2+}@CD. (c) UV/Vis absorption spectra of **2**$^{+}$:β-CD mixtures (pH = 10); overall concentration of a single solution is 0.12 mM.

Mass spectrometry (MS) analysis of the complexes with **2**$^{+}$ were troublesome since the protonation state of the bipyridine moiety during the ionization process could not be assured, therefore, MS was conducted with the complexes of ethylated **8**$^{2+}$. The MS spectrum of **8**$^{2+}$@CD is shown in Figure 48. The 1:1 complex **8**$^{2+}$@CD (*m/z* 736) can be clearly seen, but due to the weak binding between the guest and the host, dissociation during the ionization process could take place. Because of charge separation, the uncomplexed guests either loses an electron resulting in [**8**-e]$^{+}$ (*m/z* 338) or fragments to [**8**-C_2H_5]$^{+}$ (*m/z* 309).

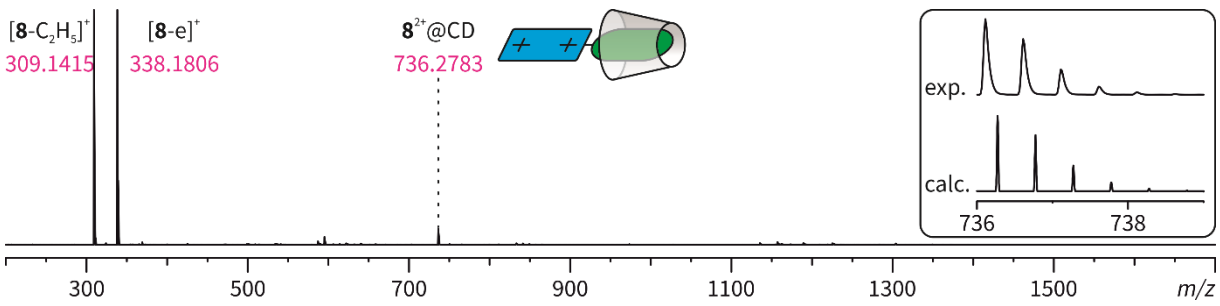

Figure 48. ESI-TOF mass spectra of a mixture of **8**$^{2+}$ and β-CD with isotope pattern.

The photophysical properties of the complexes with β-CD were analyzed. The complexation has only minor effects on the emission properties of the fluorophore compared to its free state since the host is neither rigid, nor changing the polarity of around the guest significantly (Figure 49, Table 8). Therefore, the TICT mechanism still takes place and results in quenching of the fluorescence.

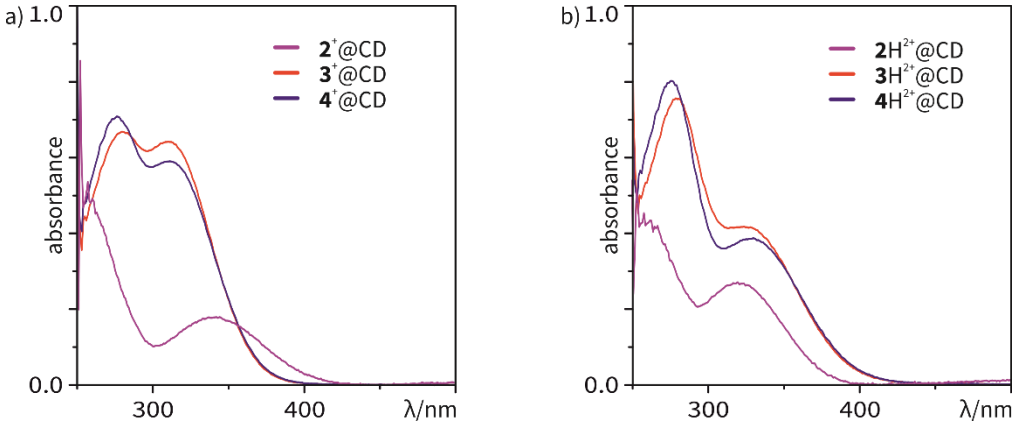

Figure 49. UV/Vis spectra of (a) **2**$^{+}$@CD–**4**$^{+}$@CD and (b) **2**H^{2+}@CD–**4**H^{2+}@CD; c = 0.06 mM.

4.1.5 Complexation of the Dye with CB[7]

CB[*n*]s are more rigid host than β-CD and feature an apolar cavity, which could have a drastic impact on the emission properties of the fluorophores. Therefore, as a first step, the complexation with CB[7] was investigated. The structures of the host-guest complexes with CB[7] can be derived from typical ^{1}H NMR shifts (Figure 50). The change of the shifts of the signals of the bipyridine protons from (a) to (b) indicate complexation of the bipyridine moiety by the cucurbituril furnishing 1:1 complex **2**H^{2+}@CB[7]. The broadening of the signals illustrate complexation of the fluorophore and the complexation induced high field shifts (d to c) indicate formation of the 1:1 complex **2**$^{+}$@CB[7].

The ^{1}H NMR spectra of the CB[7] complexes of **3**H^{2+}–**7**H^{2+} and **3**$^{+}$–**7**$^{+}$ are shown at the end of the Chapter 4.1 in Figure 61. The complexations follow the same trend and, therefore, the formation of the similar complexes can be assumed.

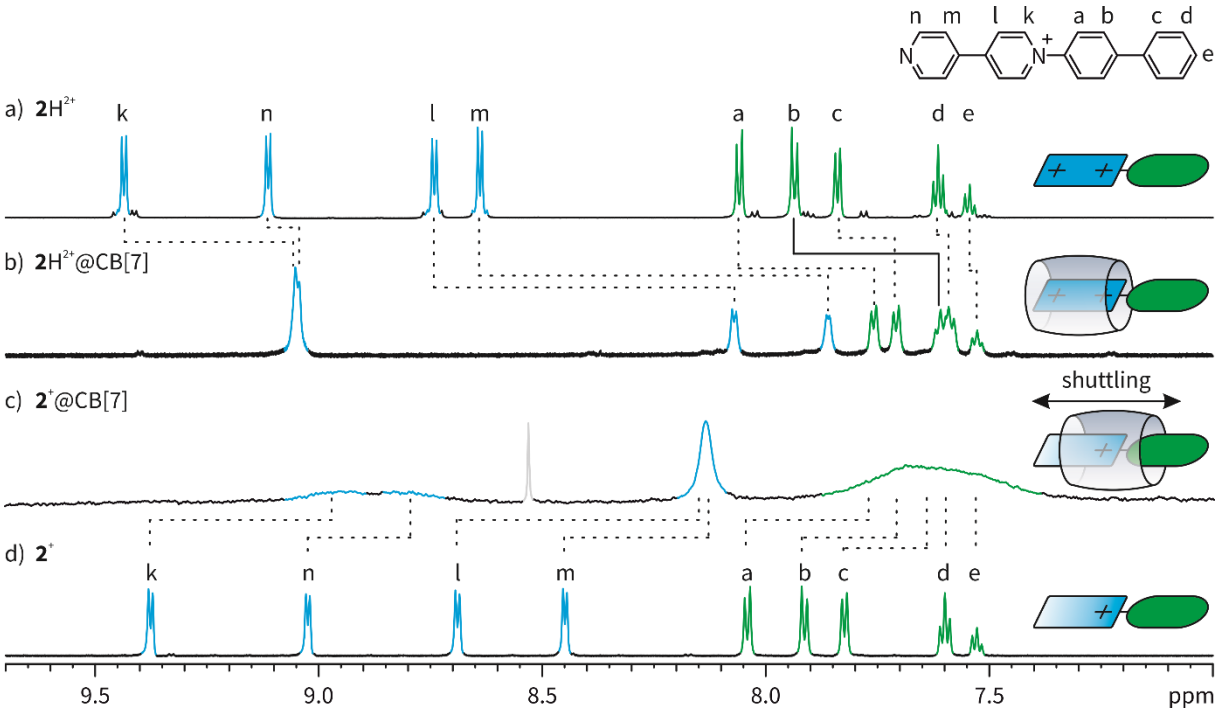

Figure 50. Partial ^{1}H NMR spectra (700 MHz, 298 K, D_2O, 1.0 mM) of (a) **2**H^{2+}, (b) a 1:1 mixture of **2**H^{2+} and CB[7], (c) a 1:1 mixture of **2**$^{+}$ and CB[7] and (d) **2**$^{+}$; DCl (35% in D_2O) and K_2CO_3 were used to (de)protonate.

MS analysis of **8**$^{2+}$@CB[7] was conducted to validate the stoichiometry of the complex (Figure 51). The 1:1 complex **8**$^{2+}$@CB[7] (*m/z* 750) can be clearly seen. Uncomplexed guests either loses an electron resulting in [**8**e]$^{+}$ (*m/z* 338) or fragments to [**8**-C_2H_5]$^{+}$ (*m/z* 309) because of the charge separation.

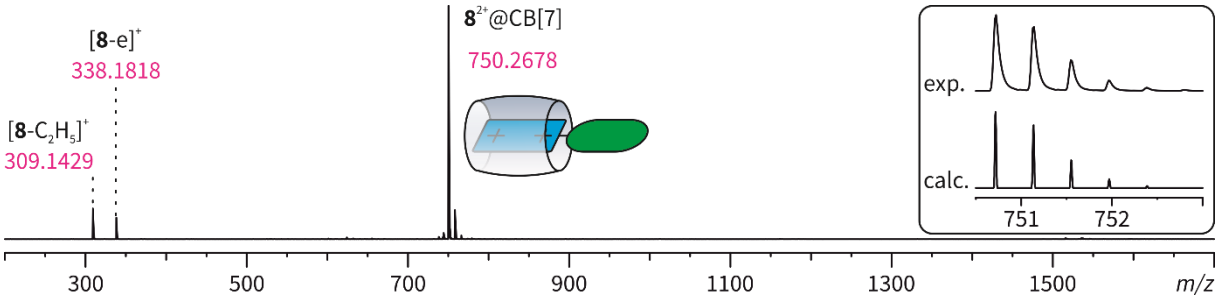

Figure 51. ESI-TOF mass spectra of a mixture of **8**$^{2+}$ and CB[7] with isotope pattern.

Compared to β-CD, the complexation with CB[7] has a significant impact on the photophysical properties of the fluorophore. Encapsulation inside CB[7] induces a bathochromic shift of the π–π* absorption band, which can be contributed to the change in the chemical environment and is in line with literature reports (Figure 52).[120] The emission wavelengths exhibit a blueshift compared to the free dyes (Table 5).

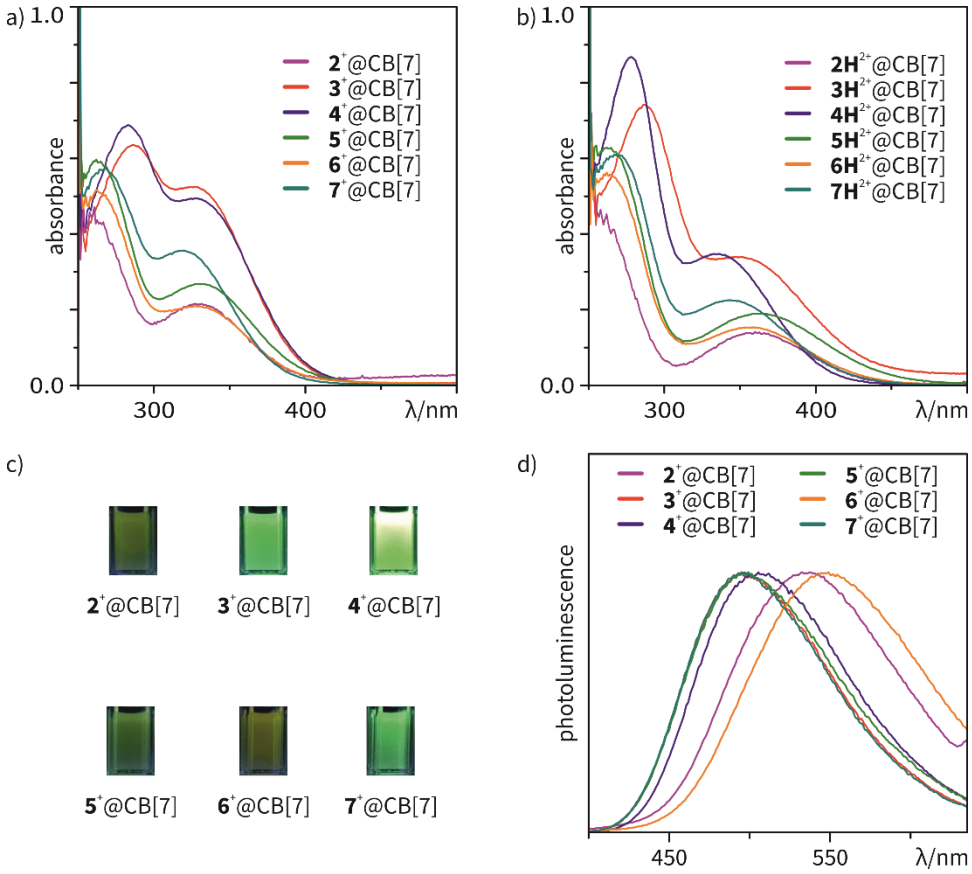

Figure 52. UV/Vis absorption spectra of (a) **2**$^{+}$@CB[7]–**4**$^{+}$@CB[7] (pH = 10), (b) **2**H^{2+}@CB[7]–**4**H^{2+}@CB[7] (pH = 4), (c) photographs (λ_{ex} = 366 nm) of **2**$^{+}$@CB[7]–**4**$^{+}$@CB[7] (pH = 10) and (d) PL spectra of ($\lambda_{ex} = \lambda_{abs}$) of **2**$^{+}$@CB[7]–**4**$^{+}$@CB[7] (pH = 10) ; c = 0.06 mM.

Additionally, the quantum yields increase due to complexation by three- and four-fold for **2**H^{2+}@CB[7] and **2**$^{+}$@CB[7], respectively. This can be attributed to the unpolar chemical environment in the host.[121] This change in polarity shifts the equilibrium from the TICT state to the LE state.[106a] Even though the excited fluorophore is well stabilized inside the cavity of the CB[7], there is no restriction of intramolecular motion (RIM).[93] The molecule can still rotate around the single bonds, bend and twist, and since any molecular motion is able to consume energy, non-radiative decay still takes place.[99c]

Table 5. Photophysical and electrochemical parameters of **2**$^{+}$–**7**$^{+}$ in aqueous solution.

	R =	λ_{abs} [nm]	λ_{em} [nm][a]	λ_s [10^3 cm^{-1}]	Φ [%][a]
2^{+}@CB[7]	H	328	528	11.5	10
3^{+}@CB[7]	CHO	312	491	11.7	50
4^{+}@CB[7]	$COCH_3$	315	499	11.7	36
5^{+}@CB[7]	CH_3	330	499	10.2	8
6^{+}@CB[7]	Br	327	549	12.4	4
7^{+}@CB[7]	CH_2OH	320	496	11.3	30

[a] $\lambda_{ex} = \lambda_{abs}$.

4.1.6 Complexation of the Dyes with CB[8]

The complexation of the fluorophores with CB[8] will be described exemplarily for **2**H^{2+} and **2**$^{+}$. One equivalent of **2**H^{2+} with one equivalent of CB[8] leads to the formation of the 2:2 complex **2**H$^{2+}_2$@CB[8]$_2$ (Figure 53b). The signals of the bipyridine protons experience the typical complexation induced high field shifts. Furthermore, the significant high field shifts of the signals of the outer phenyl protons suggest them to be in the cavity of the cucurbituril as well. The inner phenyl ring, however, is located in between the cucurbiturils experiencing a high field shift due to of encapsulation as well as a low field shift due to the interaction with the carbonyl rim of the host. The ^{1}H NMR spectrum shows that deprotonation of the guest molecule does not change the 2:2 complex stoichiometry(c).

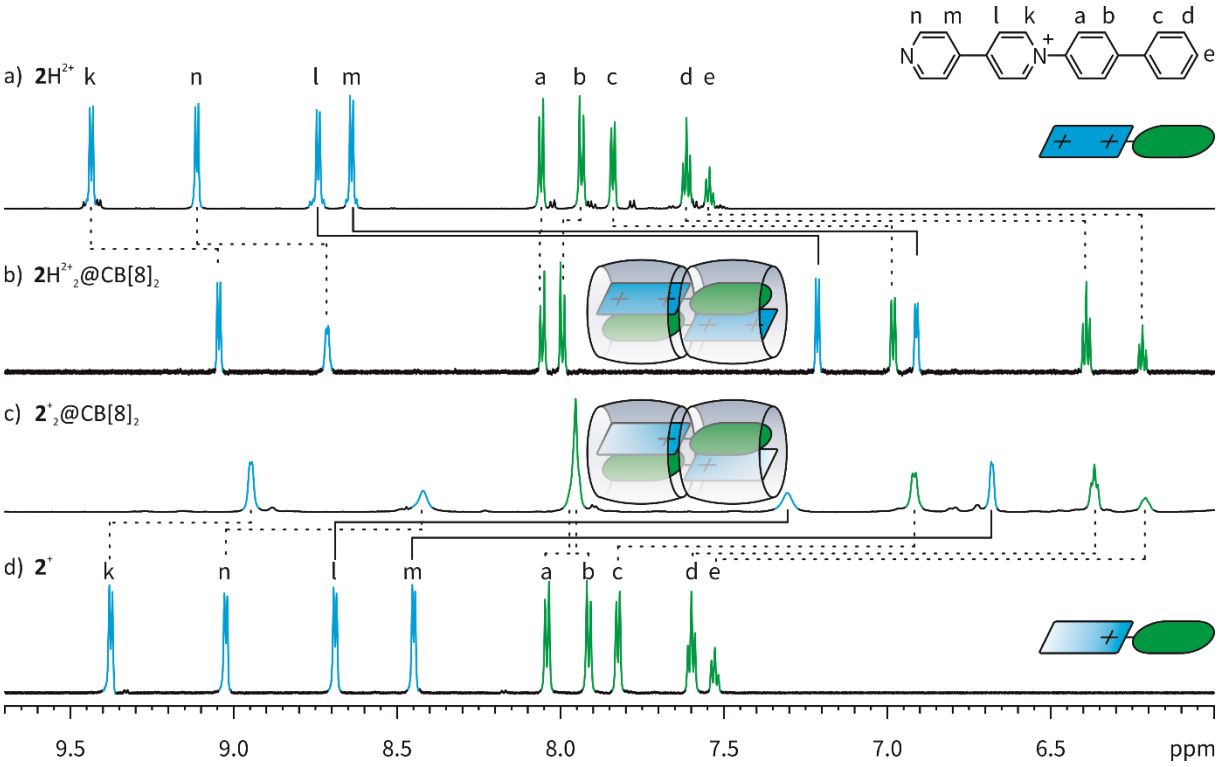

Figure 53. Partial ^{1}H NMR spectra (700 MHz, 298 K, D_2O, 1.0 mM) of (a) **2**H^{2+}, (b) a 1:1 mixture of **2**H^{2+} and CB[8], (c) a 1:1 mixture of **2**$^{+}$ and CB[8] and (d) **2**$^{+}$.

The ^{1}H NMR spectra of the CB[8] complexes of **3**H^{2+}–**7**H^{2+} and **3**$^{+}$–**7**$^{+}$ are shown at the end of the Chapter 4.1 in Figure 62. The complexations follow the same trend and, therefore, the formation of the similar 2:2 complexes can be assumed.

The complex stoichiometry was confirmed by a crystal structure (Figure 54). Two guests stack in an antiparallel fashion inside CB[8] with C–C shortest aromatic centroid-to-centroid contacts, 3.75 Å [shift distance, 1.12 Å]. The average of C···C contacts, *ca.* 3.6 Å, is in line with the reported distances (3.3-3.8 Å) for π-donor-π-acceptor complex between the electron deficient viologen unit and the relatively electron-rich biphenyl moiety.[122] The π-π dimer also manifests

several weak C–H···(O=C)$_{host}$ and C–H···(C=O)$_{host}$ interactions ranging between 3.00 and 3.20 Å. Overall it can be said that the guests are constrained into a planar conformation and hindered in their motion due to the confined space in the complex.

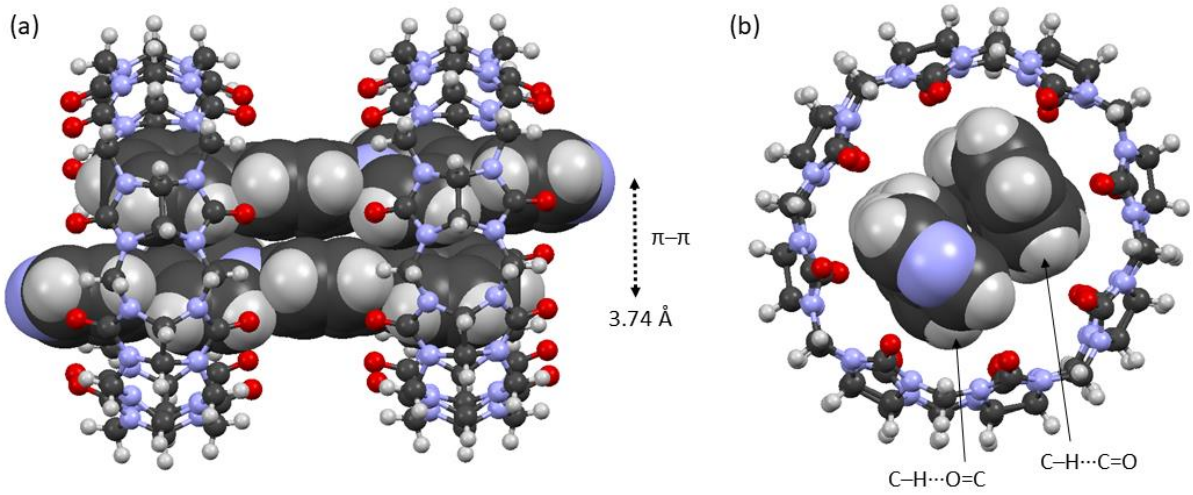

Figure 54. Crystal structure of **2**H_2^{+2}@CB[8]$_2$ (a) side-view and (b) top-view; counterions and disordered solvent molecules are omitted for clarity.

Table 6. Solid-state X-ray crystal structure bond parameters.

Complex	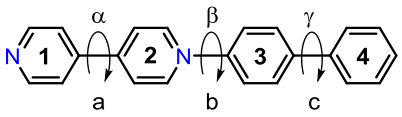 (**2**$^+$)		
	α [a, Å]	β [b, Å]	γ [c, Å]
(**2**H^{+2})$_2$@CB[8]$_2$	162.4(16) [1.485(16)]	22.7(16) [1.457(12)]	162.3(13) [1.481(14)]
	144.7(12) [1.503(17)]	34.5(14) [1.467(14)]	153.1(11) [1.517(16)]
The asymmetric unit contains two crystallographically independent **2**H^{+2} molecules.			

Additionally, based on the ^{1}H NMR signals, it was observed that excess of CB[8] does not change the complex stoichiometry, in case of a shortfall of CB[8], however, a new set of signals appears for a 2:1 complex (Figure 55). During the addition of CB[8] to **8**$^{2+}$ ((a) to (e)) signals of a new complex arise (green). The newly formed complex can be contributed to **8**$^{2+}{}_2$@CB[8] as represented in the cartoon. An excess of CB[8] (e) has no influence on the complex **8**$^{2+}{}_2$@CB[8]$_2$.

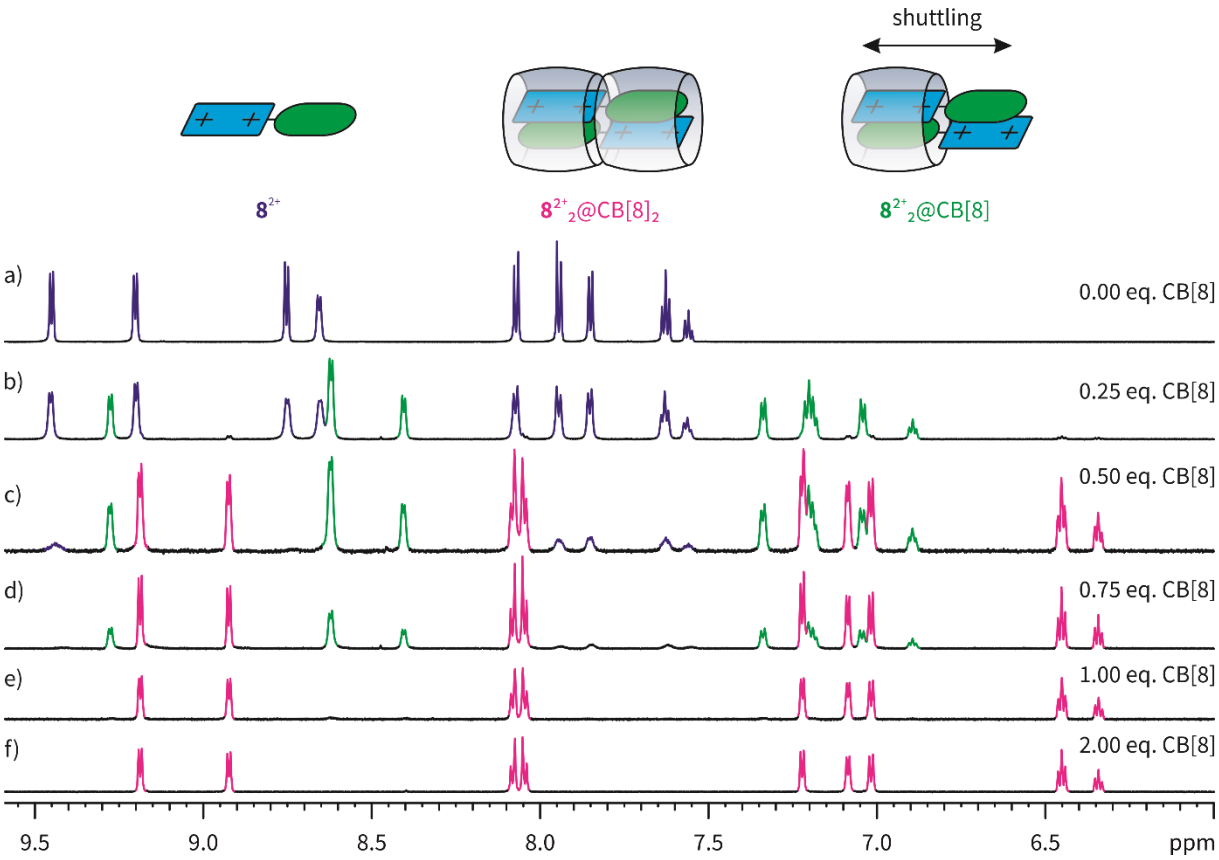

Figure 55. Partial ^{1}H NMR spectra (700 MHz, 298 K, D_2O, 1.0 mM) of (a) **8**$^{2+}$, (b) a 1.00:0.25 mixture of **8**$^{2+}$ and CB[8], (c) a 1.0:0.5 mixture of **8**$^{2+}$ and CB[8], (d) a 1.00:0.75 mixture of **8**$^{2+}$ and CB[8], (e) a 1:1 mixture of **8**$^{2+}$ and CB[8] and (f) a 1:2 mixture of **8**$^{2+}$ and CB[8].

The complexation with CB[8], compared to the other investigated hosts, has the strongest effect on the photophysical properties of the fluorophores. The UV/Vis spectra of all CB[8] complexes show a bathochromic shift indicating the formation of an excimer (Figure 56).[123] Compared to the respective CB[7] complexes, the CB[8] complexes of **2**H^{2+}–**7**H^{2+} have significantly higher quantum yields, up to ϕ = 26% for **3**H^{2+} (Table 7). A very strong emission enhancement after deprotonation for all CB[8] complexes can be observed (d). For example, **2**$^+_2$@CB[8]$_2$ displays a quantum yield of ϕ = 82% which corresponds to a 27-fold increase in comparison to the free luminophore **2**$^+$ and the fluorescence decay increases drastically by a factor of 100 (τ = 15.20 ns). It is assumed that the unpolar environment hinders the TICT mechanism just like in the smaller CB[7]. In addition, the excimer formation restricts the fluorophores in its intramolecular motion since the host and the second guest occupy the cavity of the CB[8] and conceive a confined space. Therefore, the strong fluorescence enhancement cannot only be attributed to the prevention of the TICT state, but furthermore the combination of RIM and excimer formation inside the cucurbituril. Complex **6**$^+_2$@CB[8]$_2$ with the bromo substituted guest seems to be an outlier, but the relatively low quantum yield and especially the modest enhancement compared to the CB[7] complex (ϕ = 4% to 5%) can be contributed to quenching by the heavy-atom effect of the dimers inside the cavity of CB[8].[124]

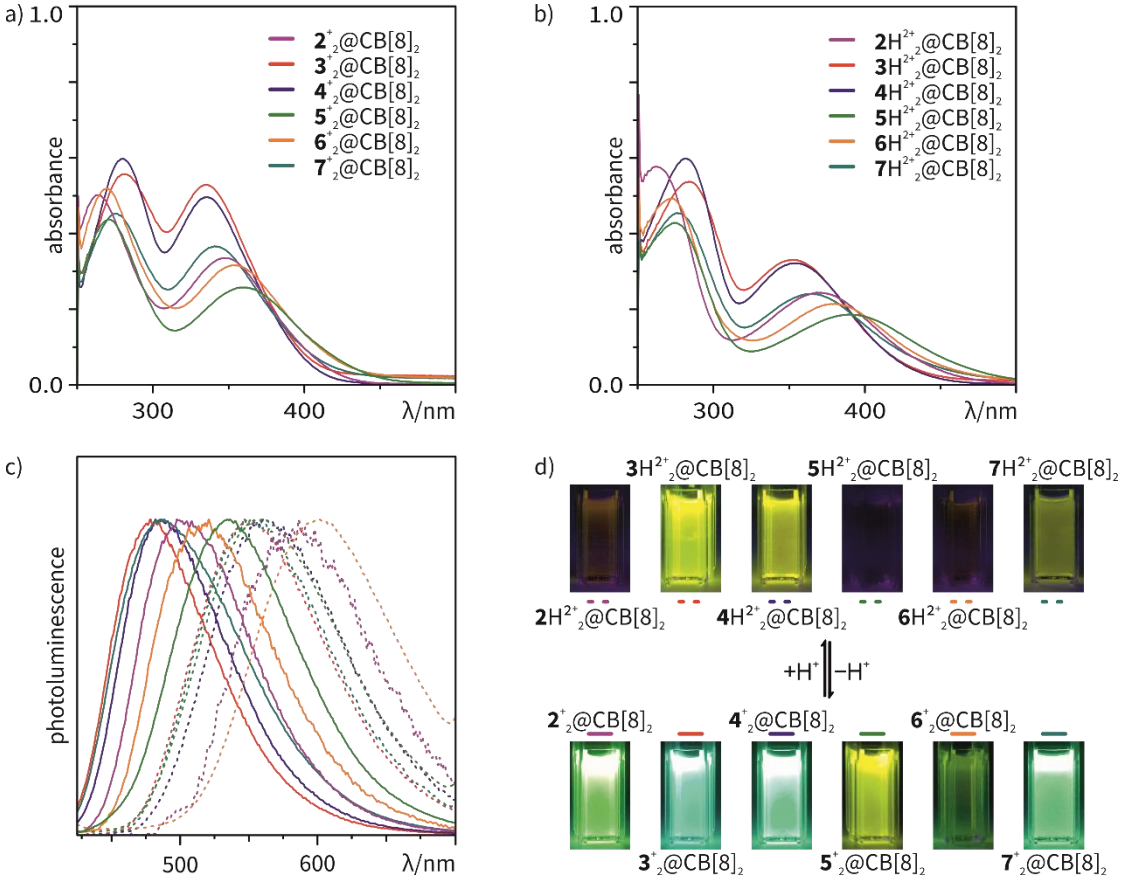

Figure 56. UV/Vis absorption spectra of (a) **2**$^{+}_{2}$@CB[8]$_2$–**7**$^{+}_{2}$@CB[8]$_2$ (pH = 10) and (b) **2**H$^{2+}_{2}$@CB[8]$_2$–**7**H$^{2+}_{2}$@CB[8]$_2$ (pH = 4), (c) normalized PL spectra (λ_{ex} = λ_{abs}) and (b) photographs (λ_{ex} = 366 nm) of **2**$^{+}_{2}$@CB[8]$_2$–**7**$^{+}_{2}$@CB[8]$_2$ (pH = 10) and (d) **2**H$^{2+}_{2}$@CB[8]$_2$–**7**H$^{2+}_{2}$@CB[8]$_2$ (pH = 4); c = 0.06 mM.

Table 7. Photophysical and electrochemical parameters of **2**$^{+}$–**7**$^{+}$ in aqueous solution.

	R =	λ_{abs} [nm]	λ_{em} [nm][a]	λ_s [10^3 cm^{-1}]	ϕ [%][a]
2$^{+}_{2}$@CB[8]$_2$	H	328	528	8.6	82
3$^{+}_{2}$@CB[8]$_2$	CHO	336	491	8.8	80
4$^{+}_{2}$@CB[8]$_2$	$COCH_3$	336	499	9.0	78
5$^{+}_{2}$@CB[8]$_2$	CH_3	360	499	9.1	42
6$^{+}_{2}$@CB[8]$_2$	Br	353	549	9.1	5
7$^{+}_{2}$@CB[8]$_2$	CH_2OH	341	496	8.9	43
2H$^{2+}_{2}$@CB[8]$_2$	H	367	587	10.2	4
3H$^{2+}_{2}$@CB[8]$_2$	CHO	353	547	10.0	26
4H$^{2+}_{2}$@CB[8]$_2$	$COCH_3$	354	561	10.0	18
5H$^{2+}_{2}$@CB[8]$_2$	CH_3	391	560	7.7	10
6H$^{2+}_{2}$@CB[8]$_2$	Br	380	601	9.7	2
7H$^{2+}_{2}$@CB[8]$_2$	CH_2OH	366	551	9.2	12

[a] λ_{ex} = λ_{abs}.

4.1.7 A Second Functionalization Site

A second functionalization of the guests is possible on the pyridine side by simple alkylation. By doing this, the pH switch is eliminated; however, other functional groups for further applications can be introduced. To demonstrate this, complexation of simply ethylated $\mathbf{8}^{2+}$ leads to the same encapsulation induced shifts like discussed with $\mathbf{2}H^{2+}$, furnishing the complexes $\mathbf{8}^{2+}$@CD, $\mathbf{8}^{2+}$@CB[7] and $\mathbf{8}^{2+}_2$@CB[8]$_2$ (Figure 57).

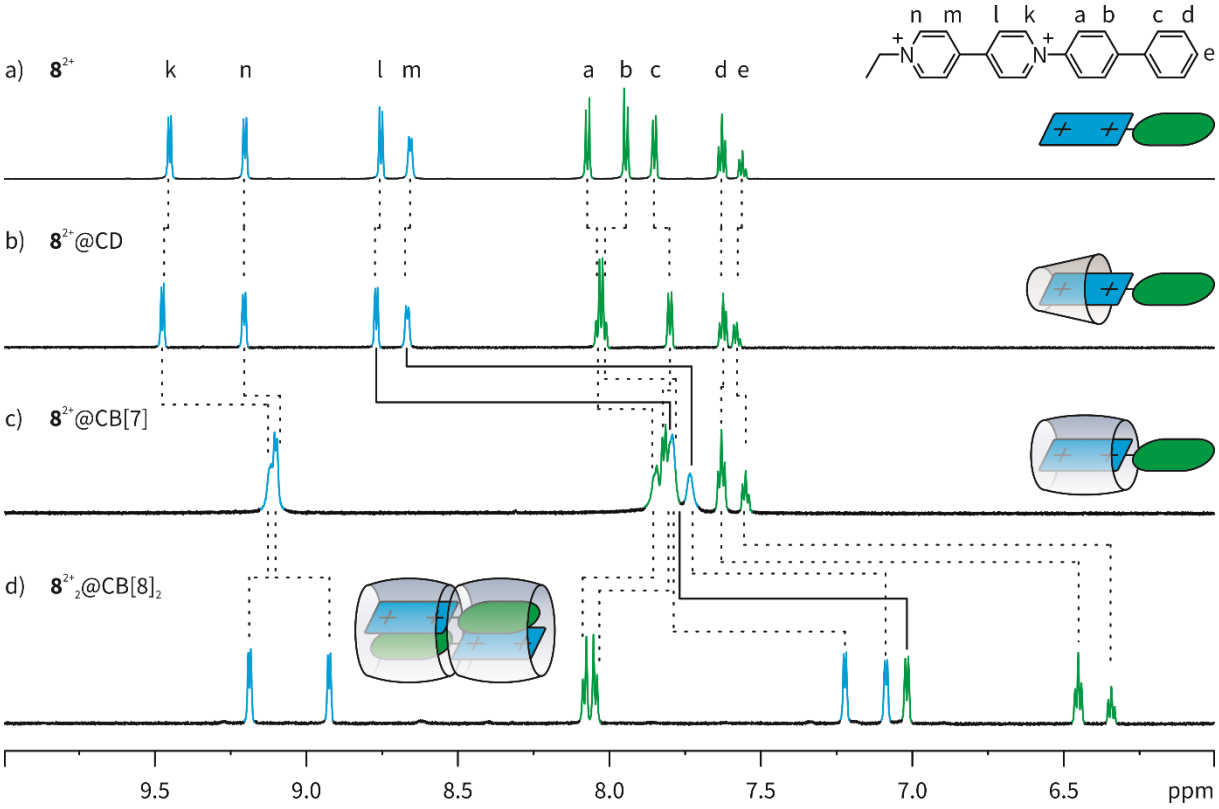

Figure 57. Partial ^{1}H NMR spectra (700 MHz, 298 K, D_2O, 1.0 mM) of (a) $\mathbf{8}^{2+}$, (b) a 1:1 mixture of $\mathbf{8}^{2+}$ and β-CD, (c) a 1:1 mixture of $\mathbf{8}^{2+}$ and CB[7], (d) a 1:1 mixture of $\mathbf{8}^{2+}$ and CB[8

The compound features a strong luminescence enhancement after addition of a host; e.g. from 0.2% to 7.8% for $\mathbf{8}^{2+}_2$@CB[8]$_2$ (Figure 58). This shows that a second functionalization site can be introduced even though the quantum yields drop drastically. But this problem could be overcome by functionalizing $\mathbf{3}^+$, which still has high quantum yields in its protonated form.

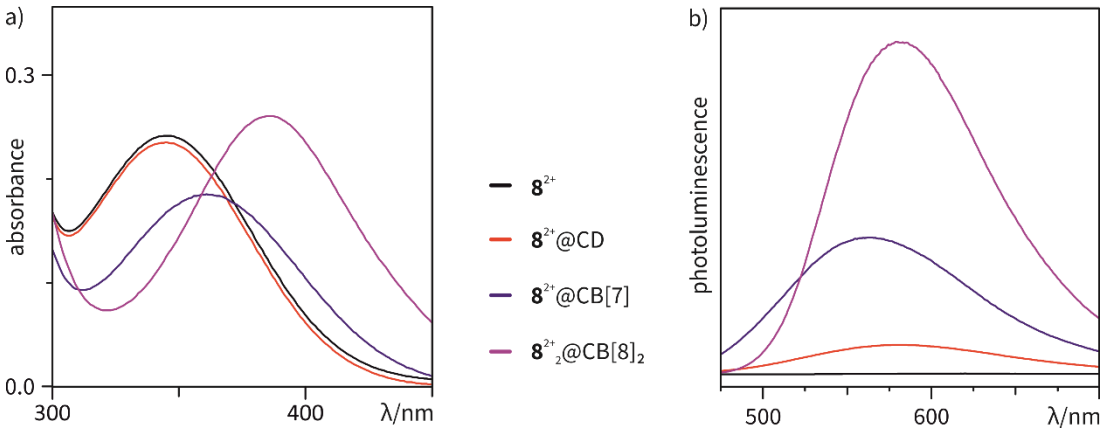

Figure 58. (a) UV/Vis and (b) Pl spectra of $\mathbf{8}^{2+}$, $\mathbf{8}^{2+}$@CD, $\mathbf{8}^{2+}$@CB[7] and $\mathbf{8}^{2+}{}_2$@CB[8]$_2$; c = 0.06 mM.

In conclusion, the effect of supramolecular complexation on the photophysical properties of simple charge transfer dyes $\mathbf{2}^{+}$–$\mathbf{7}^{+}$ and their protonated forms in aqueous solution is demonstrated. The uncomplexed luminophores are weakly emissive due to the presence of a TICT state as indicated by experimental and computational evidence. However, the compounds exhibit strong luminescence in solid-state and in polymer blends. Addition of β-CD shows small influences on the emission properties. Complexation with CB[7] results in the formation of 1:1 complexes and the TICT mechanism is hindered due to the unpolar environment inside the cavity. Addition of CB[8] yields 2:2 complexes with a cofacial *trans* arrangement of the dyes as shown by ^{1}H NMR and a crystal structure. The 2:2 complexes exhibit a very strong emission increase due to RIM and excimer formation (27-fold increase for $\mathbf{2}^{+}$ to ϕ = 82%). This novel, yet simple strategy to implement a RIM triggered luminescence enhancement in stimuli-responsive supramolecular CB[8] complexes is highly promising to obtain strongly emissive luminophores for biological and material solution or solid-sate applications.

4.1.8 Appendix for Chapter 4.1

Table 8. Experimental photophysical properties of the compounds and their complexes.

#		R =	λ_{abs} [nm]	λ_{em} [nm]	λ_s [cm^{-1}]	Φ [%]	τ [ns]
1	**2**$^{+}$	H	318	541	12962	2.54	0.15
2	**2**$^{+}$@CD	H	317	537	12923	3.14	0.19
3	**2**$^{+}$@CB[7]	H	328	528	11548	10.29	0.76 3.88
4	**2**$^{+}{}_2$@CB[8]$_2$	H	328	498	8655	81.98	15.20
5	**2**H^{2+}	H	340	601	12773	0.64	*
6	**2**H^{2+}@CD	H	342	598	12517	1.65	*
7	**2**H^{2+}@CB[7]	H	360	570	10234	2.00	*
8	**2**H$^{2+}{}_2$@CB[8]$_2$	H	367	587	10212	4.05	2.54
9	**3**$^{+}$	CHO	310	499	12218	24.78	*
10	**3**$^{+}$@CD	CHO	311	498	12074	24.11	*
11	**3**$^{+}$@CB[7]	CHO	312	491	11685	50.08	*
12	**3**$^{+}{}_2$@CB[8]$_2$	CHO	336	478	8841	79.94	7.12
13	**3**H^{2+}	CHO	324	*	-	5.79	*
14	**3**H^{2+}@CD	CHO	324	526	11853	5.69	*
15	**3**H^{2+}@CB[7]	CHO	331	492	9886	8.28	*
16	**3**H$^{2+}{}_2$@CB[8]$_2$	CHO	353	547	10047	25.48	5.54
17	**4**$^{+}$	$COCH_3$	313	513	12456	16.62	*
18	**4**$^{+}$@CB[7]	$COCH_3$	315	499	11706	36.19	*
19	**4**$^{+}{}_2$@CB[8]$_2$	$COCH_3$	336	482	9015	77.49	*
20	**4**H^{2+}	$COCH_3$	331	*	-	*	*
21	**4**H^{2+}@CB[7]	$COCH_3$	337	544	11291	6.78	*
22	**4**H$^{2+}{}_2$@CB[8]$_2$	$COCH_3$	354	561	10423	18.27	*
23	**5**$^{+}$	CH_3	321	501	11193	3.45	*
24	**5**$^{+}$@CB[7]	CH_3	330	499	10263	7.83	*
25	**5**$^{+}{}_2$@CB[8]$_2$	CH_3	360	536	9121	42.42	*
26	**5**H^{2+}	CH_3	344	*	-	*	*
27	**5**H^{2+}@CB[7]	CH_3	363	*	-	0.70	*
28	**5**H$^{2+}{}_2$@CB[8]$_2$	CH_3	391	560	7718	10.12	*
29	**6**$^{+}$	Br	318	638	15773	2.00	*
30	**6**$^{+}$@CB[7]	Br	327	549	12366	4.31	*
31	**6**$^{+}{}_2$@CB[8]$_2$	Br	353	521	9135	4.50	*
32	**6**H^{2+}	Br	343	*	-	*	*
33	**6**H^{2+}@CB[7]	Br	353	*	-	0.52	*
34	**6**H$^{2+}{}_2$@CB[8]$_2$	Br	380	601	9677	1.98	*

35	**7**$^{+}$	CH_2OH	314	497	11726	12.64	*
36	**7**$^{+}$@CB[7]	CH_2OH	320	544	11291	29.46	*
37	**7**$^{+}{}_2$@CB[8]$_2$	CH_2OH	341	489	8876	42.49	*
38	**7**H^{2+}	CH_2OH	331	*	-	*	*
39	**7**H^{2+}@CB[7]	CH_2OH	342	*	-	2.35	*
40	**7**$H^{2+}{}_2$@CB[8]$_2$	CH_2OH	366	551	9174	11.95	*
41	**8**$^{2+}$	H	345	620	12856	0.16	*
42	**8**$^{2+}$@CD	H	345	582	11803	0.30	*
43	**8**$^{2+}$@CB[7]	H	362	617	11417	0.38	*
44	**8**$^{2+}{}_2$@CB[8]$_2$	H	385	580	8733	7.81	5.28

$\lambda_{ex} = \lambda_{abs}$; * values were not determined

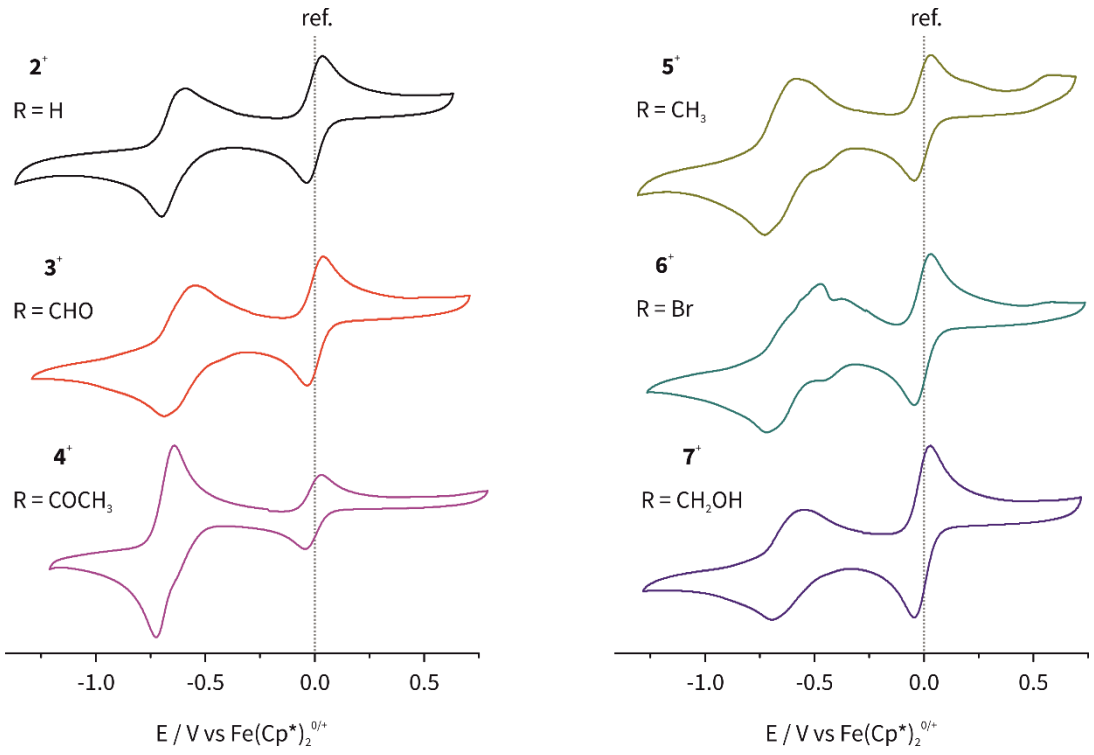

Figure 59. Cyclic voltammograms (DMF, 298 K, 1 mM, 100 mV·s^{-1}) of bipyridinium species **2**$^{+}$–**7**$^{+}$ using *n*-Bu_4NPF_6 (0.1 M) as the electrolyte. Decamethylferrocene ($Fe(Cp^*)_2$) was used as the internal standard.

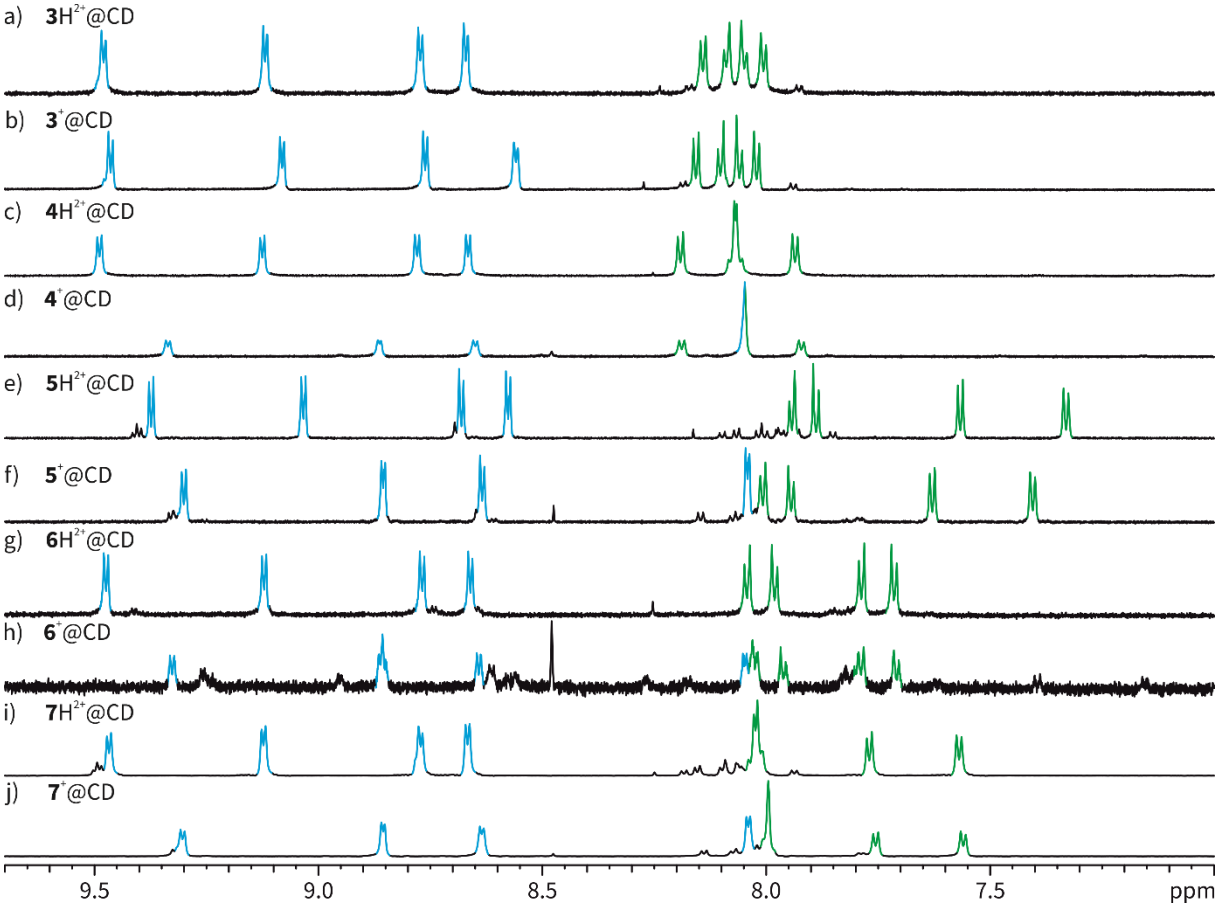

Figure 60. Partial ^{1}H NMR spectra (700 MHz, 298 K, D_2O, 1.0 mM) of (a) a 1:1 mixture of **3**H^{2+} and β-CD, (b) a 1:1 mixture of **3**$^{+}$ and β-CD, (c) a 1:1 mixture of **4**H^{2+} and β-CD, (d) a 1:1 mixture of **4**$^{+}$ and β-CD, (e) a 1:1 mixture of **5**H^{2+} and β-CD, (f) a 1:1 mixture of **5**$^{+}$ and β-CD, (g) a 1:1 mixture of **6**H^{2+} and β-CD, (h) a 1:1 mixture of **6**$^{+}$ and β-CD, (i) a 1:1 mixture of **7**H^{2+} and β-CD and (j) a 1:1 mixture of **7**$^{+}$ and β-CD; DCl (35% in D_2O) and K_2CO_3 were used to (de)protonate.

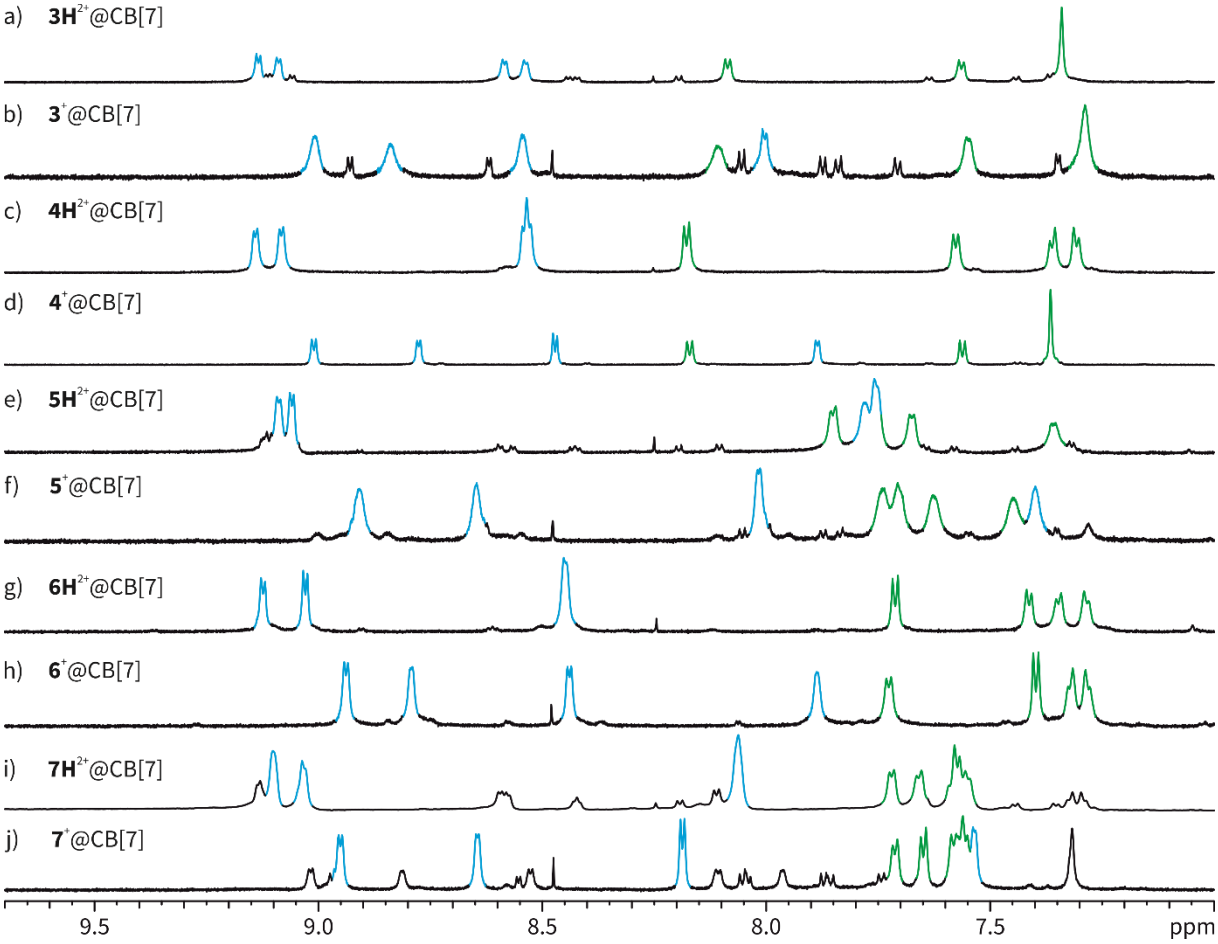

Figure 61. Partial ^{1}H NMR spectra (700 MHz, 298 K, D_2O, 1.0 mM) of (a) a 1:1 mixture of **3**H^{2+} and CB[7], (b) a 1:1 mixture of **3**$^{+}$ and CB[7], (c) a 1:1 mixture of **4**H^{2+} and CB[7], (d) a 1:1 mixture of **4**$^{+}$ and CB[7], (e) a 1:1 mixture of **5**H^{2+} and CB[7], (f) a 1:1 mixture of **5**$^{+}$ and CB[7], (g) a 1:1 mixture of **6**H^{2+} and CB[7], (h) a 1:1 mixture of **6**$^{+}$ and CB[7], (i) a 1:1 mixture of **7**H^{2+} and CB[7] and (j) a 1:1 mixture of **7**$^{+}$ and CB[7]; DCl (35% in D_2O) and K_2CO_3 were used to (de)protonate.

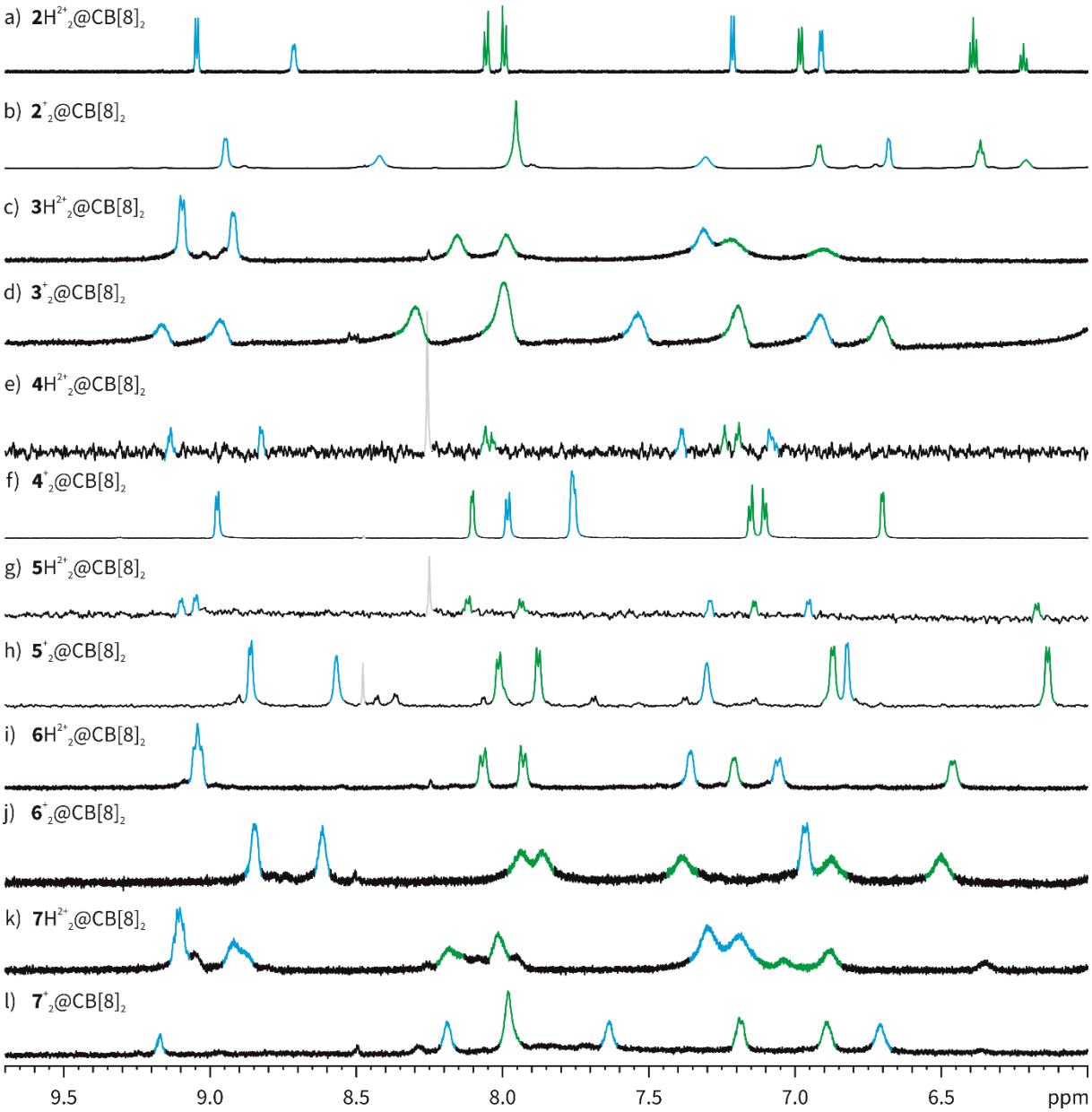

Figure 62. Partial ^{1}H NMR spectra (700 MHz, D_2O, 1.0 mM) of (a) a 1:1 mixture of **3**H^{2+} and CB[8], (b) a 1:1 mixture of **3**$^{+}$ and CB[8], (c) a 1:1 mixture of **4**H^{2+} and CB[8], (d) a 1:1 mixture of **4**$^{+}$ and CB[8], (e) a 1:1 mixture of **5**H^{2+} and CB[8], (f) a 1:1 mixture of **5**$^{+}$ and CB[8], (g) a 1:1 mixture of **6**H^{2+} and CB[8], (h) a 1:1 mixture of **6**$^{+}$ and CB[8], (i) a 1:1 mixture of **7**H^{2+} and CB[8] and (j) a 1:1 mixture of **7**$^{+}$ and CB[8]; a, b, e, f, g, h at 298 K, c, d, i, j, k, l at 333 K; DCl (35% in D_2O) and K_2CO_3 were used to (de)protonate.

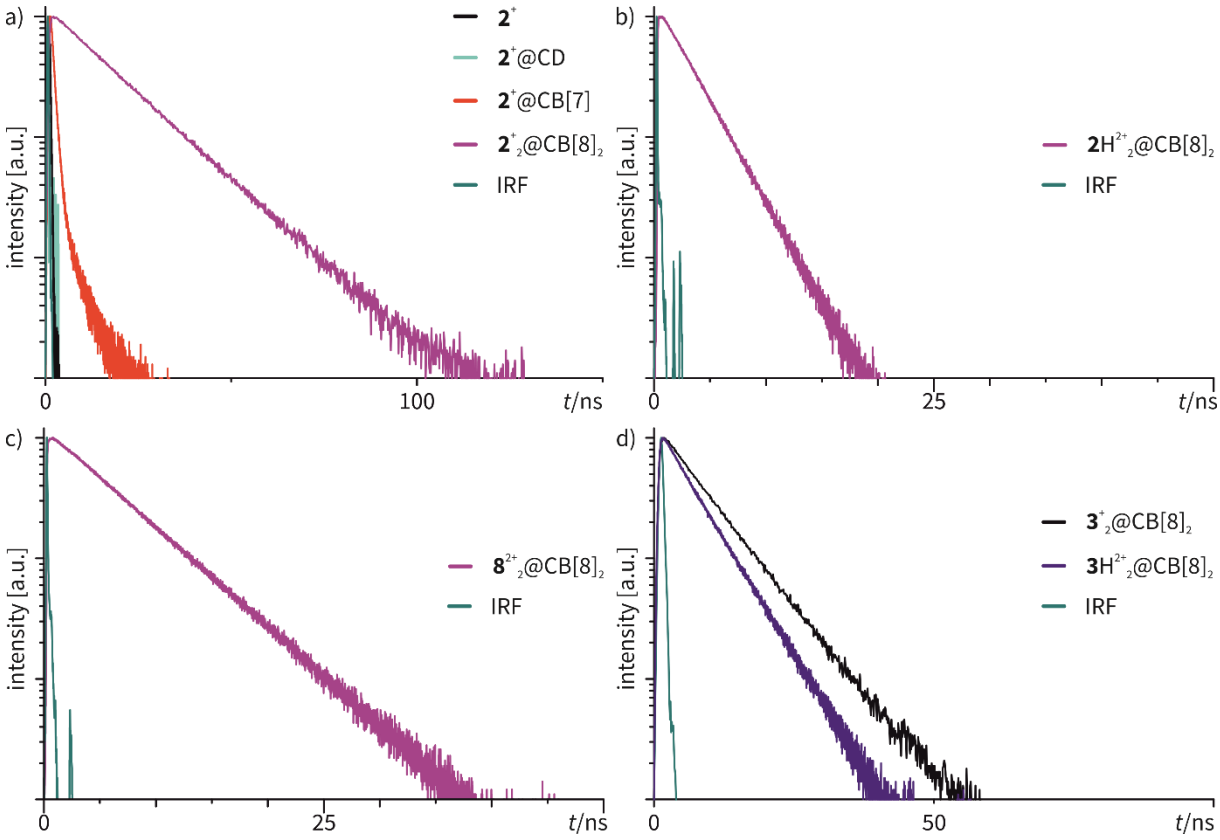

Figure 63. Fluorescence decays of (a) **2**$^{+}$ and its complexes, (b) **2**H^{2+}@CB[8], (c) **8**$^{2+}$@CB[8] and (d) **3**H^{2+}@CB[8] and **3**$^{+}$@CB[8] ($\lambda_{ex} = \lambda_{abs}$).

4.2 Complexation of 4-Phenylpyridinium Derivatives with Cucurbit[8]uril

The stimuli-responsive 2:2 CB[8] complexes of the last Chapter changed their emission properties upon (de)protonation, but kept their 2:2 conformation. Therefore, a host–guest system should be designed that changes its guests upon addition of an external input. As a first step, the complex formation of 4-phenylpyridinium derivatives with CB[*n*]s and the characteristics as potential building blocks should be evaluated (Chapter 4.2) and on the basis of these results a stimulus-responsive system should be designed (Chapter 4.3).

A series of compounds was synthesized and the host-guest complexation was investigated. The common motifs are the 4-phenylpyridinium moieties, which is either protonated at the nitrogen atom or substituted by an alkyl chain with different functional groups or electron rich aromatic systems. Furthermore, two 4-phenylpyridiniums are connected by a short and a longer alkyl chain to test the possibility of supramolecular polymerization.

4.2.1 A Simple 4-Phenylpyridinium Derivative

Since phenylpyridine is barely soluble in aqueous solutions even in its protonated form, 4-(pyridine-4-yl)phenol (**9**) was synthesized *via* Suzuki reaction of commercially available 4-hydroxyphenylboronic acid and 4-bromopyridine hydrochloride with 54% yield (Scheme 2). The quantity of the product was sufficient and so no optimization was conducted. Compound **9** is water soluble upon protonation.

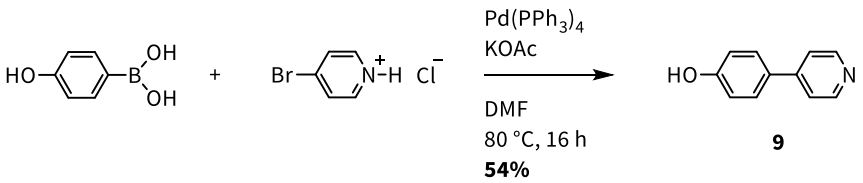

Scheme 2. Synthesis of 4-phenylpyridinium derivative **9** *via* Suzuki reaction.

The ^{1}H NMR spectrum of protonated **9**H^{+} in D_2O shows four clear cut signals for the aromatic protons without any overlap (Figure 64a). Upon addition of 1 equivalents of CB[7] all signals exhibit a high field shift and a strong broadening (b). These complexation induced shifts speak in favor for the formation of the 1:1 complex **9**H^{+}@CB[7]. MS analysis shows the complex at *m/z* 1334, but decomplexation occurs because of the harsh conditions during the ionization process resulting in free guest at *m/z* 172 (Figure 66). A 2.1:1.0 mixture of **9**H^{+} and the bigger host CB[8] clearly shows two set of signals (Figure 64c), one for the free guest an one for a newly formed 1:2 homoternary complex **9**H$^{+}_2$@CB[8] with complexation induced shifts similar to phenylpyridine derivative complexes in the literature.[45a] The presence of two set of signals indicate that the formation of the complex is faster

than the NMR time scale, which is expected for cucurbituril complexes.[6] An excess of CB[8] has no influence on the 1:2 complex (d).

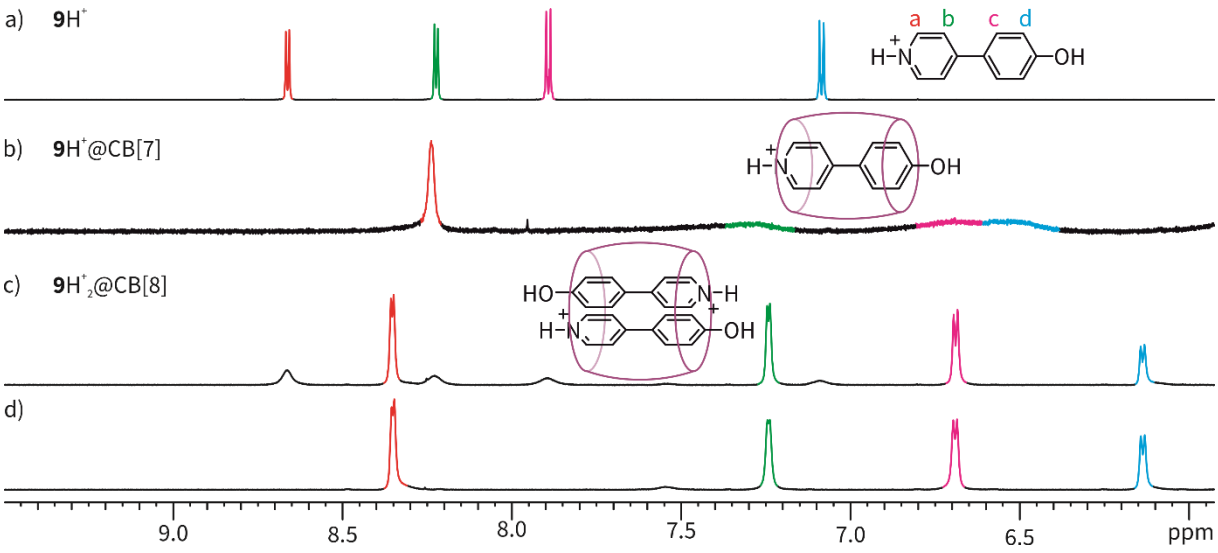

Figure 64 Partial ^{1}H NMR spectra (700 MHz, 298 K, D_2O, 1.0 mM) of (a) **9**H$^+$, (b) a 1:1 mixture of **9**H$^+$ and CB[7], (c) a 2.1:1 mixture of **9**H$^+$ and CB[8] and (d) a 1:1 mixture of **9**H$^+$ and CB[8]; all at pH 4, DCl (35% in D_2O) was used to protonate.

The stoichiometry of **9**H$^+_2$@CB[8] was validated by Job plot analysis as shown in Figure 65.[119] The intersection of the fitted lines of the Job plot is not exactly at 0.33, as it would be for a 1:2 complex. This can be attributed to the poor solubility of the host in aqueous solutions. Therefore it was complicated to match the concentration of the CB[8] solution and the values are not on point.

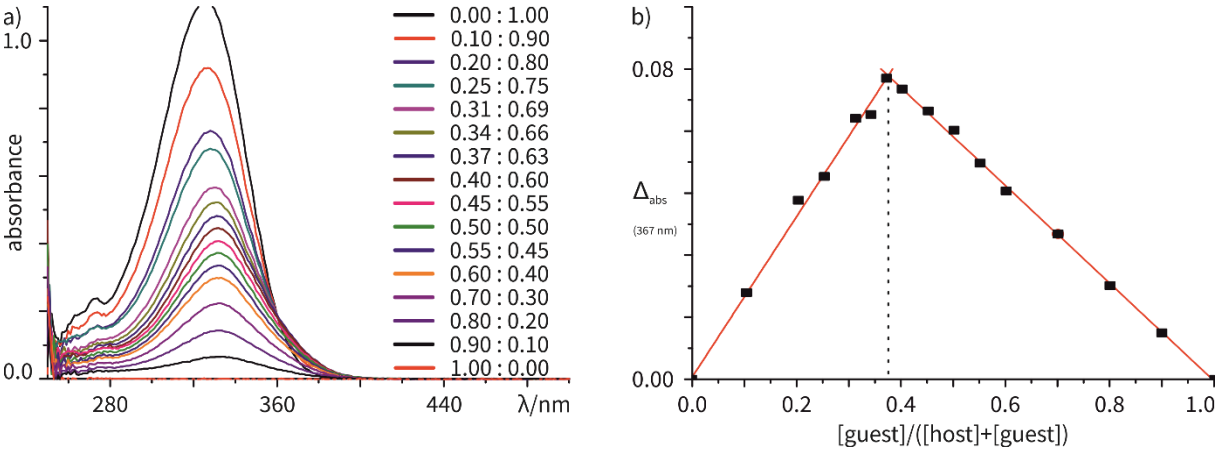

Figure 65. (a) UV/Vis spectra of host–guest mixtures of **9**H$^+$ and CB[8] (c = 0.12 mM) and (b) Job plot analysis at 367 nm.

The charge repulsion of the two guests inside the CB[8] leads to quick dissociation in the gas phase which makes MS analysis challenging (Figure 66). An aqueous solution of **9**H$^+_2$@CB[8] was measured at a ESI-TOF instrument with different fragmentor voltages. At 430 V only the 1:1 complex **9**H$^+$@CB[8] at *m/z* 1500 and free guest can be observed (b). Reducing the voltage to 200 V, however, results in complete disappearance of the 1:1 complex and the free guest, but a signal for the doubly charged 2:1 complex **9**H$^+_2$@CB[8] at *m/z* 836 can be detected (c).

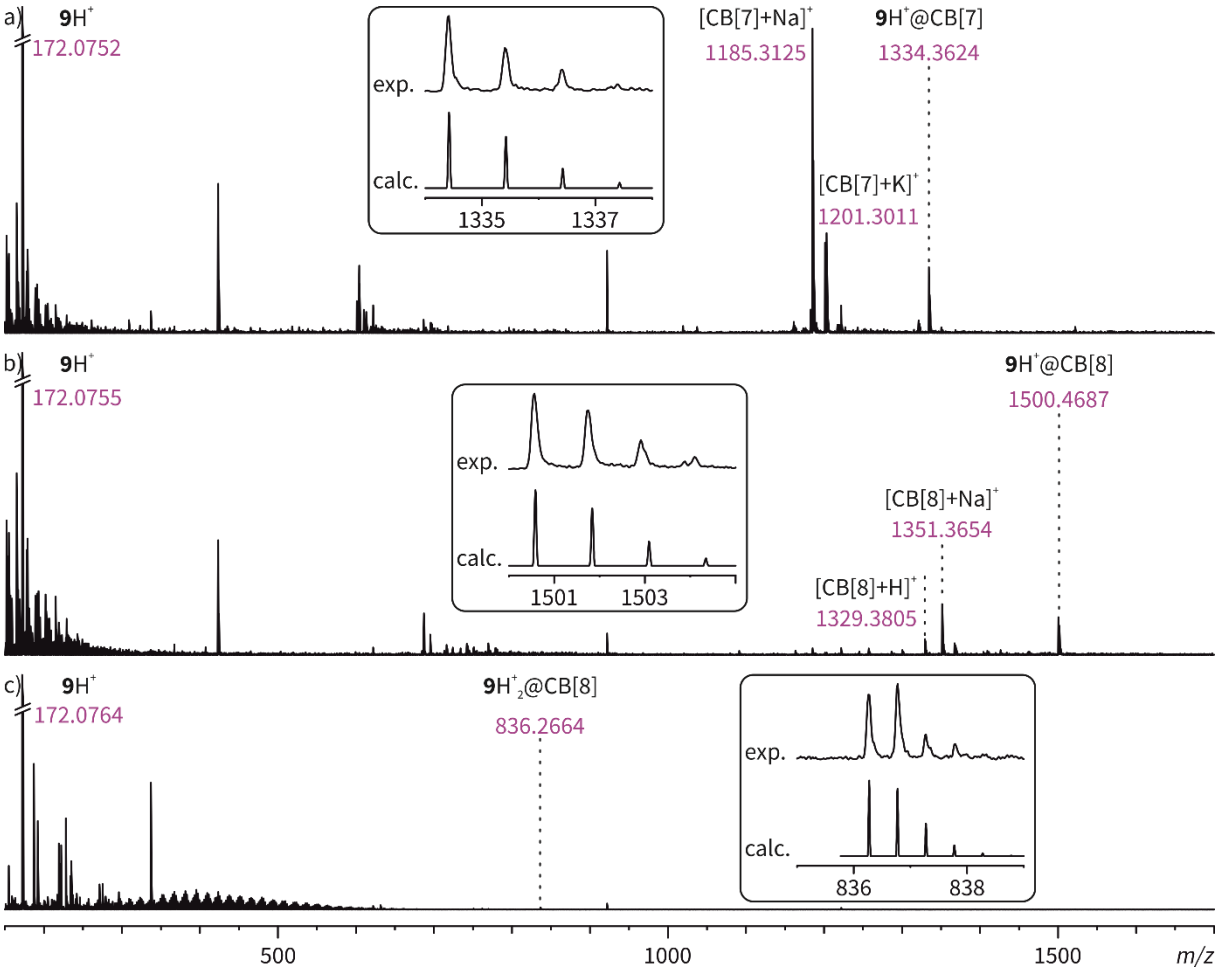

Figure 66. ESI-ToF spectra of (a) **9**H$^+$@CB[7] at a fragmentor voltage of 430 V, (b) **9**H$^+_2$@CB[8] at a fragmentor voltage of 430 V and (c) **9**H$^+_2$@CB[8] at a fragmentor voltage of 200 V with isotope patterns.

In literature methyl viologen (**MV**$^{2+}$) is used as a standard viologen derivative. The very toxic and volatile methyl iodide is the starting material for preparation of **MV**$^{2+}$. Due to the toxicity this strategy was abandoned and ethyl viologen (**V**$^{2+}$), deriving from the non-toxic ethyl iodide, was used in the cause of this thesis. The association constants of the phenylpyridinium–CB[8] 2:1 complexes are higher than the one of the viologen–CB[8] 1:1 complexes.[6] To see if this holds true for **9**H$^+$ and **V**$^{2+}$, the ^{1}H NMR spectra a 2:1:1 mixture of **9**H$^+$, **V**$^{2+}$ and CB[8] was compared to the ones of **9**H$^+_2$@CB[8], **V**$^{2+}$@CB[8] and **V**$^{2+}$ (Figure 67). The mixture of the two different guests and the host clearly show the signals of uncomplexed **V**$^{2+}$ and the complex **9**H$^+_2$@CB[8]. This means there is no unexpected interaction between the components of the mixture and no formation of a new complex.

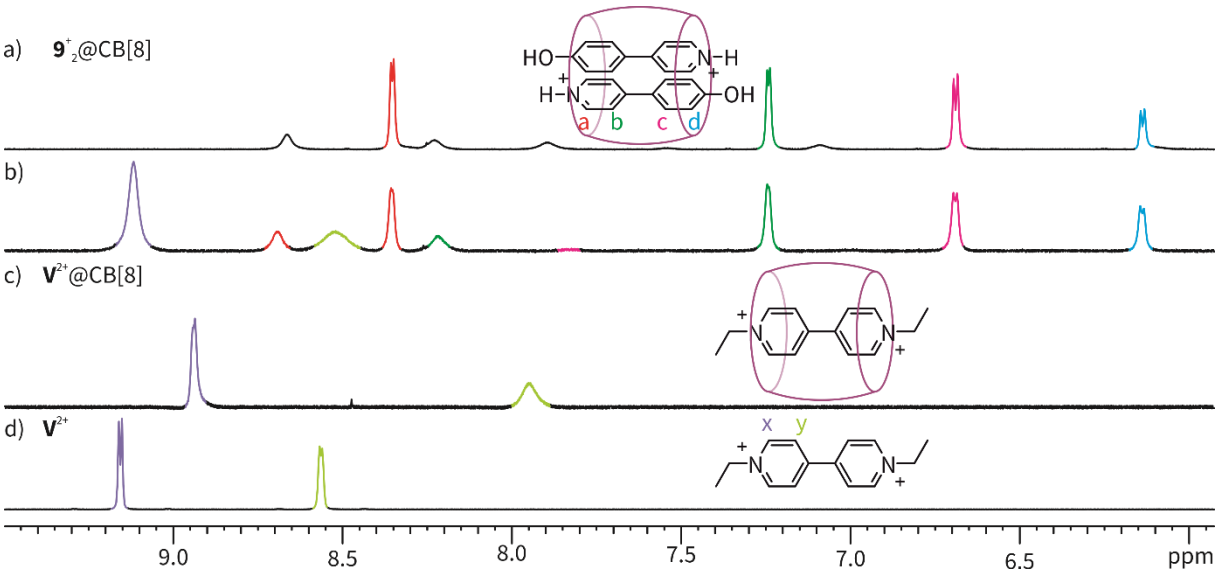

Figure 67. Partial ^{1}H NMR spectra (700 MHz, 298 K, D_2O, 1.0 mM) of (a) **9**H^+_2@CB[8], (b) a 2:1:1 mixture of **9**H^+, $\mathbf{V}^{2+}$ and CB[8], (c) a 1:1 mixture of $\mathbf{V}^{2+}$ and CB[8] and (d) $\mathbf{V}^{2+}$; (a) and (b) at pH 4, DCl (35% in D_2O) was used to protonate.

4.2.2 Phenylpyridinium with Functionalizable *N*-Substituents

For the development of larger supramolecular architectures with CB[8]s, it is important to be able to further substitute the guests after complex formation. In this context, the complexation of 4-phenylpyridinium derivatives with *N*-substitution that bear different functional groups was investigated.

1-(11-Hydroxyundecyl)-4-phenylpyridin-1-ium chloride (**10**$^+$) was chosen as an example with nucleophilic functional group at the side chain. Compound **10**$^+$ was synthesized from commercially available 4-phenylpyridine and 11-bromo-1-undecanol by nucleophilic substitution in DMF and subsequent anion exchange in 35% yield as the chloride salt (Scheme 3), which is soluble in water.

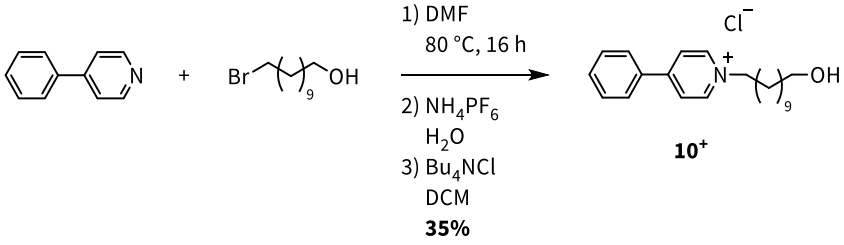

Scheme 3. Synthesis of 4-phenylpyridinium derivative **10**$^+$.

Figure 68 shows the ^{1}H NMR spectra of **10**$^+$ and its homoternary CB[8] complex **10**$^+_2$@CB[8] in D_2O. The signals of the aromatic protons H_d and H_e of the free guests overlap, and the CB[8] complex exhibits the complexation induced shifts as seen before. Since there are no more signals of the free guest after addition of 0.5 equivalents of host formation of a 2:1 complex can be assumed. The signals of the protons of the host at ~5.8 ppm and ~5.5 ppm are shown in the Figure.

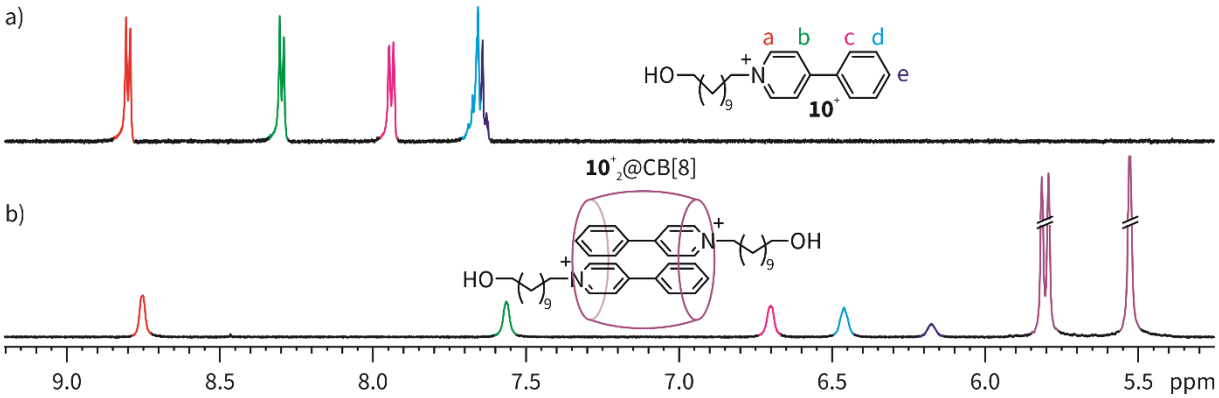

Figure 68. Partial ^{1}H NMR spectra (700 MHz, 298 K, D_2O, 1.0 mM) of (a) **10**$^+$ and (b) a 2:1 mixture of **10**$^+$ and CB[8].

The stoichiometry of the complex is validated by mass spectrometry (Figure 69). As before, high fragmentor voltage (430 V) leads to complete dissociation of the 2:1 complex **10**$^+_2$@CB[8] (*m/z* 990) to the 1:1 complex **10**$^+$@CB[8] (*m/z* 1655). Furthermore, the guest **10**$^+$ fragments to protonated 4-phenylpyridine (*m/z* 156). If the fragmentor voltage is reduced to 200 V, the 2:1 complex **1**$^+_2$@CB[8] (*m/z* 990) can be observed besides a doubly charged dissociation complex at *m/z* 827 which corresponds to the 1:1 complex [**10**@CB[8]+H]$^{2+}$.

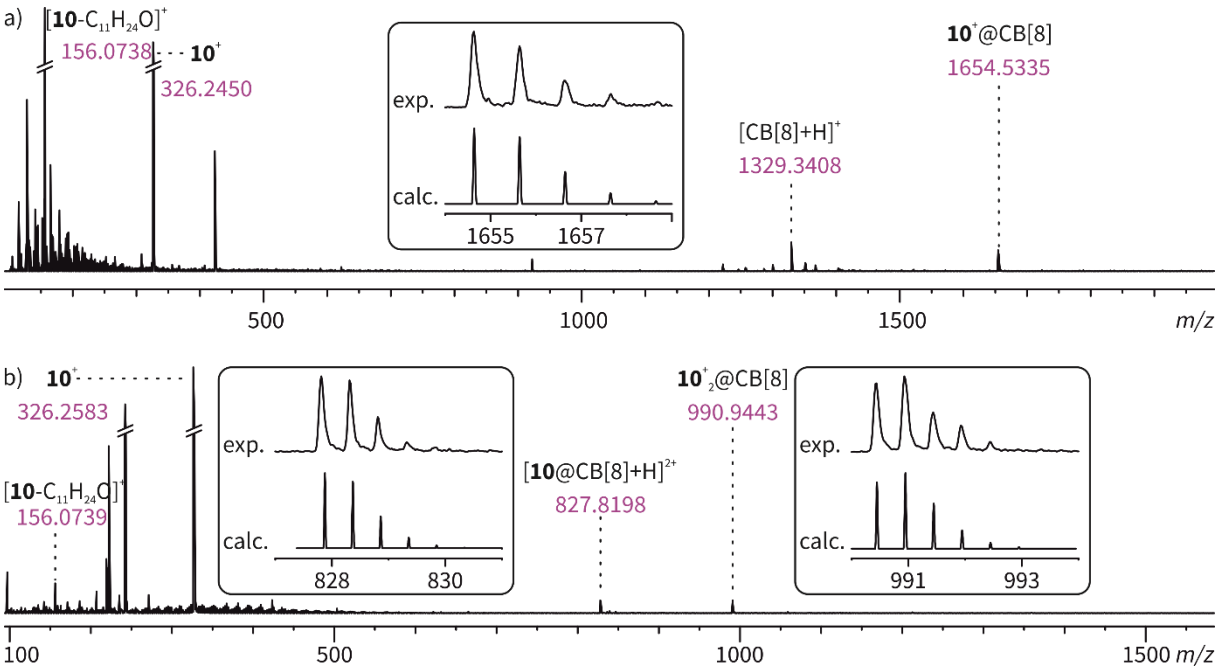

Figure 69. ESI-ToF spectra of (a) **10**$^+_2$@CB[8] at 430 V and (b) **10**$^+_2$@CB[8] at a fragmentor voltage 200 V with isotope patterns.

The substitution of the phenylpyridinium derivative with a nucleophilic functional group has no influence on the host–guest properties with CB[8]. Therefore, further reactions at the hydroxy group are possible and allow the application of **10**$^+$ as a nucleophilic building block.

1-(4-Bromobutyl)-4-phenylpyridin-1-ium bromide (**11**$^+$) was investigated as phenylpyridinium derivative with electrophilic functional group at the side chain. Compound **11**$^+$ was synthesized from

commercially available 4-phenylpyridine and 1,4-dibromobutane in DMF by nucleophilic substitution in 93% yield (Scheme 4). Purification was not necessary.

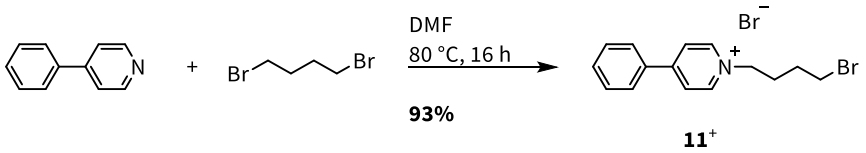

Scheme 4. Synthesis of 4-phenylpyridinium derivative **11**$^+$.

The ^{1}H NMR spectra of **11**$^+$ and the 2:1 mixture of **11**$^+$ and CB[8] in D_2O show the formation of the complex **11**$^+_2$@CB[8] with the complexation induced high field shifts analogous to the complexes shown before (Figure 70). Additionally, the signals of the protons of the host at 5.8 ppm and 5.5 ppm are shown in the Figure.

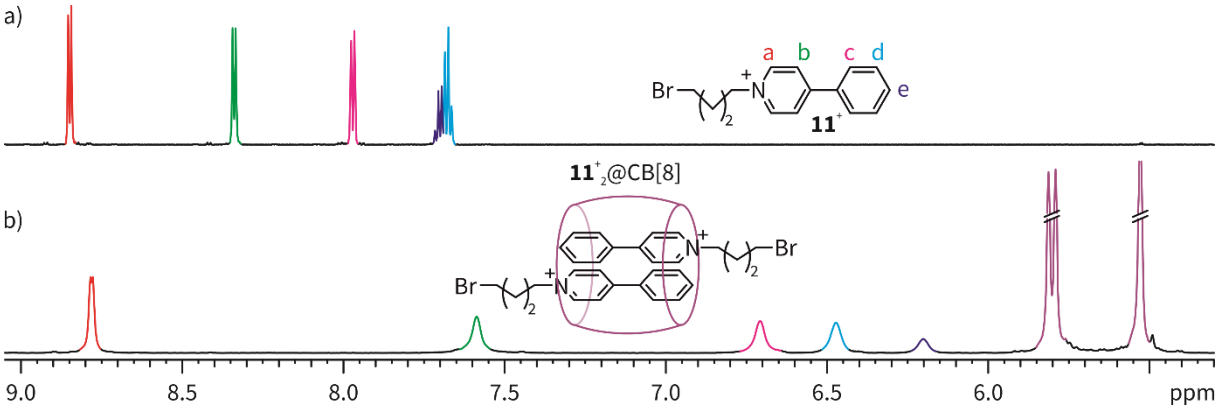

Figure 70. Partial ^{1}H NMR spectra (700 MHz, 298 K, D_2O, 1.0 mM) of (a) **11**$^+$ and (b) a 2:1 mixture of **11**$^+$ and CB[8].

The substitution of the phenylpyridinium derivative with an electrophilic functional group has no influence on the host–guest properties with CB[8]. Therefore, further reactions are possible and allow the application of **11**$^+$ as an electrophilic building block.

4.2.3 4-Phenylpyridinium with Electron-Rich Moieties

The complexation of 4-phenylpyridinium derivatives with different electron-rich apolar substituents were studied to investigate the solubility of the formed complex and the potential formation of π-donor-π-acceptor complexes inside the cavity of the CB[8].

The solubility in aqueous media is a crucial condition for the host–guest chemistry with CB[8]. Both the guest as well as the product need to be soluble. If the two charges of the formed complex are located deep inside the cavity of the host, the formed supramolecular complex precipitates. In order to pinpoint the limitations arising from low solubility the CB[8] complex of 1-(Anthracen-9-ylmethyl)-4-phenylpyridin-1-ium chloride (**12**$^+$) was investigated. The large unpolar anthracene moiety of **12**$^+$ could impair the solubility of the complex. It was synthesized from commercially available

4-phenylpyridine and 9-(chloromethyl)anthracene in DMF by nucleophilic substitution in 31% yield (Scheme 5). Purification *via* ion exchange was not necessary and the quantity of the product was sufficient, so no optimization was conducted. Compound **12**$^+$ is water soluble despite the large apolar moiety.

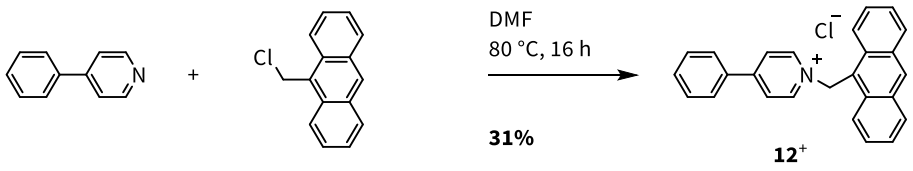

Scheme 5. Synthesis of 4-phenylpyridinium derivative **12**$^+$.

The ^{1}H NMR spectrum of **12**$^+$ in D_2O exhibits one clear set of signals (Figure 71a). Addition of 0.5 equiv. of CB[8] changes the spectrum in an unexpected manner (b). First, there are no signals for the host, which usually appear between 5.5 and 6.0 ppm (see Figure 68 and 70). Second, no complexation induced high field shifts can be observed and third, it seems like all signals exhibit a low field shift. Since there is no indication for host or complexed guest, it is assumed, that all the formed complex precipitated. And the presumable low field shift of the remaining guest may be due to disturbances during the measurement because of the precipitate in NMR tube.

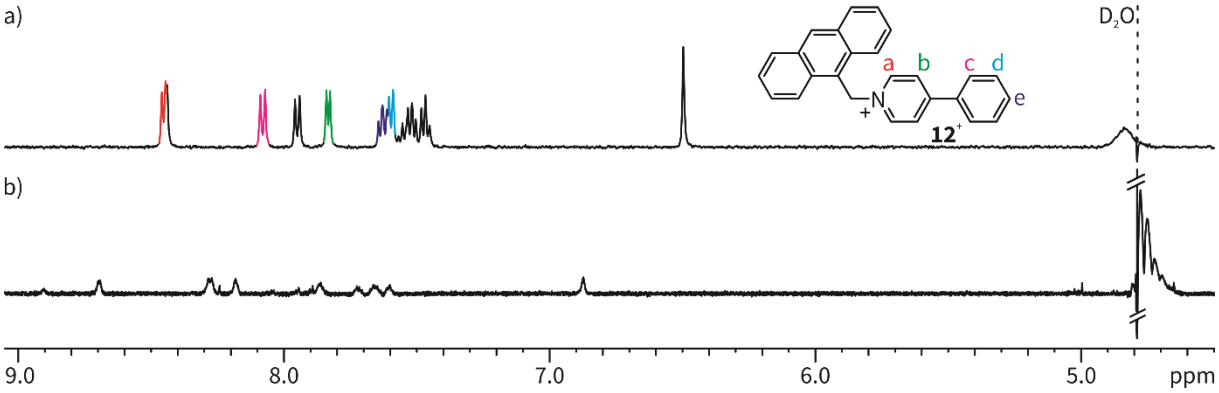

Figure 71. Partial ^{1}H NMR spectra (700 MHz, 298 K, D_2O, 1.0 mM) of (a) **12**$^+$ and (b) a 2:1 mixture of **12**$^+$ and CB[8].

This result shows that complex formation presumably takes place, but that the solubility of the formed product is too poor to perform NMR measurements. Since UV/Vis measurements can be performed at lower concentrations, a Job plot analysis was conducted and indicated the 2:1 stoichiometry of the complex **12**$^+_2$@CB[8] (Figure 72). Consequentially, the solubility of complexes with apolar moieties can be very poor which leads to precipitation. This should be kept in mind while designing potential 4-phenylpyridinium guests for CB[8].

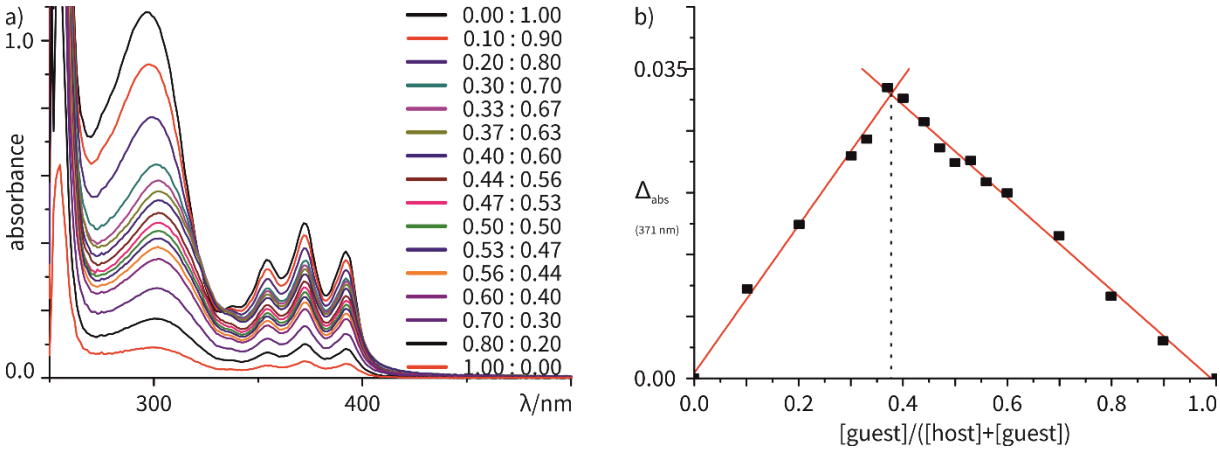

Figure 72. (a) UV/Vis spectra of host–guest mixtures of **12**$^+$ and CB[8] (c = 0.12 mM) and (b) Job plot analysis at 371 nm.

The electron poor viologen and an electron rich counterpart are known to form π-donor-π-acceptor complexes in the cavity of the CB[8] (see Chapter 3.1.2).[44a] To see if the phenylpyridinium derivates behave similar, 1-(2-(Naphthalen-2-yloxy)ethyl)-4-phenylpyridin-1-ium chloride (**13**$^+$) was investigated. It was synthesized from commercially available 4-phenylpyridine and 2-(2-bromoethoxy)naphthalene[2] in DMF by nucleophilic substitution and subsequent ion exchange in 9% yield (Scheme 6). The quantity of the product was sufficient, so no optimization was conducted.

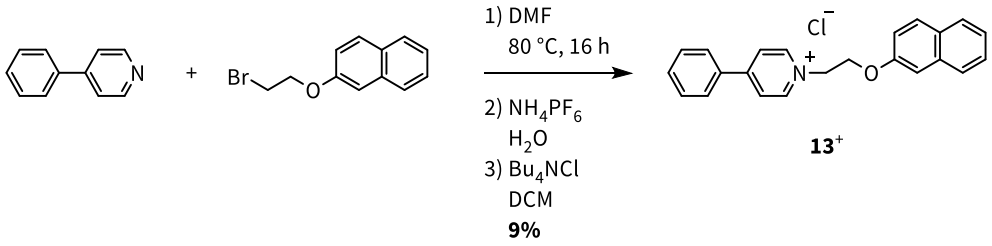

Scheme 6. Synthesis of 4-phenylpyridinium derivative **13**$^+$.

The ^{1}H NMR spectra of **13**$^+$ and of the 2:1 mixture of **13**$^+$ and CB[8] in D_2O show that the formed complex is not soluble in aqueous medium and precipitates (Figure 73). Complexation with CB[8] can have two possible outcomes. Either the phenylpyridinium moiety forms a homoternary CB[8] complex with another phenylpyridinium resulting in **13**$^+_2$@CB[8] or a heteroternary CB[8] complex with the naphthalene moiety as **13**$^+_2$@CB[8]$_2$. The stoichiometry of the complex cannot be determined based on the NMR, but the large amount of free **13**$^+$ in the mixture solution speaks in favor of the heteroternary complex.

[2] Synthesis and Analysis by Dr. Wei Jiang.

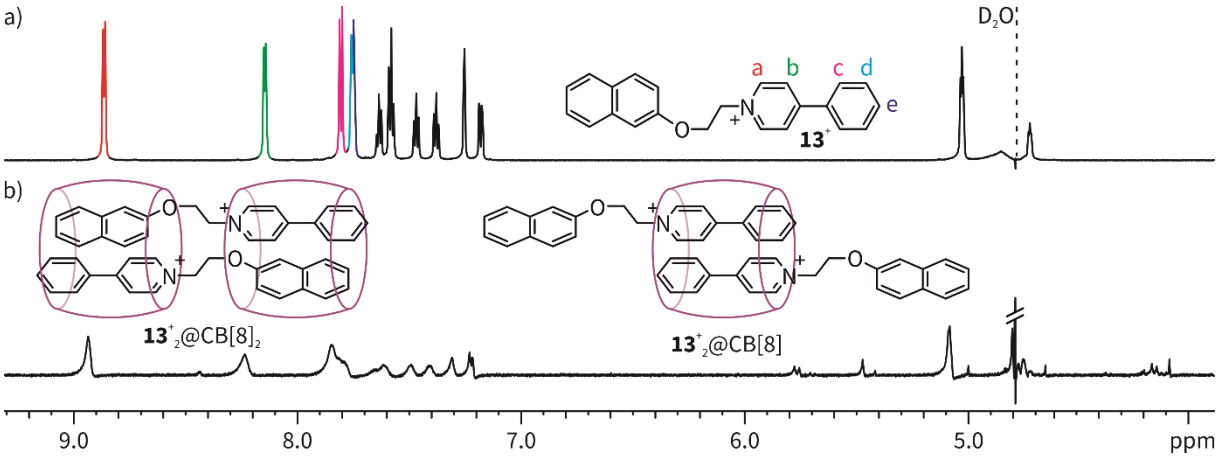

Figure 73. Partial ^{1}H NMR spectra (700 MHz, 298 K, D_2O, 1.0 mM) of (a) **13**$^{+}$ and (b) a 2:1 mixture of **13**$^{+}$ and CB[8].

The stoichiometry differs for homo- (1:2) and heteroternary (2:2) complexes (Figure 74). Job plot analysis delivers a *n*:*n* complex as a result which means that a heteroternary 2:2 complex **13**$^{+}_2$@CB[8]$_2$ is formed. Consequentially, a π-donor-π-acceptor complex of electron-poor phenylpyridinium and electron-rich naphthalene is possible.

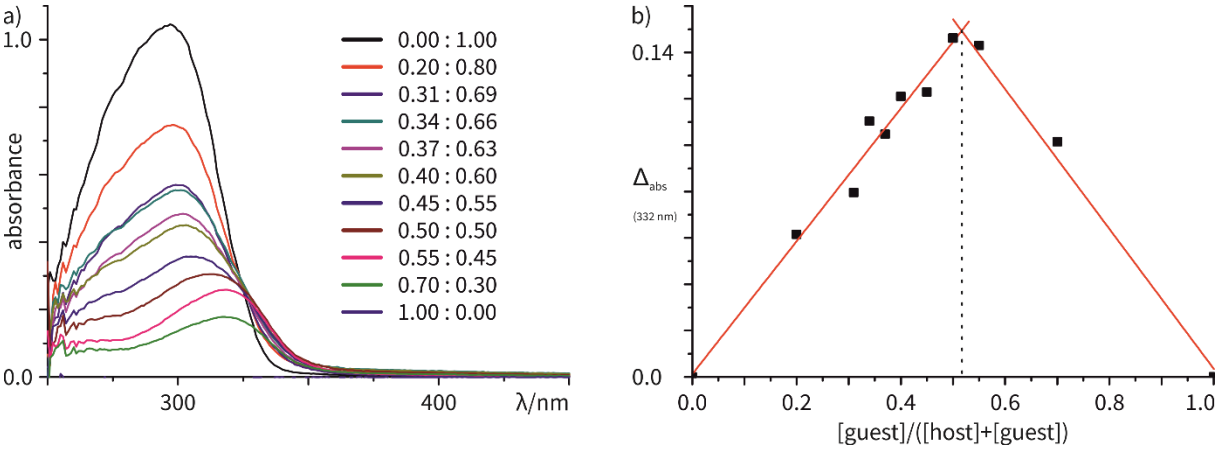

Figure 74. (a) UV/Vis spectra of host–guest mixtures of **13**$^{+}$ and CB[8] (c = 0.12 mM) and (b) Job plot analysis at 332 nm.

4.2.4 Supramolecular Polymers Based on 4-Phenylpyridines

The formation of supramolecular polymers gains great attention and can be achieved by linear molecules with binding sites for CB[8] on both ends.[46] For this reason 1,1'-(dodecane-1,12-diyl)bis(4-phenylpyridin-1-ium) bromide (**14**$^{2+}$), which consists of two phenylpyridine moieties connected by a relatively long alkyl chain, was investigated. It was synthesized from commercially available 4-phenylpyridine and 1,12-dibromododecane in DMF by nucleophilic substitution in 49% yield (Scheme 7). Purification was not necessary and the quantity of the product was sufficient, so no optimization was conducted.

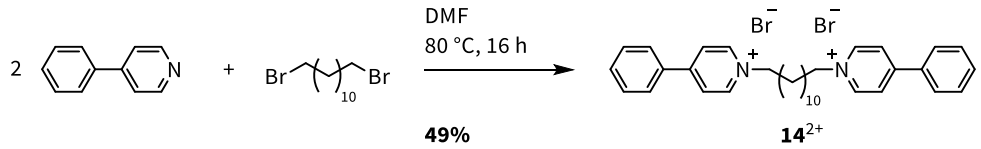

Scheme 7. Synthesis of 4-phenylpyridinium derivative **14**$^{2+}$.

The ^{1}H NMR spectrum of a 1:1 mixture of compound **14**$^{2+}$ and CB[8] in D_2O recorded after 1 h shows the expected complexation induced shifts of the dimer formation of the phenylpyridinium moieties inside the cavity of the host (Figure 75), whereby it should be noted, that the signal at 8.75 ppm cannot be assigned. It can be assumed that a supramolecular polymer SP-**14**$^{2+}$@CB[8] formed as represented by the cartoon. If the same solution is measured again after 16 h, a new set of signals appears. The signals of the new species exhibit a less pronounced high field shift and are broadened. The new complex cannot be clearly identified. It could be possibly attributed to the formation of a *syn* dimer inside the cavity of complex **14**$^{2+}$@CB[8] in a similar way as represented by the cartoon. A somewhat similar *syn* CB[8] complex was reported for styrylpyridiniums which are *N*-substituted with differently sized alkyl chains.[125] Although, a complex of a phenylpyridinium derivative with a head to head arrangement in this manner is not reported yet. It should be noted that the ratio of the complexes should be concentration dependent, but the measurements were only conducted at a CB[8] concentration of 1 mM.

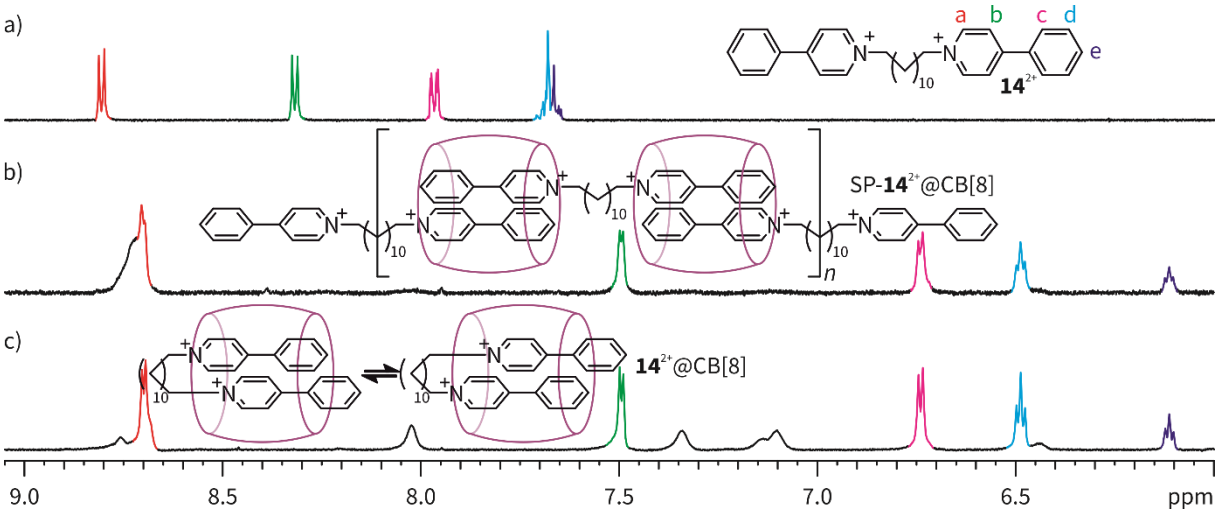

Figure 75. Partial ^{1}H NMR spectra (700 MHz, 298 K, D_2O, 1.0 mM) of (a) **14**$^{2+}$, and a 1:1 mixture of **14**$^{2+}$ and CB[8] after (b) 1 h and (c) 16 h.

A Job plot analysis was conducted, and the intersection of the fitted lines is at 0.49 which is in line with the two proposed *n*:*n* complexes SP-**14**$^{2+}$@CB[8] and **14**$^{2+}$@CB[8] (Figure 76). Still, since there is more than one complex formed in the solution, the result should be interpreted with caution.[126]

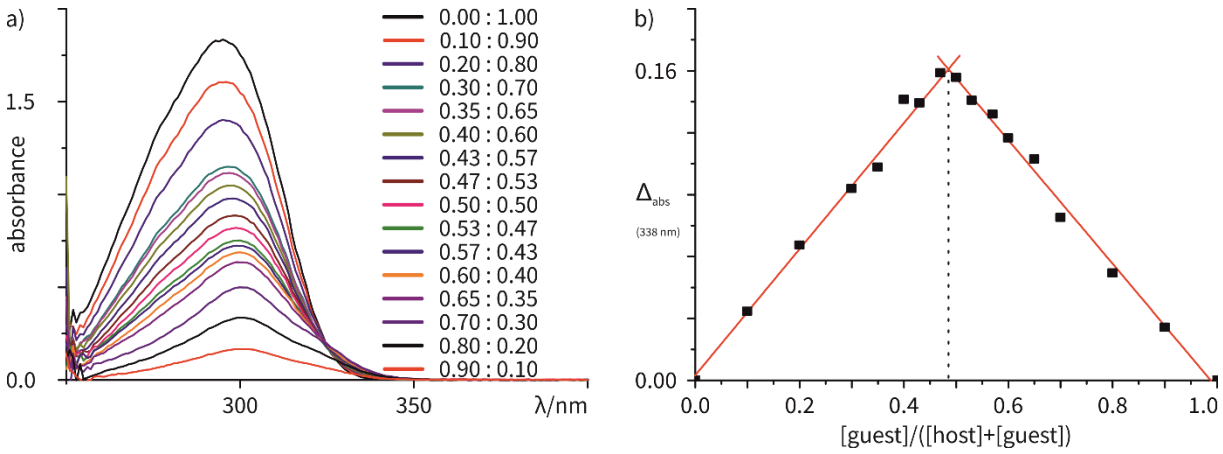

Figure 76. (a) UV/Vis spectra of host–guest mixtures of **14**$^{2+}$ and CB[8] (c = 0.12 mM) and (b) Job plot analysis at 338 nm.

As a second compound for the potential formation of a supramolecular polymer 1,1'-(propane-1,3-diyl)bis(4-phenylpyridin-1-ium) chloride (**15**$^{2+}$) was synthesized from commercially available 4-phenylpyridine and 1,3-dibromopropane in DMF by nucleophilic substitution and subsequent ion exchange in 23% yield (Scheme 8). The quantity of the product was sufficient, so no optimization was conducted.

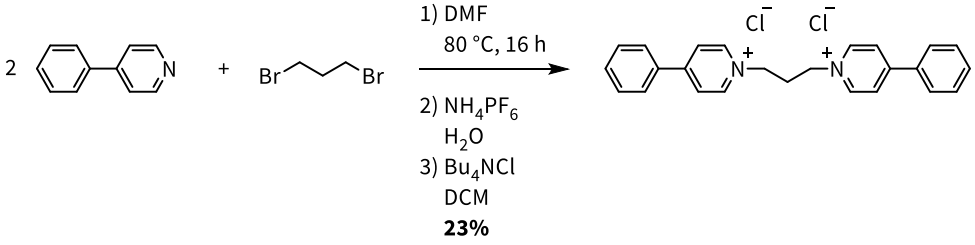

Scheme 8. Synthesis of 4-phenylpyridinium derivative **15**$^{2+}$.

The ^{1}H NMR spectrum of a 1:1 mixture of compound **15**$^{2+}$ and CB[8] in D_2O recorded after 1 h shows three sets of signals (Figure 77, each set is marked in a different color). It can be assumed, that analogues to before, the supramolecular polymer SP-**15**$^{2+}$@CB[8] (green) and the proposed *syn* dimer complex **15**$^{2+}$@CB[8] (dark blue) form. The third set of signals (orange) exhibit a down field shift of H_a to 9.2 ppm. The possible structure *l***15**$^{2+}$@CB[8] of this complex is represented as a cartoon. The host is located on the alkyl linker with both rims stabilizing the positive charges as shown with similar viologen derivatives.[127] The ^{1}H NMR spectrum of the same solution after 16 h shows only slight changes in the ratio of the three complexes, but no formation of a new one. As in the experiment above (Chapter 4.2.6), the ratio of the complexes should be concentration dependent, but the measurements were only conducted at a CB[8] concentration of 1 mM.

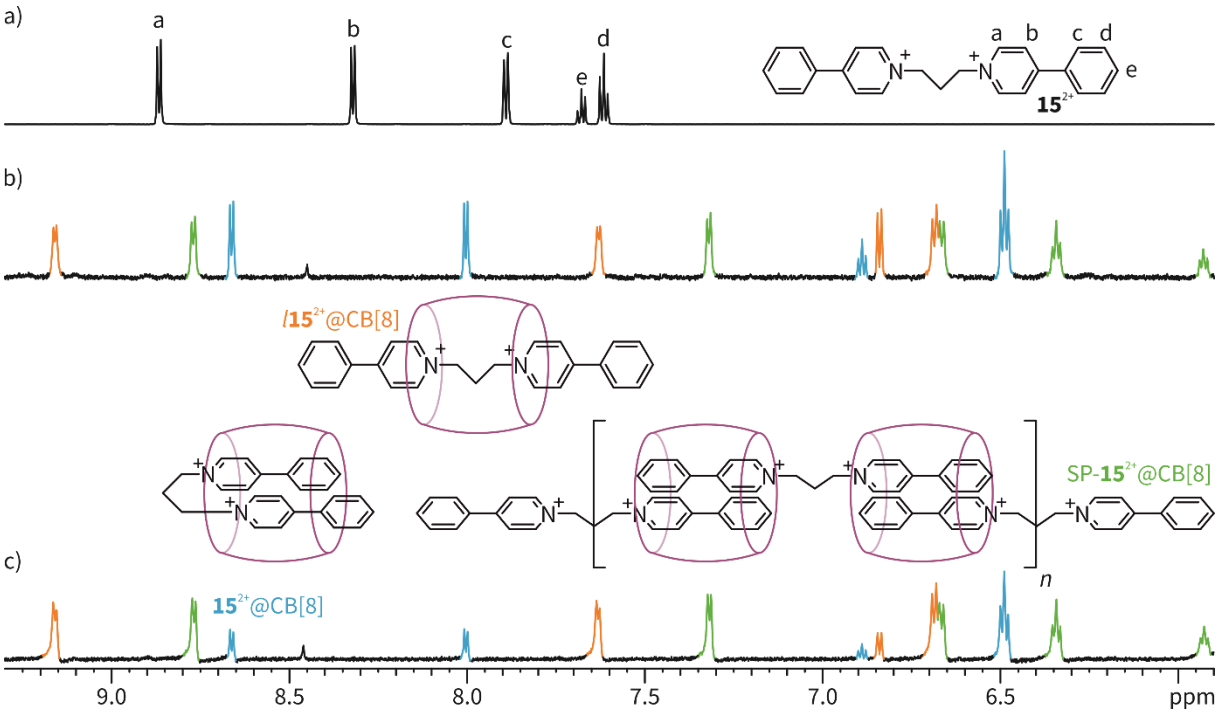

Figure 77. Partial ^{1}H NMR spectra (700 MHz, 298 K, D_2O, 1.0 mM) of (a) **15**$^{2+}$, and a 1:1 mixture of **15**$^{2+}$ and CB[8] after (b) 1 h and (c) 16 h; the three set of signals are marked in different colors.

The Job plot analysis points to a *n*:*n* stoichiometry which is in line with the three proposed structures (Figure 78). However, as before the result should be interpreted with care, since more than one complex is formed in the solution.[126]

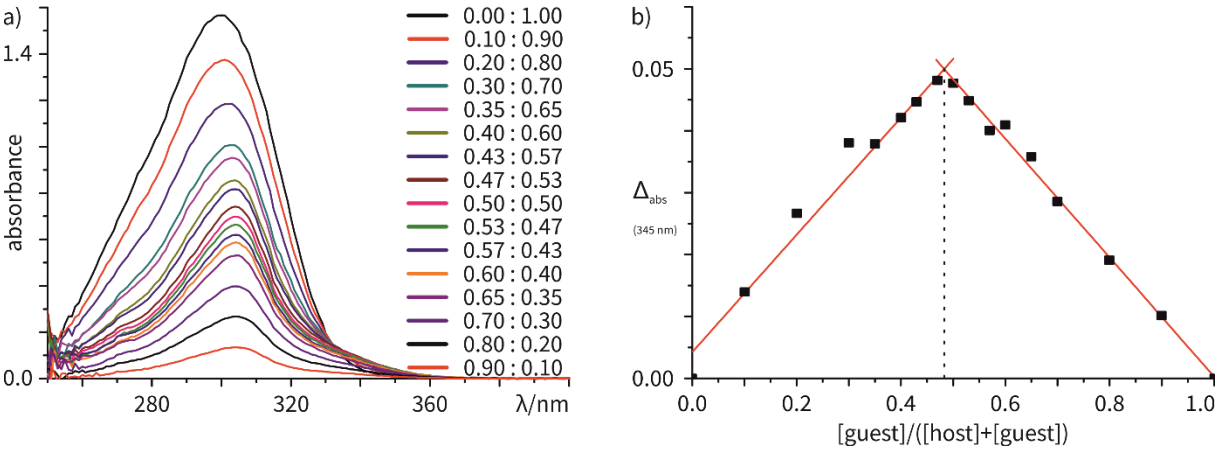

Figure 78. (a) UV/Vis spectra of host–guest mixtures of **15**$^{+}$ and CB[8] (c = 0.12 mM) and (b) Job plot analysis at 345 nm.

Overall, a series of 4-phenylpyridinium derivatives was investigated. If substituted with nucleophilic and electrophilic functional groups, complex formation to the 2:1 complex takes place. This allows for further reactions and incorporation of the guest into larger architectures. Functionalization with apolar groups results in complex formation, but poor solubility can result in precipitation. If the phenylpyridine is functionalized with a naphthalene moiety, a π-donor-π-acceptor complex between the electron-poor phenylpyridinium and the electron-rich naphthalene is formed. The two

phenylpyridinium derivatives **14**$^{2+}$ and **15**$^{2+}$ form the supramolecular polymers SP-**14**$^{2+}$@CB[8] and SP-**15**$^{2+}$@CB[8]. Furthermore, the formation of *syn* dimers in the cavity of CB[8] can be observed in **14**$^{2+}$@CB[8] and **15**$^{2+}$@CB[8]. In the case of the shorter linker, complex *l***15**$^{2+}$@CB[8] with the CB[8] located on the alkyl chain is formed. The complexes coexist in equilibrium and no further analysis was conducted. The findings of this Chapter enhance the understanding of the complexation of the 4-phenylpyridinium guest with CB[8].

4.3 Orthogonal Switching of Self-Sorting Processes in a Stimuli-Responsive Library of Cucurbit[8]uril Complexes†

The distinct feature of monocationic 4-phenylpyridinium derivatives is the formation of 2:1 homoternary complexes (Figure 79a).[45a] If this holds also true for protonated rather than methylated 4-phenylpyridinium, switching between a charged and a neutral state becomes possible by (de)protonation (b). Consequently, this guest becomes controllable by external stimuli. This enables the switching between the CB[8] complex and the dissociation to the free guests (c).

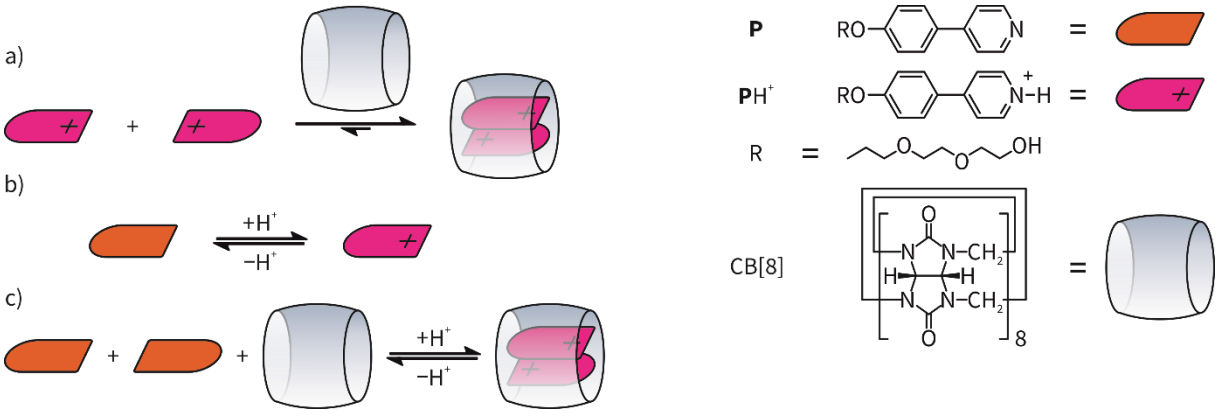

Figure 79. (a) Complexation of 4-pyenylpyridinium derivative **P**H⁺ with CB[8], (b) (de)protonation of **P** and (c) (de)complexation upon (de)protonation of **P**.

4.3.1 Formation of a pH-Responsive Homoternary Complex

In order to study the complexation of a (de)protonated phenylpyridine, compound **P** was synthesized in two reaction steps (Scheme 9). **SI3** derived from 4-iodophenol and the tosylated glycol chain **SI0**[3] in 64% yield. Subsequent Suzuki reaction with pyridine-4-ylboronic acid gave the 4-phenylpyridinium derivative **P** in 21% yield. The quantity was sufficient and so no optimization was conducted. The corresponding protonated species **P**H⁺ can be generated reversibly by simple acid/base addition.

---

† Parts of this chapter have been published and are reproduced in here with kind permission of The Royal Society of Chemistry.

Stefan Schoder and Christoph A. Schalley, *Chem. Commun.* **2017**, *53*, 9546-9549.

Design, Synthesis and Analysis were conducted by S. Schoder. The manuscript was written by S. Schoder. All authors contributed to the final version of the manuscript.

[3] Synthesis and Analysis by Dr. Bo Zheng.

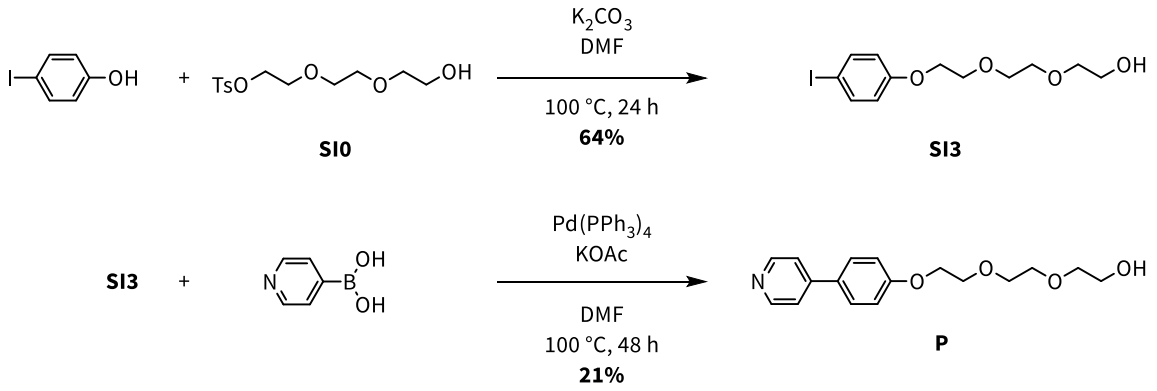

Scheme 9. Synthesis of 4-phenylpyridinium derivative **P**.

Figure 80 shows ^{1}H NMR spectra of neutral **P** (a) and protonated **P**H$^+$ (b) in D_2O. After complex formation in acidic medium a new set of signals occurs that can be assigned to the 2:1 complex (**P**H$^+$)$_2$@CB[8] (c). The complex exhibits a well-defined, somewhat broadened set of signals with significant complexation-induced signal shifts in agreement with those reported for the methylated analogue.[45b] Upon deprotonation, the signals of the free guest **P** are observed (d) suggesting the complete dissociation of (**P**H$^+$)$_2$@CB[8].

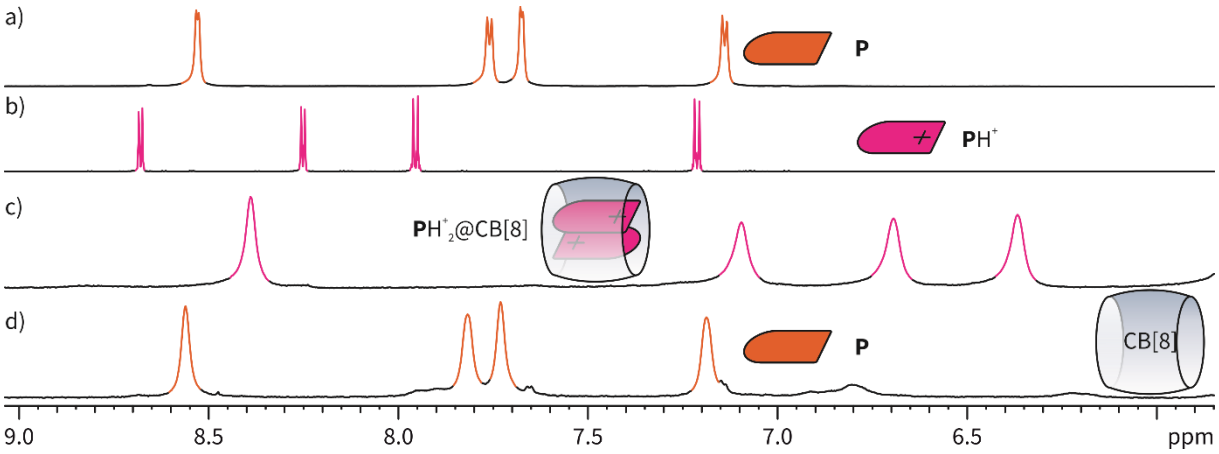

Figure 80. Partial ^{1}H NMR spectra (700 MHz, 298 K, D_2O, 1.0 mM) of (a) **P**, (b) **P**H$^+$, a 2:1 mixture of **P**H$^+$ and CB[8] (c) in acidic (pH 4) and(d) in basic (pH 10) medium; DCl (35% in D_2O) and K_2CO_3 were used to (de)protonate.

The switching can also be observed by UV/Vis spectroscopy and is fully reversible over several cycles (Figure 81a). The photophysical properties are listed in Table 9. Compound **P** is fluorescent under irradiation at 285 nm (ϕ = 9.7%), **P**H$^+$ features a blue emission at 418 nm upon excitation at 366 nm (ϕ = 13.5%). The corresponding cucurbituril complex (**P**H$^+$)$_2$@CB[8] exhibits a fluorescence red shift to 439 nm with a remarkable increase in emission (ϕ = 67.3%) (b), which speaks in favor of an excimer formation and is in line with literature for similar phenylpyridinium derivatives.[45b] This corresponds to a five-fold increase in emission upon complexation.

Table 9. Photophysical properties of **P**, **P**H$^+$ and (**P**H$^+$)$_2$@CB[8]

	P		**P**H$^+$	(**P**H$^+$)$_2$@CB[8]
λ_{abs} [nm]	366	278	325	332
λ_{em} [nm] [a]	-	413	418	439
λ_s [10^3 cm^{-1}]	-	11.8	6.8	7.3
Φ [%][a]	0.0	9.7	13.5	67.3

[a] $\lambda_{ex} = \lambda_{abs}$

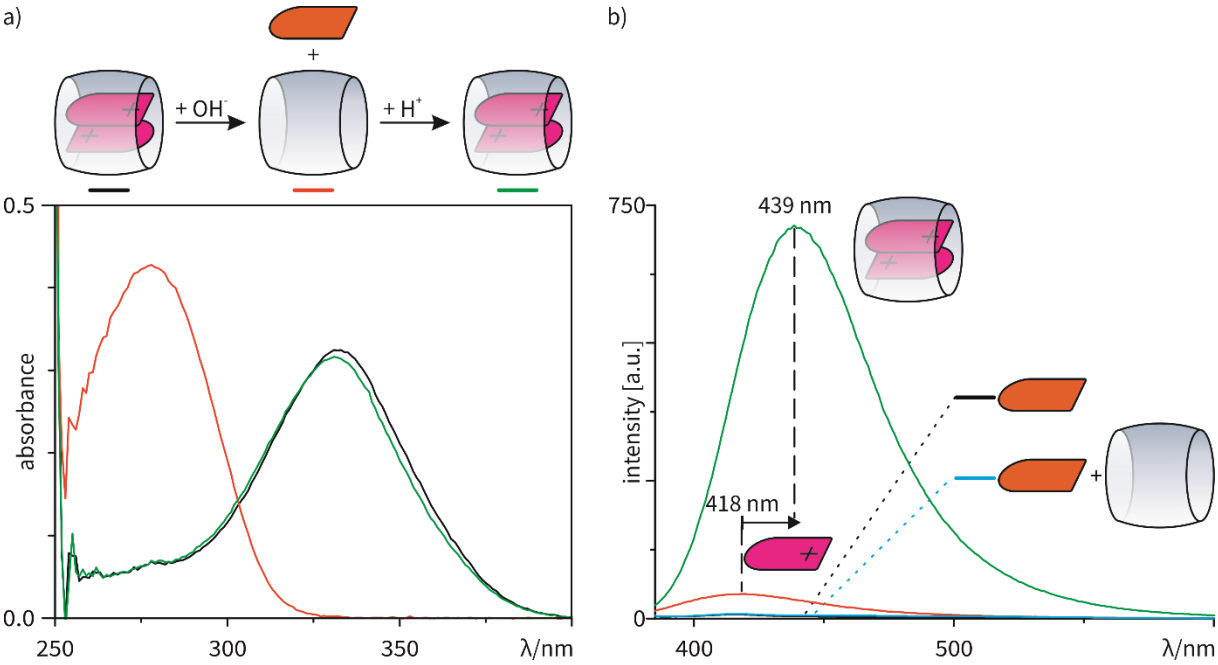

Figure 81. (a) UV/Vis spectra of (**P**H$^+$)$_2$@CB[8] (black curve), after deprotonation (red curve) and after subsequent protonation (green curve) and (b) PL spectra of **P**, **P**H$^+$, (**P**H$^+$)$_2$@CB[8] and a mixture of **P** and CB[8]; $\lambda_{ex} = \lambda_{abs}$, c = 0.06 mM.

The equilibrium association constants for the (**P**H$^+$)$_2$@CB[8] were investigated by isothermal titration calorimetry (ITC). Since the complex has two guests, a constant for the first and for the second binding event was determined and are K_1 = $1.66 \cdot 10^7$ M^{-1} and K_2 = $0.97 \cdot 10^5$ M^{-1}, consequentially, $K_1 \times K_2 = 1.61 \cdot 10^{12}$ M^{-2} (Figure 82). The association constantans agree well with those of the methylated analogue.[45b]

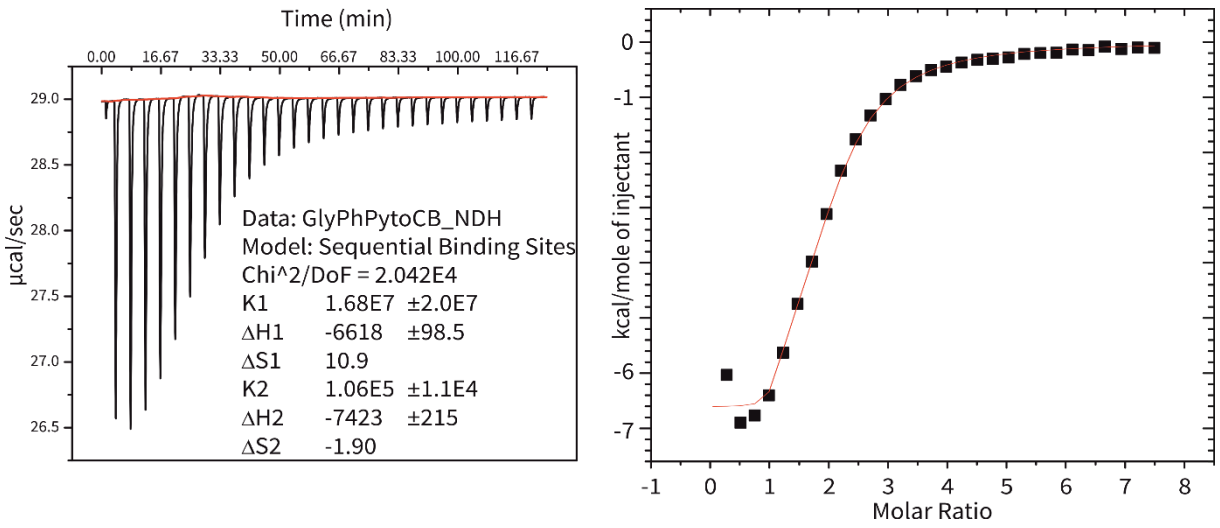

Figure 82. ITC data for the titration of CB[8] (0.03 mM) with **P**H$^+$ (1.0 mM) in a 60 mM phosphate buffer (pH = 5) at 25 °C; ΔH_1 = -6618 cal/mole, ΔS_1 = 10.9 cal/mole*K, ΔG_1 = -9867 cal/mole; ΔH_2 = 7423 cal/mole, ΔS_2 = -1.9 cal/mole*K, ΔG_2 = -6857 cal/mole.

The complex (**P**H$^+$)$_2$@CB[8] formation was also confirmed with mass spectrometry. A clear peak corresponding to the complex was detected at *m/z* 969 (Figure 83). However, this signal is not very intense as charge repulsion leads to quick fragmentation in the gas phase.

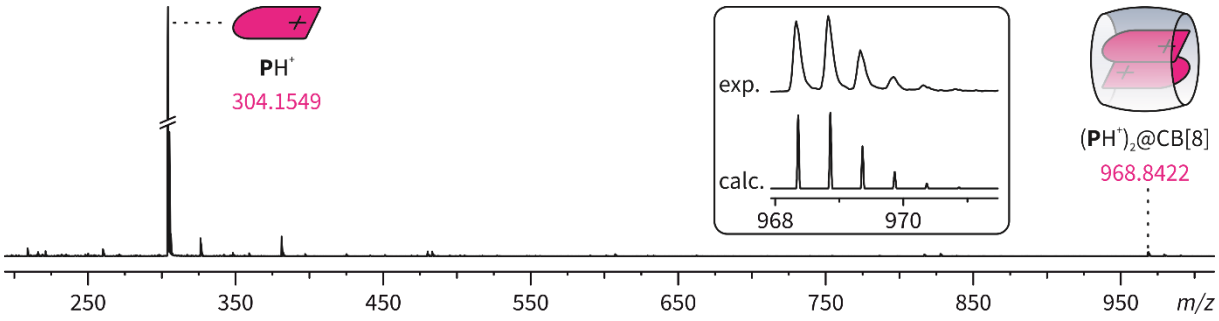

Figure 83. ESI-TOF mass spectrum of a mixture of **P**H$^+$ and CB[8] with isotope pattern.

4.3.2 Formation of a pH-Responsive Heteroternary Complex

In analogy to the literature-known viologen-naphthalene dimer complex **V**$^{2+}$**N**@CB[8],[44a] a π-donor-π-acceptor complex with water soluble naphthalene derivative **N** was investigated (Figure 84). A charge transfer complex in that manner was already proposed in Chapter 4.2.3, but ^{1}H NMR analysis was not possible because of the poor solubility of the formed complex.

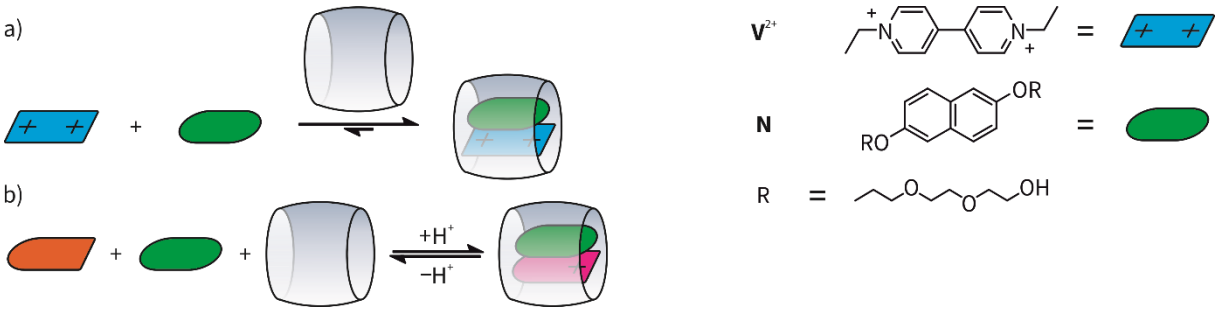

Figure 84. (a) Complexation of the π-donor-π-acceptor complex with viologen derivative $\mathbf{V}^{2+}$ and naphthalene derivative **N** and (b) (de)complexation of $\mathbf{P}H^+$ and **N** upon (de)protonation.

Compound **N** was synthesized following a Williamson ether synthesis starting from 2,6-dihydroxynaphthalene with tosylated glycol chain **SI0** in 23% yield (Scheme 10). The quantity was sufficient and so no optimization was conducted.

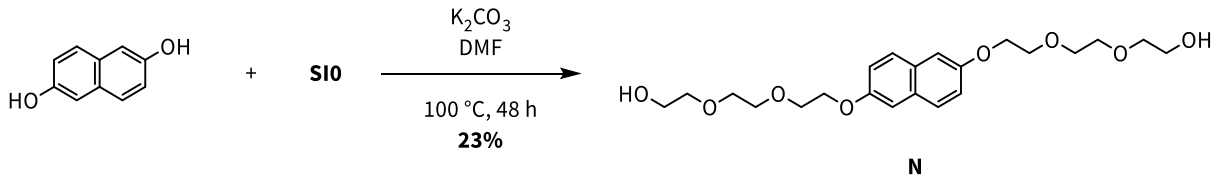

Scheme 10. Synthesis of water soluble naphthalene derivative **N**.

Figure 85 shows the ^{1}H NMR spectra of viologen derivative $\mathbf{V}^{2+}$ (a), naphthalene derivative **N** (b), 1:1 complex $\mathbf{V}^{2+}$@CB[8] (c) and of the 1:1:1 heteroternary complex $\mathbf{V}^{2+}$**N@Q** (d). Both complexes exhibit well-defined sets of signals with complexation induced high field shifts. Due to the charge transfer in the ternary complex between the electron-rich **N** and the electron poor $\mathbf{V}^{2+}$ the signals for the naphthalene shift by more than 1.0 ppm.

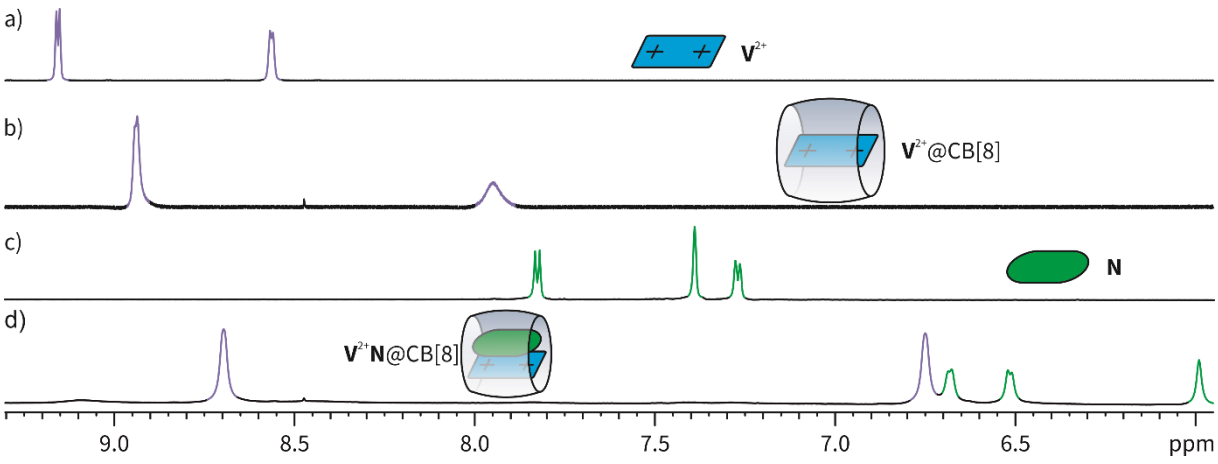

Figure 85. Partial ^{1}H NMR spectra (700 MHz, 298 K, D_2O, 1.0 mM) of (a) $\mathbf{V}^{2+}$, (b) a 1:1 mixture of $\mathbf{V}^{2+}$ and CB[8], (c) **N** and (d) a 1:1:1 mixture of $\mathbf{V}^{2+}$, **N** and CB[8].

Figure 86 shows ^{1}H NMR spectra of the introduced 2:1 complex $(\mathbf{P}H^+)_2$@CB[8] (b) and a 3:1:2 mixture of $\mathbf{P}H^+$, **N** and CB[8] in acidic medium (c). Two sets of signals are observed, one for the $(\mathbf{P}H^+)_2$@CB[8] complex described above and a second one for $\mathbf{P}H^+$**N**@CB[8]. The strong high field shifts of the

signals of **N** indicate its presence inside the cucurbituril cavity, where it experiences the anisotropy of the aromatic rings of **P** in close analogy to the known complex $\mathbf{V}^{2+}\mathbf{N}$@CB[8] (Figure 85). A confirmation of the formation of $\mathbf{P}H^{+}\mathbf{N}$@CB[8] by ESI-MS is not possible because of complex dissociation and loss of the uncharged **N** during the ionization process. After deprotonation, the region of guest signals in the ^{1}H NMR spectrum (d) matches the superposition of the signals of the free guests (a and e), indicating the complete dissociation of $(\mathbf{P}H^{+})_2$@CB[8] and $\mathbf{P}H^{+}\mathbf{N}$@CB[8].

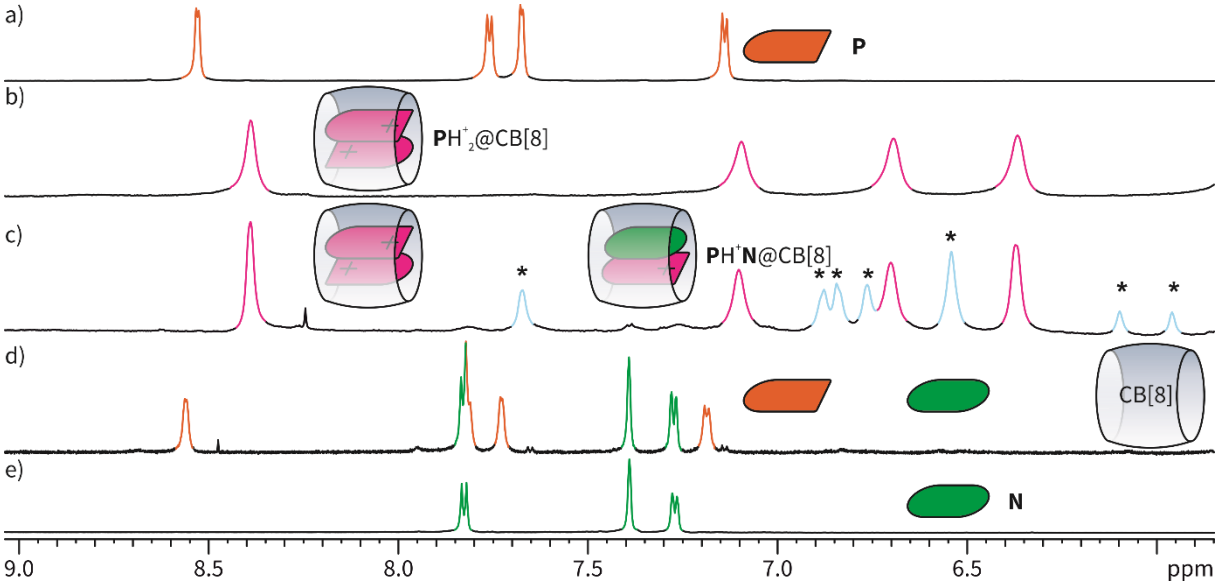

Figure 86. Partial ^{1}H NMR spectra (700 MHz, 298 K, D_2O, 1.0 mM) of (a) **P** (b) complex $(\mathbf{P}H^{+})_2$@CB[8], (c) a 3:1:2 mixture of $\mathbf{P}H^{+}$, **N** and CB[8] in acidic medium (pH 4; asterisks mark the newly formed complex), (d) an equimolar mixture of $\mathbf{P}H^{+}$, **N** and CB[8] in basic medium (pH 10) and (e) **N**; DCl (35% in D_2O) and K_2CO_3 were used to (de)protonate.

The homoternary complex $(\mathbf{P}H^{+})_2$@CB[8] and the heteroternary complex $\mathbf{P}H^{+}\mathbf{N}$@CB[8] feature different emission properties. $(\mathbf{P}H^{+})_2$@CB[8] exhibits a bright fluorescence enhancement after complex formation since an excimer is formed inside the cavity of the host. $\mathbf{P}H^{+}\mathbf{N}$@CB[8], however, quenches the fluorescence due to of exciplex formation. The UV/Vis spectra of mixtures of $\mathbf{P}H^{+}$, **N** and CB[8] at different ration are shown in Figure 87. An increase in concentration of **N** quenches the fluorescence since more of complex $\mathbf{P}H^{+}\mathbf{N}$@CB[8] is formed.

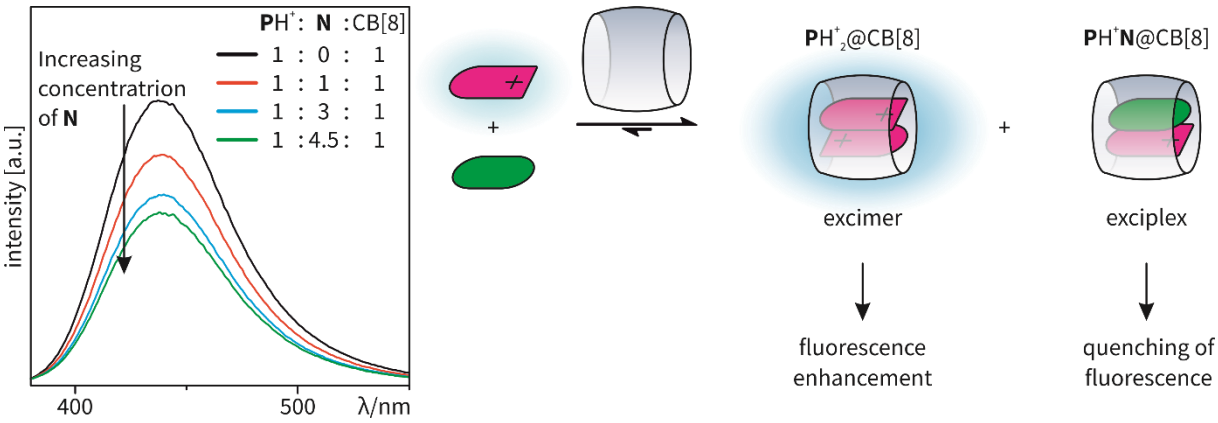

Figure 87. PL spectra of **P**H$^+$, **N** and CB[8] at different ratios and cartoons representing the complexation; λ_{ex} = 332 nm, c = 0.06 mM.

4.3.3 Formation of an Orthogonally Stimuli-Responsive Heteroternary Complex

Since the viologen derivative **V**$^{2+}$ forms a π-donor-π-acceptor complex with the electron rich **N** in CB[8], it can be assumed, that it forms a heteroternary complex with deprotonated compound **P** as well (Figure 88a). This enables switching between a homoternary complex (**P**H$^+$)$_2$@CB[8] and a heteroternary complex (b). Furthermore, **V**$^{2+}$ can be reduced to the monocation radical that can dimerize and is stabilized in CB[8] forming homoternary 2:1 complex **V**$^{+\bullet}$@CB[8].

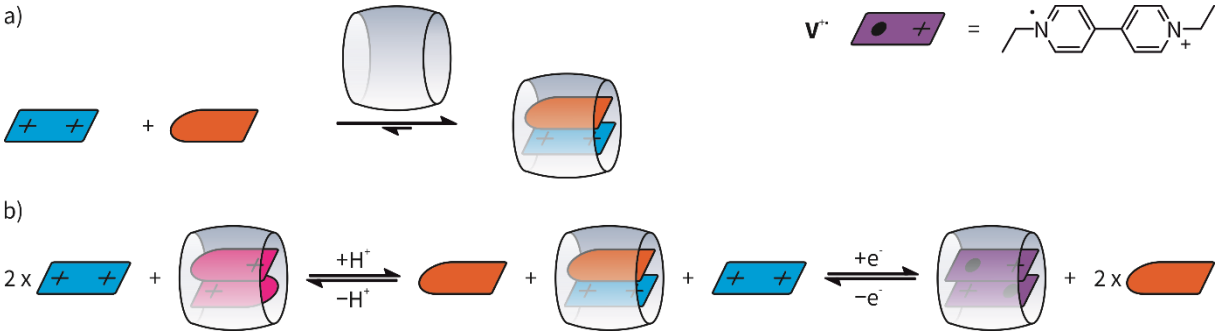

Figure 88. (a) Complexation of the π-donor-π-acceptor complex with viologen derivative **V**$^{2+}$ and phenylpyridine derivative **P** and (b) orthogonal switching between three ternary CB[8] complexes.

Figure 89 shows the ^{1}H NMR spectrum of a 2:1:1 mixture of **P**H$^+$, **V**$^{2+}$ and CB[8] in acidic medium (c) which clearly is a superposition of the spectra of **V**$^{2+}$ and (**P**H$^+$)$_2$@CB[8]. This is in agreement with the binding constants determined for the possible complexes (**P**H$^+$)$_2$@CB[8] and **V**$^{2+}$@CB[8], already the first binding constant of **P**H$^+$ to CB[8] (K_1 = 6.63 · 10^6 M^{-1}) is higher than that of **V**$^{2+}$ to CB[8] (K = 1.1 · 10^5 M^{-1})[45k] by a factor of about 60. The ^{1}H NMR spectrum of the mixture after deprotonation of **P**H$^+$ shows a new set of signals (d), indicating the formation of the 1:1:1 complex **PV**$^{2+}$@CB[8].

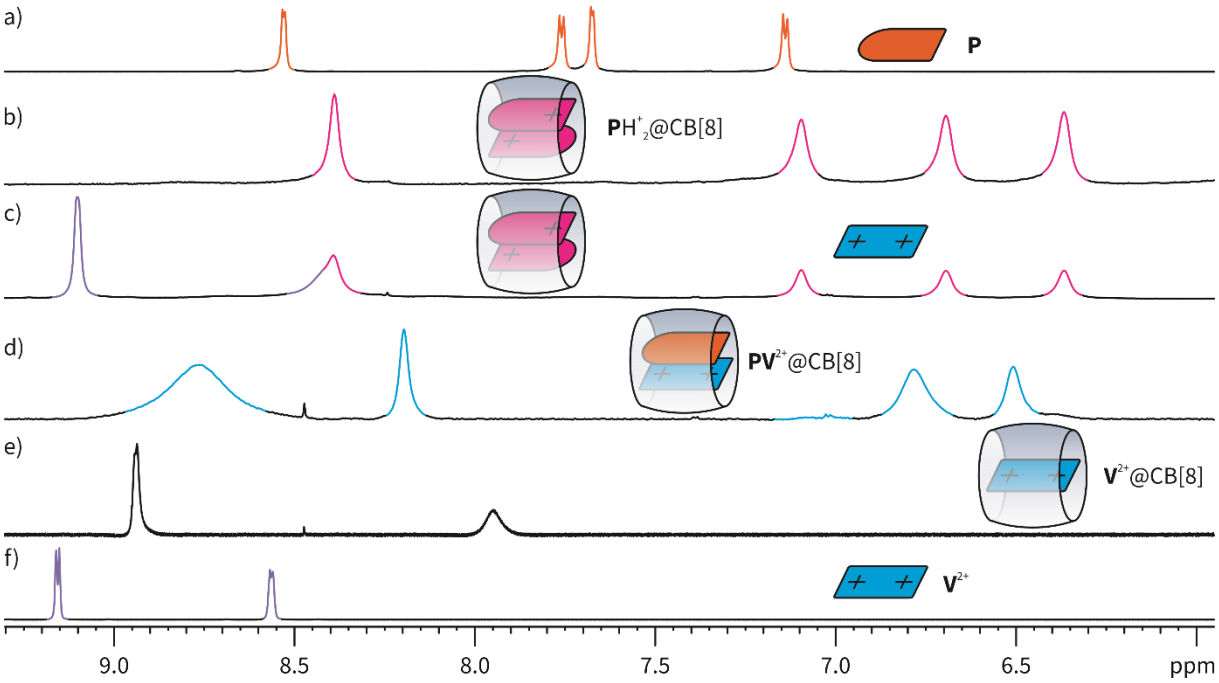

Figure 89. Partial ^{1}H NMR spectra (700 MHz, 298 K, D_2O, 1.0 mM) of (a) **P**, (b) complex (**P**H$^+$)$_2$@CB[8], (c) a 2:1:1 mixture of **P**, **V**$^{2+}$ and CB[8] in acidic medium (pH 4), (d) an equimolar mixture of **P**, **V**$^{2+}$ and CB[8] in basic medium (pH 10), (e) complex **V**$^{2+}$@CB[8], and (f) **V**$^{2+}$; DCl (35% in D_2O) and K_2CO_3 were used to (de)protonate.

The signal at 6.75 ppm can be attributed to two different protons of **P** and one set of signals of the viologen protons is broadened (Figure 90). The signals for the complex **V**$^{2+}$@CB[8] are known and can be assigned. Because of the low solubility of the complex and because of the shielding of the cucurbituril the cross peaks for the complex cannot be seen. The new set of signals (marked with dashed squares) are attributed to the new viologen containing complex **PV**$^{2+}$@CB[8]. The viologen experiences the same shielding resulting in no visible cross peaks at this low concentration.

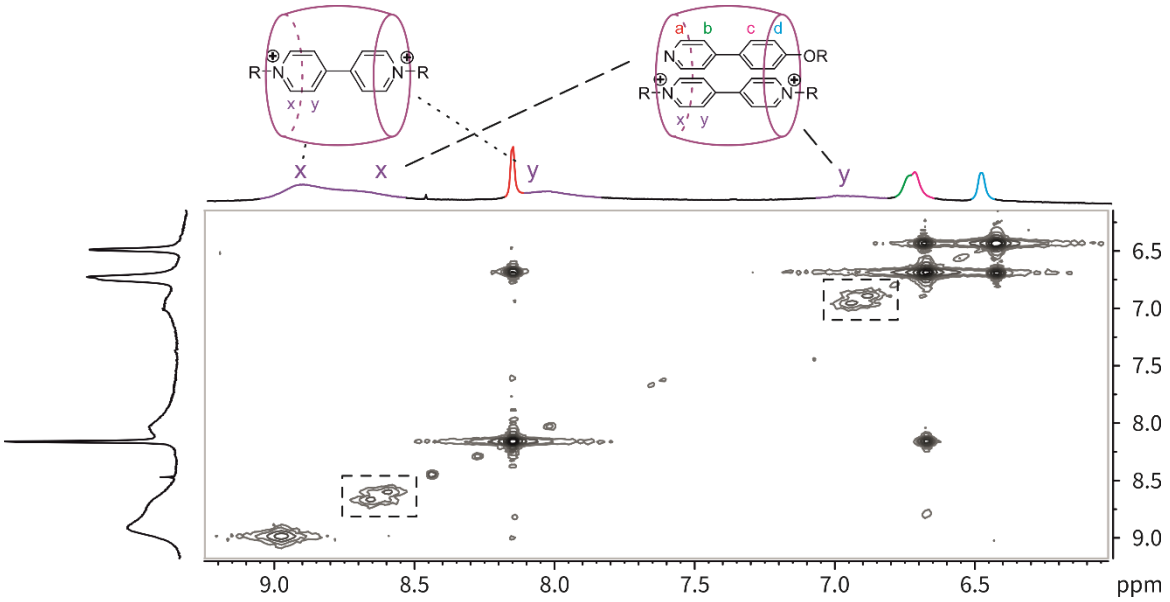

Figure 90. Partial ^{1}H ^{1}H COSY NMR spectra (700 MHz, 278 K, D_2O, 1.0 mM) of a 1:1:1 mixture of **P**, **V**$^{2+}$ and CB[8] in basic conditions (pH = 10); K_2CO_3 was used to deprotonate.

The formation of **PV**$^{2+}$@CB[8] is also confirmed by its characteristic charge transfer band at around 450 nm in the UV/Vis spectrum of the complex. Again, the switching is fully reversible upon protonation, which is shown by the recovery of the original band after the (de)protonation (Figure 91).

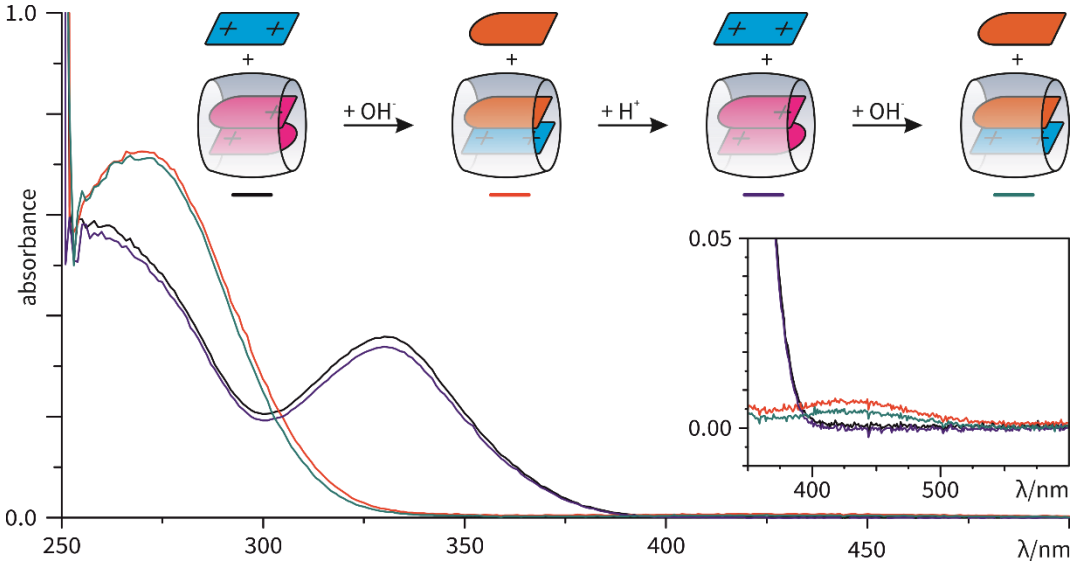

Figure 91. UV/Vis spectra of a 1:1:1 mixture of **P**H^{+}, **V**$^{2+}$ and CB[8] in acidic conditions (black curve), after deprotonation (red curve), after consecutive protonation (blue curve) and subsequent deprotonation (cyan curve) (6 µM **V**$^{2+}$). Inlay shows the charge transfer band of the formed complex **PV**$^{2+}$@CB[8].

It is well known that viologen dications can be reduced to the corresponding radical cations, which tend to dimerize inside the cucurbituril cavity, yielding (**V**$^{+\bullet}$)$_2$@CB[8] ($K_2 = 2.0 \cdot 10^7$ M^{-1}).[45k] Formation of this complex is favored over the charge transfer complex **V**$^{2+}$**N**@CB[8] ($K_2 = 5.9 \cdot 10^5$ M^{-1}).[6] Consequently, it should be favored over **PV**$^{2+}$@CB[8] as well, considering the fact that **N** is more electron rich than **P**. This allows us to use redox chemistry as a stimulus in this system. The reduction potentials of **V**$^{2+}$ ($E^1_{1/2}$ = -0.66 V) and cucurbituril complex **V**$^{2+}$@CB[8] ($E^1_{1/2}$ = -0.58 V) were determined by cyclic voltammetry (Figure 92). Neither the compounds **P** and **P**H^{+}, nor complex (**P**H^{+})$_2$@CB[8] are reduced under these conditions.

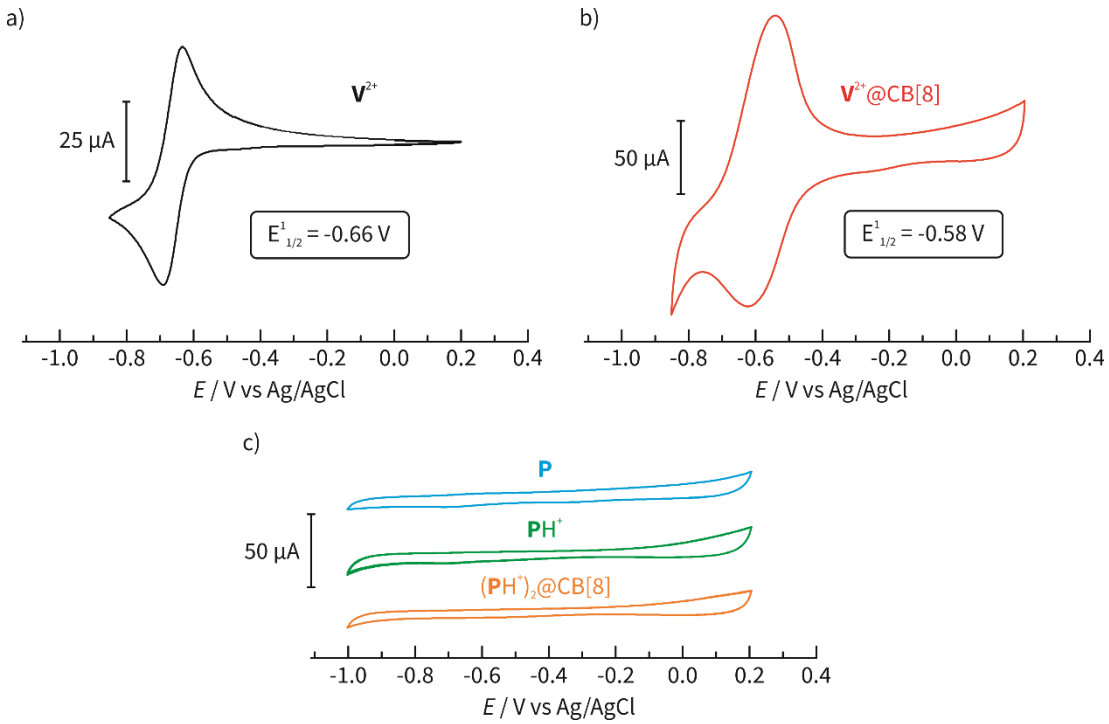

Figure 92. Cyclic voltammetry measurements of (a) $\mathbf{V}^{2+}$, (b) $(\mathbf{V}^{+\bullet})_2$@CB[8] and (c) measurements of **P**, $\mathbf{P}H^+$ and $(\mathbf{P}H^+)_2$@CB[8].

When sodium dithionite is used for chemical reduction of viologen to its cation radical $\mathbf{V}^{+\bullet}$ the 2:1 complex $(\mathbf{V}^{+\bullet})_2$@CB[8] forms as clearly indicated by the typical absorption bands at 541 nm and 982 nm (Figure 93a). The same bands are observed when the literature-known charge transfer complex $\mathbf{V}^{2+}$**N**@CB[8] and when independently prepared $\mathbf{PV}^{2+}$@CB[8] are reduced (b and c). These results clearly indicate the formation of $(\mathbf{V}^{+\bullet})_2$@CB[8] in both cases together with the release of **N** or **P**, respectively.

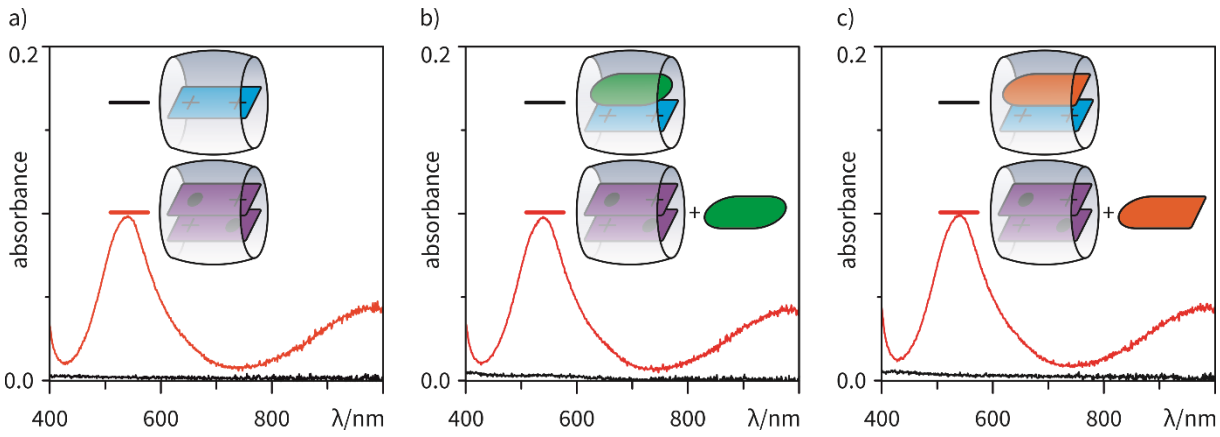

Figure 93. UV/Vis spectra of (a) a mixture of $\mathbf{V}^{2+}$ and CB[8] before and after reduction, (b) $\mathbf{V}^{2+}$, **N** and CB[8] before and after reduction and (c) **P**, $\mathbf{V}^{2+}$ and CB[8] before and after reduction; 10 equiv. $Na_2S_2O_4$ was used as reducing agent (24 mM $\mathbf{V}^{2+}$).

4.3.4 An Orthogonally Stimuli-Responsive Self-Sorting Network

Based on this simple library of complexes, a more complex four-step self-sorting network was designed, which is responsive to redox and pH stimuli. It consists of two equivalents of pH-responsive phenylpyridine derivative **P**, redox-responsive viologen derivative $\mathbf{V}^{2+}$ and electron-rich naphthalene derivative **N**, one equivalent each, and two equivalents of the macrocyclic host CB[8] (Figurer 94).

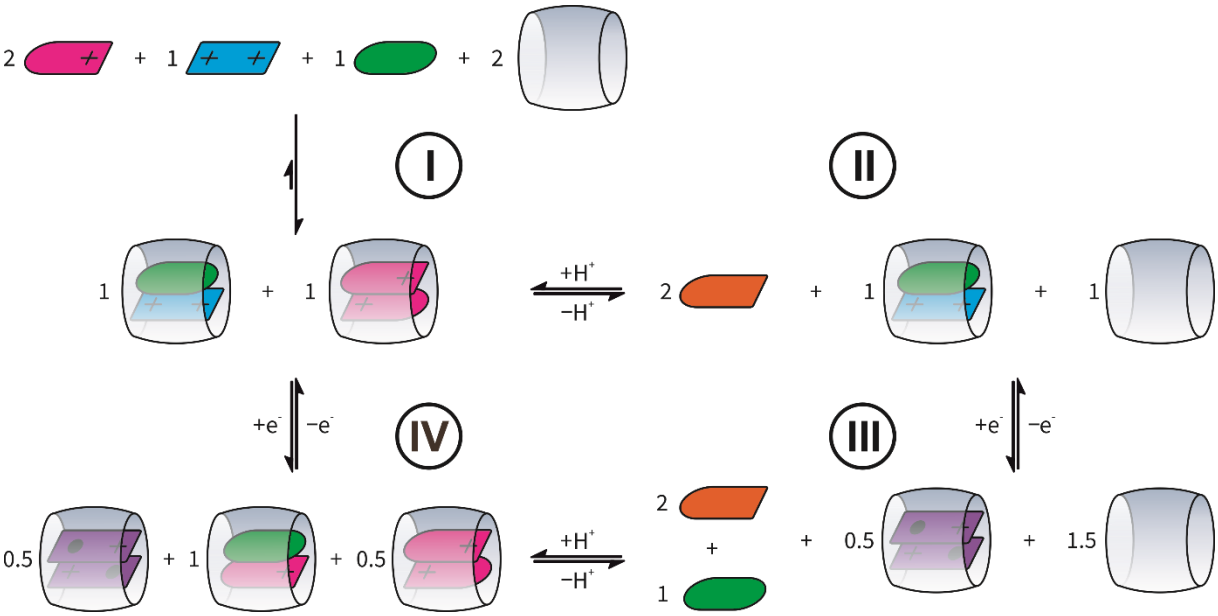

Figure 94. Four-step self-sorting square with two switches based on pH and redox with states **I** to **IV**.

The 2:1:1:2 mixture of $\mathbf{P}H^+$, $\mathbf{V}^{2+}$, **N** and CB[8] contains the two complexes $(\mathbf{P}H^+)_2$@CB[8] and $\mathbf{V}^{2+}$**N**@CB[8] and corresponds to state **I**. The ^{1}H NMR spectrum is a superposition of the spectra of independently prepared complexes and is shown in Figure 95b. Deprotonation (d) gives state **II** with viologen-naphthalene complex $\mathbf{V}^{2+}$**N**@CB[8] still intact and the signals of free **P** indicate the complete dissociation of $(\mathbf{P}H^+)_2$@CB[8]. To avoid formation of $\mathbf{PV}^{2+}$@CB[8] a slight excess of **N** was used, thus resulting in a set of signals for free **N**.

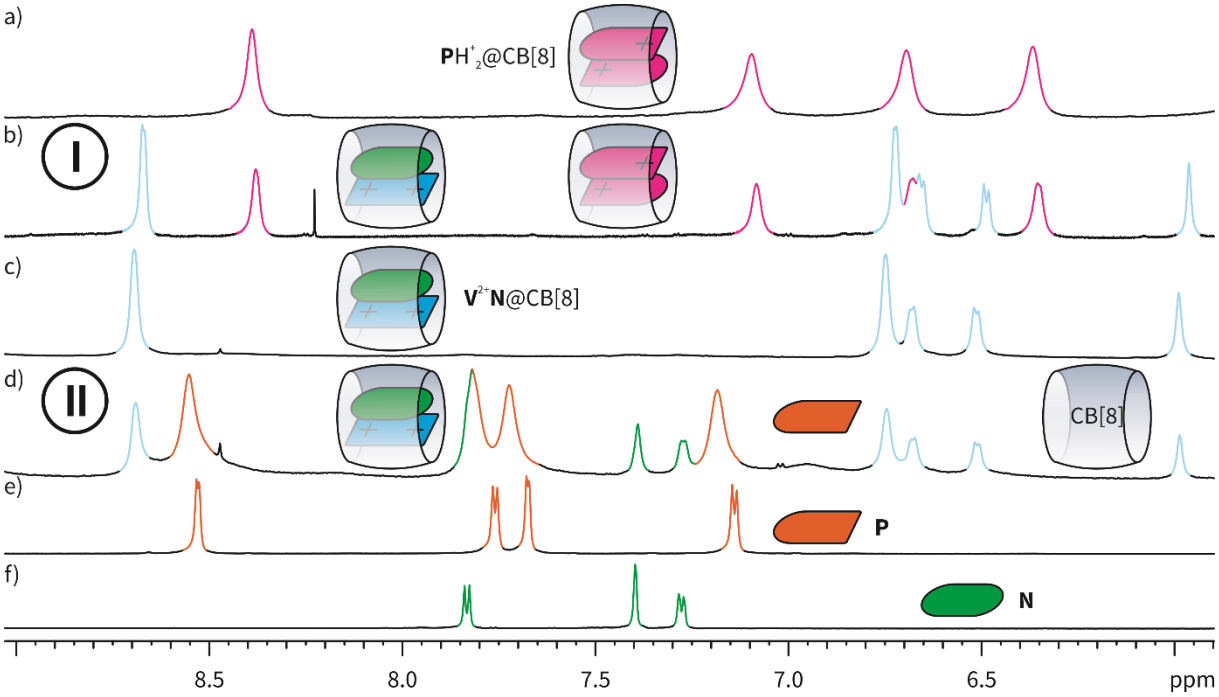

Figure 95. Partial ^{1}H NMR spectra (700 MHz, 298 K, D_2O, 1.0 mM) of (a) (**P**H$^+$)$_2$@CB[8], (b) a 2:1:1:2 mixture of **P**H$^+$, **V**$^{2+}$, **N** and CB[8], (c) **PV**$^{2+}$@CB[8], (d) a 2:1:1.1:2 mixture of **P**, **V**$^{2+}$, **N** and CB[8], (e) **P**, (f) **N**; (a) and (b) pH 4, (d) and (e) pH 10; DCl (35% in D_2O) and K_2CO_3 were used to (de)protonate.

Subsequent reduction of state **II** with $Na_2S_2O_4$ results in the distinct UV/Vis absorption spectrum of complex (**V**$^{+\bullet}$)$_2$@CB[8] with the radical cation viologen dimer inside the cucurbituril cavity (red curve) (Figure 96).

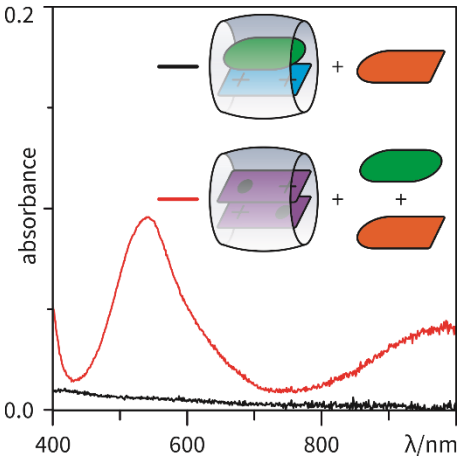

Figure 96. UV/Vis spectra of a mixture of **P**, **V**$^{2+}$, **N** and CB[8] before and after reduction; 10 equiv. $Na_2S_2O_4$ was used as reducing agent (24 mM **V**$^{2+}$).

P and **N** in the four-component mixture are not affected by the reduction as shown by ^{1}H NMR experiments. Figure 97a and (d) correspond to state **I** and **II** without the viologen derivative **V**$^{2+}$. Addition of reductant to the acidic mixture (a to b) does not result in the formation of a new complex. Therefore, the reaction mixture is not affected by the addition of $Na_2S_2O_4$. The same is true under

basic conditions (d) which is a superposition of the signals of the free guests (e and f). Consequently, after reduction of state **II** with $Na_2S_2O_4$, state **III** is obtained.

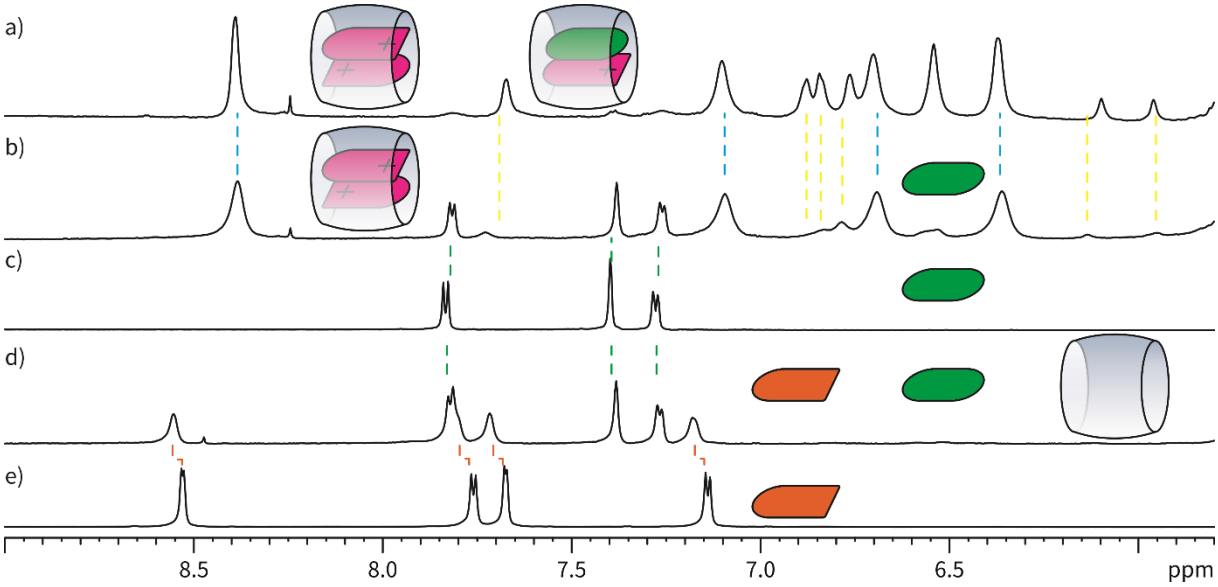

Figure 97. Partial ^{1}H NMR spectra (700 MHz, 298 K, D_2O, 1.0 mM) of a) a 2:1:2 mixture of **P**H$^+$, **N** and CB[8] in acidic (pH 4) medium (corresponding to state **I** without **V**$^{2+}$), b) the same solution after addition of $Na_2S_2O_4$, c) **N**, d) a 2:1:2 mixture of **P**, **N** and CB[8] in basic (pH 10) medium (corresponding to state **II** without **V**$^{2+}$) after addition of $Na_2S_2O_4$, e) **P** (pH 10); DCl (35% in D_2O) and K_2CO_3 were used to (de)protonate.

The reduction of the viologen in acidic medium is possible, but subsequent reoxidation occurs rapidly. Hence, the solution of state **III** was prepared slightly acidic (Figure 98a). The black curve corresponds to a 2:1:1:2 mixture of **P**H$^+$, **V**$^{2+}$, **N** and CB[8] in H_2O (24 µM **V**$^{2+}$). It should be noted that due to solubility reasons the solution is slightly acidic. To assure just a slightly acidic solution the original mixture (black curve) was deprotonated with NaOH (2 µL, 1.5M, red curve; lying under the blue curve) and slowly acidified. After the first addition of HCl (1.4 µL, 1M, blue curve) the solution is still basic. After the second addition of HCl (1.4 µL, 1M, green curve) the solution is acidic representing state **I**. Reduction with $Na_2S_2O_4$ (pink curve) results in the unique absorption maxima of (**V**$^{+\bullet}$)$_2$@CB[8] and, therefore, indicating state **IV**. The intensity of the signal is weak, because of the fast reoxidation during the measurement.

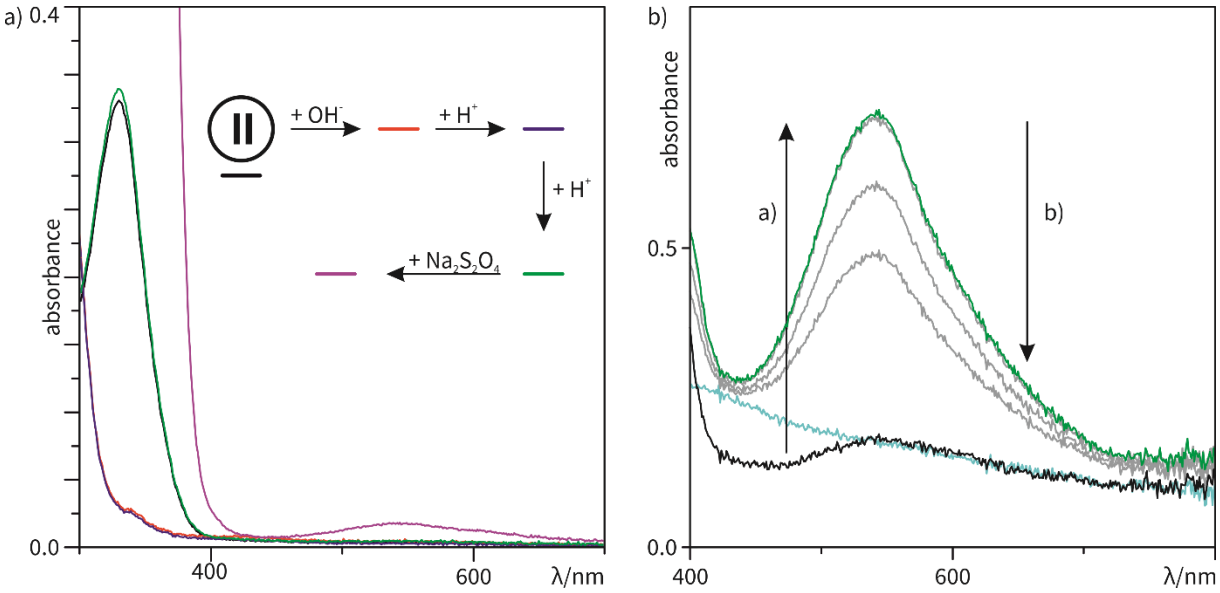

Figure 98. UV/Vis spectra of (a) preparation of a slightly acidic state **II** and subsequent reduction and (b) switching between the reduced states **III** and **IV**; 10 equiv. $Na_2S_2O_4$ was used as reducing agent (24 mM $\mathbf{V}^{2+}$).

To demonstrate the pH switching of the system between the reduced states **III** and **IV**, the more oxidation stable state **III** was prepared and acidified (Figure 98b). The black curve corresponds to a 2:1:1:2 mixture of **P**, $\mathbf{V}^{2+}$, **N** and CB[8] in H_2O (24 µM $\mathbf{V}^{2+}$) after addition of NaOH (1 µL, 1.5M, black curve). It should be noted that due to solubility reasons the solution was acidic before. Reduction with $Na_2S_2O_4$ (green curve) results in the expected absorption maxima of state **III** (depicted by arrow a). After addition of HCl (1.4 µL, 1M, grey curves), complex $(\mathbf{V}^{+\bullet})_2$@CB[8] is still present and state **IV** is reached. Fast re-oxidation can be observed by consecutive measurements over the span of two minutes resulting in the reoxidized state (blue curve) (arrow b).

In conclusion, an orthogonally switchable self-sorting network consisting of $\mathbf{P}H^+$, $\mathbf{V}^{2+}$, **N** and CB[8] was realized with pH and redox signals as the external stimuli. The new acid/base-sensitive guest $\mathbf{P}H^+$ can form the 2:1 complex $(\mathbf{P}H^+)_2$@CB[8]. In combination with the electron rich partner **N** it can form the π-donor-π-acceptor complex $\mathbf{P}H^+\mathbf{N}$@CB[8]. In its deprotonated form, **P** can act as the electron rich counterpart to $\mathbf{V}^{2+}$, forming π-donor-π-acceptor complex $\mathbf{PV}^{2+}$@CB[8]. Both compounds, **P** and $\mathbf{P}H^+$, are electrochemical stable and, thus, allow an orthogonal redox-switching of $\mathbf{V}^{2+}$ generating $(\mathbf{V}^{+\bullet})_2$@CB[8]. This is the first example of a cucurbituril-based self-sorting system which is orthogonally switchable by pH and electrochemical inputs. The high tolerance of this system is shown with a simple fully controllable square network. This work is unique, as it is possible to switch its self-sorting behavior between the three ternary cucurbituril complexes $(\mathbf{P}H^+)_2$@CB[8], $\mathbf{PV}^{2+}$@CB[8] and $(\mathbf{V}^{+\bullet})_2$@CB[8].

4.4 Synthesis and Analysis of an Axle for an Electrostatically Interlocked Cucurbit[8]uril Rotaxane

A recurring problem in the Chapters shown above is that mass spectrometric (MS) analysis of ternary CB[8] complexes can be very challenging. Charge repulsion endorses the dissociation of homoternary complexes in the gas phase and neutral binding partners decomplex since the concept of high-energy water does not apply in the gas phase. These limitations of this otherwise powerful analytic method restrict the usefulness of this method for characterization of CB[8] complexes in aqueous solutions.

The concept of the electrostatically interlocked rotaxane (EsiRot) is based on the idea that a complex consisting of two doubly charged viologen moieties inside the cavity of a CB[8] is unfavored due to charge repulsion (Figure 99). Two identical axles, each consisting of a viologen binding site, a stopper and a linker between those two, are complexed in CB[8] in a way represented in Figure 99. In structure **I**, the host can shuttle between the two identical binding stations, but the sterically demanding groups prevent dethreading over the stopper terminated ends of the complex. Consequently, in a potential decomplexation pathway structure **II** must be passed which is blocked because of the high energy necessary to overcome the charge repulsion of the two bipyridinium moieties. Therefore, dissociation of the complex in the ionization process or in the gas phase could be prevented and MS analysis should be possible.

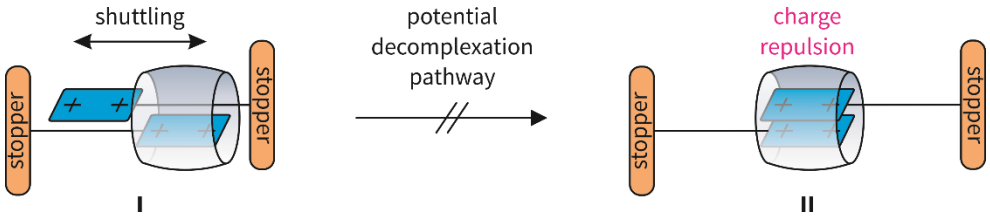

Figure 99. Concept of the electrostatically interlocked rotaxane.

4.4.1 Design and Synthesis of an Axle

An axle like the one shown above would not form the desired complex, since there would be no driving force for the formation of a 2:1 complex. So, an electron rich moiety at the linker is necessary. The designed axle $\mathbf{A}^{2+}$ consists of a viologen terminus, a naphthalene moiety and a propargyl group terminus for introduction of a stopper *via* click reaction (Figure 100).

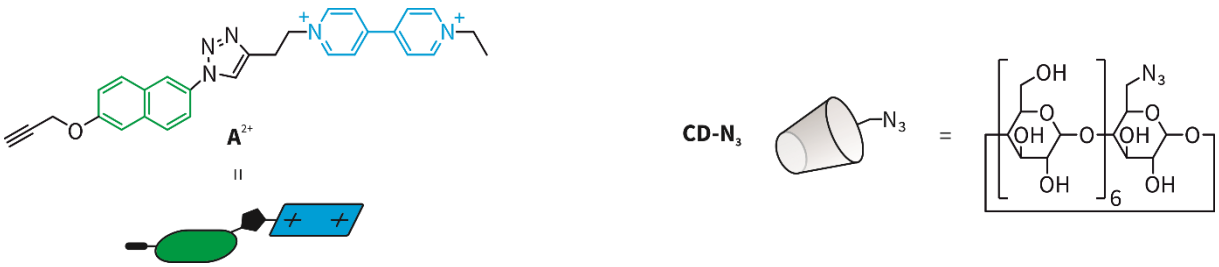

Figure 100. Structure of the designed axle $\mathbf{A}^{2+}$ and the potential stopper **CD-N₃** and the representative cartoon.

As a potential stopper, the azide-functionalized β-CD **CD-N₃**[4] was selected.[128] The square scheme in Figure 101 shows reaction and complexation pathways to accomplish the electrostatically interlocked rotaxane. The reaction of axle $\mathbf{A}^{2+}$ with the stopper **CD-N₃** should yield $\mathbf{CD\text{-}A}^{2+}$. The latter cannot form the 2:2 EsiRot complex since it would be the opposite mechanism of the EsiRot concept. Therefore, to prepare EsiRot complex, $\mathbf{A}^{2+}{}_2$@CB[8]$_2$ should be formed first and then stoppered. The mild reaction conditions of the click reaction should not interfere with the complex.

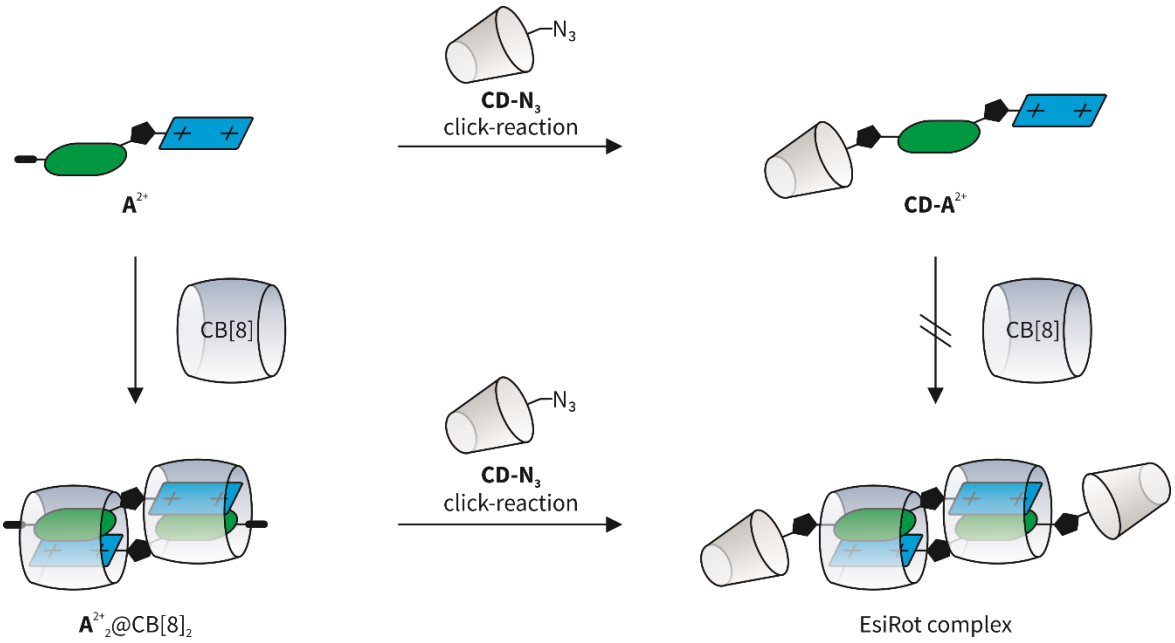

Figure 101. Square scheme showing the reaction and complexation pathways to accomplish the EsiRot complex.

Compound $\mathbf{19}^{+}$ can act as precursor for axle $\mathbf{A}^{2+}$ and was synthesized in four steps (Scheme 11). The naphthalene derivative **17** was synthesized from commercially available 6-bromonaphthalen-2-ol in two steps.[129] Monosubstitution of 4,4'-bipyridine with 1-butyne furnished bipyridinium derivative $\mathbf{18}^{+}$. The crucial step is the click reaction of naphthalene derivative **17** with bipyridinium derivative $\mathbf{18}^{+}$.

[4] Synthesis and analysis by Dr. Anneli Kruve-Viil.

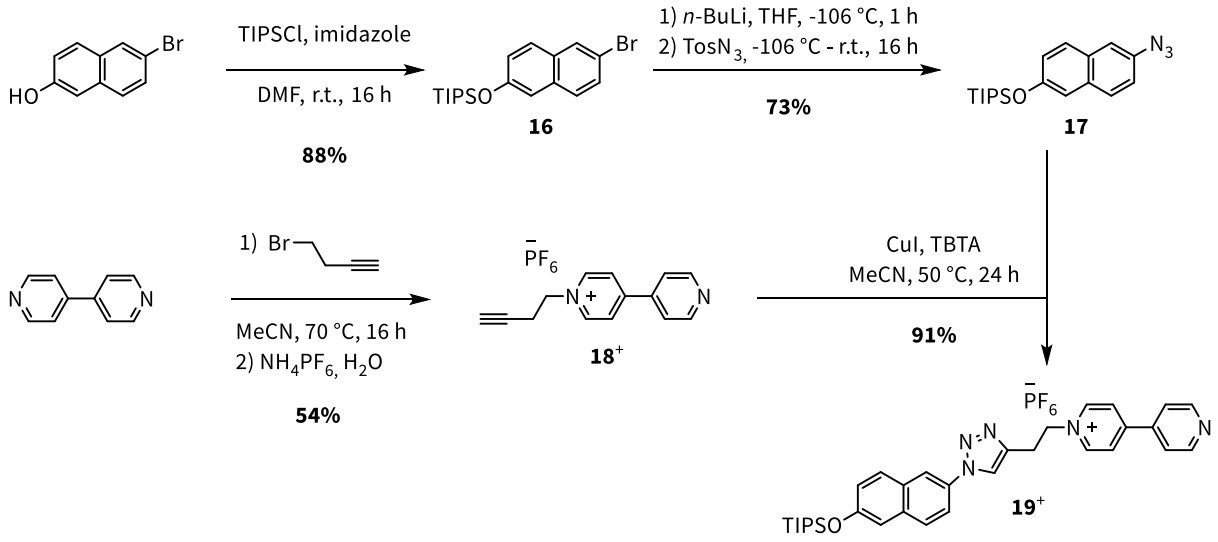

Scheme 11. Synthesis of axle precursor **19**$^{+}$ starting form commercially available compounds.

The synthetic pathway to axle compound **A**$^{2+}$ is shown in Scheme 12. The synthesis of compound **20**$^{+}$ is cumbersome, since deprotection of **19**$^{+}$ with TBAF in THF leads to immediate precipitation of deprotected alcohol **21**$^{+}$. Therefore, **19**$^{+}$ and propargyl bromide was dissolved in THF and TBAF was added yielding a precipitate with ratio of 1:9 of desired **20**$^{+}$ and **21**$^{+}$, which could be separated by column chromatography. Propargylation of **21**$^{+}$ in DMF yields **20**$^{+}$ in poor yield. Further optimization attempts were not successful, but after combining the products of several reaction attempts, the quantity of the combined products was sufficient. Ethylation of **21**$^{+}$and subsequent ion exchange gave the desired compound **A**$^{2+}$ in excellent yield.

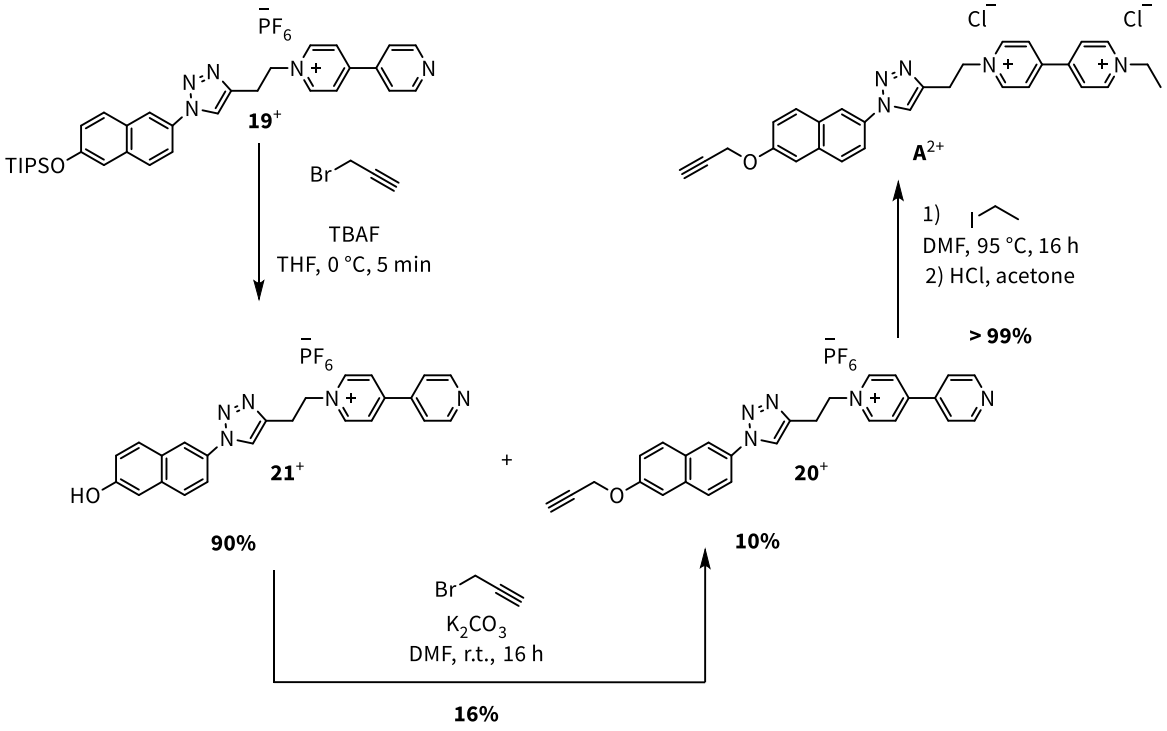

Scheme 12. Synthesis of axle compound **A**$^{2+}$.

As an alternative pathway for the synthesis of $\mathbf{A}^{2+}$, alkyne free axle $\mathbf{C}^{2+}$ was synthesized by click reaction in MeCN of **17** and $\mathbf{22}^{2+}$ (Scheme 13). Compound $\mathbf{C}^{2+}$ could not be converted to axle $\mathbf{A}^{2+}$. It was possible to obtain a crystal structure of $\mathbf{C}^{2+}$.

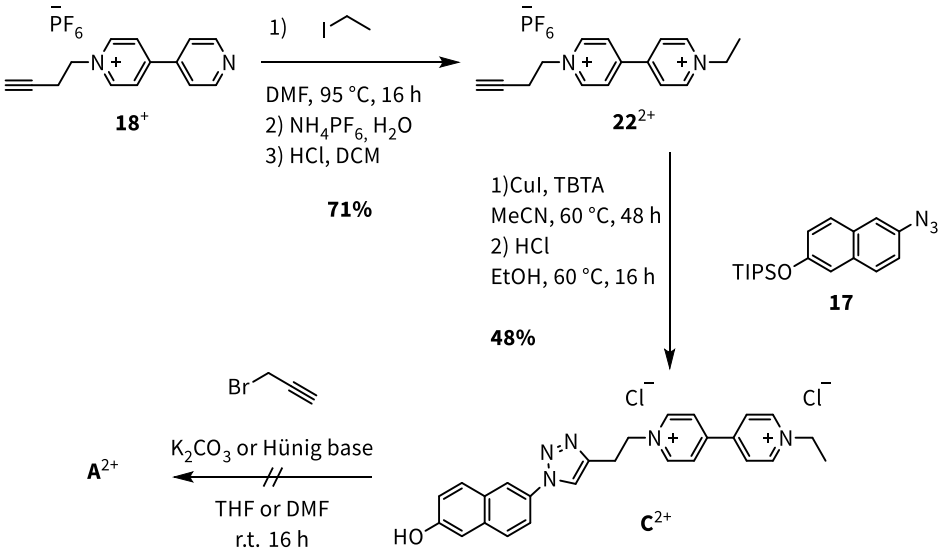

Scheme 13. Synthesis of compound $\mathbf{C}^{2+}$ by click reaction of **17** and $\mathbf{22}^{2+}$ in MeCN.

To investigate the complexation of the axle with the host, an equimolar mixture of $\mathbf{A}^{2+}$ and CB[8] in D_2O was prepared. The ^1H NMR spectra of $\mathbf{A}^{2+}$ and its CB[8] complex is shown in Figure 102. The highfield shifts of the signals of the viologen protons (blue) as well as the ones of the naphthalene (green) indicate the complexation of both parts of the molecule. The signal of the triazole (orange) exhibits a downfield shift, which is typical for protons that are located at the rim of the host. It is unclear why the signal splits into two signals; however, the presence of two complex isomers can be assumed. One with the triazole protons directed in the same direction and a second one with triazole protons directed to the opposite sides to each other. The conversion between those to complexes must be slower than the NMR time scale to exhibit two individual signals. Overall the complexation induced shifts hint to the formation of the desired 2:2 complex $\mathbf{A}^{2+}{}_2$@CB[8]$_2$.

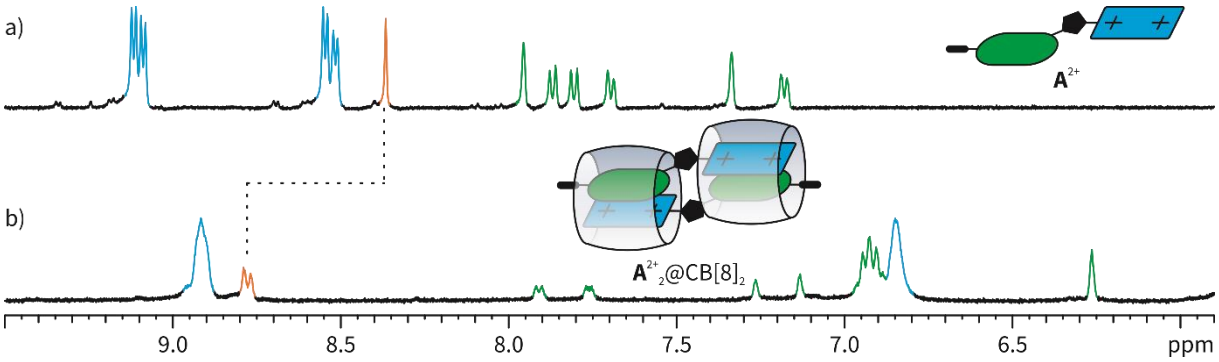

Figure 102. Partial ^1H NMR spectra (700 MHz, 298 K, D_2O, 1.0 mM) of (a) $\mathbf{A}^{2+}$ and (b) a 1:1 mixture of $\mathbf{A}^{2+}$ and CB[8].

The complexation was additionally confirmed by UV/Vis analysis. The UV/Vis spectra of $\mathbf{A}^{2+}$ and $\mathbf{A}^{2+}{}_2$@CB[8]$_2$ are shown in Figure 103. Complexation with CB[8] results in a bathochromic shift of the π–π* absorption band and in the formation of a charge transfer (CT) band between 360 to 390 nm. The existence of the CT band validates the formation of the 2:2 complex, as only then a π-donor-π-acceptor dimer inside the hosts is possible.

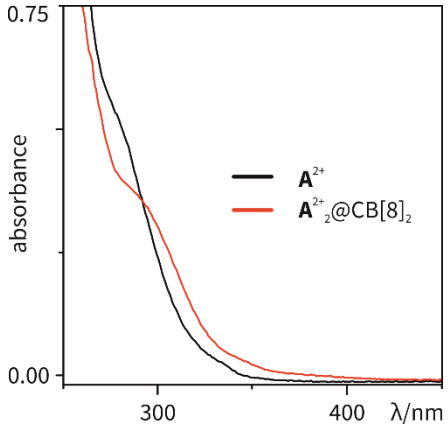

Figure 103. UV/Vis spectra of $\mathbf{A}^{2+}$ and $\mathbf{A}^{2+}{}_2$@CB[8]$_2$; c = 0.06 mM.

The formation of the 2:2 complex $\mathbf{A}^{2+}{}_2$@CB[8]$_2$ is the first crucial condition for the realization of the EsiRot complex. The second is, of course, the complex stability regarding interactions with the stopper. For this reason a 1:1 mixture of $\mathbf{A}^{2+}{}_2$@CB[8]$_2$ and the selected stopper **CD-N$_3$** in D_2O was prepared and the ^{1}H NMR spectrum was compared with the one of the complex alone (Figure 104). The signals are unchanged, which means that there is no unwanted interaction between the complex and the stopper.

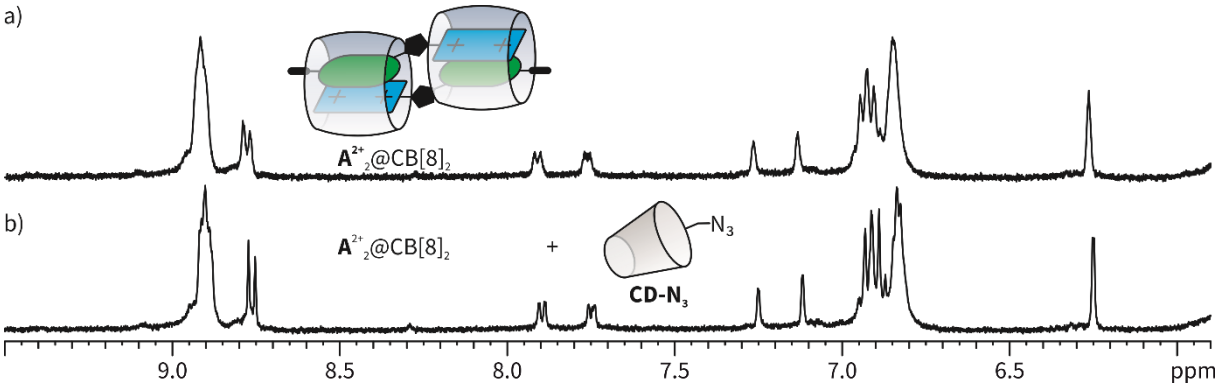

Figure 104. Partial ^{1}H NMR spectra (700 MHz, 298 K, D_2O, 1.0 mM) of (a) $\mathbf{A}^{2+}{}_2$@CB[8]$_2$ and (b) a 1:1 mixture of $\mathbf{A}^{2+}{}_2$@CB[8]$_2$ and the stopper **CD-N$_3$**.

The formation of the EsiRot complex and MS analysis was not conducted by me during this thesis. However, it seems like the designed axle does not meet the requirements of the concept of the electrostatically interlocked rotaxane. Even after stoppering the 2:2 complex with the bulky cyclodextrin stopper, MS analysis shows only the 1:1 complex. Therefore, it is assumed that the axle is too flexible because of the short linker and the dissociation takes place either during the ionization

process or the charge repulsion in the gas phase prevents the MS analysis of the EsiRot complex. Attempts to optimize the measurement conditions failed.

4.4.2 Redox Behavior of the Axle and its CB[8] Complex

The special feature of viologens, besides the complexation by cucurbiturils, is their redox behavior as explained in Chapter 4.3. Figure 105 shows the UV/Vis spectra of the axle $\mathbf{A}^{2+}$ before and after reduction with $Na_2S_2O_4$ (black and blue curve, respectively). The reduced species exhibits the typical absorption bands for the monocation radical dimer (*dimer*)[5] at 529 nm demonstrating the formation of the dimer $\mathbf{A}^{+\bullet}{}_2$ as represented as cartoon. If complex $\mathbf{A}^{2+}{}_2$@CB[8]$_2$ is reduced, however, the unique *dimer* band does not occur (red and green curve). Instead, four bands at 576, 618, 676 and 746 nm can be observed, which are identified as the bands of the monocation radical monomer (*monomer*)[6].[129] Consequently that means, that the reduced viologen moiety still form a π-donor-π-acceptor complex with the naphthalene moiety in the 2:2 complex $\mathbf{A}^{+\bullet}{}_2$@CB[8]$_2$.

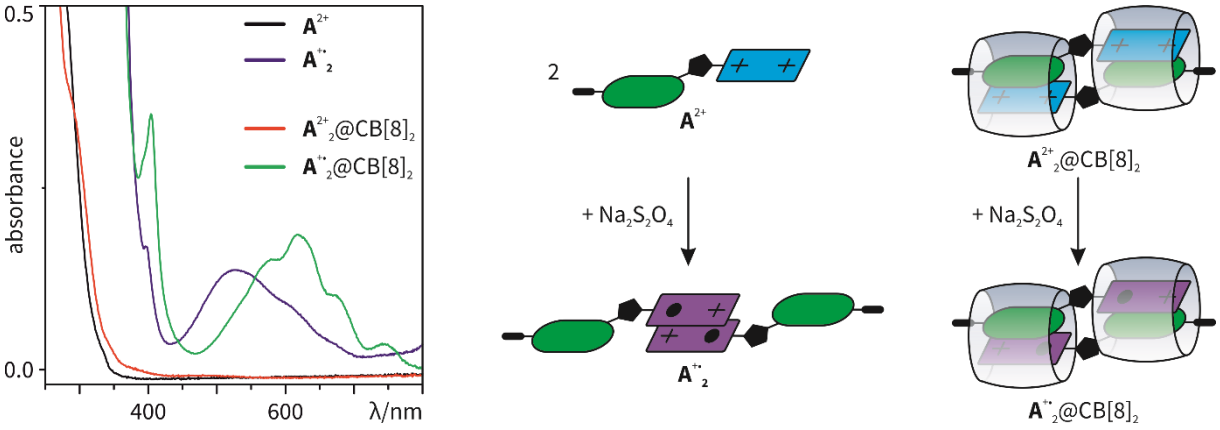

Figure 105. UV/Vis spectra of $\mathbf{A}^{2+}$ and $\mathbf{A}^{2+}{}_2$@CB[8]$_2$ in the normal (black and red curve) and the reduced (blue and green curve) state and the proposed conformations shown as cartoons; c = 0.06 mM, 10 equiv. $Na_2S_2O_4$ was used as reducing agent.

One possibility for such properties is that the 2:2 complex $\mathbf{A}^{+\bullet}{}_2$@CB[8]$_2$ is a stable intermediate and the 2:1 complex $\mathbf{A}^{+\bullet}{}_2$@CB[8] with a *dimer* band in the UV/Vis spectrum is formed over time. Therefore, the reduced solution was measured consecutive over a span of 120 minutes (Figure 106). The intensity of the *monomer* bands decreased, since the viologen moieties slowly oxidized, but no absorption band at 525 nm was observed, which means that the 2:2 complex $\mathbf{A}^{+\bullet}{}_2$@CB[8]$_2$ is thermodynamically favored over the 2:1 complex $\mathbf{A}^{+\bullet}{}_2$@CB[8].

[5] In the following, the italic word *dimer* specifically refers to the dimeric configuration of two viologen monocation radical moieties.
[6] The italic written word *monomer* refers to a configuration with just one viologen monocation radical moiety.

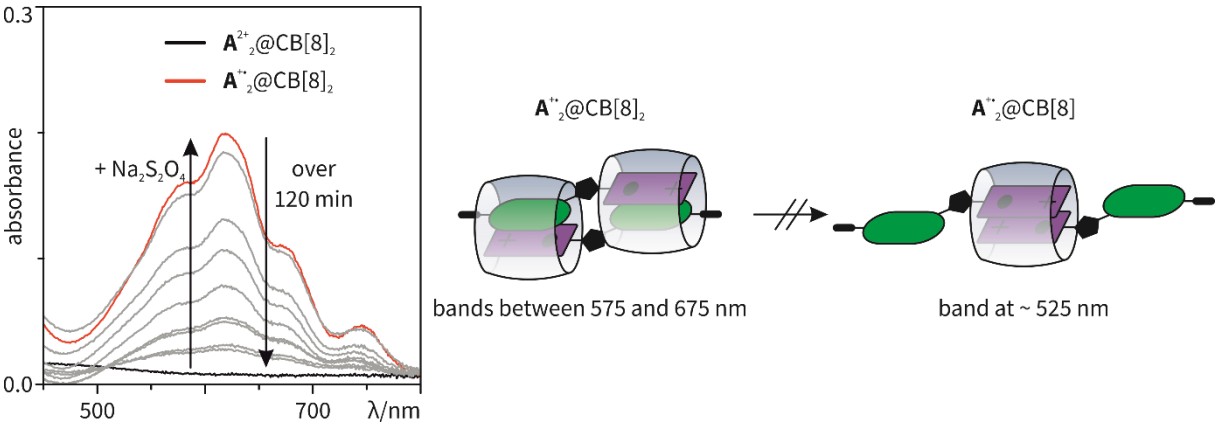

Figure 106. UV/Vis spectra of $\mathbf{A}^{2+}_2$@CB[8]$_2$ and $\mathbf{A}^{+\bullet}_2$@CB[8]$_2$ with consecutive measurements over 120 minutes and the proposed conformations shown as cartoons; c = 0.06 mM, 10 equiv. $Na_2S_2O_4$ was used as reducing agent.

The redox behavior is unusual and the formation of heteroternary π-donor-π-acceptor complexes with reduced viologen are rarely reported.[130] However, the co-conformation of the non-reduced complex $\mathbf{A}^{2+}_2$@CB[8]$_2$ and the reduced complex $\mathbf{A}^{+\bullet}_2$@CB[8]$_2$ does not change. If a second stimulus would be introduced into the system, a switching between the 2:2 and the 2:1 complex in the reduced state could be possible.

4.5 Switching between Two Cucurbit[8]uril Complex Conformations in the Reduced State

The viologen monocation radical tends to dimerize in aqueous solutions[131] and host–guest assisted stabilization of the monomer are rare in literature.[132] The 2:2 complex $\mathbf{A}^{+\bullet}_2$@CB[8]$_2$ described in Chapter 4.4.2 features the formation of a π-donor-π-acceptor dimer of a viologen monocation radical and a naphthalene moiety. If a guest would be stimuli-responsive to a second input, switching between the two states, a *monomer* and a *dimer* state, could be realized (Figure 107).[7]

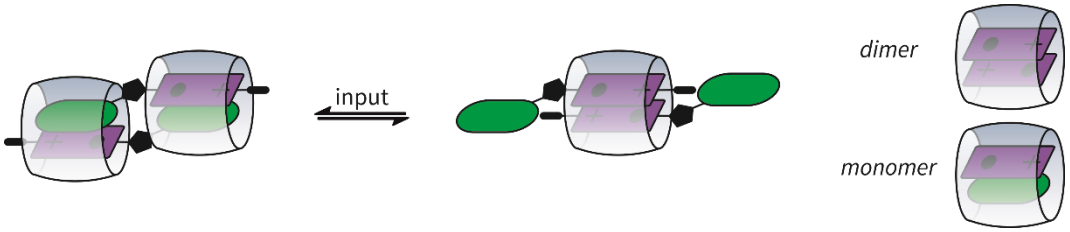

Figure 107. Concept of a molecular switch in the reduced state upon (de)protonation.

4.5.1 Synthesis and Complex Formation with Cucurbiturils

As a test compound for the electrostatically interlocked rotaxane in Chapter 4.4.1, compound **B**H^{2+} was prepared. Propargylation of axle precursor **19**$^+$ with 1-butyne and *in situ* deprotection yielded axle **B**H^{2+} in moderate yield (Scheme 14). The quantity of the product was sufficient, so no optimization was conducted. The special feature of water soluble **B**H^{2+} is the hydroxy group on the naphthalene moiety. Deprotonation changes the electronic properties of the electron rich part of the molecule giving **B**$^{2+}$.[8]

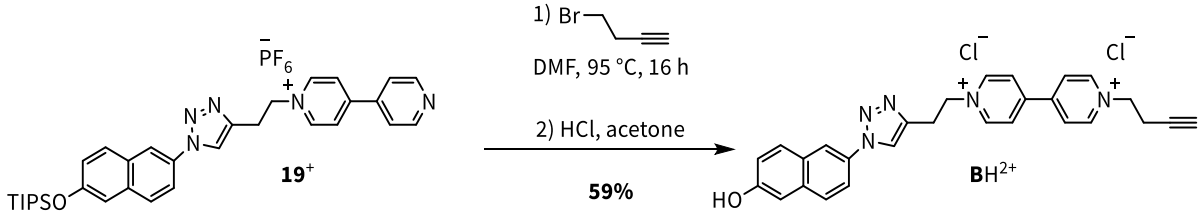

Scheme 14. Synthesis of **B**H^{2+} by alkylation and subsequent deprotection of **19**$^+$.

Figure 108 shows the ^{1}H NMR spectra of compound **B**H^{2+} and its CB[7] and CB[8] complexes in acidic and basic media. Under acidic conditions (a–c), **B**H^{2+} is well soluble in D_2O and addition of CB[7]

[7] The italic written word *dimer* specifically refers to the dimeric configuration of two viologen monocation radical moieties and the italic written word *monomer* refers in contrast to a configuration with just one viologen monocation radical moiety.

[8] The charge state in the name refers to the viologen dication and to avoid confusion, the resulting negative charge upon deprotonation is ignored in the naming of the compound.

broadens all the signals and induces the typical high field shifts of the viologen (blue) proton signals and indicate the complexation of the dicationic moiety as shown in Figure 109. Upon complexation with CB[8], all signals experience a strong highfield shift speaking in favor for the formation of the 2:2 complex **B**H$^{2+}{}_2$@CB[8]$_2$ analogous to complex **A**$^{2+}{}_2$@CB[8]$_2$ (Chapter 4.4.1). The triazole signal (orange) shifts downfield and splits to two singlets because it is located close to the rim of the host. This hints to the formation of two complex isomers with triazole protons directed in the same or the opposite direction. The spectrum exhibits two individual signals for the protons of the triazole because the conversion of the two complexes is slower than the NMR time scale. **B**$^{2+}$ has low solubility in basic aqueous solutions (d-e). The shifts of the proton signals of the complexation with CB[7] and CB[8] follow the same trends as in the acidic case, indicating formation of 1:1 complex **B**$^{2+}$@CB[7] and 2:2 complex **B**$^{2+}{}_2$@CB[8]$_2$.

This means, the complexation behavior with CB[7] and CB[8] is independent of the protonation state of the hydroxy group. Consequentially, the system is pH-responsive, but does not change its co-conformation upon (de)protonation.

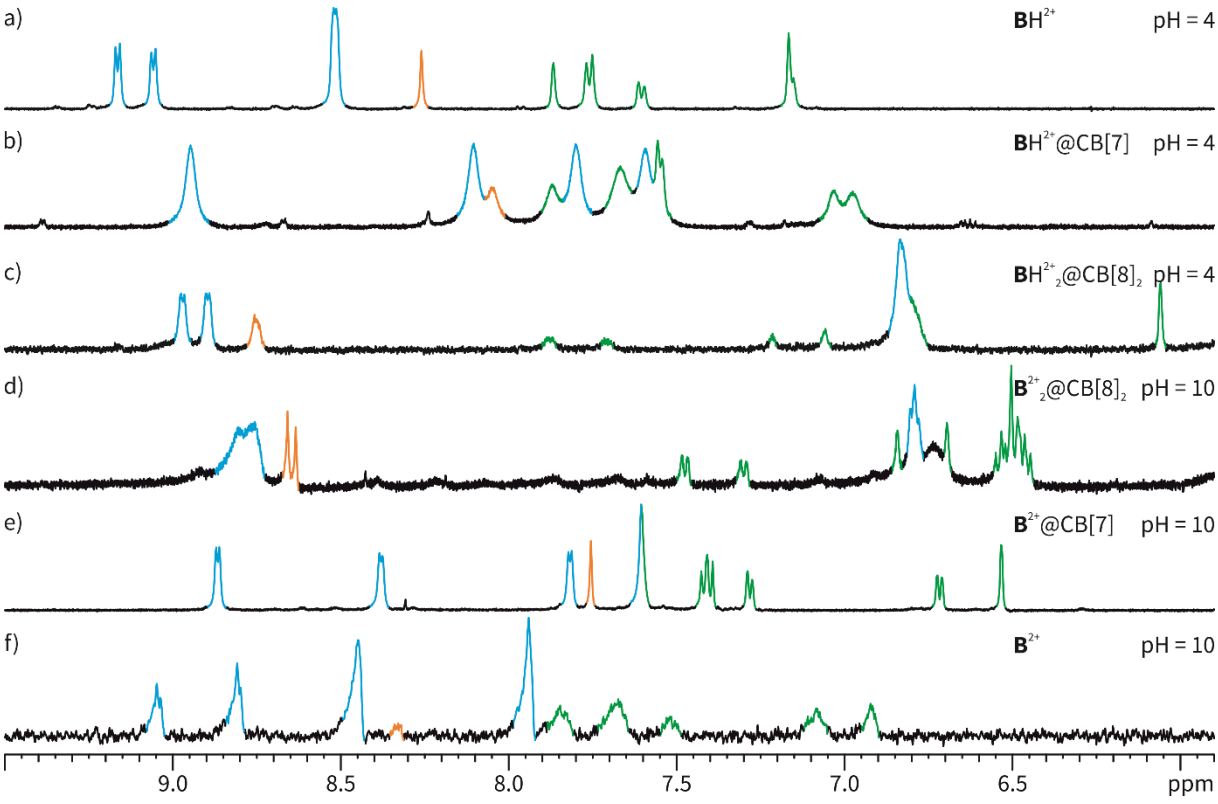

Figure 108. Partial ^{1}H NMR spectra (700 MHz, 298 K, D_2O, 1.0 mM) of (a) **B**H^{2+} (pH 4), (b) a 1:1 mixture of **B**H^{2+} and CB[7] (pH 4), (c) a 1:1 mixture of **B**H^{2+} and CB[8] (pH 4), (d) a 1:1 mixture of **B**$^{2+}$ and CB[8] (pH 10), (e) a 1:1 mixture of **B**$^{2+}$ and CB[7] (pH 10), and (f) **B**$^{2+}$ (pH 10); DCl (35% in D_2O) and K_2CO_3 were used to (de)protonate.

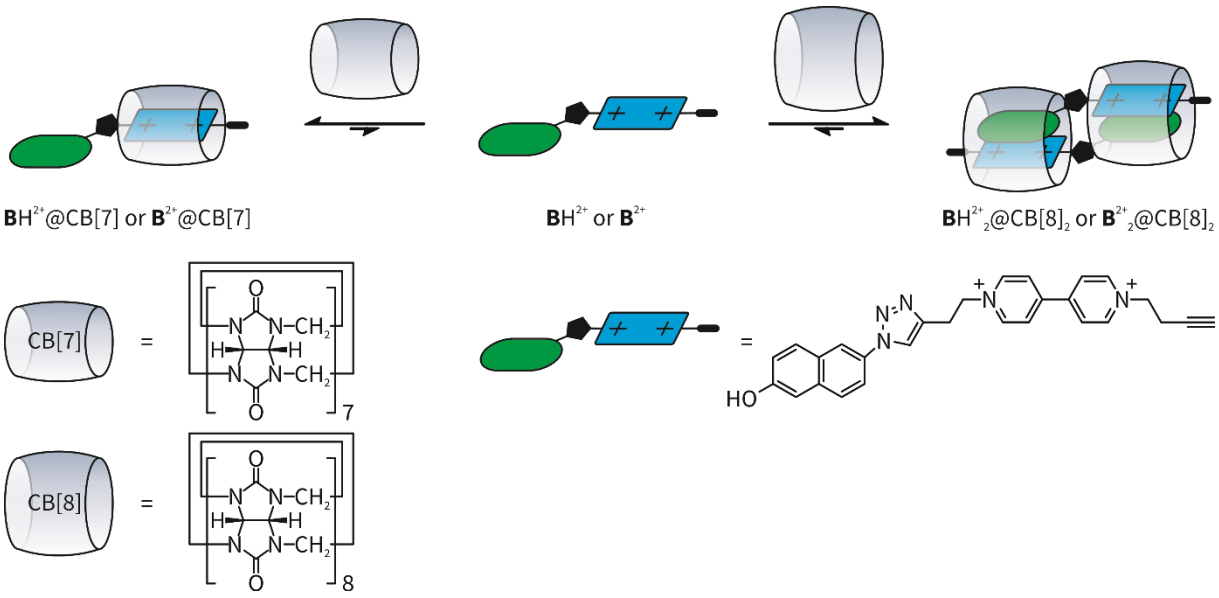

Figure 109. Complexation of **B**H^{2+} and **B**$^{2+}$ with CB[7] and CB[8].

The UV/Vis spectra of **B**H^{2+} and **B**$^{2+}$ their complexes are shown in Figure 110. In the protonated form (a), the spectra exhibit a bathochromic shift upon complexation, which can be contributed to the apolar environment inside the cavity of the host. Furthermore, for **B**H$^{2+}{}_2$@CB[8]$_2$ a charge transfer (CT) band can be observed between 360 and 390 nm, which can be attributed to the formation of a π-donor-π-acceptor 2:2 complex. The bathochromic shifts for the deprotonated forms (b) are less obvious; nevertheless, a CT band can only be observed for the CB[8] complex between 400 and 420 nm.

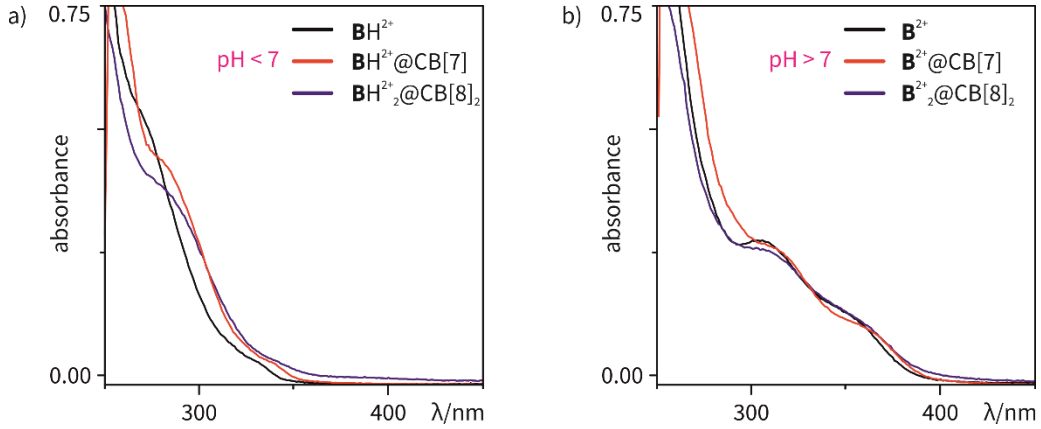

Figure 110. UV/Vis spectra of (a) **B**H^{2+} and its complexes and (b) **B**$^{2+}$ and its complexes; c = 0.06 mM.

4.5.2 Reduction Behavior of the Guest

Since the molecular switch should work in the reduced state the reduction behavior of the guest alone was investigated. The reduction of **B**H^{2+} and **B**$^{2+}$ with $Na_2S_2O_4$ is followed by the formation of the typical *dimer* bands in the UV/Vis spectra independent on the pH of the aqueous solution (Figure 111).[133] Therefore, the dimers **B**H$^{+\bullet}{}_2$ and **B**$^{+\bullet}{}_2$ are formed in acidic and basic medium.

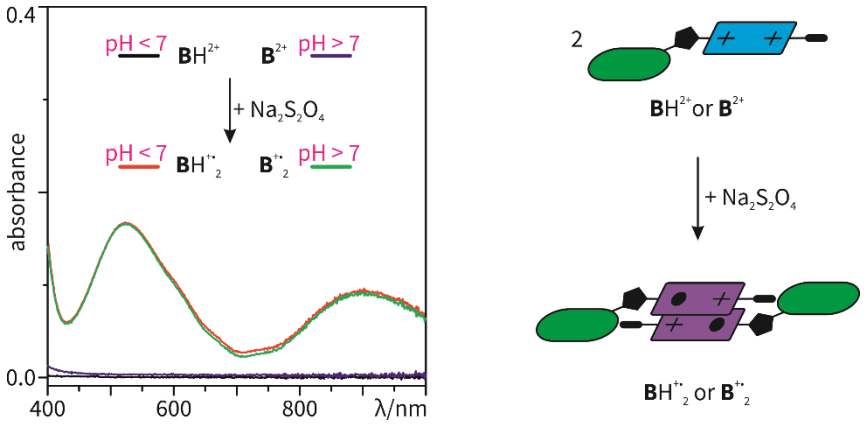

Figure 111. UV/Vis spectra of **B**H^{2+} and **B**$^{2+}$ before and after reduction and the proposed formation of the dimers **B**H$^{+\bullet}_2$ and **B**$^{+\bullet}_2$ shown as cartoons; c = 0.06 mM, 10 equiv. $Na_2S_2O_4$ was used as reducing agent.

4.5.3 Reduction Behavior of the CB[7] Complexes

The 1:1 complex **B**H^{2+}@CB[7] was reduced with $Na_2S_2O_4$ to investigate if the complexation with CB[7] has an influence on the dimerization of the viologen moieties. **B**H^{2+}@CB[7] was reduced in acidic medium and the viologen *dimer* bands can be observed in the UV/Vis spectra (Figure 112a). The same is true for **B**$^{2+}$@CB[7] in basic medium (b). Subsequent acidification has no influence on the spectrum. Therefore, the formation of **B**H$^{+\bullet}_2$ and **B**$^{+\bullet}_2$ is not prevented by any host–guest interaction with CB[7].

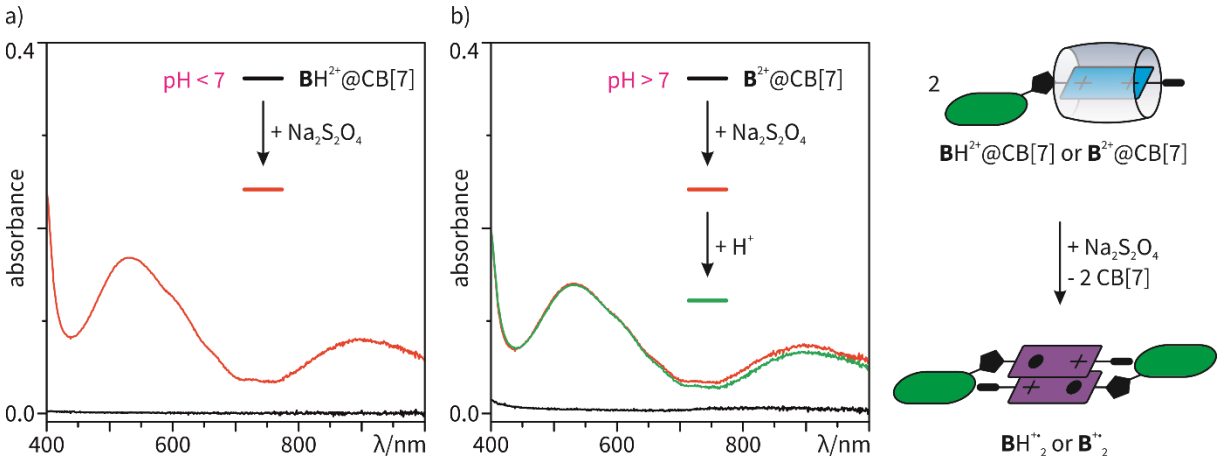

Figure 112. UV/Vis spectra of (a) **B**$^{2+}$@CB[7] in the normal (black curve) and the reduced (red curve) state in acidic medium (pH 4) and (b) **B**$^{2+}$@CB[7] in the normal (black curve) and the reduced (red curve) state in basic medium (pH 10) and subsequent protonation (green curve) and the proposed conformations shown as cartoons; c = 0.06 mM, 10 equiv. $Na_2S_2O_4$ was used as reducing agent.

4.5.4 Reduction Behavior of the CB[8] Complexes

The redox behavior of the CB[8] complexes is shown in Figure 113. The reduction of **B**H^{2+}_2@CB[8]$_2$ is analogous to the one of **A**$^{2+}_2$@CB[8]$_2$. The absorption bands for the *monomer* occur at 595, 614, 672 and 739 nm. This indicates the formation of the 2:2 complex **B**$H^{+\bullet}_2$@CB[8]$_2$. In this complex, the reduced viologen moiety is interaction with the naphthalene moiety. On the contrary, in basic medium for **B**$^{2+}_2$@CB[8]$_2$ the unique *dimer* band at 540 nm can be observed. This is only possible for the 2:1 complex **B**$^{+\bullet}_2$@CB[8].

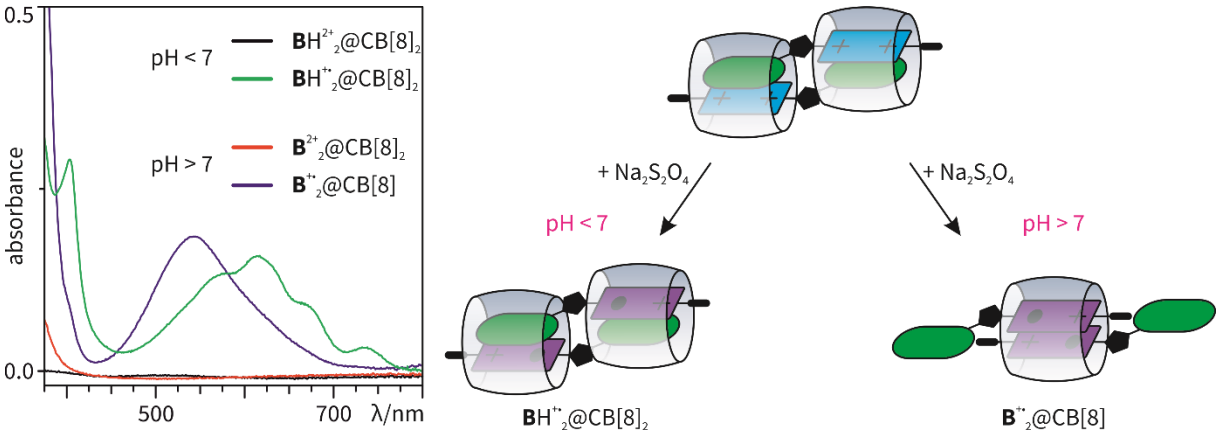

Figure 113. UV/Vis spectra of **B**H^{2+}_2@CB[8]$_2$ and **B**$^{2+}_2$@CB[8]$_2$ in the normal (black and red curve) and the reduced (blue and green curve) state and the proposed conformations of **B**$H^{+\bullet}_2$@CB[8]$_2$ and **B**$^{+\bullet}_2$@CB[8] shown as cartoons; c = 0.06 mM, 10 equiv. $Na_2S_2O_4$ was used as reducing agent.

The different complex conformations of the 2:1 and the 2:2 complex are also visible to the naked eye (Figure 114). The 2:1 complex **B**$^{+\bullet}_2$@CB[8] has the typical violet color of the viologen *dimer*.[134] The 2:2 complex **B**$H^{+\bullet}_2$@CB[8]$_2$ has a blue color.

Figure 114. Photograph of solutions of **B**$^{+\bullet}_2$@CB[8] (left) and **B**$H^{+\bullet}_2$@CB[8]$_2$ (right) and the proposed conformations shown as cartoons; c = 0.06 mM, 10 equiv. $Na_2S_2O_4$ was used as reducing agent.

Since the two proposed complexes **B**$H^{+\bullet}_2$@CB[8]$_2$ and **B**$^{+\bullet}_2$@CB[8] form at different pH, a switching between these two could be possible. To investigate if the complexes are the thermodynamic products, UV/Vis analysis was conducted over time. Oxidation of the viologen monocation radical in basic conditions is slow and therefore, 2:1 complex **B**$^{+\bullet}_2$@CB[8] is stable over the span of at least 10 minutes.[135] In acidic condition oxidation occurs faster and the UV/Vis bands of the 2:2 complex **B**$H^{+\bullet}_2$@CB[8]$_2$ vanish after 5 minutes. Therefore, transformation of the 2:2 to the 2:1 complex does not take place (Figure 115).

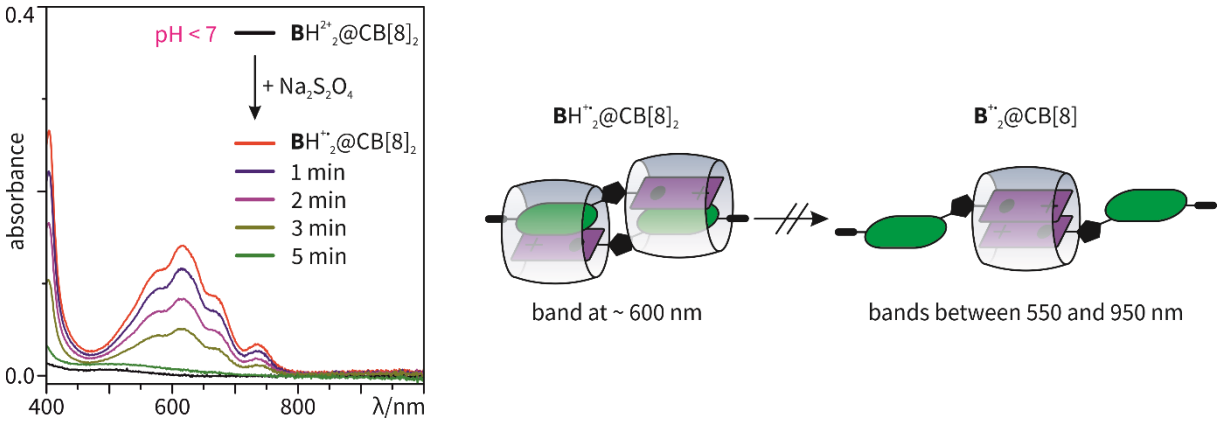

Figure 115. UV/Vis spectra of **B**H$^{2+}_2$@CB[8]$_2$ in acidic medium before and after reduction and subsequent measurements over a span of 5 min and the proposed conformations shown as cartoons; c = 0.06 mM, 10 equiv. $Na_2S_2O_4$ was used as reducing agent.

4.5.5 A Molecular Switch in the Reduced State

To test the switching between the two complexes (Figure 116), a CB[8] complex solution was acidified with HCl (1 µL, 1M, black curve) and reduced exhibiting the *monomer* bands in the UV/Vis spectrum (red curve). Neutralization with NaOH (1 µL, 1M, blue curve) shows the coexistence of both species with bands for the *monomer* (around 600 nm) and the *dimer* (around 550 and 950 nm). After addition of NaOH (1 µL, 1M, orange curve) a basic medium is reached, which results in the exclusive formation of the *dimer* bands. And after protonation with HCl (3 µL, 1M, green curve) the spectrum exhibits again the *monomer* bands. This demonstrates the reversible switching between the two complexes **B**H$^{+\bullet}_2$@CB[8]$_2$ and **B**$^{+\bullet}_2$@CB[8] by pH stimuli. The stimuli induced conformational changes of the two complexes can be identified as a molecular switch.

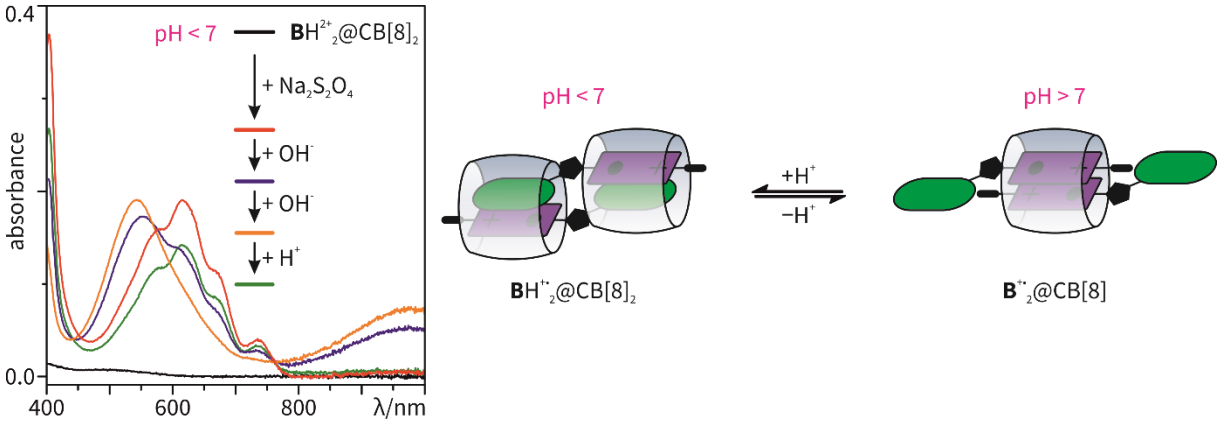

Figure 116. UV/Vis spectra of the switching between the complexes **B**H$^{+\bullet}_2$@CB[8]$_2$ and **B**$^{+\bullet}_2$@CB[8] by (de)protonation and the proposed conformations shown as cartoons; c = 0.06 mM, 10 equiv. $Na_2S_2O_4$ was used as reducing agent, 1M HCl and 1M NaOH was used to (de)protonate.

4.5.6 Complex Formation in the Reduced State

To test if the complexation with CB[8] takes place with the already reduced guest **B**H$^{+\bullet}_2$, a solution of **B**H^{2+} was reduced in acidic medium and a host solution was added (Figure 117). The reduced guest **B**H$^{+\bullet}_2$ alone exhibits the bands for the viologen *dimer* as shown before. After addition of CB[8] the *monomer* bands for the 2:2 complex **B**H$^{+\bullet}_2$@CB[8]$_2$ occur. This demonstrates the complex formation takes place even in the reduced state.

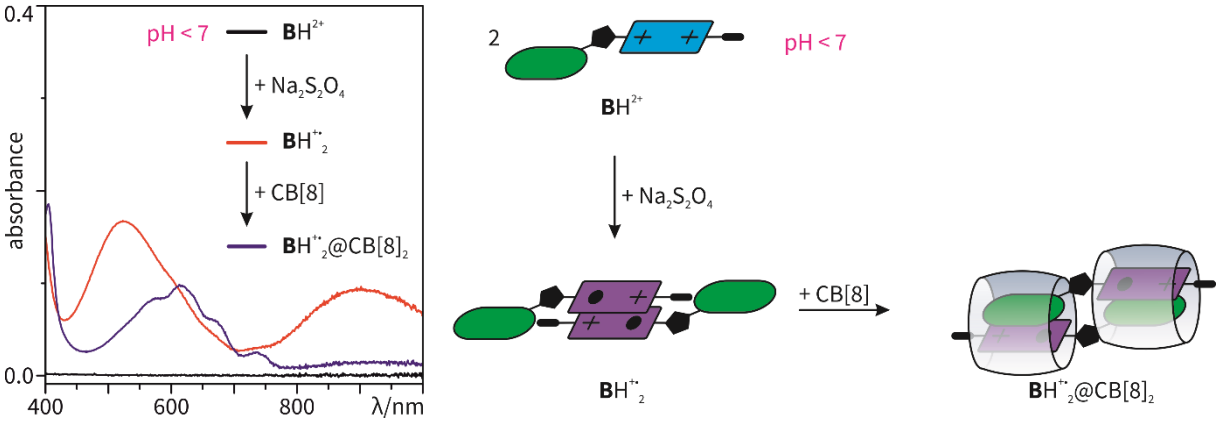

Figure 117. UV/Vis spectra of **B**H^{2+} in acidic medium before and after reduction (c = 0.06 mM) and subsequent addition of 1 equiv. CB[8] in H_2O forming 2:2 complex **B**H$^{+\bullet}_2$@CB[8]$_2$ (c = 0.04 mM) and the proposed conformations shown as cartoons; 10 equiv. $Na_2S_2O_4$ was used as reducing agent.

In conclusion, a pH-responsive molecular switch in the reduced state was realized. The conformational change from the 2:2 complex **B**H$^{+\bullet}_2$@CB[8]$_2$ to the 2:1 complex **B**$^{+\bullet}_2$@CB[8] is possible by simple acid/base titration. The switch is fully reversible and can be observed by the naked eye since the two complex solutions have different colors.

5 Conclusion

The aim of this thesis was the design and synthesis novel stimuli-responsive host–guest systems based on cucurbit[8]urils (CB[8]) as molecular switches in water. The conformational and electronic changes of these complexes upon external inputs were investigated and the emerging properties resulting from of novel functional supramolecular systems were elucidated.

The new guests for CB[8] were designed based on the following simple components: a dicationic bipyridinium and a monocationic phenylpyridinium, as well as an electron-rich counterpart, in this case either a biphenyl or a naphthalene moiety. Furthermore, the components are in part pH- or redox-responsive. Combining these two stimuli within one network results in an orthogonally addressable multicomponent system.

Overall, three stimuli-responsive supramolecular systems in water have been presented which are based on novel cucubit[8]uril complexes and their different functionalities emerging upon (de)protonation. These are (i) the tuning of the fluorescence properties of a 2:2 complex, (ii) the exchange of the guests in ternary complexes and (iii) conformational changes between a 2:2 and a 2:1 complex (Figure 118).

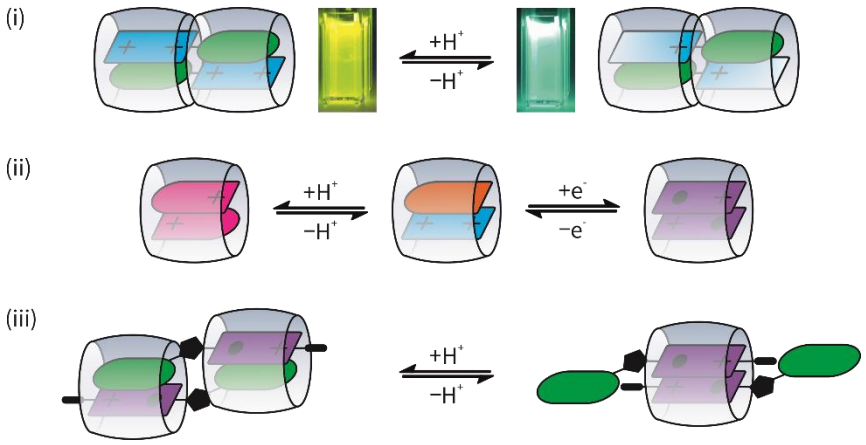

Figure 118. Schematic representations of the pH-responsive cucurbit[8]uril complexes and the behavior upon (de)protonation: (i) Changes of emission properties of a 2:2 complex, (ii) orthogonal switching between three ternary cucurbit[8]uril complexes and (iii) conformational changes from a 2:2 to a 2:1 cucurbit[8]uril complex in the reduced state.

(i) A series of pH-responsive guests based on covalently linked bipyridinium and biphenyl moieties were investigated that exhibit a strong fluorescence enhancement upon complexation within CB[8]. While examples of fluorophore encapsulation in CB[*n*]s were reported before, the combining the prevention of a twisted intramolecular charge transfer (TICT) fluorescence-quenching mechanism with excimer formation of the fluorophore upon complexation by CB[8] is a novel concept. Tuning the emission properties of the system is possible by covalent modification of the dye itself and, after complexation, by (de)protonation of the host–guest complex. Besides the investigated fluorescence properties, the 2:2 complex can be used as a potential linker in aqueous solutions. This allows the

formation of larger architectures based on two identical guests, similar to earlier presented phenylpyridinium derivatives.[48] The incorporation of a bipyridinium unit yields a redox-responsive guest which can undergo an one-electron reduction. This offers the possibility to investigate the behavior of 2:2 CB[8] complex with two identical guests upon redox-stimuli in future studies.

(ii) A series of phenylpyridinium derivatives was prepared bearing different reactive functional groups for potential post-modification. The CB[8] complex formation regarding the tolerance of the different electrophilic and nucleophilic functional groups and regarding the presence of different electron-rich aromatic systems was investigated. In addition, compounds with two binding stations for the potential formation of supramolecular polymers were studied. Based on these findings, an orthogonally switchable multicomponent system was developed. The interplay of a pH-responsive phenylpyridine derivative, a redox-responsive bipyridinium derivative and CB[8] results in a system, in which the switching between three ternary complexes is possible. Furthermore, an orthogonally stimuli-responsive self-sorting network based on four components demonstrated the robustness of the complex formation. The ternary complexes change their guests upon a stimulus. Orthogonal switching between three ternary CB[8] complexes is unique. The redox-responsive viologen-naphthalene motif is widely used in supramolecular architectures with CB[8].[6] As an extension, SCHERMAN introduced an orthogonally light-responsive second guest that can be combined with viologens for the formation of host-guest complexes with CB[8].[86] The system presented herein offers an alternative with a third orthogonal input by (de)protonation. Since the introduced phenylpyridine derivative can act as a typical first or second guest – depending on its protonation state – it can be combined with either redox active viologens or light-responsive guests. Since the phenylpyridine can be substituted without losing its pH-sensitivity, it can be used as a stimuli-responsive linker in larger supramolecular architectures.

(iii) An axle consisting of a covalently linked redox-responsive bipyridinium and a pH-responsive naphthalene was designed. The complexation with CB[8] results in an orthogonally stimuli-responsive 2:2 complex. Reduction of the CB[8] complex results in the formation of two different conformations depending on the protonation state. While the dimerization of bipyridinium moieties upon reduction is well-known, reports on the formation of π-donor-π-acceptor complex within CB[8] of a reduced bipyridinium unit and an electron-rich second guest are still rare. Not only does the system developed in this project feature such a structure, but also does (de)protonation result in a formerly unreported reversible change from a 2:2 to a 2:1 host-guest complex. The latter features the reduced viologen dimer inside the cavity of one host. The switching changes the offset of the guests towards each other. Since the guest can be substituted on one side, introduction into larger supramolecular architecture without eliminating the redox- or pH-responsiveness could be possible, potentially enabling the development of a system able to conduct muscle-like motion in future studies. With this axle, the concept of an electrostatically interlocked rotaxane in water was

developed. The axle forms a 2:2 complex with CB[8], but does not seem to meet the requirements for the realization of the concept because of its flexibility.

Two potential supramolecular systems containing the CB[8] complexes developed in this work will be presented as perspective to demonstrate their versatility. It is assumed that the work on the electrostatically interlocked rotaxane could not be completed successfully within the course of this thesis, since the linker between the viologen unit and the electron-rich counterpart is too flexible and allows for decomplexation. Therefore, the introduced bipyridinium derivative with the shorter linker might offer a solution (Figure 119). The 2:2 CB[8] complex could only dissociate to a 1:1 complex by a reaction mechanism which includes an intermediate complex with two doubly charged viologen moieties inside the cavity of a single CB[8], which is unfavored due to charge repulsion. This would result in the successful generation of an electrostatically interlocked rotaxane which will be further explored in the future.

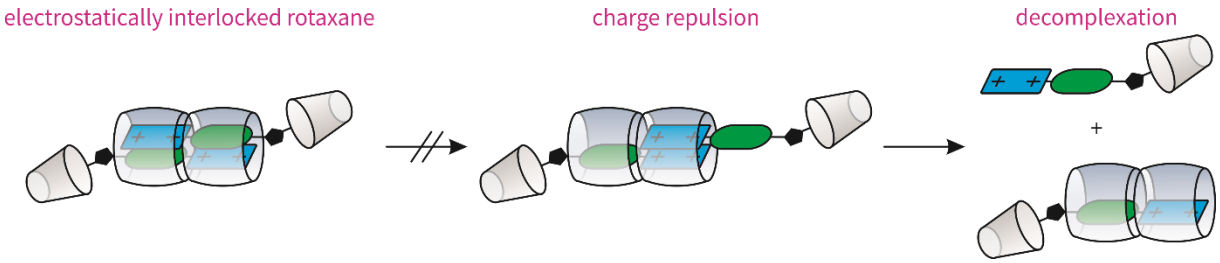

Figure 119. An electrostatically interlocked rotaxane based on the rigid guest introduced in Chapter 4.1.

The developed system of ternary 2:1 complexes which exchange their guests orthogonally switch by pH- and redox-input could be translated to the macroscopic scale by the construction of a self-sorting gel (Figure 120). It could be envisaged to functionalize a first polymer strand with the phenylpyridine moiety and a second one with a bipyridinium moiety. Under basic conditions, it could be possible to form heteroternary complexes which results in a gel that incorporates both polymers strands. Acidification or reduction of the system might result in the formation of homoternary CB[8] complexes, leading to the separation of the gelated and the non-gelated polymer strands. By color coding the polymer strands with different dyes, it might even be possible to visualize the self-sorting and to make it observable with the naked eye.

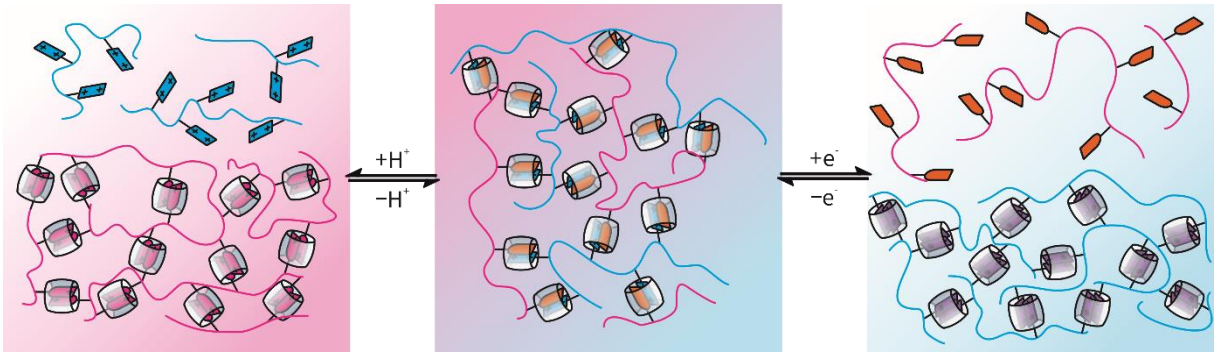

Figure 120. A self-sorting gel based on the orthogonal switching of a single cucurbit[8]uril complex between three ternary complexes introduced in Chapter 4.3.

The presented novel stimuli-responsive cucurbituril complexes extend the toolkit for supramolecular chemistry in aqueous solution. As easy to handle building blocks, the complexes can be utilized as connecting elements or building blocks for large and functional assemblies featuring intriguing emergent properties.

6 Experimental part

6.1 General Methods

All reagents were commercially available and used without further purification. Thin-layer chromatography (TLC) was performed on aluminum sheets coated with silica gel 60/F254 (Merck KGaA) or ALOX N/UV_{254} (Macherey-Nagel). Column chromatography was performed on silica gel 60 (Merck 40 – 60 nm, 230 – 400 mesh) or ALOX I, neutral (Acros Organics 50 – 200 µm, 60A). The yields refer to chromatographically homogeneous and spectroscopically pure materials (^{1}H-NMR spectroscopy).

Melting points were determined on a Stuart SMP30 apparatus and are uncorrected.

^{1}H NMR, ^{13}C NMR and ^{1}H, ^{1}H COSY spectra were recorded with Bruker (AV 500, AVIII 700) or JEOL (ECX 400, ECP 500) instruments. All chemical shifts are reported in ppm with the residual undeuterated solvents as the internal standards. Coupling constants (*J*) are given in Hz.

UV/Vis spectra were recorded on Varian Cary 50 Bio spectrophotometer. Fluorescence spectra were recorded on a PERKIN ELMER LS50B spectrophotometer. Quantum yields were recorded on a HAMAMATSU Absolute PL Quantum Yield Spectrometer C11347. Fluorescence decay measurements were conducted on an Edinburgh Instruments FLS920 with Czerny-Turner double monochromators (λ = 330 nm: Edinburgh Instrument EPLED-330 (picosecond pulsed light emitting diode); λ = 375 nm: Edinburgh Instrument EPL-375 (picosecond pulsed diode laser)) and a Hamamatsu R3809U-50 (range 200–850 nm, response width < 25 ps), Multi-Channel Plate (MCP) detector. Fit was performed with Edinburgh Instruments FAST Software.

Electrospray-ionization time-of-flight-resolution mass spectrometric (ESI-TOF-HRMS) experiments were conducted on an Agilent 6210 ESI-TOF mass spectrometer.

Redox-potentials reported in this study were obtained by cyclic voltammetry. Measurements were carried out in aqueous solutions with 0.1 M electrolyte and 1 mM analyte concentration using a three-electrode configuration (glassy carbon working electrodes, Pt counter electrode, Ag wire as pseudoreference) and an Autolab PGSTAT302N potentiostat. The decamethylferrocene/decamethylferrocenium ($[FeCp_2^*]^{+/0}$) couple was used as the internal reference for all measurements to ensure maximum comparability. Energy differences were calculated according to the equation $\Delta G = -n F \Delta E$.

The crystal data and experimental details for the data collections are given below. Single-crystal X-ray data for $\mathbf{2}^+OTf^-$, $\mathbf{2}^+BF_4^-$, $\mathbf{2}H^{+2}{}_2$@CB[8]$_2$ and $\mathbf{C}^{2+}$ was measured using a Rigaku SuperNova dual-

source Oxford diffractometer equipped with an Atlas detector using mirror-monochromated Cu-Kα (λ = 1.54184 Å) radiation. The data for $\mathbf{2}^{+}ClO_4^{-}$, $\mathbf{2}^{+}NO_3^{-}$ and $\mathbf{8}^{2+}$ were collected using a Rigaku SuperNova single-source Oxford diffractometer[125] with an Atlas EoS CCD detector using mirror-monochromated Mo-Kα (λ = 0.71073 Å) radiation. The data collection and reduction for data sets collected using Rigaku instruments were performed using the program CrysAlisPro[125] and Gaussian face index absorption correction method[125] was applied. The data for $\mathbf{2}^{+}\cdot PF_6^{-}$ was collected using a Bruker D8 Venture Photon diffractometer using mirror-monochromated Mo-Kα (λ = 0.71073 Å) radiation. The intensities for data were corrected for absorption using SADABS with multi-scan absorption correction type method. All structures were solved with direct methods (SHELXS)[136] and refined by full-matrix least squares on F^2 using the *OLEX2* software,[137] which utilizes the SHELXL-2013 module.[136] Constraints and restraints were used where appropriate for disordered models.

6.2 Synthetic Procedures for Chapter 4.1

General Procedure 1 (GP1), Suzuki Reaction in Water: Compound **1** (1 equiv., maximum of 250 mg), 4-R-boronic acid or its pinacol ester (1.3 equiv.) and Na_2CO_3 (2 equiv.) were dissolved in H_2O (0.02 mL/µmol) and argon was purged though the solution for 10 min. Afterwards, $Pd(OAc)_2$ was added and the reaction mixture was heated to 100 °C for 4 h. After cooling to r.t., sat. NH_4PF_6 (aq.) was added. The precipitate was filtered off and dried. Afterwards, the PF_6^- salt was dissolved in acetone and HCl (aq., 36%) was added. The precipitate was filtered off and dried furnishing the desired product as the corresponding Cl^- salt.

1-(2,4-Dinitrophenyl)-[4,4'-bipyridin]-1-ium chloride (**SI1**)[138]

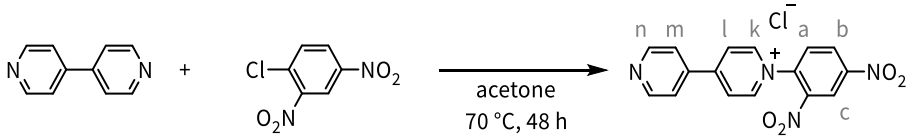

51%

4,4'-Bipyridine (3.12 g, 20.0 mmol, 1 equiv.) and 1-chloro-2,4-dinitrobenzene (4.06 g, 20.0 mmol, 1 equiv.) were dissolved in acetone (30 mL) and stirred at 70 °C for 48 h. The resulting solid was filtered off, washed with *n*-pentane and DCM furnishing **SI1** (3.69 g, 10.3 mmol, 51%) as a grey powder.

^{1}H NMR (500 MHz, DMSO-d_6) δ = 9.56 (d, *J* = 6.7 Hz, 2H, H_k), 9.15 (d, *J* = 2.5 Hz, 1H, H_c), 8.99 (dd, *J* = 8.7, 2.5 Hz, 1H, H_b), 8.95 – 8.93 (m, 4H, H_n & H_l), 8.46 (d, *J* = 8.7 Hz, 1H, H_a), 8.19 (d, *J* = 6.2 Hz, 2H, H_m) ppm.

The spectroscopic data agrees with previously published results.[138]

1-(4-Iodophenyl)-[4,4'-bipyridin]-1-ium chloride (**1**)[138]

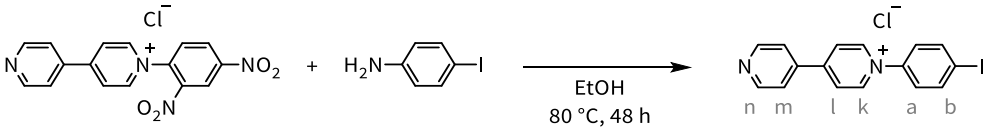

92%

Compound **SI1** (3.35 g, 9.33 mmol, 1 equiv.) and 4-iodoaniline (4.09 g, 18.66 mmol, 2 equiv.) were dissolved in EtOH (68 mL) and stirred at 80 °C for 48 h. The solvent was evaporated and the solid washed with acetone furnishing **1** (3.40 g, 8.62 mmol, 92%) as a greenish-grey powder.

^{1}H NMR (400 MHz, DMSO-d_6) δ = 9.50 (d, *J* = 7.0 Hz, 2H, H_k), 8.91 (d, *J* = 6.2 Hz, 2H, H_n), 8.80 (d, *J* = 7.0 Hz, 2H, H_l), 8.18 – 8.13 (m, 4H, H_m & H_a), 7.74 (d, *J* = 8.9 Hz, 2H, H_b) ppm.

The spectroscopic data agrees with previously published results.[138]

1-([1,1'-Biphenyl]-4-yl)-[4,4'-bipyridin]-1-ium chloride (**2**$^+$)

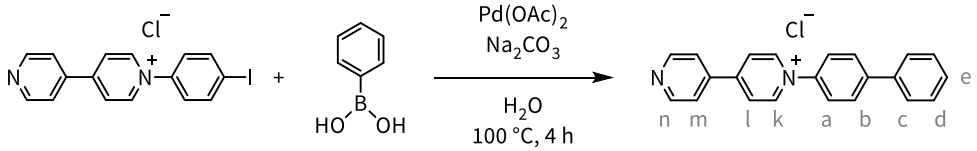

89%

According to GP1, **1** (200 mg, 506 µmol, 1.0 equiv.), phenylboronic acid (80.0 mg, 658 µmol, 1.3 equiv.), Na_2CO_3 (108 mg, 1012 µmol, 2 equiv.) and $Pd(OAc)_2$ (22.0 mg, 102 µmol, 0.2 equiv.) were dissolved in H_2O (10 mL) and stirred at 100 °C for 4 h. Anion exchanges furnished **2**$^+$ (156 mg, 452 µmol, 89%) as a yellow powder.

M.P.: > 250 °C.

^{1}H NMR (500 MHz, DMSO-d_6) δ = 9.60 (d, *J* = 6.9 Hz, 2H, H_k), 9.01 (d, *J* = 5.4 Hz, 2H, H_n), 8.85 (d, *J* = 6.9 Hz, 2H, H_l), 8.33 (d, *J* = 5.4 Hz, 2H, H_m), 8.08 (d, *J* = 8.9 Hz, 2H, Ha), 8.04 (d, *J* = 8.9 Hz, 2H, H_b), 7.82 (d, *J* = 7.4 Hz, 2H, H_c), 7.56 (t, *J* = 7.4 Hz, 2H, H_d), 7.49 (d, *J* = 7.4 Hz, 1H, H_e) ppm.

^{1}H NMR (500 MHz, D_2O) δ = 9.38 (d, *J* = 6.4 Hz, 2H, H_k), 9.02 (d, *J* = 5.9 Hz, 2H, H_n), 8.69 (d, *J* = 6.4 Hz, 2H, H_l), 8.45 (d, *J* = 5.9 Hz, 2H, H_m), 8.04 (d, *J* = 8.2 Hz, 2H, H_a), 7.91 (d, *J* = 8.2 Hz, 2H, H_b), 7.82 (d, *J* = 7.6 Hz, 2H, H_c), 7.60 (t, *J* = 7.6 Hz, 2H, H_d), 7.53 (d, *J* = 7.6 Hz, 1H, H_e).

HRMS (ESI-TOF) *m/z* calcd. for $[C_{22}H_{17}N_2]^+$ 309.1386, found 309.1404.

The spectroscopic data agrees with previously published results.[139]

It was possible to obtain several crystal structures of **2**$^+$ with different counterions: [**2**][PF_6], [**2**H][ClO_4]$_2$, [**2**][OTf], [**2**][BF_4] and [**2**H][NO_3]$_2$.

1-(4'-Formyl-[1,1'-biphenyl]-4-yl)-[4,4'-bipyridin]-1-ium chloride (**3**$^+$)

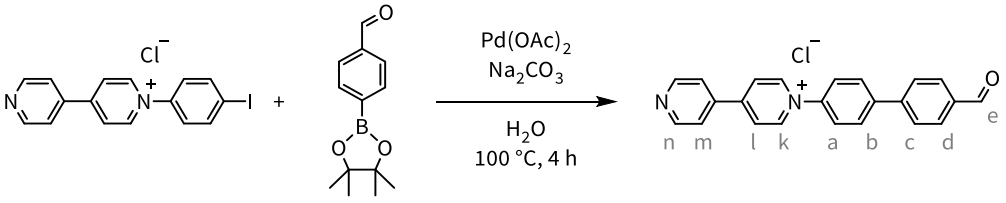

98%

According to GP1, **1** (250 mg, 633 µmol, 1.0 equiv.), 4-formylphenylboronic acid pinacol ester (191 mg, 823 µmol, 1.3 equiv.), Na_2CO_3 (134 mg, 1.27 mmol, 2 equiv.) and $Pd(OAc)_2$ (29.0 mg, 127 µmol, 0.2 equiv.) were dissolved in H_2O (12.5 mL) and stirred at 100 °C for 4 h. Anion exchanges furnished **3**$^+$ (209 mg, 619 µmol, 98%) as a yellow powder.

M.P.: > 250 °C.

^{1}H NMR (500 MHz, DMSO-d_6) δ = 10.11 (s, 1H, H_e), 9.59 (d, *J* = 7.0 Hz, 2H, H_k), 8.98 (d, *J* = 6.3 Hz, 2H, H_n), 8.84 (d, *J* = 7.0 Hz, 2H, H_l), 8.27 (d, *J* = 6.3 Hz, 2H, H_m), 8.19 (d, *J* = 8.7 Hz, 2H, H_a), 8.13 – 8.03 (m, 6H, H_b & H_c & H_d) ppm.

^{13}C NMR (176 MHz, DMSO-d_6) δ = 192.9, 152.3, 148.5, 145.5, 143.7, 142.2, 141.6, 135.9, 130.3, 128.8, 127.9, 125.7, 125.6, 123.4 ppm.

HRMS (ESI-TOF) *m/z* calcd. for $[C_{23}H_{17}N_2O]^+$ 337.1335, found 337.1357.

1-(4'-Acetyl-[1,1'-biphenyl]-4-yl)-[4,4'-bipyridin]-1-ium chloride (**4**$^+$)

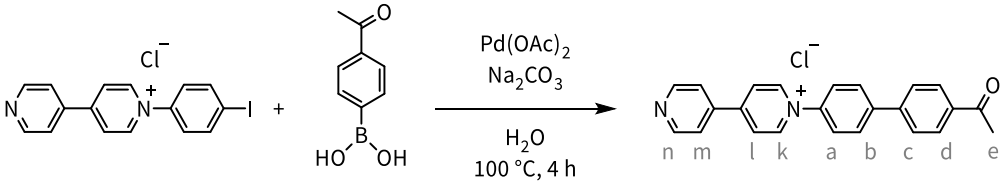

37%

According to GP1, **1** (100 mg, 253 µmol, 1.0 equiv.), 4-acetylphenylboronic acid (54.0 mg, 329 µmol, 1.3 equiv.), Na_2CO_3 (54.0 mg, 506 µmol, 2 equiv.) and $Pd(OAc)_2$ (11.0 mg, 51.0 µmol, 0.2 equiv.) were dissolved in H_2O (5 mL) and stirred at 100 °C for 4 h. Anion exchanges furnished **4**$^+$ (36.0 mg, 93.1 µmol, 37%) as a yellow powder.

M.P.: 241 °C.

^{1}H NMR (700 MHz, DMSO-d_6) δ = 9.56 (d, *J* = 6.9 Hz, 2H, H_k), 8.93 (d, *J* = 6.2 Hz, 1H, H_n), 8.82 (d, *J* = 6.9 Hz, 2H, H_l), 8.19 – 8.16 (m, 4H, H_m & H_a), 8.12 (d, *J* = 8.4 Hz, 2H, H_d), 8.07 (d, *J* = 8.6 Hz, 2H, H_b), 7.99 (d, *J* = 8.4 Hz, 2H, H_c), 2.65 (s, 3H, H_e) ppm.

^{13}C NMR (176 MHz, DMSO-d_6) δ = 197.5, 153.3, 151.1, 145.3, 142.4, 142.02, 141.6, 140.6, 136.5, 129.0, 128.6, 127.4, 125.3, 122.1, 26.9 ppm.

HRMS (ESI-TOF) *m/z* calcd. for $[C_{24}H_{19}N_2O]^+$ 351.1492, found 351.1499.

1-(4'-Methyl-[1,1'-biphenyl]-4-yl)-[4,4'-bipyridin]-1-ium chloride (**5**$^+$)

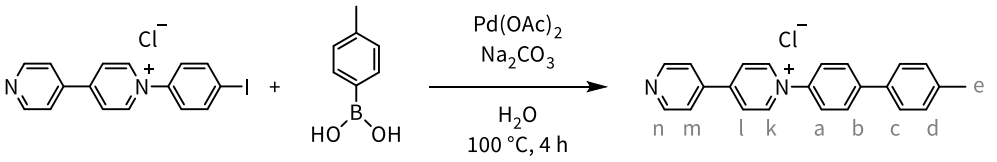

67%

According to GP1, **1** (100 mg, 253 µmol, 1.0 equiv.), 4-methylphenylboronic acid (45.0 mg, 329 µmol, 1.3 equiv.), Na_2CO_3 (54.0 mg, 506 µmol, 2 equiv.) and $Pd(OAc)_2$ (11.0 mg, 51.0 µmol, 0.2 equiv.) were

dissolved in H_2O (5 mL) and stirred at 100 °C for 4 h. Anion exchanges furnished **5**$^+$ (61.0 mg, 170 µmol, 67%) as a brownish powder.

M.P.: 247 °C.

^{1}H NMR (700 MHz, DMSO-d_6) δ = 9.58 (d, J = 6.9 Hz, 2H, H_k), 8.99 (d, J = 6.3 Hz, 2H, H_n), 8.84 (d, J = 6.9 Hz, 2H, H_l), 8.30 (d, J = 6.3 Hz, 2H, H_m), 8.05 (d, J = 8.8 Hz, 2H, H_a), 8.02 (d, J = 8.8 Hz, 2H, H_b), 7.72 (d, J = 8.0 Hz, 2H, H_c), 7.36 (t, J = 8.0 Hz, 2H, H_d), 2.38 (s, 3H, H_e) ppm.

^{13}C-NMR (176 MHz, DMSO-d_6) δ = 152.5, 149.5, 145.4, 142.9, 141.1, 138.2, 135.2, 129.8, 127.9, 126.9, 125.6, 125.3, 122.9, 20.7 ppm.

HRMS (ESI-TOF) *m/z* calcd. for $[C_{23}H_{19}N_2]^+$ 323.1543, found 323.1549.

1-(4'-Bromo-[1,1'-biphenyl]-4-yl)-[4,4'-bipyridin]-1-ium chloride (**6**$^+$)

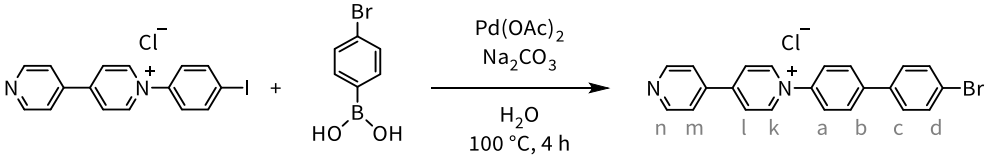

31%

According to GP1, **1** (100 mg, 253 µmol, 1.0 equiv.), 4-bromophenylboronic acid (66.0 mg, 329 µmol, 1.3 equiv.), Na_2CO_3 (54.0 mg, 506 µmol, 2 equiv.) and $Pd(OAc)_2$ (11.0 mg, 51.0 µmol, 0.2 equiv.) were dissolved in H_2O (5 mL) and stirred at 100 °C for 4 h. Anion exchanges furnished **6**$^+$ (30.0 mg, 77.3 µmol, 31%) as a brownish powder.

M.P.: > 250 °C.

^{1}H NMR (700 MHz, DMSO-d_6) δ = 9.57 (d, J = 6.9 Hz, 2H, H_k), 8.96 (d, J = 6.3 Hz, 2H, H_n), 8.83 (d, J = 6.9 Hz, 2H, H_l), 8.24 (d, J = 6.3 Hz, 2H, H_m), 8.09 (d, J = 8.7 Hz, 2H, H_a), 8.04 (d, J = 8.7 Hz, 2H, H_b), 7.79 (d, J = 8.5 Hz, 2H, H_c), 7.75 (d, J = 8.5 Hz, 2H, H_d) ppm.

^{13}C NMR (176 MHz, DMSO-d_6) δ = 152.9, 150.2, 145.4, 141.7, 137.3, 132.1, 129.2, 128.2, 125.4, 125.4, 122.5, 122.2 ppm.

HRMS (ESI-TOF) *m/z* calcd. for $[C_{22}H_{16}BrN_2]^+$ 387.0491, found 387.0514.

1-(4'-(Hydroxymethyl)-[1,1'-biphenyl]-4-yl)-[4,4'-bipyridin]-1-ium chloride (**7**$^+$)

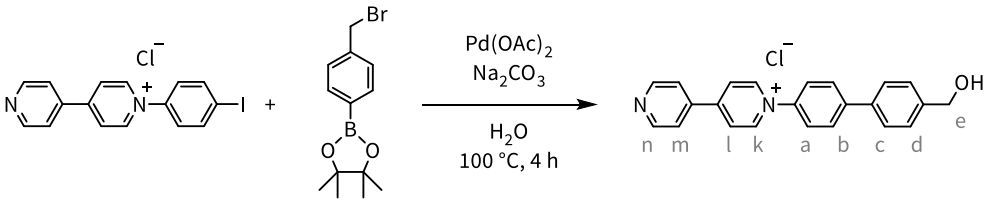

99%

According to GP1, **1** (100 mg, 253 µmol, 1.0 equiv.), 4-bromomethylphenylboronic acid pinacol ester (98.0 mg, 329 µmol, 1.3 equiv.), Na_2CO_3 (54.0 mg, 506 µmol, 2 equiv.) and $Pd(OAc)_2$ (11.0 mg, 51.0 µmol, 0.2 equiv.) were dissolved in H_2O (5 mL) and stirred at 100 °C for 4 h. Anion exchanges furnished **7**$^+$ (94.0 mg, 251 µmol, 99%) as a brownish powder.

M.P.: > 250 °C.

^{1}H NMR (700 MHz, DMSO-d_6) δ = 9.55 (d, *J* = 7.0 Hz, 2H, H_k), 8.94 (d, *J* = 6.2 Hz, 2H, H_n), 8.81 (d, *J* = 7.0 Hz, 2H, H_l), 8.21 (d, *J* = 6.2 Hz, 2H, H_m), 8.07 (d, *J* = 8.8 Hz, 2H, H_a), 8.02 (d, *J* = 8.8 Hz, 2H, H_b), 7.79 (d, *J* = 8.2 Hz, 2H, H_c), 7.49 (t, *J* = 8.2 Hz, 2H, H_d), 4.58 (s, 2H, H_e) ppm.

^{13}C NMR (176 MHz, DMSO-d_6) δ = 152.6, 149.8, 145.3, 143.1, 142.9, 141.2, 136.4, 130.3, 128.0, 127.2, 126.8, 125.5, 125.3, 122.7, 62.5 ppm.

HRMS (ESI-TOF) *m/z* calcd. for $[C_{23}H_{19}N_2O]^+$ 339.1492, found 339.1495.

1-([1,1'-Biphenyl]-4-yl)-1'-ethyl-[4,4'-bipyridine]-1,1'-diium chloride (**8**$^{2+}$)

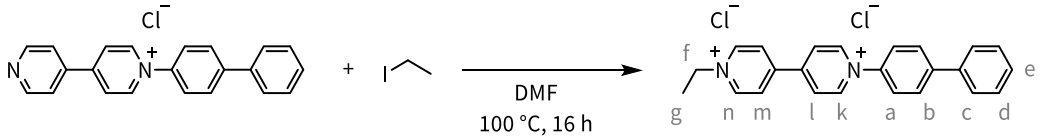

82%

Compound **2**$^+$ (100 mg, 0.290 mmol, 1.00 equiv.) and iodoethane (0.25 mL, 0.129 mg, 0.827 mmol, 2.85 equiv.) were dissolved in DMF (3 mL) and stirred at 100 °C for 16 h. For purification anion exchanges were conducted. The solvent of the reaction mixture was evaporated, the residue was dissolved in H_2O and sat. NH_4PF_6 (aq.) was added. The precipitate was filtered off and dried. Afterwards the PF_6^- salt was dissolved in acetone and HCl (aq., conc.) was added. The precipitate was filtered off and dried furnishing **8**$^{2+}$ (97.0 mg, 0.237 mmol, 82%) as a yellow powder.

M.P.: 248 °C.

^{1}H NMR (700 MHz, D_2O) δ = 9.44 (d, *J* = 7.0 Hz, 2H, H_k), 9.20 (d, *J* = 6.4 Hz, 2H, H_n), 8.74 (d, *J* = 7.0 Hz, 2H, H_l), 8.65 (d, *J* = 6.4 Hz, 2H, H_m), 8.06 (d, *J* = 8.7 Hz, 2H, H_a), 7.94 (d, *J* = 8.7 Hz, 2H, H_b), 7.84 (d, *J* =

7.1 Hz, 2H, H_c), 7.62 (t, *J* = 7.4, 7.1 Hz, 2H, H_d), 7.55 (t, *J* = 7.4 Hz, 1H, H_e), 4.82 (d, *J* = 7.3 Hz, 2H, H_f), 1.75 (t, *J* = 7.3 Hz, 3H, H_g) ppm.

^{1}H NMR (500 MHz, DMSO-d_6) δ = 9.72 (d, *J* = 6.5 Hz, 2H, H_k), 9.42 (d, *J* = 6.4 Hz, 2H, H_n), 8.96 (d, *J* = 6.5 Hz, 2H, H_l), 8.90 (d, *J* = 6.4 Hz, 2H, H_m), 8.11 (d, *J* = 8.7 Hz, 2H, H_a), 8.05 (d, *J* = 8.7 Hz, 2H, H_b), 7.83 (d, *J* = 7.6 Hz, 2H, H_c), 7.57 (dd, *J* = 7.6, 7.4 Hz, 2H, H_d), 7.49 (t, *J* = 7.4 Hz, 1H, H_e), 4.75 (q, *J* = 7.3 Hz, 2H, H_f), 1.63 (t, *J* = 7.3 Hz, 3H, H_g) ppm.

^{13}C NMR (176 MHz, DMSO-d_6) δ = 149.3, 148.2, 145.8, 143.2, 141.3, 138.1, 129.3, 128.7, 128.3, 127.1, 126.7, 126.5, 125.4, 56.6, 16.3 ppm.

HRMS (ESI-TOF) *m/z* calcd. for $[C_{24}H_{22}N_2]^{2+}$ 169.0886, found 169.0884; calcd. for $[C_{24}H_{21}N_2]^{+}$ 337.1699, found 337.1699; $[C_{24}H_{22}N_2]^{+}$ 338.1778, found 338.1776.

It was possible to obtain a crystal structure of [**8**][Cl]$_2$.

6.3 Synthetic Procedures for Chapter 4.2

4-(Pyridine-4-yl)phenol (**9**)[140]

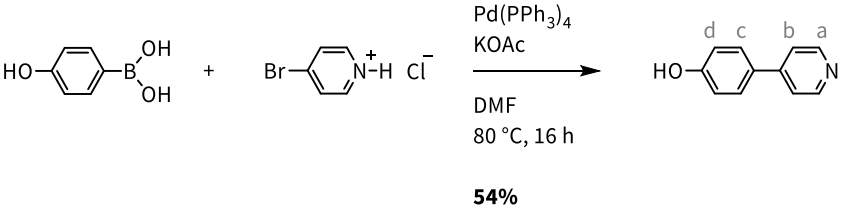

4-Bromopyridine hydrochloride (1.66 g, 8.52 mmol, 1.2 equiv.), 4-hydroxyphenylboronic acid (0.98 g, 7.03 mmol, 1.0 equiv.), $Pd(PPh_3)_4$ (428 mg, 0.37 mmol, 5 mol-%) and K_2CO_3 (2.89 g, 29.4 mmol, 4.2 equiv.) was dissolved in DMF (35 mL) under Ar atmosphere and heated to 80 °C for 16 h. The reaction was quenched with sat. K_2CO_3 (aq.), extracted with DCM (3 x 50 mL) and dried with $MgSO_4$. The crude product was purified by column chromatography (SiO_2, DCM/MeOH/NEt_3 = 95:5:0.5) giving **9** (655 mg, 4.60 mmol, 54%) as a brown powder.

^{1}H NMR (700 MHz, D_2O) δ = 8.66 (d, *J* = 7.1 Hz, 2H, H_a), 8.22 (d, *J* = 7.1 Hz, 2H, H_b), 7.89 (d, *J* = 8.8 Hz, 2H, H_c), 7.09 (d, *J* = 8.8 Hz, 2H, H_d) ppm.

^{1}H-NMR (400 MHz, CD_3OD): δ = 8.49 (d, 2H, *J* = 6.4 Hz, H_a), 7.66 - 7.62 (m, 4H, H_c & H_d), 6.91 (d, 2H, *J* = 8.7 Hz, H_d) ppm.

^{13}C-NMR (176 MHz, CD_3OD): δ = 160.4, 150.6, 150.3, 129.6, 129.3, 122.3, 117.1 ppm.

HRMS (ESI-TOF) *m/z* calcd for $[C_{11}H_{10}NO]^+$ 172.0757, found 172.0755.

The spectroscopic data agrees with previously published results.[140]

1-(11-Hydroxyundecyl)-4-phenylpyridin-1-ium chloride (**10**$^+$)

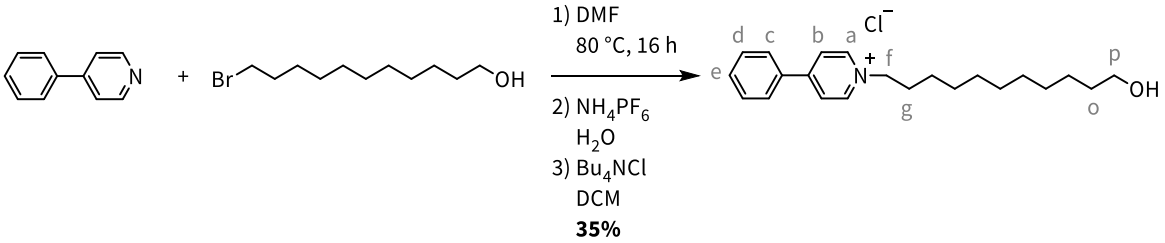

4-Phenylpyridine (155 mg, 1.00 mmol, 1.0 equiv.) and 11-bromoundecanol (327 mg, 1.30 mmol, 1.3 equiv.) is dissolved in DMF (6 mL) and heated to 80 °C for 16 h. The solvent was evaporated *in vacuo*, sat. NH_4PF_6 (aq.) was added and sonicated for 30 min. The precipitate was filtered off, washed with H_2O and dried. Then it was dissolved in DCM and an excess of Bu_4NCl in DCM was added. The precipitate was filtered off, washed with DCM and dried furnishing **10**$^+$ (127 mg, 0.35 mmol, 35%) as a white powder.

^{1}H NMR (700 MHz, D_2O) δ = 8.80 (d, 2H, *J* = 6.9 Hz, H_a), 8.30 (d, 2H, J = 6.9 Hz, H_b), 7.95 – 7.93 (m, 2H, H_c), 7.69 – 7.63 (m, 3H, H_d & H_e), 4.58 (t, 2H, *J* = 7.1 Hz, H_f), 3.54 (t, 2H, *J* = 6.7 Hz, H_p), 2.05 – 1.99 (m, 2H, H_g), 1.50 –1.45 (m, 2H, H_o), 1.36 – 1.32 (m, 4H, CH_2), 1.27 – 1.21 (m, 10H, CH_2) ppm.

^{13}C NMR (176 MHz, D_2O) δ = 156.5, 144.0, 133.9, 132.1, 129.7, 127.9, 125.0, 61.8, 61.1, 31.2, 30.2, 28.5, 28.5, 28.4, 28.2, 27.9, 25.0, 25.0 ppm.

HRMS (ESI-TOF) *m/z* calcd for $[C_{22}H_{32}NO]^+$ 326.2478, found 326.2465.

1-(4-Bromobutyl)-4-phenylpyridin-1-ium bromide (**11**$^+$)

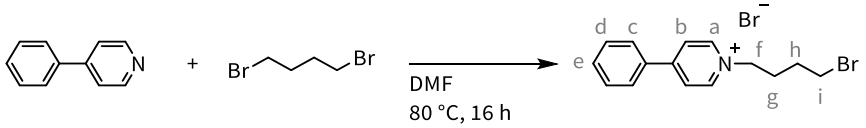

93%

4-Phenylpyridine (155 mg, 1.00 mmol, 1.0 equiv.) and 1,4-dibromobutane (5.9 mL, 10.8 g, 50.0 mmol, 50 equiv.) is dissolved in DMF (6 mL) and heated to 80 °C for 16 h. The solvent was evaporated *in vacuo*, the residue was washed with EtOAc and dried furnishing **11**$^+$ (344 mg, 0.93 mmol, 93%) as a black powder.

^{1}H NMR (700 MHz, D_2O) δ = 8.85 (d, 2H, *J* = 6.9 Hz, H_a), 8.34 (d, 2H, *J* = 6.9 Hz, H_b), 7.97 – 7.95 (m, 2H, H_c), 7.69 – 7.64 (m, 3H, H_d & H_e), 4.66 (t, 2H, *J* = 7.4 Hz, H_f), 3.56 (t, 2H, *J* = 6.5 Hz, H_i) 2.25 – 2.18 (m, 2H, H_g), 1.99 – 1.93 (m, 2H, H_h) ppm.

^{13}C NMR (176 MHz, D_2O) δ = 144.2, 134.0, 132.3 129.9, 128.1, 125.3, 60.3, 34.7, 33.3, 29.4, 28.6 ppm.

HRMS (ESI-TOF) *m/z* calcd for $[C_{15}H_{17}BrN]^+$ 290.0539, found 290.0561.

1-(Anthracen-9-ylmethyl)-4-phenylpyridin-1-ium chloride (**12**$^+$)

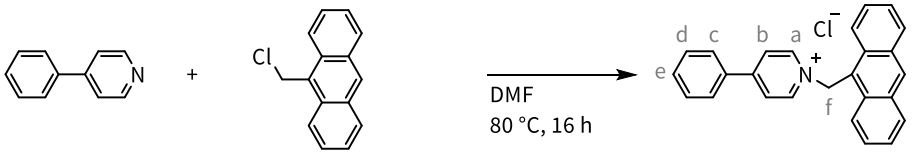

31%

4-Phenylpyridine (155 mg, 1.00 mmol, 1.0 equiv.) and 9-(chloromethyl)anthracene (295 mg, 1.30 mmol, 1.3 equiv.) is dissolved in DMF (6 mL) and heated to 80 °C for 16 h. The solvent was evaporated *in vacuo*, the residue was washed with EtOAc and dried furnishing **12**$^+$ (117 mg, 0.31 mmol, 31%) as a yellow powder.

^{1}H NMR (500 MHz, D_2O) δ = 8.45 (d, *J* = 6.8 Hz, 2H, H_a), 8.44 (s, 2H, $H_{arom.}$), 8.08 (d, *J* = 8.9 Hz, 2H, H_c), 7.95 (d, *J* = 8.5 Hz, 2H, $H_{arom.}$), 7.83 (d, *J* = 6.8 Hz, 2H, H_b), 7.69 – 7.57 (m, 3H, H_d & H_e), 7.57 – 7.49 (m, 2H, $H_{arom.}$), 7.49 – 7.42 (m, 1H, $H_{arom.}$), 6.50 (s, 2H, H_f) ppm.

^{13}C-NMR (176 MHz, D_2O) δ = 156.3, 143.0, 133.1, 132.3, 131.4, 131.0, 129.6, 129.6, 128.5, 127.7, 125.8, 124.6, 122.2, 120.6, 55.3 ppm.

HRMS (ESI-TOF) *m/z* calcd for $[C_{26}H_{20}N]^+$ 346.1590, found 346.1622.

1-(2-(Naphthalen-2-yloxy)ethyl)-4-phenylpyridin-1-ium chloride (**13**$^+$)

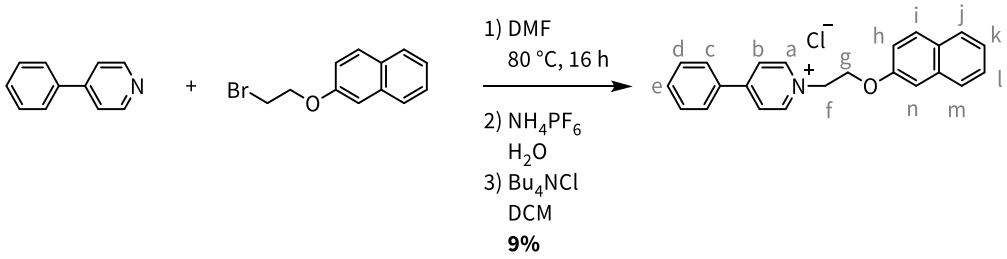

4-Phenylpyridine (100 mg, 0.640 mmol, 1.0 equiv.) and 2-(2-bromoethoxy)naphthalene (215 mg, 0.840 mmol, 1.3 equiv.) is dissolved in DMF (6 mL) and heated to 80 °C for 16 h. The solvent was evaporated *in vacuo*, sat. NH_4PF_6 (aq.) was added and sonicated for 30 min. The precipitate was filtered off, washed with H_2O and dried. Then it was dissolved in DCM and an excess of Bu_4NCl in DCM was added. The precipitate was filtered off, washed with DCM and dried furnishing **13**$^+$ (21 mg, 0.060 mmol, 9%) as a white powder.

^{1}H NMR (700 MHz, D_2O) δ = 8.87 (d, 2H, *J* = 6.4 Hz, H_a), 8.15 (d, 2H, *J* = 6.4 Hz, H_b), 7.81 (d, 2H, *J* = 8.6 Hz, H_c), 7.76 – 7.74 (m, 3H, H_d & H_e), 7.64 (t, *J* = 7.3 Hz, 1H, H_m), 7.59 (d, *J* = 7.6 Hz, 2H, H_j), 7.57 (d, *J* = 8.9 Hz, 1H, H_i), 7.47 (t, *J* = 7.6 Hz, 1H, H_k), 7.38 (t, *J* = 7.5 Hz, 1H, H_l), 7.25 (d, *J* = 2.6 Hz, 1H, H_n), 7.18 (dd, *J* = 8.9, 2.6 Hz, 1H, H_h), 5.03 (t, 2H, *J* = 4.8 Hz, H_f), 4.73 (t, 2H, *J* = 4.8 Hz, H_g) ppm.

^{1}H NMR (700 MHz, DMSO-d_6) δ = 9.23 (d, *J* = 6.5 Hz, 2H, H_a), 8.58 (d, *J* = 7.0 Hz, 2H, H_b), 8.09 (d, *J* = 6.5 Hz, 2H, H_c), 7.83 (dd, *J* = 8.5, 4.0 Hz, 1H, H_l), 7.81 (d, *J* = 8.3 Hz, 1H, H_m), 7.72 – 7.61 (m, 4H, H_d & H_e & H_j), 7.47 (ddd, *J* = 8.2, 6.8, 1.2 Hz, 1H, H_k), 7.40 – 7.33 (m, 2H, H_n & H_i), 7.15 (dd, *J* = 9.0, 2.6 Hz, 1H, H_h), 5.13 (t, *J* = 5.0 Hz, 2H, H_f), 4.69 (t, *J* = 5.0 Hz, 2H, H_g) ppm.

^{13}C NMR (176 MHz, DMSO-d_6) δ = 155.3, 155.2, 145.5, 134.0, 133.5, 132.2, 129.7, 129.5, 128.8, 128.2, 127.5, 126.7, 126.6, 124.3, 124.0, 118.3, 107.4, 66.2, 59.0 ppm.

HRMS (ESI-TOF) *m/z* calcd for $[C_{23}H_{20}NO]^+$ 326.1539, found 326.1561.

1,1'-(Dodecane-1,12-diyl)bis(4-phenylpyridin-1-ium) bromide (**14**$^{2+}$)

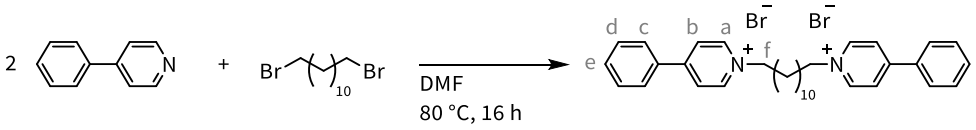

4-Phenylpyridine (381 mg, 2.38 mmol, 2.4 equiv.) and 1,12-dibromododecan (314 mg, 1.00 mmol, 1.0 equiv.) is dissolved in DMF (6 mL) and heated to 80 °C for 16 h. The emerging precipitate was filtered off, washed with acetone and dried furnishing **14**$^{2+}$ (313 mg, 0.49 mmol, 49%) as a white powder.

^{1}H NMR (500 MHz, DMSO-d_6) δ = 8.81 (d, 4H, J = 6.9 Hz, H_a), 8.32 (d, 4H, J = 6.9 Hz, H_b), 7.98 – 7.96 (m, 4H, H_c), 7.69 – 7.65 (m, 6H, H_d & H_e), 4.58 (t, 4H, J = 7.1 Hz, H_a), 2.03 – 1.97 (m, 4H, CH_2), 1.33 – 1.25 (m, 8H, CH_2), 1.22 – 1.99 (m, 8H, CH_2) ppm.

^{13}C NMR (176 MHz, D_2O) δ = 156.4, 144.0 133.8, 132.1, 129.7, 127.9, 124.9, 61.0, 30.1, 28.2, 28.2, 27.8, 24.9 ppm.

HRMS (ESI-TOF) *m/z* calcd for $[C_{34}H_{42}N_2]^{2+}$ 239.1669, found 239.1695.

1,1'-(Propane-1,3-diyl)bis(4-phenylpyridin-1-ium) chloride (**15**$^{2+}$)

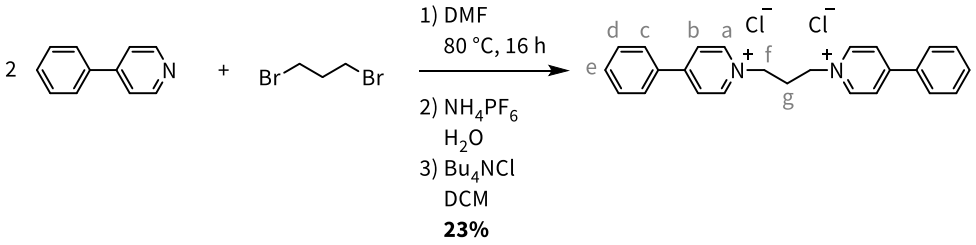

4-Phenylpyridine (400 mg, 2.58 mmol, 2.1 equiv.) and 1,3-dibromopropane (0.13 mL, 248 mg, 1.23 mmol, 1.0 equiv.) is dissolved in DMF (6 mL) and heated to 80 °C for 16 h. The solvent was evaporated *in vacuo*, sat. NH_4PF_6 (aq.) was added and sonicated for 30 min. The precipitate was filtered off, washed with H_2O and dried. Then it was dissolved in DCM and an excess of Bu_4NCl in DCM was added. The precipitate was filtered off, washed with DCM and dried furnishing **15**$^{2+}$ (118 mg, 0.280 mmol, 23%) as a white powder.

^{1}H NMR (500 MHz, D_2O) δ = 9.22 (d, 4H, J = 6.9 Hz, H_a), 8.58 (d, 4H, J = 6.9 Hz, H_b), 8.11 – 8.09 (m, 4H, H_c), 7.70 – 7.63 (m, 6H, H_d & H_e), 4.80 (t, 4H, J = 7.3 Hz, H_f), 2.74 (p, 2H, J = 7.3 Hz, H_g) ppm.

^{13}C NMR (176 MHz, D_2O) δ = 157.2, 144.1, 133.3, 132.5, 129.7, 127.9, 125.3, 57.7, 31.0 ppm.

HRMS (ESI-TOF) *m/z* calcd for $[C_{25}H_{24}N_2]^{2+}$ 176.0964, found 176.0977.

1,1'-Diethyl-[4,4'-bipyridine]-1,1'-diium iodide (**V**$^{2+}$)[141]

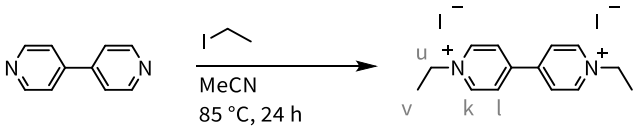

> **99%**

4,4'-Bipyridine (1.00 g, 6.40 mmol, 1 equiv.) and ethyl iodide (1.54 mL, 3.00 g, 19.2 mmol, 3 equiv.) were dissolved in MeCN (12 mL) and heated to 85 °C for 24 h. The solvent was evaporated *in vacuo* and the residue was washed with acetone and dried furnishing **V**$^{2+}$ (3.12 g, 6.40 mmol, > 99%) as a yellow powder.

^{1}H NMR (700 MHz, D_2O) δ = 9.16 (d, *J* = 6.2 Hz, 4H, H_k), 8.56 (d, *J* = 6.2 Hz, 4H, H_l), 4.84 – 4.75 (m, 4H, H_u), 1.73 (t, *J* = 7.5 Hz, 6H, H_v) ppm.

The spectroscopic data agrees with previously published results.[141]

1-Ethyl-[4,4'-bipyridin]-1-ium iodide (**SI2**$^+$)[132c]

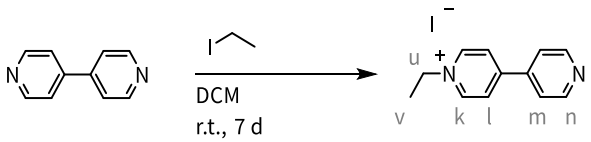

54%

4,4'-Bipyridine (2.00 g, 12.8 mmol, 1 equiv.) and ethyl iodide (1.30 mL, 2.50 g, 16.0 mmol, 1.25 equiv.) were dissolved in DCM (30 mL) and stirred at r.t. for 7 d. The precipitate was filtered off, washed with DCM and dried furnishing **SI2**$^+$ (2.15 mg, 6.89 mmol, 54%) as a yellow powder.

^{1}H NMR (250 MHz, DMSO-d_6) δ = 9.25 (d, *J* = 7.0 Hz, 2H, H_k), 8.87 (d, *J* = 6.2 Hz, 2H, H_n), 8.64 (d, *J* = 7.0 Hz, 2H, H_l), 8.04 (d, *J* = 6.2 Hz, 2H, H_m), 4.67 (q, *J* = 7.3 Hz, 2H, H_u), 1.58 (t, *J* = 7.3 Hz, 3H, H_v) ppm.

The spectroscopic data agrees with previously published results.[132c]

6.4 Synthetic Procedures for Chapter 4.3

2-(2-(2-(4-Iodophenoxy)ethoxy)ethoxy)ethan-1-ol (**SI3**)

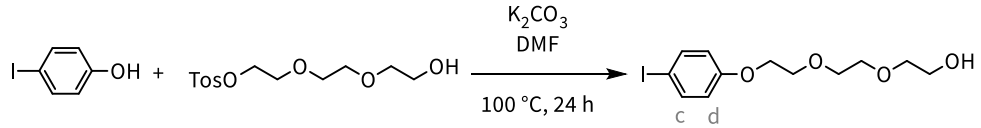

64%

Compound **SI3** was prepared according to a modified literature procedure.[142] 4-Iodophenol (1.00 g, 4.55 mmol, 1.0 equiv.), 2-(2-(2-hydroxyethoxy)ethoxy)ethyl 4-methylbenzenesulfonate (**SI0**) (1.66 g, 5.46 mmol, 1.2 equiv.) and K_2CO_3 (1.57 g, 11.38 mmol, 2.5 equiv.) were dissolved in DMF (15 mL) and heated to 100 °C for 24 h. The reaction was quenched with a sat. NH_4Cl (aq.) solution, extracted with EtOAc (3 x 15 mL) and dried with $MgSO_4$. The crude product was purified by column chromatography (SiO_2, DCM/MeOH = 100:0, 100:1 – 10:1) furnishing **SI3** (1.02 g, 2.90 mmol, 64%) as a yellowish oil.

^{1}H NMR (400 MHz, $CDCl_3$) δ = 7.53 (d, *J* = 9.1 Hz, 2H, H_d), 6.69 (d, *J* = 9.1 Hz, 2H, H_c), 4.10 – 4.06 (m, 2H, OCH_2), 3.86 – 3.82 (m, 2H, OCH_2), 3.75 – 3.67 (m, 6H, OCH_2), 3.62 – 3.58 (m, 2H, OCH_2) ppm.

The spectroscopic data agrees with previously published results.[142]

2-(2-(2-(4-(Pyridine-4-yl)phenoxy)ethoxy)ethoxy)ethan-1-ol (**P**)

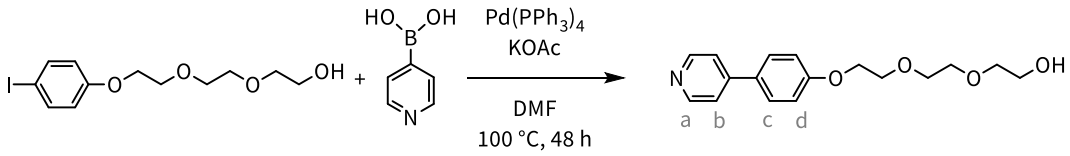

21%

SI3 (863 mg, 2.45 mmol, 1 equiv.), pyridin-4-ylboronic acid (903 mg, 7.35 mmol, 3 equiv.), $Pd(PPh_3)_4$ (113 mg, 0.49 mmol, 4 mol-%) and KOAc (962 mg, 9.8 mmol, 4 equiv.) were dissolved in DMF (50 mL) under Ar atmosphere and heated to 100 °C for 48 h. The reaction was quenched with H_2O, extracted with EtOAc (3 x 50 mL), filtered over celite, washed with sat NaCl aq. (1 x 25 mL) and dried with $MgSO_4$. The crude product was purified by column chromatography (SiO_2, DCM/MeOH = 150:0, 150:1 – 15:1) furnishing **P** (153 mg, 0.500 mmol, 21%) as a colorless powder.

M.P. 110.2 – 110.7 °C.

^{1}H NMR (700 MHz, D_2O) δ = 8.68 (d, *J* = 6.9 Hz, 2H, H_a), 8.25 (d, *J* = 7.0 Hz, 2H, H_b), 7.95 (d, *J* = 8.8 Hz, 2H, H_c), 7.21 (d, *J* = 8.8 Hz, 2H, H_d), 4.34 – 4.31 (m, 2H, OCH_2), 3.96 – 3.94 (m, 2H, OCH_2), 3.80 – 3.78 (m, 2H, OCH_2), 3.74 – 3.72 (m, 2H, OCH_2), 3.72 – 3.70 (m, 2H, OCH_2), 3.65 – 3.62 (m, 2H, OCH_2) ppm.

^{13}C NMR (176 MHz, D_2O) δ = 161.41, 157.27, 140.60, 129.87, 126.93, 123.23, 115.68, 71.67, 69.81, 69.41, 68.92, 67.26, 60.32 ppm.

HRMS (ESI-TOF) *m/z* calcd for $[C_{17}H_{21}NO_4+H]^+$ 304.1543, found 304.1565; calcd for $[C_{17}H_{21}NO_4+Na]^+$ 326.1363, found 326.1353.

2,2'-(((((Naphthalene-2,6-diylbis(oxy))bis(ethane-2,1-diyl))bis(oxy))bis(ethane-2,1-diyl))bis(oxy))bis(ethan-1-ol) (**N**)

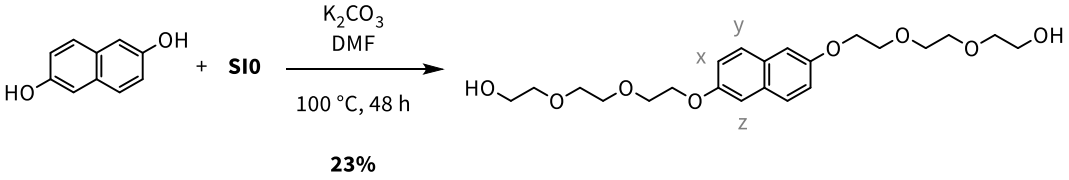

Compound **N** was prepared according to a modified literature procedure.[143] 2,6-Dihydroxynaphthalene (500 mg, 3.12 mmol, 1 equiv.), 2-(2-(2-hydroxyethoxy)ethoxy)ethyl 4-methylbenzenesulfonate (**SI0**) (2.48 g, 7.80 mmol, 2.5 equiv.) and K_2CO_3 (2.18 g, 15.6 mmol, 5 equiv.) were dissolved in DMF (15 mL) and heated to 100 °C for 48 h. The reaction was quenched with H_2O, extracted with EtOAc (3 x 15 mL), washed with sat. NaCl aq. (1 x 15 mL) and dried with $MgSO_4$. The crude product was purified by column chromatography (SiO_2, DCM/MeOH = 100:0, 100:1 – 10:1) furnishing **N** (303 mg, 0.713 mmol, 23%) as a colorless powder.

^{1}H NMR (700 MHz, D_2O) δ = 7.83 (d, *J* = 8.9 Hz, 2H, H_y), 7.40 (d, *J* = 2.5 Hz, 2H, H_z), 7.28 (dd, *J* = 8.9, 2.5 Hz, 2H, H_x), 4.38 – 4.33 (m, 4H, OCH_2), 4.00 – 3.96 (m, 4H, OCH_2), 3.83 – 3.79 (m, 4H, OCH_2), 3.77 – 3.73 (m, 4H, OCH_2), 3.74 – 3.70 (m, 4H, OCH_2), 3.67 – 3.63 (m, 4H, OCH_2) ppm.

The spectroscopic data agrees with previously published results.[143]

6.5 Synthetic Procedures for Chapter 4.4

4-Methylbenzenesulfonyl azide (**SI3**)[144]

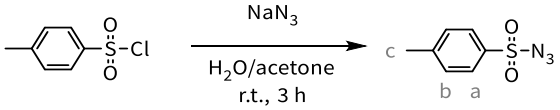

4-Toluenesulfonyl chloride (10.0 g, 52.5 mmol, 1 equiv.) was dissolved in an acetone/H_2O mixture (45:5 mL), NaN_3 (7.90 g, 120.8 mmol, 2.3 equiv.) was added and stirred at r.t. After 1 h each, H_2O (2 x 50 mL) is added and subsequent the acetone is removed *in vacuo*. The water phase is extracted with DCM (3 x 50 mL), the combined organic phases were washed with H_2O (50 mL) and dried with $MgSO_4$. The crude product **SI3** (10.4 g, 52.5 mmol, > 99%), a colorless powder, could be used without purification.

^{1}H NMR (400 MHz, $CDCl_3$) δ = 7.84 (d, *J* = 8.6 Hz, 2H, H_a), 7.41 (d, *J* = 8.6 Hz, 1H, H_b), 2.48 (s, 1H, H_c) ppm.

The spectroscopic data agrees with previously published results.[144]

((6-Bromonaphthalen-2-yl)oxy)triisopropylsilane (**16**)[145]

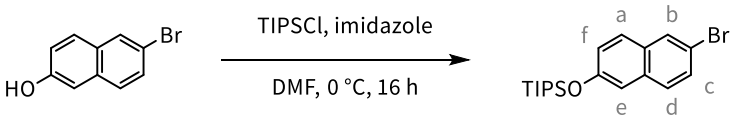

6-Bromo-2-naphthol (2.50 g, 12.2 mmol, 1 equiv.) and imidazole (837 mg, 12.3 mmol, 1.1 equiv.) were dissolved in DMF (15 mL) and cooled to 0 °C. TIPSCl (3.8 mL, 3.45 g, 17.9 mmol, 1.6 equiv.) was added dropwise and the reaction solution was stirred at r.t. 16 h. The solvent was evaporated *in vacuo*, and the residue was dissolved in DCM (30 mL), washed with sat NH_4Cl (aq., 30mL) and dried with $MgSO_4$. The crude product was purified by column chromatography (SiO_2, Hex/DCM = 8:1) furnishing **16** (3.75 g, 9.88 mmol, 88%) as a yellow oil.

^{1}H NMR (400 MHz, $CDCl_3$) δ = 7.91 (d, *J* = 2.0 Hz, 1H, H_b), 7.63 (d, *J* = 8.8 Hz, 1H, H_d), 7.56 (d, *J* = 8.8 Hz, 1H, H_a), 7.47 (dd, *J* = 8.8, 2.0 Hz, 1H, H_c), 7.18 (d, *J* = 2.5 Hz, 1H, H_e), 7.15 (dd, *J* = 8.8, 2.5 Hz, 1H, H_f), 1.39 – 1.26 (m, 3H, OTIPS), 1.13 (d, *J* = 7.3 Hz, 18H, OTIPS) ppm.

The spectroscopic data agrees with previously published results.[145]

((6-Azidonaphthalen-2-yl)oxy)triisopropylsilane (**17**)

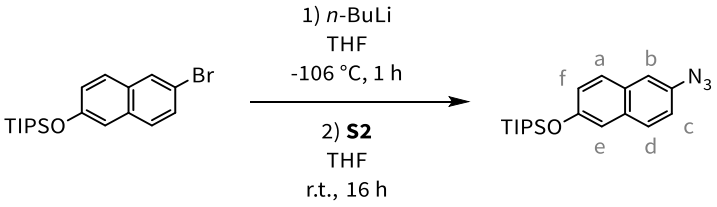

88%

Compound **16** (3.70 g, 9.75 mmol, 1 equiv.) was dissolved in dry THF (60 mL) under Ar and cooled to -106 °C. *n*-BuLi (2.5M in hexane, 4.30 mL, 10.7 mmol, 1.1 equiv.) was added dropwise. After 1 h at this temperature, **SI3** (2.90 g, 14.6 mmol, 1.5 equiv.) dissolved in dry THF (25 mL) was added and the reaction solution was stirred at r.t. for 16 h. The solvent was evaporated *in vacuo*, then the residue was dissolved in EtOAc (45 mL), washed with NaCl (aq., 45mL) and dried with $MgSO_4$. The crude product was purified by column chromatography (SiO_2, Hex/DCM = 20:1 – 8:1) furnishing **17** (2.92 g, 8.56 mmol, 88%) as a yellow oil.

^{1}H NMR (400 MHz, $CDCl_3$) δ = 7.67 (d, *J* = 8.8 Hz, 1H, H_d), 7.64 (d, *J* = 8.9 Hz, 1H, H_a), 7.38 (d, *J* = 2.3 Hz, 1H, H_b), 7.20 (d, *J* = 2.4 Hz, 1H, H_e), 7.15 (dd, *J* = 8.9, 2.4 Hz, 1H, H_f), 7.10 (dd, *J* = 8.8, 2.3 Hz, 1H, H_c), 1.38 – 1.26 (m, 3H, OTIPS), 1.13 (d, *J* = 7.4 Hz, 18H, OTIPS) ppm.

The spectroscopic data agrees with previously published results.[145]

1-(But-3-yn-1-yl)-[4,4'-bipyridin]-1-ium bromide (**18**$^+$)

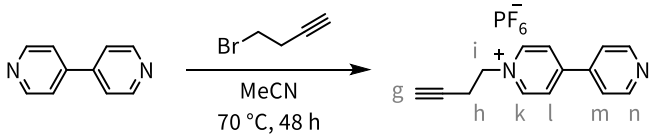

49%

4,4'-Bipyridine (1.05 g, 6.75 mmol, 1 equiv.) and 4-bromo-1-butyne (0.64 mL, 901 mg, 6.77 mmol, 1 equiv.) were dissolved in MeCN (12 mL) and heated to 70 °C for 48 h. The precipitate was filtered off, washed with MeCN, dissolved in H_2O and sat. NH_4PF_6 (aq.) was added. The precipitate was filtered off and dried furnishing **18**$^+$ (1.17 g, 3.30 mmol, 49%) as a white powder.

^{1}H NMR (400 MHz, DMSO-d_6) δ = 9.25 (d, *J* = 7.0 Hz, 2H, H_k), 8.88 (d, *J* = 6.2 Hz, 2H, H_n), 8.69 (d, *J* = 7.0 Hz, 2H, H_l), 8.06 (d, *J* = 6.2 Hz, 2H, H_m), 4.79 (t, *J* = 6.6 Hz, 2H, H_i), 3.10 (t, *J* = 2.6 Hz, 1H, H_g), 3.01 (td, *J* = 6.6, 2.6 Hz, 2H, H_h) ppm.

The spectroscopic data agrees with previously published results.[146]

1-(2-(1-(6-((Triisopropylsilyl)oxy)naphthalen-2-yl)-1H-1,2,3-triazol-4-yl)ethyl)-[4,4'-bipyridin]-1-ium hexafluorophosphate(V) (**19**$^+$)

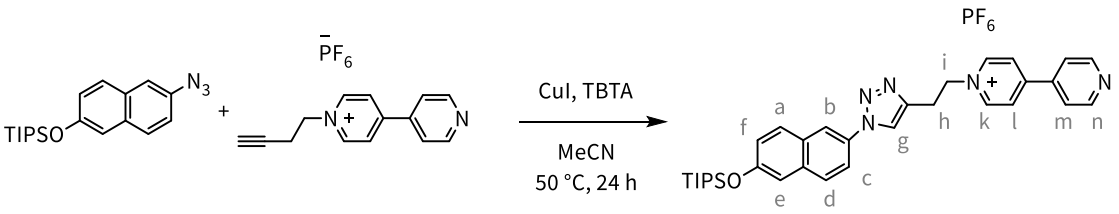

91%

Compound **17** (834 mg, 2.65 mmol, 1.1 equiv.), compound **18**$^+$ (845 mg, 2.39 mmol, 1 equiv.), CuI (25.0 mg, 0.13 mmol, 0.05 equiv.) and tris((1-benzyl-4-triazolyl)methyl)amine (69.0 mg, 0.13 mmol, 0.05 mmol) were dissolved in MeCN (50 mL) and stirred at 50 °C for 24 h. The reaction solution was filtered over celite and the solvent was evaporated *in vacuo*. The crude product was purified by column chromatography (ALOX, DCM/MeOH = 50:1 – 8:1) furnishing **19**$^+$ (1.52 g, 2.18 mmol, 91%) as a grey powder.

^{1}H NMR (500 MHz, DMSO-d_6) δ = 9.28 (d, J = 7.0 Hz, 2H, H_k), 8.89 (s_{br}, 2H, H_n), 8.74 (s, 1H, H_g), 8.66 (d, J = 7.0 Hz, 2H, H_l), 8.33 (d, J = 2.2 Hz, 1H, H_b), 8.07 - 8.04 (m, 3H, H_m & H_d), 7.97 (d, J = 8.9 Hz, 1H, H_a), 7.93 (dd, J = 8.9, 2.2 Hz, 1H, H_c), 7.41 (d, J = 2.5 Hz, 1H, H_e), 7.26 (dd, J = 8.9, 2.5 Hz, 1H, H_f), 5.06 (t, J = 7.0 Hz, 2H, H_i), 3.56 (t, J = 7.0 Hz, 2H, H_h), 1.33 (hept, J = 7.5 Hz, 3H, OTIPS), 1.09 (d, J = 7.5 Hz, 18H, OTIPS) ppm.

^{13}C NMR (126 MHz, DMSO-d_6) δ = 154.1, 152.6, 151.0, 145.7, 142.9, 133.8, 132.5, 130.0, 128.7, 128.6, 128.3, 125.2, 123.2, 121.6, 119.0, 117.7, 114.2, 59.4, 26.7, 17.8, 12.1 ppm.

HRMS (ESI-TOF) *m/z* calcd for $[C_{33}H_{40}N_5OSi]^+$ 550.2997, found 550.3012.

1-(2-(1-(6-(Prop-2-yn-1-yloxy)naphthalen-2-yl)-1H-1,2,3-triazol-4-yl)ethyl)-[4,4'-bipyridin]-1-ium hexafluorophosphate(V) (**20**$^+$)

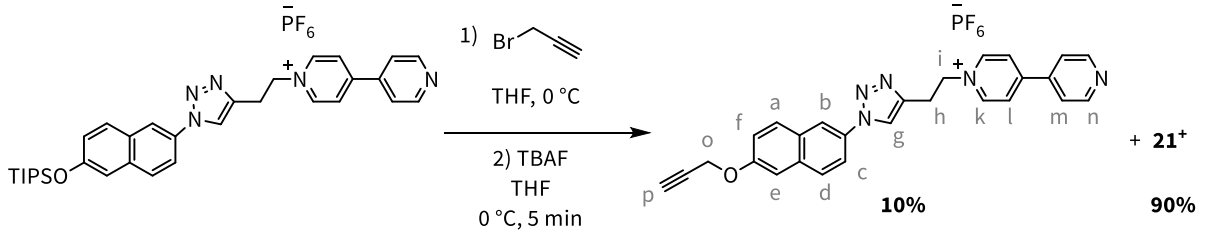

Compound **19**$^+$ (200 mg, 0.364 mmol, 1 equiv.) and propargyl bromide (in toluene) (0.6 mL, 5.52 mmol, 15 equiv.) were dissolved in dry THF (8 mL) and cooled to 0 °C. TBAF (138 mg, 0.437 mmol, 1.2 equiv.) dissolved in THF (2 mL) was added slowly and the reaction mixture stirred at this temperature for 5 min. The precipitate was filtered off. The crude product was purified by

column chromatography (ALOX, DCM/MeOH = 50:1 – 4:1) furnishing desired product **20**$^+$ (19 mg, 0.033 mmol, 9%) as a grey powder and side product **21**$^+$ (167 mg, 0.309 mmol, 85%) as a grey powder.

^{1}H NMR (700 MHz, DMSO-d_6) δ = 9.28 (d, J = 6.4 Hz, 2H, H_k), 8.87 (d, J = 6.2 Hz, 1H, H_n), 8.77 (s, 1H, H_g), 8.66 (d, J = 6.4 Hz, 2H, H_l), 8.36 (d, J = 2.2 Hz, 1H, H_c), 8.05 (d, J = 6.2 Hz, 2H, H_m), 8.04 (d, J = 8.9 Hz, 1H, H_d), 7.99 (d, J = 9.1 Hz, 1H, H_a), 7.97 (dd, J = 8.9, 2.3 Hz, 1H, H_f), 7.51 (d, J = 2.2 Hz, 1H, H_b), 7.33 (dd, J = 8.9, 2.5 Hz, 1H, H_e), 5.06 (t, J = 7.0 Hz, 2H, H_i), 4.96 (d, J = 2.1 Hz, 2H, H_o), 3.64 (t, J = 2.1 Hz, 1H, H_p), 3.56 (t, J = 7.0 Hz, 2H, H_h) ppm.

^{13}C NMR (176 MHz, DMSO-d_6) δ = 155.8, 152.5, 151.0, 145.6, 142.9, 140.7, 133.5, 132.4, 129.9, 128.7, 128.3, 125.2, 121.9, 121.6, 120.1, 119.1, 117.8, 107.8, 79.0, 78.6, 59.3, 55.6, 26.7 ppm.

HRMS (ESI-TOF) *m/z* calcd for $[C_{27}H_{22}N_5O]^+$ 432.1819, found 432.1820.

1-(2-(1-(6-Hydroxynaphthalen-2-yl)-1H-1,2,3-triazol-4-yl)ethyl)-[4,4'-bipyridin]-1-ium hexafluorophosphate(V) (**21**$^+$)

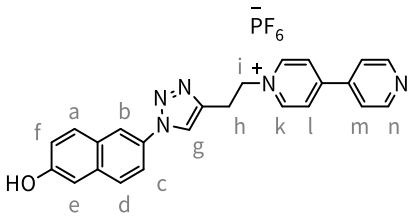

Compound **21**$^+$ was the side product of the synthesis of **20**$^+$.

^{1}H NMR (700 MHz, DMSO-d_6) δ = 10.09 (s, 1H, OH), 9.30 (d, J = 6.2 Hz, 2H, H_k), 8.86 (d, J = 5.2 Hz, 2H, H_n), 8.75 (s, 1H, H_g), 8.66 (d, J = 6.6 Hz, 2H, H_l), 8.26 (d, J = 2.2 Hz, 1H, H_b), 8.05 (d, J = 6.1 Hz, 2H, H_m), 7.90 (d, J = 8.7 Hz, 1H), 7.88 (d, J = 8.8 Hz, 1H, H_d), 7.86 (dd, J = 8.8, 2.2 Hz, 1H, H_c), 7.24 (d, J = 2.4 Hz, 1H, H_e), 7.21 (dd, J = 8.7, 2.4 Hz, 1H, H_f), 5.07 (t, J = 7.0 Hz, 2H, H_i), 3.55 (t, J = 6.9 Hz, 2H, H_h) ppm.

^{13}C NMR (176 MHz, DMSO-d_6) δ = 156.3, 152.5, 151.0, 145.6, 142.8, 140.7, 134.1, 131.5, 129.8, 127.9, 127.1, 125.2, 121.9, 121.6, 120.2, 118.8, 117.9, 108.8, 59.3, 26.7 ppm.

HRMS (ESI-TOF) *m/z* calcd for $[C_{24}H_{20}N_5O]^+$ 394.1662, found 394.1669.

1-Ethyl-1'-(2-(1-(6-(prop-2-yn-1-yloxy)naphthalen-2-yl)-1H-1,2,3-triazol-4-yl)ethyl)-[4,4'-bipyridine]-1,1'-diium chloride (**A**$^{2+}$)

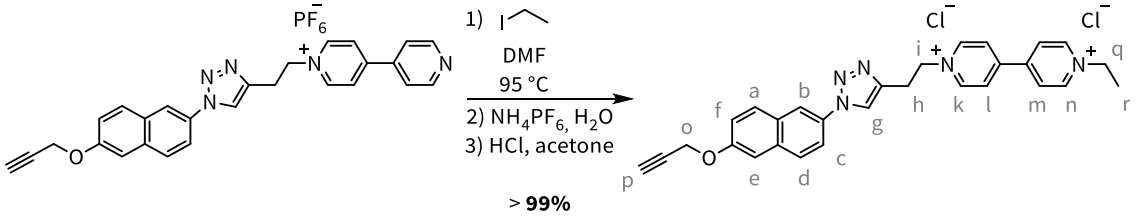

Compound **20**$^{+}$ (50 mg, 0.087 mmol, 1 equiv.) and ethyl iodide (0.1 mL, 190 mg, 1.22 mmol, 14 equiv.) were dissolved in DMF (5 mL) and heated to 95 °C for 4 h. The solvent was evaporated *in vacuo* and sat. NH_4PF_6 (aq.) was added. The precipitate was filtered off, dried, dissolved in acetone and HCl (aq., 36%) was added. The precipitate was filtered off and dried furnishing **A**$^{2+}$ (46 mg, 0.087 mmol, > 99%) as a brown powder.

^{1}H NMR (700 MHz, D_2O) δ = 9.11 (d, *J* = 6.6 Hz, 2H, H_k), 9.08 (d, *J* = 6.4 Hz, 2H, H_n), 8.54 (d, *J* = 6.3 Hz, 2H, H_m), 8.51 (d, *J* = 6.4 Hz, 2H, H_l), 8.36 (s, 1H, H_g), 7.95 (d, *J* = 2.2 Hz, 1H, H_b), 7.86 (d, *J* = 8.8 Hz, 1H, H_d), 7.80 (d, *J* = 8.9 Hz, 1H, H_a), 7.69 (dd, *J* = 8.8, 2.2 Hz, 1H, H_c), 7.33 (d, *J* = 2.6 Hz, 1H, H_e), 7.17 (dd, *J* = 8.9, 2.5 Hz, 1H, H_f), 5.12 (t, *J* = 6.8 Hz, 2H, H_i), 4.85 (d, *J* = 2.3 Hz, 2H, H_o), 4.76 (q, *J* = 7.3 Hz, 2H, H_q), 3.63 (t, *J* = 6.8 Hz, 1H, H_h), 3.05 – 3.02 (m, 1H, H_p), 1.70 (t, *J* = 7.3 Hz, 1H, H_r) ppm.

^{13}C NMR (176 MHz, D_2O) δ = 155.6, 150.5, 149.6, 145.6, 145.2, 142.6, 133.8, 132.1, 130.1, 128.8, 128.3, 127.0, 126.9, 122.7, 119.8, 119.2, 118.6, 107.7, 78.5, 76.9, 61.1, 57.7, 55.9, 26.6, 15.5 ppm.

HRMS (ESI-TOF) *m/z* calcd for $[C_{29}H_{27}N_5O]^+$ 461.2205, found 461.2193.

1-(But-3-yn-1-yl)-1'-ethyl-[4,4'-bipyridine]-1,1'-diium chloride (**22**$^{2+}$)

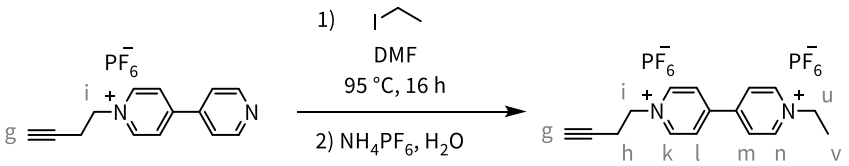

71%

Compound **18**$^{+}$ (150 mg, 0.529 mmol. 1 equiv.) and iodoethane (0.2 mL, 386 mg, 2.48 mmol, 4.7 equiv.) were dissolved in DMF (4 mL) and heated to 95 °C for 16 h. The solvent was evaporated *in vacuo*. The residue was dissolved in H_2O, sat. NH_4PF_6 (aq.) was added, the precipitate was filtered off, washed with H_2O and dried furnishing **22**$^{2+}$ (200 mg, 0.378 mmol, 71%) as a grey powder.

^{1}H NMR (400 MHz, DMSO-d_6) δ = 9.39 (d, *J* = 6.3 Hz, 2H, H_k), 8.83 (d, *J* = 6.8 Hz, 2H, H_n), 8.79 (d, *J* = 6.5 Hz, 2H, H_l), 8.05 (d, *J* = 6.2 Hz, 2H, H_m), 4.84 (t, *J* = 6.5 Hz, 2H, H_i), 4.72 (q, *J* = 7.4 Hz, 2H, H_u), 3.11 (t, *J* = 2.6 Hz, 1H, H_g), 3.01 (td, *J* = 6.6, 2.6 Hz, 2H, H_h), 1.61 (t, *J* = 7.3 Hz, 3H, H_v) ppm.

The spectroscopic data agrees with previously published results.[147]

1-Ethyl-1'-(2-(1-(6-hydroxynaphthalen-2-yl)-1H-1,2,3-triazol-4-yl)ethyl)-[4,4'-bipyridine]-1,1'-diium chloride (**C**$^{2+}$)

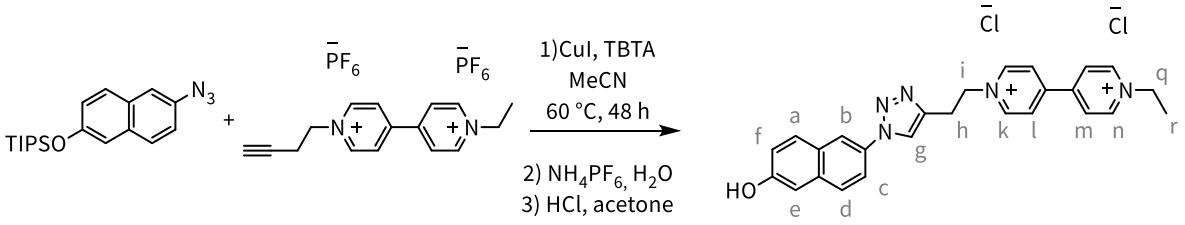

37%

Compound **17** (66 mg, 0.210 mmol, 1.1 equiv.), compound **22**$^{2+}$ (100 mg, 0.190 mmol, 1 equiv.), CuI (0.2 mg, 0.001 mmol, 5 mol-%) and tris((1-benzyl-4-triazolyl)methyl)amine (0.5 mg, 0.001 mmol, 0.05 equiv.) were dissolved in MeCN (5 mL) and stirred at 60 °C for 48 h. The solvent was evaporated *in vacuo*. The crude product was purified by column chromatography (ALOX, DCM/MeOH = 99:1, 50:1, 20:1), dissolved in H_2O and sat. NH_4PF_6 (aq.) was added. The precipitate was filtered off, dried, dissolved in acetone and HCl (aq., 36%) was added. The precipitate was filtered off and dried furnishing **C**$^{2+}$ (35.0 mg, 0.071 mmol, 37%) as a grey powder.

^{1}H NMR (500 MHz, D_2O) δ = 8.93 (d, *J* = 6.9 Hz, 2H, H_k), 8.88 (d, *J* = 7.0 Hz, 2H, H_n), 8.26 (d, *J* = 6.9 Hz, 2H, H_l), 8.22 (d, *J* = 7.0 Hz, 2H, H_m), 7.91 (s, 1H, H_g), 7.27 (d, *J* = 1.3 Hz, 1H, H_b), 7.26 (d, *J* = 8.9 Hz, 1H, H_a), 7.23 (d, *J* = 8.9 Hz, 1H, H_d), 7.14 (dd, *J* = 8.7, 2.2 Hz, 1H, H_c), 6.75 (dd, *J* = 8.7, 2.6 Hz, 1H, H_f), 6.64 (d, *J* = 2.6 Hz, 1H, H_e), 4.78 – 4.74 (m, 2H, H_i), 4.63 (q, *J* = 7.4 Hz, 2H, H_q), 3.27 (t, *J* = 7.4 Hz, 2H, H_h), 1.61 (t, *J* = 7.4 Hz, 3H, H_r) ppm.

^{13}C NMR (176 MHz, D_2O) δ = 154.6, 150.4, 149.4, 145.5, 145.1, 142.5, 134.2, 131.4, 130.3, 128.2, 127.5, 126.9, 126.8, 122.5, 119.5, 119.1, 118.6, 109.2, 61.0, 57.7, 26.5, 15.5 ppm.

HRMS (ESI-TOF) *m/z* calcd for $[C_{26}H_{25}N_5O]^{2+}$ 211.6024, found 211.6027; $[C_{26}H_{24}N_5O]^{+}$ 422.1975, found 422.1975; $[C_{26}H_{25}N_5O]^{+}$ 432.2054, found 432.2053.

It was possible to obtain a crystal structure of [**C**][Cl]$_2$.

6.6 Synthetic Procedures for Chapter 4.5

1-(But-3-yn-1-yl)-1'-(2-(1-(6-hydroxynaphthalen-2-yl)-1H-1,2,3-triazol-4-yl)ethyl)-[4,4'-bipyridine]-1,1'-diium chloride (**B**$^{2+}$)

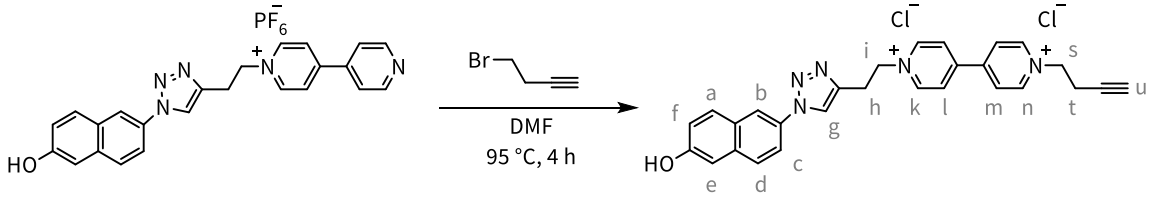

59%

Compound **19**$^{+}$ (341 mg, 0.632 mmol, 1 equiv.) and 4-bromo-1-butyne (0.2 mL, 283 mg, 2.13 mmol, 3.37 equiv.) were dissolved in DMF (5 mL) and heated to 95 °C for 4 h. The solvent was evaporated *in vacuo* and sat. NH_4PF_6 (aq.) was added. The precipitate was filtered off, dried, dissolved in acetone and HCl (aq., 36%) was added. The precipitate was filtered off and dried furnishing **B**$^{2+}$ (193 mg, 0.373 mmol, 59%) as a brown powder.

^{1}H NMR (700 MHz, DMSO-d_6) δ = 10.10 (s, 1H, OH), 9.50 (d, *J* = 6.3 Hz, 2H, H_k), 9.44 (d, *J* = 6.4 Hz, 2H, H_n), 8.89 (d, *J* = 6.3 Hz, 2H, H_m), 8.86 (d, *J* = 6.4 Hz, 2H, H_l), 8.80 (s, 1H, H_g), 8.27 (d, *J* = 2.2 Hz, 1H, H_b), 7.90 (d, *J* = 9.0 Hz, 1H, H_d), 7.89 (d, *J* = 8.9 Hz, 1H, H_a), 7.87 (dd, *J* = 9.0, 2.2 Hz, 1H, H_c), 7.24 (d, *J* = 2.4 Hz, 1H, H_e), 7.22 (dd, *J* = 8.9, 2.4 Hz, 1H, H_f), 5.14 (t, *J* = 6.9 Hz, 2H, H_i), 4.86 (t, *J* = 6.6 Hz, 2H, H_s), 3.59 (t, *J* = 6.9 Hz, 2H, H_h), 3.11 (d, *J* = 2.4 Hz, 1H, H_u), 3.05 (td, *J* = 6.6, 2.4 Hz, 2H, H_t) ppm.

^{13}C NMR (176 MHz, DMSO-d_6) δ = 156.3, 148.6, 146.1, 146.0, 142.7, 134.1, 131.5, 129.8, 127.9, 127.1, 126.5, 126.4, 121.6, 120.2, 118.8, 117.8, 108.8, 79.0, 75.3, 59.8, 58.7, 26.7, 20.4 ppm.

HRMS (ESI-TOF) calcd. for $[C_{28}H_{24}N_5O]^+$ 446.1975; found: 446.1969; calcd. for $[C_{28}H_{25}N_5O]^+$ 447.2054; found: 447.2049.

6.7 Crystallographic Data

The data is not uploaded to the Cambridge Structural Database and, therefore, have no CCDC entry.

Crystal data for $\mathbf{2}^{+}\cdot OTf^{-}$: CCDC-XXXXXX, M = 458.44, colorless plate, 0.21 x 0.12 x 0.05 mm^3, monoclinic, space group $P2_1/c$, a = 10.76354(16) Å, b = 8.10679(15) Å, c = 47.0300(7) Å, α = 90°, β = 94.2464 (14)°, γ = 90°, V = 4092.47(12) $Å^3$, Z = 8, Dc = 1.488 g/cm^3, F000 = 1888, μ= 1.916 mm^{-1} , T = 123.00(10) K, θ_{max} = 66.75°, 42632 total reflections, 6611 with Io > 2σ(Io), R_{int} = 0.0346, 7239 data, 577 parameters, 6 restraints, GooF = 1.140, R = 0.0767 and wR= 0.1791 [Io > 2σ(Io)], R = 0.0815 and wR= 0.1817 (all reflections), 0.783 < Δρ < -0.467 e/$Å^3$.

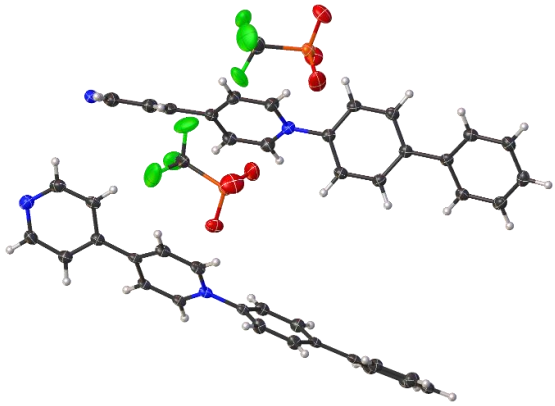

Crystal data for $\mathbf{2}^{+}\cdot BF_4^{-}$: CCDC-XXXXXX, M = 428.23, yellow block, 0.23 x 0.16 x 0.14 mm^3, orthorhombic, space group $P2_12_12_1$, a = 7.00624(8) Å, b = 16.60752(18) Å, c = 17.46005(16) Å, α = 90°, β = 90°, γ = 90°, V = 2031.59(4) $Å^3$, Z = 4, Dc = 1.400 g/cm^3, F000 = 888, μ= 0.938 mm^{-1} , T = 120.01(10) K, θ_{max} = 66.75°, 10864 reflection number, 3494 with Io > 2σ(Io), R_{int} = 0.0965, 3553 data, 282 parameters, 0 restraints, GooF = 1.062, R = 0.0422 and wR= 0.1183 [Io > 2σ(Io)], R= 0.0428 and wR= 0.1191 (all reflections), 0.650 < Δρ < -0.486 e/$Å^3$.

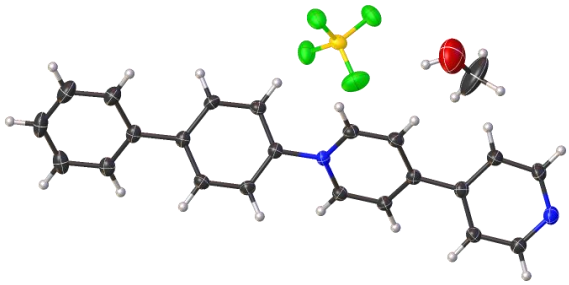

Crystal data for $\mathbf{2}H^{+}\cdot[2ClO_4^{-}]$: CCDC-XXXXXX, M = 1527.85, yellow needle, 0.08 x 0.06 x 0.05 mm^3, orthorhombic, space group $P2_1/n$, a = 14.7118(6) Å, b = 9.9969(5) Å, c = 44.7305(14) Å, α = 90°, β = 90°, γ = 90°, V = 6578.7(4) $Å^3$, Z = 4, Dc = 1.543 g/cm^3, F000 = 3144, μ= 0.350 mm^{-1}, T = 100.0(1) K, θ_{max} = 25.25°, 38727 reflection number, 9612 with Io > 2σ(Io), R_{int} = 0.0718, 11848 data, 894 parameters, 2 restraints, GooF = 1.107, R = 0.0717 and wR= 0.1583 [Io > 2σ(Io)], R = 0.0912 and wR= 0.1677 (all reflections), 0.643 < Δρ < -0.498 e/$Å^3$.

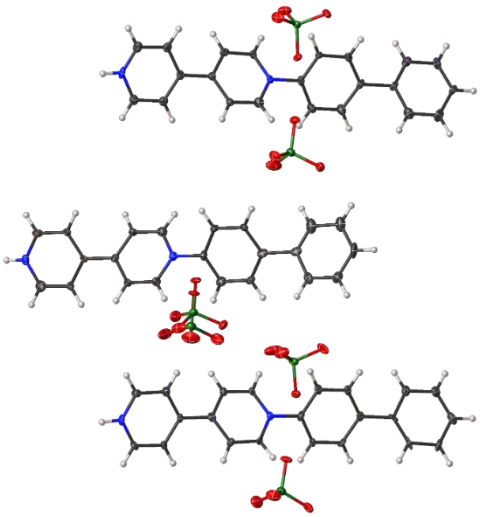

Crystal data for $\mathbf{2}^{2+}\cdot[2NO_3^-]$: CCDC-XXXXXX, M = 434.40, yellow block, 0.13 x 0.08 x 0.04 mm^3, monoclinic, space group $P2_1/c$, a = 17.4632(12) Å, b = 7.1404(4) Å, c = 16.4121(14) Å, α = 90°, β = 112.168(10)°, γ = 90°, V = 1895.2(3) $Å^3$, Z = 4, Dc = 1.522 g/cm^3, F000 = 904, μ= 0.113 mm^{-1}, T = 100 0(1) K, θ_{max} = 25.25°, 12258 reflection number, 2328 with Io > 2σ(Io), R_{int} = 0.0506, 3435 data, 289 parameters, 1 restraints, GooF = 1.053, R = 0.0476 and wR= 0.0967 [Io > 2σ(Io)], R =0.0871 and wR= 0.1148 (all reflections), 0.233 < Δρ < -0.300 e/$Å^3$.

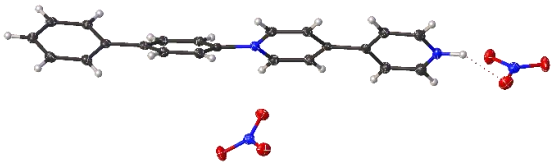

Crystal data for $\mathbf{8}^{2+}\cdot[2Cl^-]$: CCDC-XXXXXX, M = 517.43, yellow block, 0.15 x 0.13 x 0.09 mm^3, monoclinic, space group $P2_1/c$, a = 9.1891(7) Å, b = 7.4027(6)Å, c = 38.467(4) Å, α = 90°, β = 95.877(8)°, γ = 90°, V = 2602.9(4) $Å^3$, Z = 4, Dc = 1.320 g/cm^3, F000 = 1096, μ= 0.290 mm^{-1}, T = 120.0(1) K, θ_{max} = 25.25°, 9498 reflection number, 2988 with Io > 2σ(Io), R_{int} = 0.0463, 4490 data, 308 parameters, 0 restraints, GooF = 1.043, R = 0.0463 and wR= 0.1438 [Io > 2σ(Io)], R = 0.1146 and wR= 0.1637 (all reflections), 0.692 < Δρ < -0.489 e/$Å^3$.

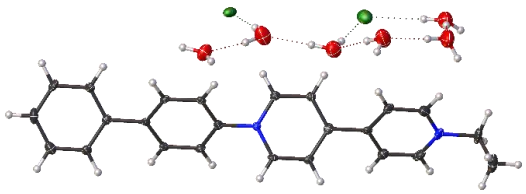

Crystal data for $\mathbf{2}^{+}\cdot PF_6^-$: CCDC-XXXXXX, M = 526.45, yellow plate, 0.50 x 0.44 x 0.16 mm^3, monoclinic, space group $P2_1/c$, a = 10.3231(7) Å, b = 16.7828(13) Å, c = 14.4791(11) Å, α = 90°, β = 108.954(2)°, γ = 90°, V = 2372.5(3)$Å^3$, Z = 4, Dc = 1.474 g/cm^3, F000 = 1088, μ= 0.186mm^{-1} , T = 100.0(1) K, θ_{max} = 27.52°,

29814 reflection number, 4769 with Io > 2σ(Io), R_{int} = 0.0287, 5464 data, 325 parameters, 0 restraints, GooF = 1.020, R = 0.0387 and wR= 0.0964 [Io > 2σ(Io)], R= 0.0459 and wR= 0.1022 (all reflections), 0.358 < Δρ < -0.508 e/Å^3.

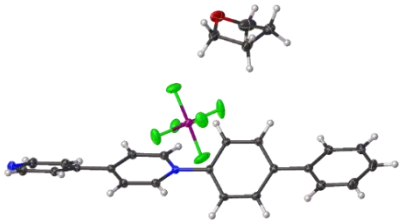

Crystal data for **2**H_2^+**2**@CB[8]$_2$: CCDC-XXXXXX, M = 8008.27, violet block, 0.13 x 0.08 x 0.04 mm^3, triclinic, space group *P*-1, a = 16.8857(15) Å, b = 22.3191(13) Å, c = 24.3440(10) Å, α = 88.408(4)°, β = 87.841(5)°, γ = 75.288(6)°, V = 8866.0(11) Å^3, Z = 1, Dc = 1.500 g/cm^3, F000 = 4179, μ= 1.609 mm^{-1} , T = 120.01(10) K, θ_{max} = 66.75°, 49807 reflection number, 13597 with Io > 2σ(Io), R_{int} = 0.1147, 299831 data, 2579 parameters, 108 restraints, GooF = 1.188, R = 0.1469 and wR= 0.3652 [Io > 2σ(Io)], R = 0.2431 and wR= 0.4393 (all reflections), 1.506 < Δρ < -1.188 e/Å^3.

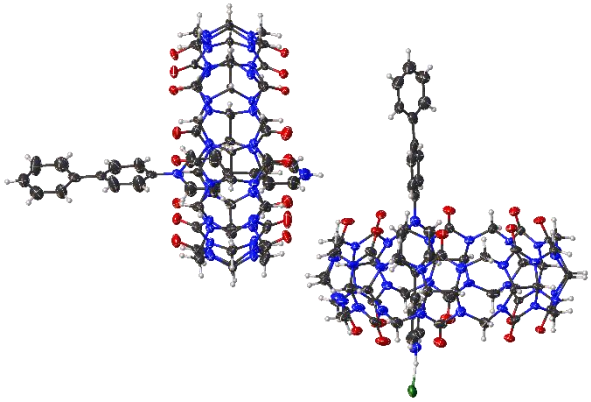

Counterions and disordered solvent molecules are omitted for clarity.

Crystal data for **C**$^{2+}$: CCDC-XXXXXX, M = 602.50, colorless plate, 0.36 x 0.21 x 0.07 mm^3, orthorhombic, space group *Pna*2$_1$, a = 7.41903(11) Å, b = 41.1592(8) Å, c = 9.7831(2) Å, α = 90°, β = 90°, γ = 90°, V = 2987.38(10) Å^3, Z = 4, Dc = 1.340 g/cm^3, F000 = 1272, μ= 2.388 mm^{-1} , T = 120.01(10) K, θ_{max} = 66.50°, 52459 total reflections, 4988 with Io > 2σ(Io), R_{int} = 0.0363, 5077 data, 396 parameters, 19 restraints, GooF = 1.037, R = 0.0715 and wR= 0.2021 [Io > 2σ(Io)], R = 0.0724 and wR= 0.2034 (all reflections), 1.175 < Δρ -0.682 e/Å^3.

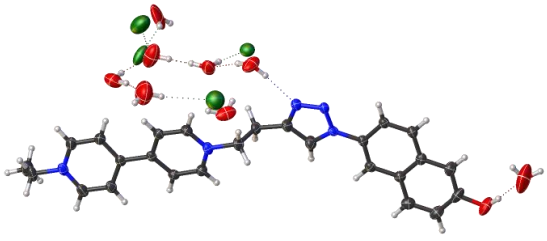

6.8 Computational Details

Starting from the crystal structure of [**2**][CF_3SO_3], the bipyridinium salt $\mathbf{2}^+$ was structurally optimized with DFT using the ORCA program package (version 3.0.3 and 4.0.1).[148] The structural optimization was performed *in vacuo* at the BP86[149] level of theory with the triple-ζ basis set def2-TZVP[150] and the auxiliary basis def2-TZVP/J[151] to enable the RI approximation (Figure 34a). The SCF Convergence tolerance was set to "TightSCF" and the DFT integration grid to a value of 5. Afterwards, a single-point calculation was performed using the hybrid functional B3LYP[152] (def2-TZVP with RijCosX approximation) to obtain a more detailed view on the electronic structure of $\mathbf{2}^+$ (Figure 34b).

Beginning with the geometry-optimized structure of $\mathbf{2}^+$, relaxed surface scans (BP86/def2-SVP) were performed by scanning the dihedral angle of the aromatic rings from 0 to 90° in 10 steps (Figure 35). Additionally, a conductor-like polarizable continuum model[153] (CPCM, ε = 80.4 for water) and the DFT-D3 dispersion corrections with Becke-Johnson damping (D3BJ)[154] as implemented in ORCA were used.

To elucidate a possible TICT mechanism, excited state energy and geometry optimization calculations were done according to the following procedure:

(A) ground state geometry optimization → (B) single-point energy evaluation → (C) excitation energies calculation → (D) excited state geometry optimization → (E) single-point energy evaluation

Excited states calculations (C) of $\mathbf{2}^+$ were performed with the hybrid time-dependent DFT (TD DFT)[155] approach (B3LYP/def2-TZVP) with D3BJ dispersion correction giving the HOMO→LUMO orbital excitation (528 nm, 2.34 eV) as the energetically lowest transition (Table 10). A second TD DFT calculation (PBE0/def2-TZVP)[156] using a solvent (CPCM, water) and dispersion (D3BJ) correction yielded similar results with a HOMO-LUMO excitation energy of 2.65 eV. The excited state geometry optimization $\mathbf{2}^+$ was performed using a TD DFT geometry optimization procedure (B3LYP/def2-TZVP). As shown in Figures 36a and 36b, the excited-state geometry optimization yields a more twisted conformation with a dihedral angle of 79.6° between the biphenyl and bipyridinium moiety. We assume that this drastic change is a consequence of a TICT mechanism. The excited TICT state is 0.42 eV lower in energy then the locally enhanced (LE) state (Figure 36c). Single-point energy calculations showed the twisted conformation to be a metastable state (MSS). As shown above, the low rotation barriers should enable a fast conformer interconversion between the ground and metastable state.

Table 10. Selected excitations obtained by TD DFT calculations (B3LYP/def2-TZVP) of **2**$^{+}$. Orbital transitions which contribute less than 1% are neglected.

state	excitation energy / nm (eV)	oscillator strength	transition
1	529 (2.34)	0.313	HOMO → LUMO
2	470 (2.64)	0.001	HOMO-1 → LUMO
3	423 (2.93)	0.001	HOMO-2 → LUMO
4	363 (3.42)	0.001	HOMO → LUMO+1
5	359 (3.45)	0.012	HOMO-3 → LUMO

7 List of Publications

[1] The Delicate Balance of Preorganisation and Adaptability in Multiply Bonded Host–Guest Complexes

Larissa K. S. von Krbek, Andreas J. Achazi, Stefan Schoder, Marius Gaedke, Tobias Biberger, Beate Paulus, and Christoph A. Schalley, *Chem. Eur. J.* **2017**, *23*, 2877-2883.

[2] PolyWhips: Directional Particle Transport by Gradient-Directed Growth and Stiffening of Supramolecular Assemblies

Luca Cera, Leonardo Chiappisi, Christoph Böttcher, Andrea Schulz, Stefan Schoder, Michael Gradzielski, and Christoph A. Schalley, *Adv. Mater.* **2017**, *29*, 1604430.

[3] Orthogonal switching of self-sorting processes in a stimuli-responsive library of cucurbit[8]uril complexes

Stefan Schoder and Christoph A. Schalley, *Chem. Commun.* **2017**, *53*, 9546-9549.

[4] Strong Emission Enhancement in pH-Responsive 2:2 Cucurbit[8]uril Complexes

Stefan Schoder, Hendrik V. Schröder, Luca Cera, Rakesh Puttreddy, Ute Resch-Genger, Kari Rissanen and Christoph A. Schalley, *manuscript in preparation*.

[5] Orthogonal Switching of a 2:2 Cucurbit[8]uril Complex

Stefan Schoder and Christoph A. Schalley, *manuscript in preparation*.

8 Danksagung

An erster Stelle möchte ich mich bei Prof. Dr. Christoph A. Schalley dafür bedanken, dass er mir die Möglichkeit gegeben hat in seiner Gruppe zu promovieren und dass er mir die Freiheit gegeben hat mein Thema so zu gestalten, dass ich daran Spaß und Freude gefunden habe.

Mein Dank gilt auch Prof. Dr. Marcelo Calderón für das Erstellen des Zweitgutachtens.

Nicht zu vergessen sind meine aktuellen und ehemaligen Kollegen, die eine gute Zusammenarbeit und das freundliche Arbeitsklima ermöglicht haben und mir stets mit etlichen Ratschlägen zur Seite standen. Dabei sind Hendrik Schröder, Bo Zheng und Anneli Kruve-Viil hervorzuheben, die mich immer ermuntert haben meinen Ergebnissen zu vertrauen. Die Erlebnisse außerhalb des Labors waren dabei auch eine Bereicherung an Erfahrung und eine Entledigung von anderen Dingen. Im Besonderen bin ich dabei natürlich dankbar Luca Cera, Fabian Klautzsch, Henrik Hupatz, Ulrike Warzok und Tuğrul Kaynak kennengelernt zu haben. Weil er sicherlich keine leichte Zeit mit mir hatte, will ich Marius Gaedke gesondert nennen. Für die großartige Unterstützung bei meinen Problemen abseits der Chemie möchte ich Carin Kietzmann und Silke Benndorf an dieser Stelle wertschätzen. Ich will mich ebenfalls bei allen Korrekturlesern erkenntlich zeigen. Diese halfen mir aus einem langweiligem Manuskript eine spannende Dissertation zu kreieren.

Darüber hinaus möchte ich mich bei meinen Studenten Lukas Fischer, Jessica Stubbe, Stefan Sander und Larissa Kapp dafür entschuldigen, dass ich ihnen nichts beigebracht habe, und schätze mich überaus glücklich, dass sie trotzdem bei mir geblieben sind.

Meine besondere Dankbarkeit gilt meiner Familie für ihre bedingungslose Liebe und weil sie mich so akzeptieren wie ich bin. Dieser Dank geht natürlich auch an Charlotte, wobei die nicht wirklich etwas Produktives beigetragen hat. Ebenfalls zu erwähnen sind meine guten Freunde Rara, Tobias und Léonie, die immer zu mir stehen und Kraft geben, das ganze hier relativ unbeschadet zu überleben. Mai-Phuong danke ich für die schöne Zeit, die Unterstützung und das Verständnis.

Mein Dank gilt auch allen anderen, die ich vergessen habe an dieser Stelle zu nennen. Ihr habt einen Platz in meinem Herzen, aber nicht in meiner Arbeit.

Und zuallerletzt muss ich auch meinen geliebten Chemikalien hoch anrechnen, dass sie mich nicht umgebracht haben und dass im Endeffekt ja doch etwas halbwegs Sinnvolles bei der ganzen Sache rausgekommen ist.

Vielen Dank!

9 References

[1] "The 2016 Nobel Prize in Chemistry - Press Release". *Nobelprize.org*. Nobel Media AB 2014. Web. 30 Apr 2018, 16:00 CET. <http://www.nobelprize.org/nobel_prizes/chemistry/laureates/2016/press.html>

[2] a) N. Koumura, R. W. J. Zijlstra, R. A. van Delden, N. Harada, B. L. Feringa, *Nature* **1999**, *401*, 152-155; b) B. L. Feringa, *Angew. Chem. Int. Ed.* **2017**, *56*, 11060-11078.

[3] a) C. Cheng, P. R. McGonigal, S. T. Schneebeli, H. Li, N. A. Vermeulen, C. Ke, J. F. Stoddart, *Nat. Nanotechnol.* **2015**, *10*, 547-553; b) C. Cheng, P. R. McGonigal, J. F. Stoddart, R. D. Astumian, *ACS Nano* **2015**, *9*, 8672-8688; c) J. F. Stoddart, *Angew. Chem. Int. Ed.* **2017**, *56*, 11094-11125.

[4] a) M. von Delius, E. M. Geertsema, D. A. Leigh, *Nat. Chem.* **2009**, *2*, 96-101; b) M. von Delius, D. A. Leigh, *Chem. Soc. Rev.* **2011**, *40*, 3656-3676; c) C. J. Martin, A. T. L. Lee, R. W. Adams, D. A. Leigh, *J. Am. Chem. Soc.* **2017**, *139*, 11998-12002.

[5] P. T. Anastas, J. C. Warner, *Green Chemistry: Theory and Practice*, Oxford University Press: New York, **1998**.

[6] S. J. Barrow, S. Kasera, M. J. Rowland, J. del Barrio, O. A. Scherman, *Chem. Rev.* **2015**, *115*, 12320-12406.

[7] J. W. Steed, P. A. Gale, *Supramolecular Chemistry: From Molecules to Nanomaterials*, Wiley-VCH, **2012**.

[8] a) A. Villiers, *Bull. Soc. Chim. Paris* **1891**, *45*, 468-471; b) A. Villiers, *C. R. Acad. Sci* **1891**, *CXII*, 435-438.

[9] A. Biwer, G. Antranikian, E. Heinzle, *Appl. Microbiol. Biotechnol.* **2002**, *59*, 609-617.

[10] G. Crini, *Chem. Rev.* **2014**, *114*, 10940-10975.

[11] J. F. Stoddart, *Carbohyd. Res.* **1989**, *192*, xii-xv.

[12] F. Cramer, *Angew. Chem.* **1952**, *64*, 437-447.

[13] M. V. Rekharsky, Y. Inoue, *Chem. Rev.* **1998**, *98*, 1875-1918.

[14] a) L. Isaacs, *Isr. J. Chem.* **2011**, *51*, 578-591; b) H. Cong, X. L. Ni, X. Xiao, Y. Huang, Q.-J. Zhu, S.-F. Xue, Z. Tao, L. F. Lindoy, G. Wei, *Org. Biomol. Chem.* **2016**, *14*, 4335-4364.

[15] J. Kim, I.-S. Jung, S.-Y. Kim, E. Lee, J.-K. Kang, S. Sakamoto, K. Yamaguchi, K. Kim, *J. Am. Chem. Soc.* **2000**, *122*, 540-541.

[16] R. Behrend, E. Meyer, F. Rusche, *Liebigs Ann.* **1905**, *339*, 1-37.

[17] W. A. Freeman, W. L. Mock, N. Y. Shih, *J. Am. Chem. Soc.* **1981**, *103*, 7367-7368.

[18] W. L. Mock, N. Y. Shih, *J. Org. Chem.* **1986**, *51*, 4440-4446.

[19] K. Kim, *Chem. Soc. Rev.* **2002**, *31*, 96-107.

[20] D. Whang, J. Heo, J. H. Park, K. Kim, *Angew. Chem. Int. Ed.* **1998**, *37*, 78-80.

[21] L. Isaacs, *Chem. Commun.* **2009**, 619-629.

[22] M. Nau Werner, M. Florea, I. Assaf Khaleel, *Isr. J. Chem.* **2011**, *51*, 559-577.

[23] a) X.-L. Ni, X. Xiao, H. Cong, L.-L. Liang, K. Cheng, X.-J. Cheng, N.-N. Ji, Q.-J. Zhu, S.-F. Xue, Z. Tao, *Chem. Soc. Rev.* **2013**, *42*, 9480-9508; b) A. G. Ol'ga, G. S. Denis, P. F. Vladimir, *Russ. Chem. Rev.* **2002**, *71*, 741-760.

[24] K. Jansen, H. J. Buschmann, A. Wego, D. Döpp, C. Mayer, H. J. Drexler, H. J. Holdt, E. Schollmeyer, *J. Incl. Phenom. Macrocycl. Chem.* **2001**, *39*, 357-363.

[25] F. Biedermann, W. M. Nau, H.-J. Schneider, *Angew. Chem. Int. Ed.* **2014**, *53*, 11158-11171.

[26] F. Biedermann, V. D. Uzunova, O. A. Scherman, W. M. Nau, A. De Simone, *J. Am. Chem. Soc.* **2012**, *134*, 15318-15323.

[27] S. Moghaddam, C. Yang, M. Rekharsky, Y. H. Ko, K. Kim, Y. Inoue, M. K. Gilson, *J. Am. Chem. Soc.* **2011**, *133*, 3570-3581.

[28] M. V. Rekharsky, T. Mori, C. Yang, Y. H. Ko, N. Selvapalam, H. Kim, D. Sobransingh, A. E. Kaifer, S. Liu, L. Isaacs, W. Chen, S. Moghaddam, M. K. Gilson, K. Kim, Y. Inoue, *Proc. Natl. Acad. Sci. U.S.A.* **2007**, *104*, 20737-20742.

[29] F. Biedermann, M. Vendruscolo, O. A. Scherman, A. De Simone, W. M. Nau, *J. Am. Chem. Soc.* **2013**, *135*, 14879-14888.

[30] a) H. J. Buschmann, E. Cleve, K. Jansen, E. Schollmeyer, *Anal. Chim. Acta* **2001**, *437*, 157-163; b) H. J. Buschmann, E. Cleve, K. Jansen, A. Wego, E. Schollmeyer, *J. Incl. Phenom. Macrocycl. Chem.* **2001**, *40*, 117-120.

[31] K. A. Kellersberger, J. D. Anderson, S. M. Ward, K. E. Krakowiak, D. V. Dearden, *J. Am. Chem. Soc.* **2001**, *123*, 11316-11317.

[32] Y. Miyahara, K. Abe, T. Inazu, *Angew. Chem. Int. Ed.* **2002**, *41*, 3020-3023.

[33] M. Florea, W. M. Nau, *Angew. Chem. Int. Ed.* **2011**, *50*, 9338-9342.

[34] W. L. Mock, N. Y. Shih, *J. Org. Chem.* **1983**, *48*, 3618-3619.

[35] a) Y. Honda, T. Hanaya, Y. Sueishi, *J. Incl. Phenom. Macrocycl. Chem.* **2017**, *88*, 253-257; b) M. I. El-Barghouthi, K. I. Assaf, A. M. M. Rawashdeh, *J. Chem. Theory Comput.* **2010**, *6*, 984-992.

[36] a) W. Ong, A. E. Kaifer, *Organometallics* **2003**, *22*, 4181-4183; b) W. S. Jeon, K. Moon, S. H. Park, H. Chun, Y. H. Ko, J. Y. Lee, E. S. Lee, S. Samal, N. Selvapalam, M. V. Rekharsky, V. Sindelar, D. Sobransingh, Y. Inoue, A. E. Kaifer, K. Kim, *J. Am. Chem. Soc.* **2005**, *127*, 12984-12989.

[37] L. Cao, M. Šekutor, P. Y. Zavalij, K. Mlinarić-Majerski, R. Glaser, L. Isaacs, *Angew. Chem. Int. Ed.* **2014**, *53*, 988-993.

[38] K. Moon, A. E. Kaifer, *Org. Lett.* **2004**, *6*, 185-188.

[39] W. Ong, M. Gómez-Kaifer, A. E. Kaifer, *Org. Lett.* **2002**, *4*, 1791-1794.

[40] J. Lagona, P. Mukhopadhyay, S. Chakrabarti, L. Isaacs, *Angew. Chem. Int. Ed.* **2005**, *44*, 4844-4870.

[41] S. Liu, C. Ruspic, P. Mukhopadhyay, S. Chakrabarti, P. Y. Zavalij, L. Isaacs, *J. Am. Chem. Soc.* **2005**, *127*, 15959-15967.

[42] a) S.-Y. Kim, I.-S. Jung, E. Lee, J. Kim, S. Sakamoto, K. Yamaguchi, K. Kim, *Angew. Chem. Int. Ed.* **2001**, *40*, 2119-2121; b) T. V. Mitkina, D. Y. Naumov, O. A. Gerasko, F. M. Dolgushin, C. Vicent, R. Llusar, M. N. Sokolov, V. P. Fedin, *Russ. Chem. Bull.* **2004**, *53*, 2519-2524; c) S. L. Hart, R. I. Haines, A. Decken, B. D. Wagner, *Inorg. Chim. Acta* **2009**, *362*, 4145-4151; d) T. V. Mitkina, D. Y. Naumov, O. A. Gerasko, V. P. Fedin, *Inorg. Chim. Acta* **2010**, *363*, 4387-4391; e) E. A.

Kovalenko, T. V. Mitkina, O. A. Geras'ko, D. G. Samsonenko, D. Y. Naumov, V. P. Fedin, *Koord. Khim.* **2011**, *37*, 161-167.

[43] G. Jiang, G. Li, *J. Photochem. Photobiol. B* **2006**, *85*, 223-227.

[44] a) H.-J. Kim, J. Heo, W. S. Jeon, E. Lee, J. Kim, S. Sakamoto, K. Yamaguchi, K. Kim, *Angew. Chem. Int. Ed.* **2001**, *40*, 1526-1529; b) M. E. Bush, N. D. Bouley, A. R. Urbach, *J. Am. Chem. Soc.* **2005**, *127*, 14511-14517; c) V. Sindelar, M. A. Cejas, F. M. Raymo, W. Chen, S. E. Parker, A. E. Kaifer, *Chem. Eur. J.* **2005**, *11*, 7054-7059; d) Y. Ling, W. Wang, A. E. Kaifer, *Chem. Commun.* **2007**, 610-612; e) F. Biedermann, U. Rauwald, M. Cziferszky, K. A. Williams, L. D. Gann, B. Y. Guo, A. R. Urbach, C. W. Bielawski, O. A. Scherman, *Chem. Eur. J.* **2010**, *16*, 13716-13722; f) D. Jiao, F. Biedermann, O. A. Scherman, *Org. Lett.* **2011**, *13*, 3044-3047; g) F. Biedermann, O. A. Scherman, *J. Phys. Chem. B* **2012**, *116*, 2842-2849.

[45] a) S. Senler, L. Cui, A. M. Broomes, E. L. Smith, J. N. Wilson, A. E. Kaifer, *J. Phys. Org. Chem.* **2012**, *25*, 592-596; b) Y. Zhang, T.-Y. Zhou, K.-D. Zhang, J.-L. Dai, Y.-Y. Zhu, X. Zhao, *Chem. Asian J.* **2014**, *9*, 1530-1534; c) R. Wang, L. Yuan, H. Ihmels, D. H. Macartney, *Chem. Eur. J.* **2007**, *13*, 6468-6473; d) R. Wang, D. Bardelang, M. Waite, K. A. Udachin, D. M. Leek, K. Yu, C. I. Ratcliffe, J. A. Ripmeester, *Org. Biomol. Chem.* **2009**, *7*, 2435-2439; e) X. Wu, X. Meng, G. Cheng, *J. Incl. Phenom. Macrocycl. Chem.* **2009**, *64*, 325-329; f) M. Shaikh, S. D. Choudhury, J. Mohanty, A. C. Bhasikuttan, H. Pal, *Phys. Chem. Chem. Phys.* **2010**, *12*, 7050-7055; g) D. Jiao, F. Biedermann, F. Tian, O. A. Scherman, *J. Am. Chem. Soc.* **2010**, *132*, 15734-15743; h) G. A. Vincil, A. R. Urbach, *Supramol. Chem.* **2008**, *20*, 681-687; i) S. Sonzini, S. T. J. Ryan, O. A. Scherman, *Chem. Commun.* **2013**, *49*, 8779-8781; j) C. P. Carvalho, Z. Dominguez, J. P. Da Silva, U. Pischel, *Chem. Commun.* **2015**, *51*, 2698-2701; k) W. S. Jeon, H.-J. Kim, C. Lee, K. Kim, *Chem. Commun.* **2002**, 1828-1829.

[46] a) J. M. Zayed, F. Biedermann, U. Rauwald, O. A. Scherman, *Polym. Chem.* **2010**, *1*, 1434-1436; b) Y. Liu, H. Yang, Z. Wang, X. Zhang, *Chem. Asian J.* **2013**, *8*, 1626-1632.

[47] a) A. S. Groombridge, A. Palma, R. M. Parker, C. Abell, O. A. Scherman, *Chem. Sci.* **2017**, *8*, 1350-1355; b) X. Xu, E. A. Appel, X. Liu, R. M. Parker, O. A. Scherman, C. Abell, *Biomacromolecules* **2015**, *16*, 2743-2749.

[48] a) J. Tian, T.-Y. Zhou, S.-C. Zhang, S. Aloni, M. V. Altoe, S.-H. Xie, H. Wang, D.-W. Zhang, X. Zhao, Y. Liu, Z.-T. Li, *Nat. Commun.* **2014**, *5*, 5574; b) K.-D. Zhang, J. Tian, D. Hanifi, Y. Zhang, A. C.-H. Sue, T.-Y. Zhou, L. Zhang, X. Zhao, Y. Liu, Z.-T. Li, *J. Am. Chem. Soc.* **2013**, *135*, 17913-17918.

[49] H. Yang, B. Yuan, X. Zhang, O. A. Scherman, *Acc. Chem. Res.* **2014**, *47*, 2106-2115.

[50] E. A. Appel, X. J. Loh, S. T. Jones, F. Biedermann, C. A. Dreiss, O. A. Scherman, *J. Am. Chem. Soc.* **2012**, *134*, 11767-11773.

[51] a) R. Nally, L. Isaacs, *Tetrahedron* **2009**, *65*, 7249-7258; b) S. Liu, P. Y. Zavalij, L. Isaacs, *J. Am. Chem. Soc.* **2005**, *127*, 16798-16799.

[52] a) W. Gong, X. Yang, Y. Zavalij Peter, L. Isaacs, Z. Zhao, S. Liu, *Chem. Eur. J.* **2016**, *22*, 17612-17618; b) X. Yang, F. Liu, Z. Zhao, F. Liang, H. Zhang, S. Liu, *Chin. Chem. Lett.* **2018**.

[53] X. J. Cheng, L. L. Liang, K. Chen, N. N. Ji, X. Xiao, J. X. Zhang, Y. Q. Zhang, S. F. Xue, Q. J. Zhu, X. L. Ni, Z. Tao, *Angew. Chem. Int. Ed.* **2013**, *52*, 7252-7255.

[54] a) J. Svec, M. Necas, V. Sindelar, *Angew. Chem. Int. Ed.* **2010**, *49*, 2378-2381; b) J. Svec, M. Dusek, K. Fejfarova, P. Stacko, P. Klán, A. E. Kaifer, W. Li, E. Hudeckova, V. Sindelar, *Chem. Eur. J.* **2011**, *17*, 5605-5612.

[55] M. A. Yawer, V. Havel, V. Sindelar, *Angew. Chem. Int. Ed.* **2015**, *54*, 276-279.

[56] K. Kim, N. Selvapalam, Y. H. Ko, K. M. Park, D. Kim, J. Kim, *Chem. Soc. Rev.* **2007**, *36*, 267-279.

[57] D. B. Amabilino, J. F. Stoddart, *Chem. Rev.* **1995**, *95*, 2725-2828.

[58] a) D. P. Fielden Stephen, A. Leigh David, L. Woltering Steffen, *Angew. Chem. Int. Ed.* **2017**, *56*, 11166-11194; b) J. J. Danon, A. Krüger, D. A. Leigh, J.-F. Lemonnier, A. J. Stephens, I. J. Vitorica-Yrezabal, S. L. Woltering, *Science* **2017**, *355*, 159-162; c) K. E. Horner, M. A. Miller, J. W. Steed, P. M. Sutcliffe, *Chem. Soc. Rev.* **2016**, *45*, 6432-6448.

[59] K. S. Chichak, S. J. Cantrill, A. R. Pease, S.-H. Chiu, G. W. V. Cave, J. L. Atwood, J. F. Stoddart, *Science* **2004**, *304*, 1308-1312.

[60] P. L. Anelli, N. Spencer, J. F. Stoddart, *J. Am. Chem. Soc.* **1991**, *113*, 5131-5133.

[61] a) S. A. Nepogodiev, J. F. Stoddart, *Chem. Rev.* **1998**, *98*, 1959-1976; b) M. C. T. Fyfe, J. F. Stoddart, *Acc. Chem. Res.* **1997**, *30*, 393-401; c) N. Nakashima, A. Kawabuchi, H. Murakami, *J. Incl. Phenom. Macrocycl. Chem.* **1998**, *32*, 363-373; d) K. B. Lipkowitz, *Chem. Rev.* **1998**, *98*, 1829-1874; e) A. Harada, J. Li, M. Kamachi, *Nature* **1992**, *356*, 325-327; f) A. Harada, J. Li, M. Kamachi, *Nature* **1993**, *364*, 516-518; g) A. Harada, *J. Synth. Org. Chem Jpn.* **2004**, *62*, 464-470; h) A. Harada, Y. Takashima, H. Yamaguchi, *Chem. Soc. Rev.* **2009**, *38*, 875-882.

[62] Y. Okumura, K. Ito, *Adv. Mater.* **2001**, *13*, 485-487.

[63] M. Hmadeh, C. Fahrenbach Albert, S. Basu, A. Trabolsi, D. Benítez, H. Li, A. M. Albrecht-Gary, M. Elhabiri, J. F. Stoddart, *Chem. Eur. J.* **2011**, *17*, 6076-6087.

[64] J. Stankiewicz, L. H. Eckardt, *Angew. Chem. Int. Ed.* **2006**, *45*, 342-344.

[65] G. M. Whitesides, R. F. Ismagilov, *Science* **1999**, *284*, 89-92.

[66] D. Newth, J. Finnigan, *Austr. J. Chem.* **2006**, *59*, 841-848.

[67] a) G. Ashkenasy, T. M. Hermans, S. Otto, A. F. Taylor, *Chem. Soc. Rev.* **2017**, *46*, 2543-2554; b) R. F. Ludlow, S. Otto, *Chem. Soc. Rev.* **2008**, *37*, 101-108.

[68] J.-M. Lehn, *Science* **2002**, *295*, 2400-2403.

[69] J.-P. Sauvage, *Angew. Chem. Int. Ed.* **2017**, *56*, 11080-11093.

[70] M. M. Safont-Sempere, G. Fernández, F. Würthner, *Chem. Rev.* **2011**, *111*, 5784-5814.

[71] A. Wu, L. Isaacs, *J. Am. Chem. Soc.* **2003**, *125*, 4831-4835.

[72] R. Kramer, J. M. Lehn, A. Marquis-Rigault, *Proc. Natl. Acad. Sci. U.S.A.* **1993**, *90*, 5394-5398.

[73] P. N. Taylor, H. L. Anderson, *J. Am. Chem. Soc.* **1999**, *121*, 11538-11545.

[74] A. Shivanyuk, J. Rebek, *J. Am. Chem. Soc.* **2002**, *124*, 12074-12075.

[75] E. A. Neal, S. M. Goldup, *Angew. Chem. Int. Ed.* **2016**, *55*, 12488-12493.

[76] Z. He, W. Jiang, C. A. Schalley, *Chem. Soc. Rev.* **2015**, *44*, 779-789.

[77] P. Mukhopadhyay, A. Wu, L. Isaacs, *J. Org. Chem.* **2004**, *69*, 6157-6164.

[78] W. Jiang, Q. Wang, I. Linder, F. Klautzsch, C. A. Schalley, *Chem. Eur. J.* **2011**, *17*, 2344-2348.

[79] R. Kay Euan , A. Leigh David , F. Zerbetto, *Angew. Chem. Int. Ed.* **2006**, *46*, 72-191.

[80] a) Q. Li, G. Fuks, E. Moulin, M. Maaloum, M. Rawiso, I. Kulic, J. T. Foy, N. Giuseppone, *Nat. Nanotechnol.* **2015**, *10*, 161-165; b) J. T. Foy, Q. Li, A. Goujon, J.-R. Colard-Itté, G. Fuks, E.

Moulin, O. Schiffmann, D. Dattler, D. P. Funeriu, N. Giuseppone, *Nat. Nanotechnol.* **2017**, *12*, 540-545.

[81] S. Erbas-Cakmak, D. A. Leigh, C. T. McTernan, A. L. Nussbaumer, *Chem. Rev.* **2015**, *115*, 10081-10206.

[82] C. Pezzato, C. Cheng, J. F. Stoddart, R. D. Astumian, *Chem. Soc. Rev.* **2017**, *46*, 5491-5507.

[83] S. Saha, J. F. Stoddart, *Chem. Soc. Rev.* **2007**, *36*, 77-92.

[84] P. R. Ashton, R. Ballardini, V. Balzani, I. Baxter, A. Credi, M. C. T. Fyfe, M. T. Gandolfi, M. Gómez-López, M. V. Martínez-Díaz, A. Piersanti, N. Spencer, J. F. Stoddart, M. Venturi, A. J. P. White, D. J. Williams, *J. Am. Chem. Soc.* **1998**, *120*, 11932-11942.

[85] I. Hwang, A. Y. Ziganshina, Y. H. Ko, G. Yun, K. Kim, *Chem. Commun.* **2009**, 416-418.

[86] F. Tian, D. Jiao, F. Biedermann, O. A. Scherman, *Nat. Commun.* **2012**, *3*, 1207.

[87] S. Erbas-Cakmak, S. D. P. Fielden, U. Karaca, D. A. Leigh, C. T. McTernan, D. J. Tetlow, M. R. Wilson, *Science* **2017**, *358*, 340-343.

[88] J. B. Birks, *Photophysics of Aromatic Molecules*, Wiley-Interscience, London, **1970**.

[89] Y. Hong, J. W. Y. Lam, B. Z. Tang, *Chem. Soc. Rev.* **2011**, *40*, 5361-5388.

[90] R. Hu, N. L. C. Leung, B. Z. Tang, *Chem. Soc. Rev.* **2014**, *43*, 4494-4562.

[91] J. Luo, Z. Xie, J. W. Y. Lam, L. Cheng, H. Chen, C. Qiu, H. S. Kwok, X. Zhan, Y. Liu, D. Zhu, B. Z. Tang, *Chem. Commun.* **2001**, 1740-1741.

[92] a) B. Z. Tang, X. Zhan, G. Yu, P. P. Sze Lee, Y. Liu, D. Zhu, *J. Mater. Chem.* **2001**, *11*, 2974-2978; b) J. Chen, C. C. W. Law, J. W. Y. Lam, Y. Dong, S. M. F. Lo, I. D. Williams, D. Zhu, B. Z. Tang, *Chem. Mater.* **2003**, *15*, 1535-1546.

[93] G. Feng, R. T. K. Kwok, B. Z. Tang, B. Liu, *Appl. Phys. Rev.* **2017**, *4*, 021307.

[94] a) C. J. Bhongale, C.-W. Chang, C.-S. Lee, E. W.-G. Diau, C.-S. Hsu, *J. Phys. Chem. B* **2005**, *109*, 13472-13482; b) Y. T. Wu, M. Y. Kuo, Y. T. Chang, C. C. Shin, T. C. Wu, C. C. Tai, T. H. Cheng, W. S. Liu, *Angew. Chem. Int. Ed.* **2008**, *47*, 9891-9894.

[95] a) C.-X. Yuan, X.-T. Tao, L. Wang, J.-X. Yang, M.-H. Jiang, *J. Phys. Chem. C* **2009**, *113*, 6809-6814; b) K. Hirano, S. Minakata, M. Komatsu, J. Mizuguchi, *J. Phys. Chem. A* **2002**, *106*, 4868-4871; c) Z. Yang, Z. Chi, T. Yu, X. Zhang, M. Chen, B. Xu, S. Liu, Y. Zhang, J. Xu, *J. Mater. Chem.* **2009**, *19*, 5541-5546.

[96] a) J. Liu, J. W. Y. Lam, B. Z. Tang, *Chem. Rev.* **2009**, *109*, 5799-5867; b) A. Qin, C. K. W. Jim, Y. Tang, J. W. Y. Lam, J. Liu, F. Mahtab, P. Gao, B. Z. Tang, *J. Phys. Chem. B* **2008**, *112*, 9281-9288.

[97] a) A. Y.-Y. Tam, K. M.-C. Wong, V. W.-W. Yam, *J. Am. Chem. Soc.* **2009**, *131*, 6253-6260; b) M. X. Zhu, W. Lu, N. Zhu, C. M. Che, *Chem. Eur. J.* **2008**, *14*, 9736-9746; c) Q. Zhao, L. Li, F. Li, M. Yu, Z. Liu, T. Yi, C. Huang, *Chem. Commun.* **2008**, 685-687.

[98] Z. Wei, Z.-Y. Gu, R. K. Arvapally, Y.-P. Chen, R. N. McDougald, J. F. Ivy, A. A. Yakovenko, D. Feng, M. A. Omary, H.-C. Zhou, *J. Am. Chem. Soc.* **2014**, *136*, 8269-8276.

[99] a) M. Wang, G. Zhang, D. Zhang, D. Zhu, B. Z. Tang, *J. Mater. Chem.* **2010**, *20*, 1858-1867; b) V. S. Vyas, R. Rathore, *Chem. Commun.* **2010**, *46*, 1065-1067; c) J. Mei, Y. Hong, W. Y. Lam Jacky, A. Qin, Y. Tang, Z. Tang Ben, *Adv. Mater.* **2014**, *26*, 5429-5479.

[100] D. L. Dexter, *J. Chem. Phys.* **1953**, *21*, 836-850.

[101] W. T. Yip, D. H. Levy, *J. Phys. Chem.* **1996**, *100*, 11539-11545.

[102] S. Sasaki, G. P. C. Drummen, G.-i. Konishi, *J. Mater. Chem. C* **2016**, *4*, 2731-2743.

[103] Z. R. Grabowski, K. Rotkiewicz, W. Rettig, *Chem. Rev.* **2003**, *103*, 3899-4032.

[104] a) S. Paudel, P. Nandhikonda, M. D. Heagy, *J. Fluoresc.* **2009**, *19*, 681-691; b) G. Wermuth, W. Rettig, *J. Phys. Chem.* **1984**, *88*, 2729-2735.

[105] W. Rettig, *Ber. Bunsenges. Phys. Chem.* **2010**, *95*, 259-263.

[106] a) N. G. a. P. Suppan, *Pure Appl. Chem.* **1993**, *65*, 1739-1743; b) J. Hicks, M. Vandersall, Z. Babarogic, K. B. Eisenthal, *Chem. Phys. Lett.* **1985**, *116*, 18-24.

[107] M. A. Haidekker, E. A. Theodorakis, *J Biol Eng* **2010**, *4*, 11.

[108] S. Sasaki, Y. Niko, A. S. Klymchenko, G.-i. Konishi, *Tetrahedron* **2014**, *70*, 7551-7559.

[109] J. Kim, T. Morozumi, H. Hiraga, H. Nakamura, *Anal. Sci.* **2009**, *25*, 1319-1325.

[110] Z.-Q. Yan, Z.-Y. Yang, H. Wang, A.-W. Li, L.-P. Wang, H. Yang, B.-R. Gao, *Spectrochim. Acta A* **2011**, *78*, 1640-1645.

[111] C. L. Schilling, E. F. Hilinski, *J. Am. Chem. Soc.* **1988**, *110*, 2296-2298.

[112] H.-H. Fang, Q.-D. Chen, J. Yang, H. Xia, B.-R. Gao, J. Feng, Y.-G. Ma, H.-B. Sun, *J. Phys. Chem. C* **2010**, *114*, 11958-11961.

[113] W. Qin, D. Ding, J. Liu, W. Z. Yuan, Y. Hu, B. Liu, B. Z. Tang, *Adv. Funct. Mater.* **2012**, *22*, 771-779.

[114] R. Hu, E. Lager, A. Aguilar-Aguilar, J. Liu, J. W. Y. Lam, H. H. Y. Sung, I. D. Williams, Y. Zhong, K. S. Wong, E. Peña-Cabrera, B. Z. Tang, *J. Phys. Chem. C* **2009**, *113*, 15845-15853.

[115] F. Biedermann, E. Elmalem, I. Ghosh, W. M. Nau, O. A. Scherman, *Angew. Chem. Int. Ed.* **2012**, *51*, 7739-7743.

[116] H.-T. Feng, X. Zheng, X. Gu, M. Chen, J. W. Y. Lam, X. Huang, B. Z. Tang, *Chem. Mater.* **2018**, *30*, 1285-1290.

[117] M. Freitag, L. Gundlach, P. Piotrowiak, E. Galoppini, *J. Am. Chem. Soc.* **2012**, *134*, 3358-3366.

[118] a) J. J. McKinnon, M. A. Spackman, A. S. Mitchell, *Acta Crystallogr. Sect. B* **2004**, *60*, 627-668; b) J. J. McKinnon, D. Jayatilaka, M. A. Spackman, *Chem. Commun.* **2007**, 3814-3816; c) M. A. Spackman, D. Jayatilaka, *CrystEngComm* **2009**, *11*, 19-32; d) M. A. Spackman, J. J. McKinnon, *CrystEngComm* **2002**, *4*, 378-392.

[119] K. Hirose, *J. Incl. Phenom. Macrocycl. Chem.* **2001**, *39*, 193-209.

[120] M. Shaikh, J. Mohanty, P. K. Singh, W. M. Nau, H. Pal, *Photochem. Photobiol. Sci.* **2008**, *7*, 408-414.

[121] A. L. Koner, W. M. Nau, *Supramol. Chem.* **2007**, *19*, 55-66.

[122] a) A. K. Blackburn, A. C. H. Sue, A. K. Shveyd, D. Cao, A. Tayi, A. Narayanan, B. S. Rolczynski, J. M. Szarko, O. A. Bozdemir, R. Wakabayashi, J. A. Lehrman, B. Kahr, L. X. Chen, M. S. Nassar, S. I. Stupp, J. F. Stoddart, *J. Am. Chem. Soc.* **2014**, *136*, 17224-17235; b) C. Janiak, *Dalton Trans.* **2000**, 3885-3896.

[123] F. Würthner, E. Kaiser Theo, R. Saha-Möller Chantu, *Angew. Chem. Int. Ed.* **2011**, *50*, 3376-3410.

[124] Y. Shao, X. Zhang, K. Liang, J. Wang, Y. Lin, S. Yang, W.-B. Zhang, M. Zhu, B. Sun, *RSC Adv.* **2017**, *7*, 16155-16162.

[125] *Rigaku Oxford Diffraction 2015, CrysAlisPro* Version 1.171.38.43.

[126] a) F. Ulatowski, K. Dąbrowa, T. Bałakier, J. Jurczak, *J. Org. Chem.* **2016**, *81*, 1746-1756; b) D. Brynn Hibbert, P. Thordarson, *Chem. Commun.* **2016**, *52*, 12792-12805.

[127] S. Deroo, U. Rauwald, C. V. Robinson, O. A. Scherman, *Chem. Commun.* **2009**, 644-646.

[128] Y.-M. Zhang, Z. Wang, Y. Chen, H.-Z. Chen, F. Ding, Y. Liu, *Org. Biomol. Chem.* **2014**, *12*, 2559-2567.

[129] E. M. Kosower, J. L. Cotter, *J. Am. Chem. Soc.* **1964**, *86*, 5524-5527.

[130] X. Song, F. Liu, S. Sun, J. Cui, J. Fan, F. Song, X. Peng, *Supramol. Chem.* **2013**, *25*, 401-408.

[131] a) P. M. S. Monk, R. D. Fairweather, M. D. Ingram, J. A. Duffy, *J. Chem. Soc., Perkin Trans. 2* **1992**, 2039-2041; b) M. R. Geraskina, A. S. Dutton, M. J. Juetten, S. A. Wood, A. H. Winter, *Angew. Chem. Int. Ed.* **2017**, *56*, 9435-9439.

[132] a) J. W. Park, N. H. Choi, J. H. Kim, *J. Phys. Chem.* **1996**, *100*, 769-774; b) M. J. Juetten, A. T. Buck, A. H. Winter, *Chem. Commun.* **2015**, *51*, 5516-5519; c) T. Zhang, S. Sun, F. Liu, J. Fan, Y. Pang, L. Sun, X. Peng, *Phys. Chem. Chem. Phys.* **2009**, *11*, 11134-11139.

[133] C. L. Bird, A. T. Kuhn, *Chem. Soc. Rev.* **1981**, *10*, 49-82.

[134] L. Michaelis, E. S. Hill, *J. Gen. Physiol.* **1933**, *16*, 859-873.

[135] S. Schoder, C. A. Schalley, *Chem. Commun.* **2017**, *53*, 9546-9549.

[136] G. Sheldrick, *Acta Cryst.* **2015**, *C71*, 3-8.

[137] O. V. Dolomanov, L. J. Bourhis, R. J. Gildea, J. A. K. Howard, H. Puschmann, *Appl. Cryst.* **2009**, *42*, 339-341.

[138] I. Yamaguchi, H. Higashi, S. Shigesue, S. Shingai, M. Sato, *Tetrahedron Lett.* **2007**, *48*, 7778-7781.

[139] F. Lin, T.-Y. Zhou, T.-G. Zhan, X. Zhao, *Tetrahedron* **2014**, *70*, 2251-2256.

[140] V. Diemer, H. Chaumeil, A. Defoin, A. Fort, A. Boeglin, C. Carré, *Eur. J. Org. Chem.* **2006**, 2727-2738.

[141] H.-H. Li, Y. Li, A.-W. Gong, C.-X. Wu, J. Zhu, H.-J. Dong, F.-S. Li, Z.-R. Chen, *Sci. Adv. Mater.* **2015**, *7*, 1793-1799.

[142] W. Qu, M.-P. Kung, C. Hou, S. Oya, H. F. Kung, *J. Med.Chem.* **2007**, *50*, 3380-3387.

[143] Y. Han, J.-B. Guo, J. Cao, C.-F. Chen, *Tetrahedron* **2013**, *69*, 4541-4545.

[144] H. Keipour, T. Ollevier, *Org. Lett.* **2017**, *19*, 5736-5739.

[145] L. Cera, C. A. Schalley, *Chem. Sci.* **2014**, *5*, 2560-2567.

[146] C. M. Gothard, C. J. Bruns, N. A. Gothard, B. A. Grzybowski, J. F. Stoddart, *Org. Lett.* **2012**, *14*, 5066-5069.

[147] A. Coskun, S. Saha, I. Aprahamian, J. F. Stoddart, *Org. Lett.* **2008**, *10*, 3187-3190.

[148] F. Neese, *WIREs Comput Mol Sci* **2012**, *2*, 73 - 78.

[149] a) A. D. Becke, *Phys. Rev. A* **1988**, *38*, 3098-3100; b) J. P. Perdew, *Phys. Rev. B* **1986**, *33*, 8822-8824.

[150] a) A. Schäfer, H. Horn, R. Ahlrichs, *J. Chem. Phys.* **1992**, *97*, 2571-2577; b) F. Weigend, R. Ahlrichs, *Phys. Chem. Chem. Phys.* **2005**, *7*, 3297-3305.

[151] F. Weigend, *Phys. Chem. Chem. Phys.* **2006**, *8*, 1057-1065.

[152] a) A. D. Becke, *J. Chem. Phys.* **1993**, *98*, 5648-5652; b) P. J. Stephens, F. J. Devlin, C. F. Chabalowski, M. J. Frisch, *J. Phys. Chem.* **1994**, *98*, 11623-11627.

[153] V. Barone, M. Cossi, *J. Phys. Chem. A* **1998**, *102*, 1995-2001.

[154] S. Grimme, S. Ehrlich, L. Goerigk, *J. Comp. Chem.* **2011**, *32*, 1456-1465.

[155] a) E. Runge, E. K. U. Gross, *Phys. Rev. Lett.* **1984**, *52*, 997-1000; b) F. Neese, *Coord. Chem. Rev.* **2009**, *253*, 526-563.

[156] a) J. P. Perdew, M. Ernzerhof, K. Burke, *J. Chem. Phys.* **1996**, *105*, 9982-9985; b) C. Adamo, V. Barone, *J. Chem. Phys.* **1999**, *110*, 6158-6170.